

# CFD Simulation of the Thermal Conversion of Solid Biomass in Packed Bed Furnaces

by

**Ramin Mehrabian Bardar**

Submitted to

the Institute for Process and Particle Engineering

Graz University of Technology

in partial fulfillment of the requirements for the degree of  
Doctor of Philosophy



Graz, November 2013

Deutsche Fassung:  
Beschluss der Curricula-Kommission für Bachelor-, Master- und Diplomstudien vom 10.11.2008  
Genehmigung des Senates am 1.12.2008

## EIDESSTÄTTLICHE ERKLÄRUNG

Ich erkläre an Eides statt, dass ich die vorliegende Arbeit selbstständig verfasst, andere als die angegebenen Quellen/Hilfsmittel nicht benutzt, und die den benutzten Quellen wörtlich und inhaltlich entnommenen Stellen als solche kenntlich gemacht habe.

Graz, am .....


.....  
(Unterschrift)

Englische Fassung:

## STATUTORY DECLARATION

I declare that I have authored this thesis independently, that I have not used other than the declared sources / resources, and that I have explicitly marked all material which has been quoted either literally or by content from the used sources.

*November 2013*  
.....  
date

  
.....  
(signature)

## Acknowledgement

Without professional and emotional support of a number of people this thesis would never been written. I would like to express my gratitude to all of them.

I would like to acknowledge my supervisor, Prof. Dr. Ingwald Obernberger for his guidance and for giving me the opportunity to work on an interesting and challenging research topic. I am very thankful to the reviewer of this work Prof. Dr. Viktor Scherer for carefully reviewing my thesis and making valuable comments on it. I am especially indebted to my scientific advisor Dr. Robert Scharler for lots of enlightening discussions, his everlasting optimism and untiring support during all these years.

At the beginning of my work in Graz I have been fortunated to work with Dr. Selma Zahirovic. I will always remember her fruitful exchange of ideas. I am also grateful to Dr. Stefan Kleditzsch from ANSYS FLUENT Germany for his consultation on various issues.

I am thankful to all my colleagues at Bioenergy2020+ GmbH for the enjoyable working atmosphere, especially Dr. Kai Schulze and Dr. Markus Gölles. I thank M.Sc. Ali Shiehnejadhesar for his close friendship and his lively conversation during the most tedious parts of this work.

Finally, this work would never been written without the constant encouragement and support of my wife, Maryam.

Graz, November 2013

Ramin Mehrabian Bardar

## Abstract

CFD calculations give an approximate overview of biomass grate firing systems, helping to diagnose and solve operational problems as well as providing assistance when dealing with new designs. At present there is no numerical simulation of biomass fixed-bed combustion systems using detailed models for both the bed and gas phases. In order to directly link the bed model with the gas phase combustion models and to simultaneously simulate the entire biomass grate furnace, it is necessary to develop an appropriate particle model which can be coupled with available CFD tools. A model for the thermal conversion of thermally thick solid biomass particles (drying, pyrolysis, and char burnout) was developed and implemented into CFD. The layer model treats the biomass particles as thermally thick particles, i.e., the temperature gradient in the particle is taken into account and, accordingly, the parallel progress of thermal conversion processes is allowed. The simulation results of the layer model were validated by the measured particle centre and surface temperatures as well as the overall particle mass loss during particles combustion in a single particle reactor.

Another important issue in simulating biomass packed bed combustion systems is modelling the hydrodynamics of the gas-solid multiphase flow. The model has to be capable of describing the influence of particle-particle interactions on the particle movements on the grate. Therefore a novel, three-dimensional model was developed by coupling Eulerian and Lagrangian multiphase flow approaches. The fluid flow is simulated with an Eulerian approach - the Euler-granular model, and the thermal conversion of biomass particles is resolved using a Lagrangian approach and the developed single particle model. The 3D packed bed model for biomass grate furnaces was applied to simulate a small-scale underfeed stoker furnace. Since no experimental data inside the packed bed were available, qualitative information about the position of the drying, pyrolysis, and char burnout zones, and the flue gas temperature measured by thermocouples at different positions in the combustion chamber above the fuel bed, was used for

comparison.

The packed bed model was further improved by considering radiation heat transfer between the particles and applying a detailed kinetic mechanism for combustion chemistry. The model performance was extensively validated using experimental data obtained in a laboratory-scale fixed-bed reactor, including CO, CO<sub>2</sub>, CH<sub>4</sub>, H<sub>2</sub>, H<sub>2</sub>O and O<sub>2</sub> concentrations above the fuel bed, temperatures at different heights in the bed and in the freeboard, and the propagation rate of the ignition front. The predicted results are in good agreement with the measured values.

# Contents

<b>List of Figures</b>	<b>III</b>
<b>List of Tables</b>	<b>IV</b>
<b>Nomenclature</b>	<b>V</b>
<b>1 Introduction</b>	<b>1</b>
1.1 Background . . . . .	2
1.2 Objectives and methodology . . . . .	3
<b>2 Combustion of biomass particles</b>	<b>6</b>
2.1 Drying . . . . .	7
2.2 Pyrolysis . . . . .	9
2.2.1 Pyrolysis products . . . . .	10
2.2.2 Pyrolysis kinetic scheme . . . . .	13
2.2.3 Effect of heating rate . . . . .	15
2.3 Char burnout . . . . .	17
2.4 Thermally thin and thick particles . . . . .	25
2.5 Layer model . . . . .	26
<b>3 Hydrodynamics of the packed bed</b>	<b>30</b>
3.1 Lagrangian approach . . . . .	31
3.1.1 Discrete phase model . . . . .	31
3.1.2 Discrete element method . . . . .	32
3.2 Eulerian approach . . . . .	32
3.3 Approach followed . . . . .	36

<b>4</b>	<b>Heat transfer in the packed bed</b>	<b>37</b>
4.1	Convective heat transfer . . . . .	38
4.2	Radiative heat transfer . . . . .	41
<b>5</b>	<b>Homogeneous reactions</b>	<b>44</b>
5.1	Reaction mechanisms . . . . .	44
5.2	Composition of volatiles . . . . .	45
5.2.1	Conservation of elements and enthalpy . . . . .	49
<b>6</b>	<b>Summary and conclusion</b>	<b>53</b>
	<b>Bibliography</b>	<b>58</b>
	<b>Annex</b>	<b>82</b>
	<b>Paper I: A CFD model for thermal conversion of thermally thick biomass particles</b>	
	<b>Paper II: Effects of pyrolysis conditions on the heating rate in biomass particles and applicability of TGA kinetic parameters in particle thermal conversion modelling</b>	
	<b>Paper III: Optimisation of biomass grate furnaces with a new 3D packed bed combustion model - on example of a small-scale underfeed stoker furnace</b>	
	<b>Paper IV: CFD simulation of biomass grate furnaces with a comprehensive 3D packed bed model</b>	
	<b>Paper V: Multi-physics modelling of packed bed biomass combustion</b>	

# List of Figures

2.1	Yields of char as a function of temperature for various biomass fuels . . . . .	11
2.2	Yields of tar as a function of temperature for various biomass fuels . . . . .	12
2.3	Yields of gas as a function of temperature for various biomass fuels . . . . .	13
2.4	Correlations for CO/CO <sub>2</sub> product ratios as a function of temperature . . . . .	24
2.5	Discretisation scheme of the Layer Model . . . . .	27
4.1	Scheme of heat transfer processes for particles in a packed bed	37
4.2	The Nusselt number as a function of the Reynolds number for packed beds . . . . .	40
4.3	Radiation control volume and neighbouring particles in the packed bed radiation model . . . . .	42
5.1	The yields of permanent gases as a function of pyrolysis temperature. . . . .	46
5.2	The mass ratios of CO, CH <sub>4</sub> , H <sub>2</sub> and H <sub>2</sub> O yields to CO <sub>2</sub> yield as functions of pyrolysis temperature. . . . .	51
5.3	The mass ratio of C <sub>2</sub> H <sub>x</sub> =C <sub>2</sub> H <sub>2</sub> +C <sub>2</sub> H <sub>4</sub> +C <sub>2</sub> H <sub>6</sub> yields to CH <sub>4</sub> yield as a function of pyrolysis temperature. . . . .	51



# List of Tables

2.1	Comparison of thermal conversion processes . . . . .	7
2.2	Heterogeneous reaction rate constants (R1-R4) . . . . .	21
2.3	CO/CO <sub>2</sub> product ratios . . . . .	23
4.1	The convective heat transfer correlations for packed beds . . .	39
5.1	The volatile compositions considered in the simulations with different mechanisms. . . . .	48

# Nomenclature

Symbol	Unit	Description
$A$	$[\text{m}^{-2}]$	area
$\mathbf{A}$	$[\text{s}^{-1}]$	pre-exponential factor
$a$	$[-]$	mass fraction of each biomass component
$c_p$	$[\text{J.kg}^{-1}.\text{K}^{-1}]$	specific heat capacity
$\mathcal{D}_a$	$[\text{m}^2.\text{s}^{-1}]$	ordinary gas molecular diffusivity
$\mathcal{D}_{ab}$	$[\text{m}^2.\text{s}^{-1}]$	binary diffusivity
$\mathcal{D}_e$	$[\text{m}^2.\text{s}^{-1}]$	effective diffusivity
$\mathcal{D}_{Ka}$	$[\text{m}^2.\text{s}^{-1}]$	Knudsen diffusivity
$d$	$[\text{m}]$	diameter
$\mathbf{E}$	$[\text{kJ.mol}^{-1}]$	activation energy
$e$	$[-]$	restitution coefficient
$F$	$[\text{kg.m.s}^{-2}]$	force
$H$	$[\text{J.kg}^{-1}]$	specific enthalpy
$\Delta H_f^\circ$	$[\text{J.kg}^{-1}]$	standard enthalpy of formation
$h_m$	$[\text{m.s}^{-1}]$	mass transfer coefficient
$\bar{I}$	$[-]$	identity matrix
$k$	$[\text{W.m}^{-1}.\text{K}^{-1}]$	thermal conductivity
$k_c$	$[\text{m.s}^{-1}]$	reaction rate constants
$m$	$[\text{kg}]$	mass
$M$	$[\text{kg.kmol}^{-1}]$	molecular weight
$\dot{m}$	$[\text{kg.s}^{-1}]$	mass flow rate
$Nu$	$[-]$	Nusselt number
$p$	$[\text{kg.m}^{-1}.\text{s}^{-2}]$	pressure
$Pr$	$[-]$	Prandtl number
$\mathbf{q}$	$[\text{W.m}^{-2}]$	heat flux
$\mathbf{R}$	$[\text{kJ.mol}^{-1}.\text{K}^{-1}]$	universal gas constant
$\mathcal{R}$	$[\text{s.m}^{-2}]$	mass transfer resistance
$Re$	$[-]$	Reynolds number
$Sc$	$[-]$	Schmidt number
$Sh$	$[-]$	Sherwood number

Symbol	Unit	Description
$T$	[K]	temperature
$t$	[s]	time
$\mathbf{v}$	[m.s <sup>-1</sup> ]	velocity
$X$	[mol.m <sup>-3</sup> ]	molar concentration of gas species
$\Delta x_0$	[m]	ratio between area of a layer left boundary to the half of the layer thickness
$\Delta x_1$	[m]	ratio between area of a layer right boundary to the half of the layer thickness

### Greek symbols:

$\alpha$	[-]	volume fraction
$\epsilon$	[-]	porosity
$\epsilon$	[-]	emissivity
$\eta$	[-]	stoichiometric coefficient of reactions
$\lambda$	[kg.m <sup>-1</sup> .s <sup>-1</sup> ]	bulk viscosity
$\mu$	[kg.m <sup>-1</sup> .s <sup>-1</sup> ]	shear viscosity
$\rho$	[kg.m <sup>-3</sup> ]	density
$\sigma$	[W.m <sup>-2</sup> .K <sup>-4</sup> ]	Stefan-Boltzmann constant
$\tau$	[-]	tortuosity
$\bar{\tau}$	[kg.m <sup>-1</sup> .s <sup>-2</sup> ]	stress tensor
$\Omega$	[-]	stoichiometric ratio of moles of carbon per mole of oxidising/gasifying agent in corresponding reaction

### Subscripts:

$B$	boundary
$c$	component (solid and gas)
$ch$	char
$conv$	convective
$diff$	diffusive
$df$	dry fuel
$g$	gas
$G$	granular
$L_i$	layer ( $L_0$ : wet fuel layer, $L_1$ : dry fuel layer, $L_2$ : char layer, $L_3$ : ash layer)

<b>Symbol</b>	<b>Description</b>
<i>lam</i>	laminar
<i>p</i>	particle
<i>rad</i>	radiative
<i>s</i>	solid
<i>turb</i>	turbulent
$\infty$	ambient condition

# Chapter 1

## Introduction

Biomass combustion plants are particularly important in the energy supply sector: by reducing dependency on fossil fuels they contribute to the mitigation of greenhouse gases and ensuring a more secure energy supply. Grate firing is one of the most widely spread combustion technologies because it can fire a wide range of fuels of varying moisture contents and requires less fuel preparation. In line with global trends, grate firing combustion units are continuously being optimised to increase process efficiency and reduce emissions. When it comes to biomass combustion plants, CFD modelling has proved to be a highly efficient tool for process analysis, providing the basis for optimising emission reduction, plant efficiency and availability. However, a number of processes have still not been sufficiently well described.

CFD modelling of biomass grate furnaces is inherently difficult. This is due to the complex biomass conversion in the fuel bed on the grate, the reactive flow in the freeboard, and the intensive interaction between them. CFD tools are successfully applied to simulate reactive flow, gas phase combustion and heat transfer in the furnace at levels of accuracy which are satisfactory for engineering purposes. At present, however, there are no commercially available numerical models for coupled bed and gas phase combustion with sufficient accuracy for use as engineering tools. This can be explained by the complexity of the thermo-chemical processes and limited computation capacities. But with the rapid improvements in computer

hardware technologies and new numerical methods, detailed modelling of such complex phenomena for engineering applications is possible within a reasonable calculation time. Therefore this thesis focused on the development of a 3D CFD model for solid biomass conversion in packed beds, for use in design studies.

## 1.1 Background

Packed bed modeling has been carried out for many years, and different model types have been developed according to the physical or chemical processes under consideration. The review of elaborations on packed bed modelling published in the literature shows a broad variety of different model approaches to describe packed bed systems. Fundamentally, they are either homogeneous or heterogeneous models. The difference lies in the calculation of the energy equation. In homogeneous models the temperatures of the gas and the solid phase are assumed to be equal, and a single, overall energy balance equation is applied [1–4]. The physical properties which appear as constants in the energy equation are described by their effective values over the entire bed. In heterogeneous models the gas phase and the solid phase have individual energy equations [5–12]. They have different temperatures, and heat and mass transfer between the two phases are described by means of Nusselt and Sherwood correlations. Where the temperature difference between gas and solid is not negligible as in packed bed combustion, then heterogeneous modelling is recommended.

Based on their treatment of the solid phase, heterogeneous models can be classified into continuous models [13–16] and discrete particle models [17–19]. Continuous heterogeneous models treat both phases as if they were distributed continuously over the whole spatial domain. At each point in space both phases exist with distinguished properties. The common limitation of the continuous packed bed models is that intra-particle effects cannot be sufficiently described. Additionally, it is very difficult to model the shrinkage of the packed bed using continuous models. The discrete particle

models enhance packed bed modelling by considering the packed bed as an ensemble of representative particles in which each particle undergoes thermal conversion processes. This enables the inter-particle effects, e.g. momentum and energy exchange, to be fully described. The main drawback of the discrete particle models is the high calculation time. However, a significant limitation of almost all existing models is that they model the packed bed and the freeboard separately, although there is an intensive interaction between them.

## 1.2 Objectives and methodology

The goal of this thesis is to gain greater insight into the conversion of biomass on the grate. The process in the fuel bed is of great significance, hence it would be extremely valuable to be able to predict the underlying processes inside the bed and not only provide boundary conditions, e.g. the distribution of gas species concentrations, velocity and temperature along the top surface of the packed bed to CFD models for the freeboard. Basically, packed bed modelling can be split into two parts: the conversion of biomass in the packed bed and the hydrodynamics of the gas-solid multiphase flow of the packed bed.

The thermal conversion processes of single solid particles are rather complex, although common to all solid fuel types (coal, biomass, waste) and all technologies (pulverised, packed-bed and fluidised bed combustion). A solid particle exposed to a hot environment heats up, dries and devolatilises until the solid residue (char) finally burns to ash. In the present work, a model for the thermal conversion of the thermally thick solid biomass particles is developed. The particle model is programmed in C/C++ and coupled to ANSYS FLUENT. The model treats the biomass particles as thermally thick particles, i.e. the temperature gradient in the particle is taken into account, and accordingly the parallel progress of thermal conversion processes is considered. In the model the drying rate is calculated using an energy balance equation at the drying front. The devolatilisation rate is assumed to consist

of three competing kinetic rates for lignin, cellulose, and hemicellulose. The char burnout reaction rate is limited by kinetic and diffusion rates. The simulation results of the model are extensively validated by measured particle centre and surface temperatures as well as the overall particle mass loss during particle pyrolysis and combustion in a single particle reactor.

Modelling the particle motion on the grate is another significant issue. In this work, the packed bed of the grate furnace is considered as a multiphase medium. The Eulerian treatment (the Euler-granular model of ANSYS FLUENT) is applied to model the dynamics of both the solid and gas phase. Therefore the solid phase equation of motion is similar to the gas phase momentum equation, with some specific terms denoting the solid behaviour. These terms are modelled using the kinetic theory of granular flow. The model proposed for particle motion inside the packed beds provides more reliable results for particle trajectories, because it has the ability to account for inter-particle interactions, i.e. friction and collision. Additionally, the volume fraction of the solid phase is accounted for in the momentum equation of the gas phase, implying gas phase displacement by means of the volume of the solid phase. However, when using the Euler-granular model it is not possible to apply the particle model to simulate the thermal conversion of the particles individually. Therefore an innovative approach is developed to combine the Euler-granular model for the hydrodynamics of packed beds with the particle model for the thermal conversion of biomass particles. A user defined function (UDF) is programmed to calculate the particle trajectories based on the velocity field of the granular phase obtained by the Euler-granular model.

Having an accurate model for homogeneous reactions is important for packed bed biomass combustion because it produces the energy required for the heating, drying and pyrolysis of the fuel bed. Additionally, species concentrations are affected by the model used for homogeneous reactions. On the other hand, apart from the radiation heat transfer from the freeboard to the packed bed, the radiation between the particles is an important mechanism of heat transfer in biomass grate firing systems. This work



therefore also involved the implementation of models for the radiation heat transfer between the particles, and detailed mechanisms for the homogeneous reactions in the packed bed as well as in the freeboard. In order to validate the entire 3D packed bed model, it was used to simulate a laboratory-scale fixed bed reactor. The model performance was extensively validated with several experimental measurements - CO, CO<sub>2</sub>, CH<sub>4</sub>, H<sub>2</sub>, H<sub>2</sub>O and O<sub>2</sub> concentrations above the fuel bed, temperatures at different heights in the bed and in the freeboard, and the propagation rate of the ignition front.

# Chapter 2

## Combustion of biomass particles

This chapter introduces the subject of combustion of biomass particles with a short description of its sub-processes, e.g. drying, pyrolysis and char burnout.

The conversion of solid biomass can be achieved through one of two major pathways, (1) biological (fermentation) and (2) thermal. Biological conversion is perhaps the most ancient means of biomass conversion. India and China produced methane gas for local energy needs through the anaerobic microbial digestion of animal wastes [20]. Thermal conversion of biomass into gases came much later. Commercial usage of small biomass gasifiers began during the Second World War. The four principal routes for thermal conversion are:

- combustion
- gasification
- pyrolysis
- liquefaction

Combustion involves the high temperature conversion biomass in excess air directly into heat. Gasification, in contrast involves a chemical reaction in an oxygen deficient environment to produce gas and char at the first stage, and the subsequent reduction of the product gases by the charcoal. Pyrolysis is the fundamental chemical reaction process that is the precursor of both

the gasification and combustion of solid fuels. Pyrolysis takes place without the participation of oxygen. In liquefaction, the large biomass molecules are decomposed into liquids with smaller molecules. This occurs in the presence of a catalyst and at a relatively low temperature. These small molecules are unstable and reactive, and can repolymerise into oily compounds with a wide range of molecular weight distribution. Table 2.1 compares these four thermochemical paths for biomass conversion.

Table 2.1: Comparison of thermal conversion processes [21]

Process	Temperature [°C]	Pressure [MPa]	Oxygen	Catalyst
combustion	700-1400	>0.1	surplus	not required
gasification	500-1300	>0.1	deficient	not required
pyrolysis	250-530	0.1-0.5	absence	not required
liquefaction	250-330	5-20	absence	essential

Combustion is perhaps the oldest method of using of biomass by means of thermal conversion. It is a complex process involving heat and mass transfers, fluid dynamics, homogeneous as well as heterogeneous reactions. When a biomass particle is exposed to heat flux, it undergoes three stages: drying, pyrolysis, and char burnout. For small particles, e.g. pulverized fuel particles, drying, pyrolysis, and char burnout occur sequentially, and the char burnout period lasts much longer than the pyrolysis and drying stages. For larger particles, drying, pyrolysis, and char burnout occur simultaneously. The following sections describe the stages involved in the combustion of the biomass particles.

## 2.1 Drying

Water embeds into a wood particle in three forms: free liquid water in the cell lumina which is held by capillary forces, bound or hygroscopic water which is bounded to the wood structure via hydrogen bonds and water vapour in the cell lumina which is in thermodynamic equilibrium with free water [22, 23]. An increase in particle temperature leads to a higher saturation pressure

of water vapour in the particle pores. It results in a higher concentration of water vapour and faster diffusion out of the particle. If the saturation pressure of the water vapour exceeds the external pressure, the vapour leaves the particle by convection. Due to a decrease in water vapour concentration in the particle pores, the free water evaporates to compensate for the loss of water vapour. Once no free water remains the bound water begins to evaporate. In addition to water vapour diffusion and convection out of the particle, the free water convection in the pores and bound water diffusion in the solid structure may contribute to the drying process. However, during fast drying, as given under biomass combustion conditions, it can be shown that the effect of the free and bound water transport on the whole drying process is negligible [23, 24].

There are different models available in the literature to calculate the evaporation rate during fast drying. They can be divided into three groups: thermal models, equilibrium models and kinetic rate models. The kinetic rate models consider drying as a heterogeneous reaction and use an Arrhenius equation to calculate its rate [25–30]. The pre-exponential factor and activation energy are set so that the drying rate significantly increases at 373.15 K. This model has the advantages of easy implementation and numerical stability. However, it is difficult to apply the given kinetic data to conditions different from those for which the data have been derived. The equilibrium models are based on the hypothesis that the liquid water and the water vapour in the gas phase are in thermodynamic equilibrium. The drying rate is thus proportional to the difference between the equilibrium concentration and the current vapour concentration in the gas phase. The equilibrium assumption is usual in low-temperature drying models [31], therefore the mass transfer coefficient, which is highly dependent on particle permeability, needs to be adjusted using experimental data gained under fast drying conditions [32, 33].

The thermal models are the ones most often used in the literature [34–51]. This model is based on the assumption that drying occurs at a fixed boiling temperature (373.15 K). Therefore, any amount of heat flow above

this temperature is consumed by the drying process. Indeed, drying acts as a heat sink. Bellais [23], Peters et al. [39–41], and Yang [42] reported numerical difficulties in applying the thermal model for drying because they use a conditional test on local temperatures which appears as a Dirac function in the energy equation. If the local temperature is higher than the boiling temperature, the drying rate is equal to the energy beyond the boiling temperature divided by the latent heat, otherwise the drying rate is zero. This Dirac function in the energy equation makes it stiff and this in turn requires a special solver.

In the present work the drying is modelled based on the thermal model and drying occurs at a fixed boiling temperature in an infinitely thin zone that separates the wet and the dry part of the particle. If the temperature is higher than the boiling temperature, the total energy needed to heat the local element beyond the boiling temperature consumes for evaporation and the boiling temperature consumes for drying and the drying rate is obtained with dividing this energy by the heat of vaporization.

## 2.2 Pyrolysis

Pyrolysis is the major decomposition process occurring in a biomass particle and involves a great number of reactions. Large hydrocarbon chains are broken down into shorter chains, some of which can break again to form smaller hydrocarbons (secondary reactions). During these reactions gas and tar species leave the solid matrix of the particle, finally leaving a very porous char structure. Usually the volatile matter (gas and tar) of a biomass particle comprises the major part of the particle mass. Because of the large number of reactions taking place it is usually the global, rather than the elementary, reactions which are investigated. These reactions describe an overall process by which reactants are converted to anticipated products at the end of the process.

### 2.2.1 Pyrolysis products

Several studies have been carried out to determine product yields in terms of char, tar and gas. Detected yields for biomass under combustion conditions ranged from 5-25 wt% for char, 10-40 wt% for gaseous and 30-60 wt% for tars [52]. These differences result from diversity in feedstock and experimental setups and procedures. Variations in heating rate and temperatures in particular lead to large changes in observed yields. A slow heating rate is associated with high char production, but rapid heating yields more tar at a low temperature peak (675-775 K), and/or gas at a high temperature peak [21]. The composition, size, shape, and physical structure of the biomass exert some influences on the pyrolysis product through their effect on the heating rate. Increasing particle size facilitates secondary cracking due to the greater resistance they offer to the escape of the primary pyrolysis product. Moreover, the hot char layer formed around the biomass particle acts as a catalyst for the tar cracking reactions, resulting in a higher gas yield. For example, Yin et al. [53] reported an increase of about 55% in the gas yield if the particle size changes from below 1 cm to 6-8 cm. Nik-Azar et al. [54] also found that, as particle size increases from 53-63  $\mu\text{m}$  to 270-500  $\mu\text{m}$  the maximum tar yield decreases from 53% to about 38% (wt% of parent fuel).

#### Char

Char is the solid residue remaining after pyrolysis. It consists of organic material and ash. Its organic material is primarily carbon, but it can also contain some oxygen and hydrogen. The lower heating value (LHV) of biomass char (32 MJ/kg [55, 56]) is much higher than that of the parent biomass, which is in the range of 19 to 21 MJ/kg dry basis.

Figure 2.1 shows char yields as a function of temperature for various biomass fuels. Data come from 32 studies on the pyrolysis of woody biomass [57-88], which primarily involved fast heating rate pyrolysis experiments. Regardless of biomass type and experimental conditions, char yield decreases with temperature. Within the range of typical combustion conditions ( $> 700^\circ\text{C}$ ) the char yields remain roughly constant.

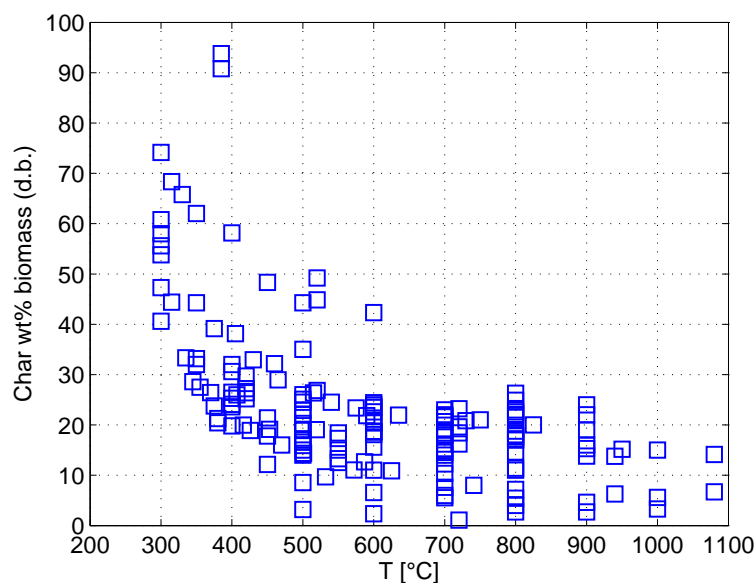


Figure 2.1: Yields of char as a function of temperature for various biomass fuels, experimental data from [57–88].

### Tar

Tar is a generic term for all organic compounds with a molecular weight higher than benzene present in the biomass volatiles that are condensable at room temperature. Although tar species form the largest mass fraction of the pyrolysis products, its definition is still a matter of discussion. This may be because the composition of tar can vary with the peak temperature, residence time at peak temperature, biomass composition and size of the particle [89, 90]. Additionally, different experimental procedures and sampling methods may result in large variations in the detected tar component, making it hard to determine the molecular composition of tar. Analyses show that the elemental composition of tar is fairly similar to that of the parent fuel [56–59]. Moreover, tar has a comparable LHV to that of the parent biomass [56, 91].

Figure 2.2 summarises some experimental data, clearly demonstrating the effect of temperature on tar yields. Maximum yields, obtained at 400–600°C,

range between 50 and 80 wt%. There are two reasons for the lower tar yields at low temperatures: incomplete devolatilisation of the solid particles and favored char formation. The lower tar yields at high temperatures are due to the effect of the secondary tar cracking reactions. The primary tar volatiles are highly susceptible to further conversion into light gas [87–89, 92, 93], secondary char [89, 92] and water [66, 89, 94].

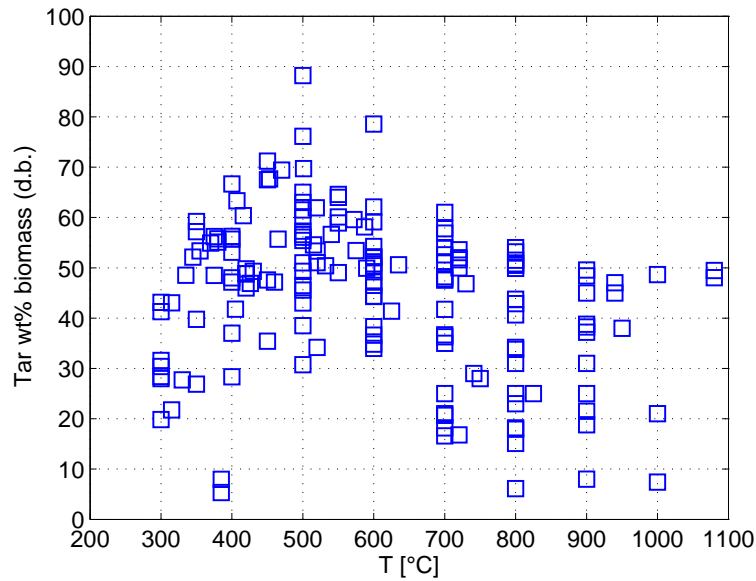


Figure 2.2: Yields of tar as a function of temperature for various biomass fuels, experimental data from [57–88].

### Gas

Gas is produced by the primary decomposition of biomass and the secondary cracking of the tar species. The light gas yields as a function of temperature are provided in Figure 2.3. A higher pyrolysis temperature promotes the formation of gaseous products at the expense of total tar and changes the gas composition. For temperatures below 500°C, when the activity of secondary tar cracking reactions for gas formation is negligible, the gas yields are small and roughly constant. In other words, the sharp decrease in char yield at temperatures below 500°C is only compensated by an increase in the tar yields, as shown in Figures 2.1 and 2.2. Comparing Figures 2.1 and 2.3



shows that char is the main product at low temperatures, maximum tar yields are observed at middle range temperatures and high temperatures favour the production of light gases. These general trends in product yields as a function of temperature are the same for both slow and fast heating rates.

A broad range of LHV has been reported in the literatures for the pyrolysis gas, from 4 to 16 MJ/kg depending on feedstock and pyrolysis peak temperature [52, 62–68]. The composition of the permanent gas has been experimentally studied by several researchers. It is addressed in more details in section 5.2.

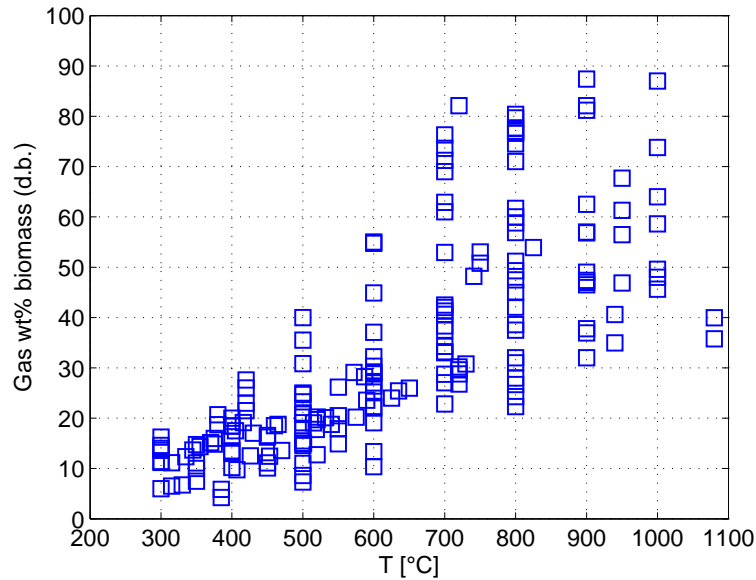


Figure 2.3: Yields of gas as a function of temperature for various biomass fuels, experimental data from [57–88].

### 2.2.2 Pyrolysis kinetic scheme

The majority of kinetic mechanisms consist of single or parallel one-step reactions for the formation of gas, tar and char. The kinetic constants must be determined experimentally, and empirical data obtained by Chan et

al. [26], Thurner and Mann [95], and Wagenaar et al. [96] are normally used in models for the thermal conversion of biomass particles. The advantage of such a pyrolysis mechanism is that both product yields and decomposition rates can be predicted. However, biomass mass loss curves present different reaction zones which can be mainly associated with the decomposition of the different biomass constituents. Hence, simplifying biomass fuels to one-component produces inaccuracies in the results. Moreover, the dependency of product yields, specially the char yield, on temperature is not well predicted in this model [97, 98]. The one-step one-component mechanism fails to describe thermogravimetric curves of biomass pyrolysis, at least with regard to the correct prediction of conversion time and the maximum pyrolysis rate [99].

Several studies suggest that primary biomass decomposition rates can be modelled in terms of the decomposition of its three major components: hemicellulose, cellulose, and lignin [98, 100–103]. The model implicitly assumes the hypothesis of independent decomposition of these three constituents. This superposition model is an appealing approach as it is able to handle different feedstocks. An Arrhenius equation is used to describe the pyrolysis of each major component. The kinetic parameters are determined by fitting to experimental results (e.g. TGA) concerning the mass loss rate versus temperature. The analysis of experimental data shows that the decomposition of hemicellulose and cellulose is associated with the shoulder and the peak of the mass loss curves respectively. Lignin decomposes slowly over a broad range of temperatures and forms the tail of the mass loss curves in the high temperature region. In addition to kinetic constants, the mass fractions of these components in a specific biomass fuel need to be determined in the superposition model. Like the kinetic parameters, they are estimated by fitting to experimental results. Alternatively, they can be determined based on chemical analyses.

Assuming first-order reactions in respect to mass fraction for the decomposition of each major component leads to the following equations

for the mass loss of a particle during pyrolysis:

$$\frac{dm_{df}}{dt} = - \sum_{i=1}^3 R_i \quad (2.1)$$

$$R_i = \mathbf{A}_i \exp\left(\frac{-\mathbf{E}_i}{\mathbf{R}T}\right) a_i m_{df} \quad (2.2)$$

where  $R_i$ ,  $\mathbf{A}_i$ ,  $\mathbf{E}_i$ ,  $\mathbf{R}$ , and  $m_{df}$  are the reaction rate, the pre-exponential factor, the activation energy, the universal gas constant, and the mass of dry fuel, respectively.  $a_i$  represents the mass fraction of cellulose, hemicellulose and lignin in the total mass of dry fuel which converts to volatiles.

This model has been subjected to extensive experimental validation and the predictions from this model correctly reproduce the experimental thermogravimetric curves during the pyrolysis of several biomass fuels [22, 104–110]. However, the three-component mechanism cannot predict the product yields, which is a deficiency of this model and it will be addressed in section 5.2. In the present work the three-component mechanism is used to model the pyrolysis. Considering  $a_i m_{df} = m_i$ , where  $m_i$  is the mass of cellulose, hemicellulose and lignin, by substituting it together with Equation 2.2 into Equation 2.1 the pyrolysis rate used in this thesis is obtained:

$$\frac{dm_{df}}{dt} = - \sum_{i=1}^3 \frac{dm_i}{dt} = - \sum_{i=1}^3 \mathbf{A}_i \exp\left(\frac{-\mathbf{E}_i}{\mathbf{R}T}\right) m_i \quad (2.3)$$

### 2.2.3 Effect of heating rate

Several studies have investigated the effect of heating rates on the characteristics of thermogravimetric curves, for example see [22, 99, 108, 109, 111]. They indicate that by increasing the heating rate the pyrolysis reactions take place at higher temperatures and the maximum mass loss rate rises. Moreover, the hemicellulose shoulder and lignin tail become less visible, thus increasing the overlap between the pyrolysis of the three major biomass components. This shift of biomass decomposition to higher temperatures may be attributed to the residence time of the biomass. The

faster the heating rate, the shorter the residence time of exposure to a given temperature range. Hence the biomass must reach a higher temperature to assure sufficient time for completion of the overall pyrolysis reaction.

The shift of pyrolysis reaction to higher temperatures by increasing the heating rate can be mathematically shown. The mass loss rate of each pseudo-component, Equation 2.3, for constant heating rate experiments  $T = \beta t + T_0$ , where  $\beta$  is the heating rate and  $t$  is the time, can be rearranged to:

$$\frac{dm_i}{dT} = \frac{\mathbf{A}_i}{\beta} \exp\left(-\frac{\mathbf{E}_i}{\mathbf{R}T}\right) m_i \quad (2.4)$$

If one looks for the temperature at which the maximum conversion rate of each pseudo-component occurs  $T_{max}$ , the second derivative of  $m_i$  in respect to temperature is required:

$$\frac{d^2m_i}{dT^2} = \frac{\mathbf{A}_i}{\beta} \exp\left(-\frac{\mathbf{E}_i}{\mathbf{R}T}\right) \left[ \frac{\mathbf{E}_i}{\mathbf{R}T^2} m_i - \frac{dm_i}{dT} \right] \quad (2.5)$$

The extrema of the conversion rate of each pseudo-component are the roots of equation  $d^2m_i/dT^2 = 0$ . Considering Equation 2.5 and Equation 2.4 results in:

$$\exp\left(\frac{\mathbf{E}_i}{\mathbf{R}T}\right) - \frac{\mathbf{R}\mathbf{A}_i}{\mathbf{E}_i\beta} T^2 = 0 \quad (2.6)$$

Equation 2.6 might have only one root. According to the DTG curves this root corresponds to the temperature at which the maximum conversion rate of each pseudo-component occurs,  $T_{max}$ . As it can be seen the second term of Eq. 2.6 is a function of the heating rate  $\beta$ . For a given set of kinetic parameters, i.e.  $\mathbf{A}_i$  and  $\mathbf{E}_i$ , any changes in the heating rate alert  $T_{max}$  and successively lead to a lateral shift of the DTG curve. In other words, as the heating rate increases, the DTG curves as well as the temperature  $T_{max}$  move towards higher temperatures.

Accordingly, the pyrolysis mass loss function, Equation 2.3, is able to predict the lateral shift of DTG curves by changing the heating rate. However, applying low heating rate kinetic parameters overestimates the increase of  $T_{max}$ . Therefore, using kinetic parameters measured at low heating rate

TGA experiments for the simulation of pyrolysis in high heating rate regime leads to an unrealistic shape of the DTG curves. It, successively, impairs the overall mass loss profile during pyrolysis.

This means that the kinetic parameters and the mass fractions of the components obtained by slow heating rate experiments (i.e. typically below 50 K/min) are not valid for fast heating rate conditions. This topic is investigated in more details in *Paper II*.

Product distribution is also found to be dependent on the heating rate. In general, fast heating rates lead to higher yields of tar at the expense of char production [98, 112]. Additionally, the composition of volatile matter is affected by the heating rate [58, 71]; for instance, the average molecular weight of tar increases with the heating rate [54]. Shen et al. [94] proposed that higher heating rates favour bond scission reactions to form tar components, while lower heating rates favour the recombination of tar components on the biomass matrix (charring reactions).

## 2.3 Char burnout

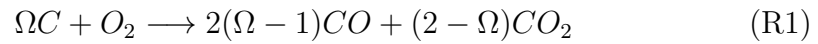
Char conversion models are more complicated than biomass pyrolysis models because they are heterogeneous reactions for which both intrinsic kinetic and transport phenomena are important. As the char conversion proceeds, the density and/or size of the char particle decreases due to mass loss, depending on the char type and operating conditions. The classical uniform char conversion model assumes that the reaction occurs uniformly throughout the entire particle, and that temperature and species fields inside the particle are flat. The reaction rate in this model can be evaluated by the char intrinsic reactivity; this model is applicable for low temperatures or low rate reactions [113].

Apart from the classical model, the char conversion models based on the location of the reaction can be classified into surface reaction models and zone reaction models. In surface reaction models the reaction is fast and occurs at a surface as soon as the reactant gas reaches the reaction surface.

As the reactions proceed, the reaction surface moves towards the centre of the particle. In this case the reaction rates are correlated to the area of the reaction surface. In zone reaction models the reactions take place in a region inside the particle which grows and travels into the particle during the conversion. Therefore the reaction rates are a function of the available contact area in the reaction zone.

Additionally, two different char conversion models can be distinguished based on the ash behaviour,. The ash remaining after the char conversion may leave the particle as soon as it is produced, or it can build up an additional layer which surrounds the char particle; the former is called a shrinking particle, the latter a shrinking core. In the shrinking particle models, the change in particle size is proportional to the conversion rate, whereas in the shrinking core models, particle size is related to char conversion, ash density and porosity. Furthermore, in the shrinking core models, the ash layer increases the resistance to mass and heat transfer.

It has been experimentally verified that char combustion is such a rapid reaction that it occurs in a very thin layer [114]. Additionally, since the surface reaction models are more compatible with the structure of the layer model, the char conversion reactions are assumed to occur at the interface between char and ash layer. The char oxidation with  $O_2$  and gasification with  $CO_2$ ,  $H_2O$  and  $H_2$  are considered as the char conversion reactions:



For most of the combustion applications the reaction of char with oxygen is much faster than char gasifications with carbon dioxide, water vapour and hydrogen [112, 114, 115]. Where the oxygen is depleted, these gasification reactions become important. The fundamental kinetic analysis

of carbonaceous solid conversion can be found in [112, 116–118].

Apart from the kinetics of the reactions, they always involve a mass transport rate because the process of a heterogeneous reaction can be divided into the following steps:

1. transport of oxidising/gasifying agent to the particle surface
2. diffusion through the ash layer
3. adsorption on the reaction surface
4. chemical reaction
5. desorption of products from the surface
6. diffusion of products through the ash layer
7. transport of products from the particle surface back to the environment

Except the chemical reaction, the remaining steps are mass transport. The overall rate of the entire process is determined by their slowest rate. Thus two main regimes can be introduced in char conversion [112, 119]: the kinetically controlled regime for low temperatures and char particles which are so small that the mass transport rate is much faster than the chemical reaction, and the transport controlled regime for high temperatures and large particles, where the intra-particle and/or external mass transfer rates become lower than the kinetic rate of the chemical reaction, leading to a limited penetration of gas species into the char particle. It is worth noting that diffusion effects during char gasification may be important even for small particles, as under the conditions of thermogravimetric analysis [120–123].

In this work the rate of char conversion reactions is a function of both the kinetic rate at the reaction surface and the mass transfer rate to/from the reaction surface. Assuming a global reaction rate to the order of one with respect to the oxidising/gasifying agent concentration at the reaction surface,

this gives a char conversion rate of:

$$\frac{dm_{ch}}{dt} = - \sum_{i=1}^4 \Omega_i M_c A k_{c,i} X_i \quad (2.7)$$

where  $i = 1$  to 4 corresponds to reactions R1-R4, respectively.  $\Omega_i$  is the stoichiometric ratio of moles of carbon per mole of oxidising/gasifying agent in the corresponding reaction.  $M_c$ ,  $A$ ,  $k_{c,i}$ , and  $X_i$  are the carbon molecular weight, the area of the reaction surface, the constant rate of reaction  $i$ , and the molar concentration of oxidising/gasifying agent of reaction  $i$  at the reaction surface, respectively.

Although the oxidising/gasifying agents molar concentration at the reaction surface is not known, it can be calculated from the continuity equation for this reacting gaseous component. By assuming the pseudo-steady state approximation, the concentration of oxidising/gasifying agent at the reaction surface can be written as a function of its concentration at the bulk gas flow:

$$X_i = \frac{1}{Ak_{c,i}(\mathcal{R}_{conv} + \mathcal{R}_{diff}) + 1} X_{\infty,i} \quad (2.8)$$

$\mathcal{R}_{conv}$  and  $\mathcal{R}_{diff}$  are resistances to convective and diffusive mass transfer, respectively.

The pseudo steady state approximation neglects the transient term in the continuity equation of reacting gaseous components. This means that the rate at which the reaction surface moves is smaller than the rate of transport of the reacting gaseous component. This condition is always satisfied for gas-solid reactions, but not necessarily for liquid-solid reactions, as was shown by [124–126].

Substituting Equation 2.8 into Equation 2.7 leads to:

$$\frac{dm_{ch}}{dt} = - \sum_{i=1}^4 \frac{\Omega_i M_c}{\frac{1}{Ak_{c,i}} + (\mathcal{R}_{conv} + \mathcal{R}_{diff})} X_{\infty,i} \quad (2.9)$$



The reaction rate constants of reactions R1-R4,  $k_{c,i}$ , are listed in Table 2.2. The mass transfer resistances are given by:

$$\mathcal{R}_{diff} = \frac{1}{\mathcal{D}_e} \int \frac{dr}{A(r)} \quad (2.10)$$

$$\mathcal{R}_{conv} = \frac{1}{h_m A} \quad (2.11)$$

where  $A$  and  $h_m$  are the area and mass transfer coefficient, respectively.  $\mathcal{D}_e$  is the effective diffusivity of the ash layer, which depends on the ash porosity,  $\epsilon$ , the tortuosity,  $\tau$ , and the molecular diffusivity of the penetrating gaseous component,  $\mathcal{D}_a$ :

$$\mathcal{D}_e = \frac{\epsilon}{\tau} \mathcal{D}_a \quad (2.12)$$

The tortuosity can be replaced by the inverse of the porosity, which is often a reasonable approximation [113, 128, 129]:

$$\mathcal{D}_e = \epsilon^2 \mathcal{D}_a \quad (2.13)$$

The molecular diffusivity of the reactive agent in the ash layer pores can be written as [113, 130]:

$$\frac{1}{\mathcal{D}_a} = \frac{1}{\mathcal{D}_{ab}} + \frac{1}{\mathcal{D}_{Ka}} \quad (2.14)$$

For the sake of simplicity, the Stefan-Maxwell equation for a binary system with equimolar counter-diffusion condition was applied in the above equation. The binary diffusivity,  $\mathcal{D}_{ab}$ , is calculated using the Chapman-Enskog kinetic theory [131]. The Knudsen diffusivity is given by:

$$\mathcal{D}_{Ka} = \frac{2}{3} d_{pore} \sqrt{\frac{2 \mathbf{R} T}{\pi M_a}} \quad (2.15)$$

Table 2.2: Heterogeneous reaction rate constants (R1-R4)

$k_{c,R1} = 1.715 \times T_{B_2} \exp(-9000/T_{B_2})$	[127]
$k_{c,R2} = k_{c,R3} = 3.42 \times T_{B_2} \exp(-15600/T_{B_2})$	[127]
$k_{c,R4} = 3.42e^{-3} \times T_{B_2} \exp(-15600/T_{B_2})$	[127]

where  $M_a$  is the molecular weight of the diffusing species and  $d_{pore}$  is the pore diameter. This equation was derived assuming random collisions of the gas molecules with the walls, which is reasonable when the pore size is larger than the molecular dimensions and much smaller than the mean free path [113].

The mass transfer coefficient of reactant species in the boundary layer around the particle,  $h_m$  in Equation 2.11, is obtained using the Sherwood number:

$$Sh = \frac{h_m d_p}{\mathcal{D}_{ab}} \quad (2.16)$$

Several experimental and theoretical investigations have been undertaken to determine the Sherwood number for a reacting particle. Scala [132] investigated many of the empirical/theoretical correlations available for Sherwood. He showed that almost all the theoretical correlations [133–139] failed to predict a Sherwood number comparable to his experimental data of a freely moving active particle in the dense phase of a fluidised bed. However, a semi-empirical correlation proposed by Hayhurst and Parmar [140], one of several empirical correlations [141–148], fits his experimental data excellently. Hayhurst and Parmar measured the temperature of freely moving single graphite spheres and coal char particles during their combustion in a fluidised bed as well as outlet gas concentrations in order to calculate the burning rate. By estimating the CO/CO<sub>2</sub> ratio as combustion products, they suggested a Frössling-type expression:

$$Sh = 2\epsilon_{bed} + 0.69(Re/\epsilon_{bed})^{1/2} Sc^{1/3} \quad (2.17)$$

where  $\epsilon_{bed}$  is the bed voidage.

It should be noted that this correlation for Sh holds for the case of equimolar counter-diffusion, although in reactions R1-R4 the diffusion of reactants towards the reaction surface and of products away from it are not equimolar and even for the oxidation reaction, the molar flux of products is temperature dependent. Hayhurst [149], Paterson and Hayhurst [150] and Scala [151] proved that assuming CO as the only product of reaction R1, which represents the biggest deviation from equimolar counter-diffusion

condition, leads to an error of less than 10%. If CO and CO<sub>2</sub> are considered as products, the error is even less and can thus be neglected in calculating the Sherwood number compared to other uncertainties, such as the determination of  $\mathcal{D}_e$ , and experimental errors [152].

Table 2.3: CO/CO<sub>2</sub> product ratios

CO/CO <sub>2</sub>	T (K)	Carbonaceous material	size (mm)	Oxygen (vol.%)	Ref.
$10^{3.4}e^{(-6240/T)}$	730-1170	coal char, graphite	0.85-2.41	5-25	[153]
$1860e^{(-7200/T)}$	790-1690	electrode carbon	o.d.: 12.1, i.d.: 8.3, L: 10	3-21	[154]
$170e^{(-3220/T)}$	800-950	graphon	fine particles	1-26	[155]
$25.7e^{(-2000/T)}$	770-920	vitreous carbon		3-15	[156]
$8.5 \cdot 10^9 e^{(-33200/T)}$	1500-1800	coal char		6-12	[157]
$120e^{(-3200/T)}$	670-890	soot particles		5-100	[158]
$1336e^{(-7643/T)}$	850-970				
$4.72 \cdot 10^{-3} e^{(4539/T)}$	970-1220	petroleum coke	3-11	21	[159, 160]
$12.41e^{(-5063/T)}$	1220-1650				
$94e^{(-2980/T)}$				5	
$70e^{(-3070/T)}$	670-1670	spherocarb char	0.18-0.24	20	[161]
$50e^{(-3070/T)}$				100	
$3 \cdot 10^8 e^{(-33237/T)}$	1400-2100	utah coal char	0.07	5-21	[162]
$4.3e^{(-3390/T)}$	1000-1370	wood charcoal	o.d.: 27, L: 114	21	[163]
$12e^{(-3300/T)}$		biomass charcoal			[164]
$218e^{(-7250/T)}$		wood charcoal			[165]

The CO/CO<sub>2</sub> product ratio in reaction R1 has been the subject of many experimental and modelling studies, as it has a significant impact on the particle temperature as well as the char oxidation rate. According to the work of Tognotti et al. [161], there is almost no doubt that both CO and CO<sub>2</sub> are primary products of char oxidation. They heated single char particles by laser irradiation and avoided CO oxidation to CO<sub>2</sub> in the particle boundary layer by maintaining the surrounding gas at room temperature. Their results clearly indicate that at high temperatures both CO and CO<sub>2</sub> are primary products of char oxidation.

Table 2.3 summarises the empirical correlations for CO/CO<sub>2</sub> product ratios

available in the literature so far. Measurement data have been correlated in all of them using an Arrhenius relation, and the product ratio increases with temperature. The  $\text{CO}/\text{CO}_2$  ratios obtained by correlations in Table 2.3 show little agreement. This is probably due to the different types of fuels used, leading to different morphologies, porosities, pore sizes and internal surface areas. Other reasons may be different experimental procedures and conditions. A comparison of the correlations in Table 2.3 is shown in Figure 2.4. The suggested correlations by Linjewile and Agarwal [159, 160] and Evans and Emmons [163] have nearly the same values for  $\text{CO}/\text{CO}_2$ . Although Evans and Emmons [163] did not report two local extrema at 970 K and 1220 K.

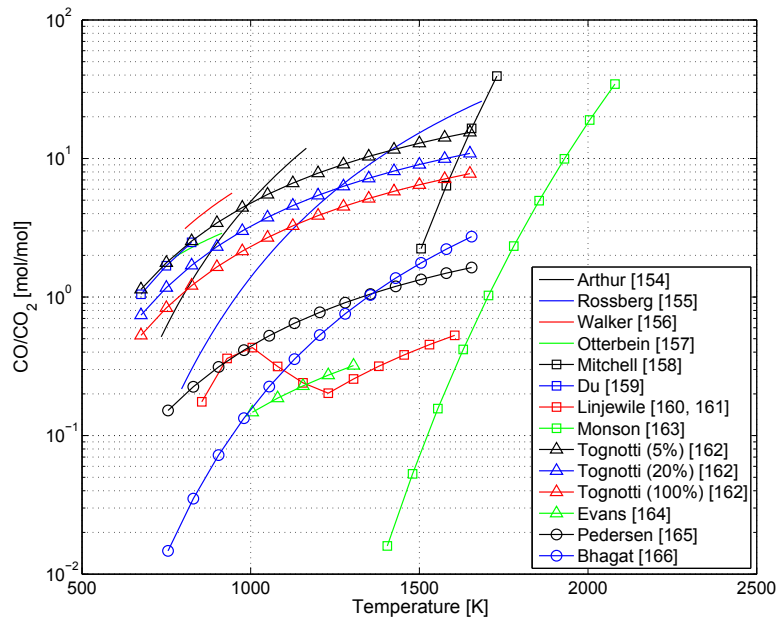


Figure 2.4: Correlations for  $\text{CO}/\text{CO}_2$  product ratios as a function of temperature, data from Table 2.3

The correlation of Evans and Emmons [163] has been selected in this study, because two independent measurements concede it. Furthermore, there are

enough evidences which show at high temperatures, approaching 1400 K, CO rapidly oxidises to CO<sub>2</sub> so close to the particle surface that it gives its heat of combustion to the particle [166–170]. Therefore the CO/CO<sub>2</sub> ratio at high temperatures should be one or even smaller than one as reported by several measurements [159, 163, 171]. Only the correlations of Linjewile and Agarwal [159, 160] as well as of Evans and Emmons [163] are able to predict the acceptable CO/CO<sub>2</sub> ratio at high temperatures.

## 2.4 Thermally thin and thick particles

Based on the Biot number,  $Bi$ , which depends on a particle length scale, the external heat transfer coefficient, and the particle thermal conductivity, particles can be classified as thermally thin or thick, the later meeting the criterion  $Bi > 0.1$ . The Biot number is an index characterising the ratio between the resistance to conductive heat transfer inside the particle and the resistance to convective heat transfer across the fluid boundary layer. This ratio makes it possible to estimate whether the temperature gradient inside the particle is negligible or not, when the surface of the particle is exposed to the external heat transfer rate.

In the case of thermally thin particles, no gradients are present inside the particle and the thermal conversion stages take place more or less uniformly throughout the particle and sequentially as the temperature of the particle increases. In contrast, thermally thick particles experience large internal temperature gradients causing intra-particle transport processes. Accordingly, the thermal conversion sub-processes can take place simultaneously in different parts of the particle. The reaction fronts of the sub-processes move progressively from the particle outer surface (higher temperature) towards the centre of the particle (lower temperature). Consequently, different zones with different physical properties and temperatures appear within a thermally thick particle. For biomass combustion systems the particle Biot number is considerably higher than 0.1. Hence modelling the combustion of biomass particles based on

thermally thick particle assumption is inevitable, otherwise it leads to large modelling errors.

## 2.5 Layer model

The layer model is proposed to account for intra-particle transport processes and simultaneous sub-processes during the combustion of thermally thick biomass particles. The layer model treats the typical particle shapes (spheres and finite cylinders) of biomass in one dimension. The description of the particle thermal conversion using one-dimensional models is an usual simplification assumption, applied to reduce model complexity and calculation time [17, 25, 32, 34–36, 130, 172, 173]. The validity of this assumption has already been addressed by Ha and Choi [174]. In order to apply the one-dimensional governing equations for the finite cylinder geometry, the Thunman approach [25] was selected to discretise the particles. This approach assumes that the particle boundary conditions are homogeneous and that every point at a certain axial or radial distance from the particle surface has the same temperature and conversion state, see Figure 2.5.

In the layer model the particle is divided into four layers, corresponding to the fuel conversion stages: wet fuel, dry fuel, char, and ash. Consequently, the boundaries between the layers are related to the conversion sub-processes drying, pyrolysis, and char burnout fronts, as illustrated in Figure 2.5. The thickness of each layer is determined by the amount of wet fuel, dry fuel, char and ash in each time step, and assumes a constant density for each layer. As the conversion proceeds, the mass of each layer changes and boundaries move towards the particle centre. Therefore particle size and density vary during thermal conversion.

The conservation equation of thermal energy is [131]:

$$\frac{\partial}{\partial t} \rho H = -\nabla \cdot \rho \mathbf{v} H - \nabla \cdot \mathbf{q} \quad (2.18)$$

where the left-hand side of the equation is the accumulation rate of enthalpy per unit volume, the first term on the right-hand side is the rate of enthalpy change by advection per unit volume and the second term represents the contribution of the conductive heat transfer per unit volume. The advection term in this equation can be interpreted as the energy transfer in/from each layer when the boundaries move towards the centre of the particle.

The internal energy equation is discretised into four layers by setting a temperature for each boundary and layer. In order to simplify the equation, the thermal energy per unit volume is replaced by the thermal energy of each layer, therefore the thermal energy balance of layer  $i$  is:

$$\begin{aligned} \frac{\partial}{\partial t} \sum_c m_{c,L_i} H_{c,L_i} = & \sum_{c=in} \dot{m}_{c,B(i-1)} H_{c,B(i-1)} - \sum_{c=out} \dot{m}_{c,B_i} H_{c,B_i} \\ & + k_{L_i} \Delta x_{0,L_i} (T_{B(i-1)} - T_{L_i}) - k_{L_i} \Delta x_{1,L_i} (T_{L_i} - T_{B_i}) \quad (2.19) \end{aligned}$$

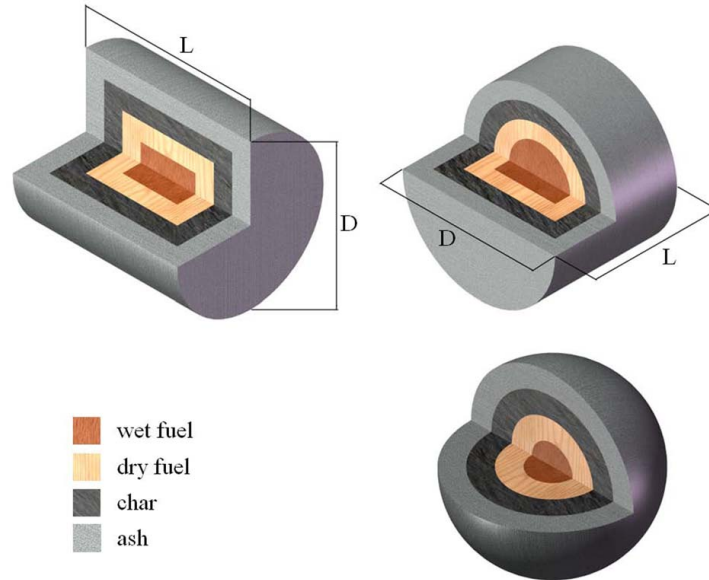


Figure 2.5: Discretisation scheme for spherical and cylindrical particles with length ( $L$ ) longer and shorter than the diameter ( $D$ )

where  $\sum_c$  is the summation over all components (solid and gas) of the layer,  $\sum_{c=in}$  represents the summation over all components which enter the layer from the previous boundary and  $\sum_{c=out}$  is the summation over all components which leave the layer to the next boundary.  $m_{c,L_i}$  and  $H_{c,L_i}$  are the mass and specific enthalpy of each component presents in the layer  $L_i$ , respectively.  $\dot{m}_{c,B_i}$  and  $H_{c,B_i}$  are the mass flow rate and specific enthalpy of each component at the boundary  $B_i$ , respectively.  $k_{L_i}$  is the thermal conductivity of the layer  $L_i$ .  $\Delta x_{0,L_i}$  is the ratio of the area of the boundary  $B_{i-1}$  to half of the layer  $L_i$  thickness.  $\Delta x_{1,L_i}$  is the ratio of the area of the boundary  $B_i$  to half of the layer  $L_i$  thickness. Finally,  $T_{L_i}$  and  $T_{B_i}$  are the temperature at the centre of the layer  $L_i$  and the temperature of the boundary  $B_i$ , respectively.

The conservation of mass of each layer reads:

$$\frac{\partial}{\partial t} \sum_c m_{c,L_i} = \sum_{c=in} \dot{m}_{c,B_{i-1}} - \sum_{c=out} \dot{m}_{c,B_i} \quad (2.20)$$

substituting Equation 2.20 and  $dH = c_p dT$  into Equation 2.19:

$$\begin{aligned} \sum_c (m_{c,L_i} c_{p,c}) \frac{dT_{L_i}}{dt} &= \sum_{c=in} [\dot{m}_{c,B_{i-1}} (H_{c,B_{i-1}} - H_{c,L_i})] \\ &\quad - \sum_{c=out} [\dot{m}_{c,B_i} (H_{c,L_i} - H_{c,B_i})] \\ &\quad + k_{L_i} \Delta x_{0,L_i} (T_{B_{i-1}} - T_{L_i}) - k_{L_i} \Delta x_{1,L_i} (T_{L_i} - T_{B_i}) \end{aligned} \quad (2.21)$$

The enthalpy of each component at every layer or boundary is calculated by:

$$H_c(T) = \Delta H_{f,c}^\circ + \int_{T_{ref}}^T c_{p,c} dT \quad (2.22)$$



The boundary temperatures are calculated by writing the energy balance for each boundary:

$$\begin{aligned} k_{L_i} \Delta x_{1,L_i} (T_{L_i} - T_{B_i}) - k_{L_{(i+1)}} \Delta x_{0,L_{(i+1)}} (T_{B_i} - T_{L_{(i+1)}}) \\ = \sum_{c=in} \dot{m}_{c,B_i} H_{c,B_i} - \sum_{c=out} \dot{m}_{c,B_i} H_{c,B_i} \end{aligned} \quad (2.23)$$

Since the reactions are assigned to the boundaries, the components which enter a certain boundary may be different from the components which leave that boundary. Hence, the right hand side of Equation 2.23 represents the enthalpy difference between products and reactants of the reactions, i.e. the enthalpies of reactions. The reaction rates,  $\dot{m}_r$ , and stoichiometric coefficients of reactions,  $\eta_r$ , determine the mass flow rate of each component from one layer over the boundary into the next layer, which implicitly determines the velocity of each boundary towards the particle centre:

$$\dot{m}_{c,B_i} = \sum_r \dot{m}_r \eta_{r,c} \quad (2.24)$$

where  $\sum_r$  is the summation over all reactions of boundary  $i$ .

A detailed description of the layer model and a summary of all reactions and correlations used in the model as well as its validation simulations are presented in *Paper I*.

## Chapter 3

# Hydrodynamics of the packed bed

The main problems encountered in modelling biomass packed bed combustion are the thermal conversion of the biomass particles and the hydrodynamics of the gas-solid multiphase flow. The former has already been addressed in the previous chapter. In biomass packed bed combustion systems the gas and solid phase flow fields are strongly interlinked. A suitable model for biomass packed bed combustion must therefore be capable of considering the interaction between particle movement and gas flow. A variety of simulation methods can be used for dense gas-solid multiphase flows (granular flows). These can generally be classified into two approaches: the Lagrangian approach, where the motion of each particle is defined by classical Newtonian mechanics, and the Eulerian approach or two-fluid model, based on the assumption that the gas and particulate phases form two inter-penetrating continua [175].

In this thesis, ANSYS FLUENT is used to simulate biomass packed bed furnaces. These two approaches are also available in ANSYS FLUENT for the numerical simulation of fluid-solid multiphase flows. A short description of each approach is given in the following sections.

## 3.1 Lagrangian approach

This approach treats the granular material as a collection of particles and each particle is simulated by applying Newton's laws of motion and followed in time. ANSYS FLUENT features two models based on the Lagrangian approach.

### 3.1.1 Discrete phase model

The discrete phase model (DPM) in ANSYS FLUENT follows the Lagrangian approach. The fluid phase is treated as a continuum by solving the mass and momentum conservation equations. The governing equation for particle tracking is derived by equating the particle inertia with the forces acting on the particle:

$$\frac{du_{p,i}}{dt} = \frac{1}{m_{p,i}} \sum F \quad (3.1)$$

where  $u_{p,i}$ ,  $m_{p,i}$ , and  $F$  are the velocity and mass of the  $i^{th}$  particle and any force exerted on the particle, respectively. The sum of forces depends on various factors such as drag, lift, gravity, buoyancy, etc. Usually one can make assumptions whether or not to include certain forces depending on the type of system to be modelled. The dispersed phase can exchange momentum, mass, and energy with the fluid phase. The interaction of phases is considered by tracking a number of representative particles through the calculated flow field.

The fundamental assumptions in this model are that the effect of solid phase volume is ignored in the continuous phase mass and momentum equations, and that the collision and friction forces can not be modelled in standard DPM. Consequently the displacement of fluid volume by the solid phase and the effect of particle-particle interactions are neglected. Therefore, the DPM model is valid if the dispersed phase occupies a low volume fraction (about  $< 10\%$ ), even though high mass loading is acceptable.

### 3.1.2 Discrete element method

The discrete element method (DEM) has been developed to overcome one of the standard DPM deficiencies - the calculation of the collision force. DEM is based on the molecular dynamics and is suitable for a high volume fraction of particles, where particle-particle interactions are important. Particle-particle collisions can be modelled by the soft sphere method [176] or hard sphere method [177]. A characteristic feature of the soft sphere method is the ability to handle multiple particle contacts which are of prime importance in modelling packed beds. In contrast, the hard sphere method is quasi-instantaneous and the particle interaction is based on binary interaction. The DEM model of ANSYS FLUENT is based on the soft sphere method.

One of the main aspects of computing the contact forces is to let the simulated particles overlap. This overlap can be seen as the displacement of a spring. The contact forces are thus computed using a relation similar to Hooke's law, in conjunction with a damper model for energy dissipation due to contact. The limiting parameter in the DEM is the number of particles. The calculation time is usually too long for industrial-scale systems.

## 3.2 Eulerian approach

The Eulerian approach assumes that the dispersed phase behaves as a fluid, hence this approach is also known as a two-fluid model (TFM). The continuity and momentum equations, with jump conditions for phase interfaces, are solved for both gas and dispersed phases. An averaging approach is used where equations are derived by space, time or the ensemble averaging of the local instantaneous balances of each of the phases. Basically a Reynolds-Averaging Navier-Stokes approach is applied [178]. As the variables are averaged, it is assumed that the point variables are averaged over a region that is larger than the particle spacing but smaller than the flow domain. Hence, a new variable is incorporated: the volume fraction of

the phases which is assumed to be a continuous function of space and time:

$$\sum_i \alpha_i = 1 \quad (3.2)$$

For simplicity only two phases will be considered: a solid phase  $s$  and a gas phase  $g$ :

$$\alpha_s + \alpha_g = 1 \quad (3.3)$$

The mass conservation equations for the gas and solid phases are:

$$\frac{\partial}{\partial t}(\alpha_g \rho_g) + \nabla \cdot (\alpha_g \rho_g \vec{v}_g) = \dot{m}_g \quad (3.4)$$

$$\frac{\partial}{\partial t}(\alpha_s \rho_s) + \nabla \cdot (\alpha_s \rho_s \vec{v}_s) = \dot{m}_s \quad (3.5)$$

where  $\rho$  denotes the bulk density,  $\vec{v}$  the velocity vector. The first term on the left-hand side of Equations 3.4 and 3.5 is the rate of mass accumulation per unit volume, and the second term is the net rate of convective mass flux.  $\dot{m}$  represents the interphase mass transfer rate.

The momentum equations have the following forms:

$$\frac{\partial}{\partial t}(\alpha_g \rho_g \vec{v}_g) + \nabla \cdot (\alpha_g \rho_g \vec{v}_g \vec{v}_g) = -\alpha_g \nabla p_g + \nabla \cdot \bar{\tau}_g + \alpha_g \rho_g \vec{g} - \vec{F} \quad (3.6)$$

$$\frac{\partial}{\partial t}(\alpha_s \rho_s \vec{v}_s) + \nabla \cdot (\alpha_s \rho_s \vec{v}_s \vec{v}_s) = -\alpha_s \nabla p_g + \nabla \cdot \bar{\tau}_s + \alpha_s \rho_s \vec{g} + \vec{F} \quad (3.7)$$

The first term on the left-hand side of both equations is the rate of increase of momentum per unit volume, the second is the rate of momentum variation due to convection per unit volume.  $\vec{F}$  is the interaction force (momentum exchange) between the phases per unit volume and  $\vec{g}$  is the specific gravity force.  $\bar{\tau}$  is the stress tensor and  $p$  the pressure.

The constitutive equations are required to close the momentum equations. For the gas phase the stress tensor takes the form of a Newtonian fluid:

$$\bar{\tau}_g = \alpha_g \mu_g \left[ (\nabla \vec{v}_g + \nabla \vec{v}_g^T) - \frac{2}{3} \nabla \cdot \vec{v}_g \bar{I} \right] \quad (3.8)$$

where  $\mu_g$  is the gas viscosity,  $\bar{I}$  is the identity matrix, and the second term on the right-hand side represents the effect of compressibility.

For the viscous or rapidly shearing regime of granular flows, in which stresses arise because of the collisional or translational transfer of momentum, the stress tensor of the solid phase is written as:

$$\bar{\tau}_s = -p_s \bar{I} + \alpha_s \mu_s (\nabla \vec{v}_s + \nabla \vec{v}_s^T) + \alpha_s \left( \lambda_s - \frac{2}{3} \mu_s \right) \nabla \cdot \vec{v}_s \bar{I} \quad (3.9)$$

where  $\mu_s$  is the solid shear viscosity and  $\lambda_s$  is the solid bulk viscosity.  $p_s$  is the solid pressure:

$$p_s = \alpha_s \rho_s T_G + 2\rho_s (1 + e) \alpha_s^2 g_0 T_G \quad (3.10)$$

where  $T_G$  is the granular temperature,  $e$  is the particle-particle restitution coefficient and  $g_0$  is the radial distribution function. The first term on the right-hand side is the kinetic term and the second term represents particle collisions. The granular temperature is associated with the kinetic energy of the fluctuating particle motion and is introduced as:

$$T_G = \frac{1}{3} \overline{u_s'^2} \quad (3.11)$$

where  $\vec{u}_s'$  is the deviation of particle instantaneous velocity from mean particle velocity, like the Reynolds decomposition in turbulence modelling. In the derivation of Equation 3.11 it is assumed that deviations of particle velocity from mean velocity in all spatial directions are equal. It can be shown that the conservation equation for particle kinetic fluctuation energy reads [178, 179]:

$$\frac{\partial}{\partial t} \left( \frac{3}{2} \alpha_s \rho_s T_G \right) + \nabla \cdot \left( \frac{3}{2} \alpha_s \rho_s T_G \vec{v}_s \right) = \nabla \cdot (\kappa \nabla T_G) + \bar{\tau}_s : \nabla \vec{v}_s - J - 3\gamma T_G \quad (3.12)$$

where the first term on the right-hand side represents the diffusion transport of granular temperature, the second term is the production of granular temperature by shear, the third term is dissipation due to inelastic collisions,

and the last term is dissipation by interaction with the gas phase.  $\gamma$  is the interphase momentum exchange coefficient and is differently defined in the various momentum exchange coefficient models [180].

According to Gidaspow et. al. [181] the diffusion coefficient for kinetic fluctuation energy is:

$$\kappa = \frac{150d_s\rho_s\sqrt{\pi T_G}}{384(1+e)g_0} \left[ 1 + \frac{6}{5}\alpha_s g_0(1+e) \right]^2 + 2d_s\rho_s\alpha_s^2 g_0(1+e)\sqrt{\frac{T_G}{\pi}} \quad (3.13)$$

and collisional kinetic energy dissipation is represented by the expression derived by Lun et. al. [179]:

$$J = \frac{12}{d_s\sqrt{\pi}}\rho_s\alpha_s^2(1-e^2)g_0T_G^{3/2} \quad (3.14)$$

where the particles are assumed to be smooth hard spheres of diameter  $d_s$  and only binary interactions (characterised by a single parameter, namely the coefficient of normal restitution,  $e$ ) are considered.

The radial distribution function,  $g_0$ , is a correction factor that modifies the probability of collisions between particles when the volume fraction of the solid phase increases up to its maximum value. A correlation for  $g_0$  which has been used successfully is [182, 183]:

$$g_0 = \frac{1}{1 - (\alpha_s/\alpha_{s,max})^{1/3}} \quad (3.15)$$

where  $\alpha_{s,max}$  is the maximum solid volume fraction or packing limit.

In TFM models all the particles are assumed to be identical, specified by their mean diameter and density. Therefore handling a poly-disperse system, i.e. a system with different particle sizes, requires several solid phases corresponding to the number of particle diameter classes. Hjertager reported a quadratic increase of computational effort with the number of phases [184].

The modelling of particle-particle collisions using this approach is rather complicated compared with the DEM models. It has been implemented in the

solid phase momentum equation by the viscosity and normal stress tensor of the solid phase, while in DEM models the particle trajectories are calculated using the Newton's laws. However, TFM models are computationally less expensive than the DEM models. The TFM's ability to simulate granular systems has been proven by numerous applications, see [185] and its references.

### 3.3 Approach followed

The commercial CFD software ANSYS FLUENT has been used in the present work to simulate the hydrodynamics of the packed bed granular flow. The Euler-Granular model was selected from the gas-solid multiphase models available in ANSYS FLUENT because it is based on the kinetic theory of granular flows and allows the consideration of inter-particle interactions, which are of key importance in modelling packed beds. This model has been successfully used for predicting the hydrodynamic behaviour of granular flows [186–189]. However, when using the Euler-granular model one cannot apply the layer model to simulate the thermal conversion of the particles.

On the other hand, the discrete phase model (DPM) used by ANSYS FLUENT is not suitable for particle tracking under packed bed conditions because it ignores the particle-particle collisions. However, its multi-component particle model provides the ability to link the layer model to ANSYS FLUENT. In order to combine the Euler-granular model for the hydrodynamics of packed beds with the layer model for the thermal conversion of the biomass particles the following innovative approach is used: a non-reacting simulation based on the Euler-granular model is performed and the simulated velocity field of the granular phase is stored as a user defined memory (UDM). Then these data are used to prescribe the particle velocities in the DPM simulation by means of a user defined function (UDF). The results of this approach are presented in *Paper III* and *Paper IV*.



# Chapter 4

## Heat transfer in the packed bed

In general, for a packed bed in which gas, particles and walls all have different temperatures, the three heat transport mechanisms, convection, conduction and radiation, are all involved. Altogether, there are 9 possible ways to heat or cool a particle in a packed bed, which are shown schematically in Figure 4.1 [116].

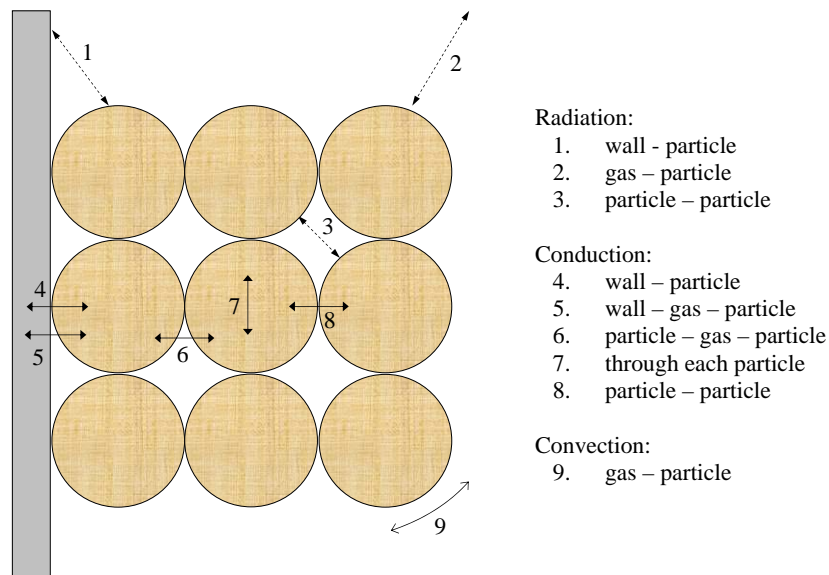


Figure 4.1: Scheme of heat transfer processes for particles in a packed bed

The mathematical description of heat transfer in the packed bed requires some assumptions and simplifications due to the complexity and irregular arrangement of the packing. As radiation is the dominant mechanism of heat transfer in combustion systems, all the radiation possibilities are considered. It is known that the conduction mechanism is important if the temperature in the packed bed is below 450 K [190]. Therefore, only the conduction inside each particle is considered, as already explained in the layer model section 2.5. In addition, gas-particle convective heat transfer is also considered in the calculations. In the following sections the convection and radiation mechanisms are explained.

## 4.1 Convective heat transfer

In the literature a variety of experimental and theoretical investigations have been published addressing the problem of convective heat transfer in a packed bed. Most of the articles describe a correlation of the mean Nusselt number as a function of the mean Reynolds number.

Achenbach [191] investigates the heat transport in fixed beds under conditions where radiant heat transfer can be neglected. He derived a correlation for the average Nusselt number by measuring the cooling of an electrically heated single sphere buried in the unheated packing. Inaba et al. [192, 193] measured the temperature of 12 test particles embedded in horizontal cylindrical beds of glass, iron and aluminum spheres to derive a correlation for the local heat transfer coefficient. Khan et al. [194] determined the heat transport coefficient by drying solid beds of porous particles with overheated steam. Bird et al. [131] derived a correlation by applying the Reynolds analogy between heat transfer and fluid friction, i.e. the Colburn factor, and also considered the effect of particle shape. Gupta et al. [195] summarised several sets of experimental data obtained by other authors for packed and fluidised beds and proposed a correlation based on these data. In his work Resnik [196] calculated the Colburn factor and the Nusselt number for a bed of catalytic spheres through which vapour passes. Wakao

and Kaguei [197] introduced the concept of axial fluid thermal dispersion, corrected the published heat transfer data for packed beds, and proposed an equation to correlate these re-evaluated experimental data. Eckert and Drake [198] suggested another equation for heat transfer in packed beds with Reynolds numbers larger than 500. Collier et al. [199] measured the temperature of a preheated phosphor-bronze sphere added to a bed of larger particles, through which air at room temperature was passed. The cooling of the bronze sphere enabled the heat transfer coefficient to be measured. Denton [200] derived an equation for the Nusselt number by measuring the rate of heat transfer from a heated sphere to a packed bed of spheres of equal size when the heated sphere and surrounding bed reached a steady state. Scott et al. [201] experimentally investigated the heat transfer to spherical particles immersed in fixed and fluidised beds and introduced a correlation for the Nusselt number in a certain range of the Reynolds number. Table 4.1 summarises the correlations proposed by the mentioned studies and their ranges of Reynolds number.

A successful semi-empirical method of calculating the heat transfer rate inside the beds was introduced by [202]. This method is based on the idea that heat transfer from arbitrary particles can be predicted by applying the equations for a flat plate using a suitable length scale and velocity. This characteristic length scale is the distance travelled by a fluid particle on its way along the

Table 4.1: The convective heat transfer correlations for packed beds

$Nu = 0.72PrRe^{0.7}$		[200]
$Nu = 0.922Pr^{1/3}Re^{0.66}$	$10 < Re$	[196]
$Nu = 0.8Pr^{1/3}Re^{0.7}$	$500 < Re$	[198]
$Nu = 0.61Pr^{1/3}Re^{0.59}(6(1 - \epsilon))^{0.41}f^{1.41}$	$f=1$ for sphere	[131]
$Nu = Pr^{1/3}/\epsilon(2.876 + 0.3023Re^{0.65})$	$20 < Re < 10^4$	[195]
$Nu = 2 + 1.1Pr^{1/3}Re^{0.6}$	$15 < Re < 8500$	[197]
$Nu = 3.15(dp/D)^{0.761}Re^{0.658}$	$80 < Re$ , D: bed diameter	[192]
$Nu = 1.8Pr^{1/3}Re^{0.585}$	$250 < Re < 780$	[194]
$Nu = ((1.18Re^{0.58})^4 + (0.23Re^{0.75})^4)^{1/4}$	$1 < Re < 10^4$	[191]
$Nu = 2 + 0.9Re^{0.62}$	$100 < Re < 680$	[199]
$Nu = 2 + 1.0 * Re^{0.6}$	$100 < Re < 830$	[201]

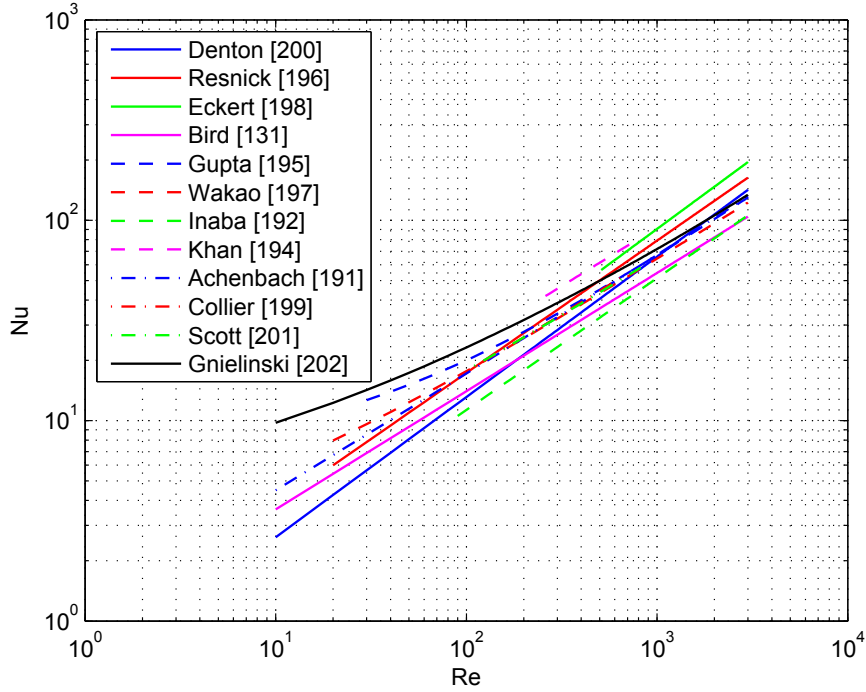


Figure 4.2: The Nusselt number as a function of the Reynolds number for packed beds, data from Table 4.1 and Equation 4.4 (Gnielinski [202])

body. The characteristic velocity is the mean velocity of the interstitial fluid. Both characteristic quantities are introduced into the asymptotic solutions for laminar and turbulent heat transfer:

$$Nu_{lam} = 0.664Pr^{1/3}(Re/\epsilon)^{1/2} \quad (4.1)$$

$$Nu_{turb} = \frac{0.037Pr(Re/\epsilon)^{0.8}}{1 + 2.443(Pr^{2/3} - 1)(Re/\epsilon)^{-0.1}} \quad (4.2)$$

The combination of the two asymptotic solutions yields the heat transfer from a single sphere:

$$Nu_p = 2 + (Nu_{lam}^2 + Nu_{turb}^2)^{1/2} \quad (4.3)$$

The 2 in this equation is the asymptotic solution for  $Re \rightarrow 0$ .

$Nu_p$  can now be used to calculate the mean Nusselt number for the packed beds;

$$Nu = f(\epsilon)Nu_p \quad (4.4)$$

where  $f(\epsilon)$  is an empirical factor which depends on the porosity of the bed:

$$f(\epsilon) = 1 + 1.5(1 - \epsilon) \quad (4.5)$$

The comparison between the correlations in Table 4.1 and Equation 4.4 are shown in Figure 4.2. The empirical correlations from the literature depict a scattering of the results due to non-uniformities in the void fraction distributions across the bed which leads to cold bypass flows as reported by [195, 202, 203]. However, the important message of Figure 4.2 is that Equation 4.4 plausibly correlates the mean Nusselt number to the Reynolds number in packed beds. Therefore, this correlation is used in this thesis to model the convective heat transfer in packed beds.

The convection model is applied as a sub-model to simulate a packed bed biomass combustion in *Paper V*.

## 4.2 Radiative heat transfer

Each particle in the packed bed emits radiation, which is absorbed by neighbouring particles. The influence of the neighbouring particles on radiative heat transfer is considered by changing the boundary condition on the particle surface:

$$\mathbf{q}_{rad,i} = \sum_{j=1}^N \epsilon \sigma F_{ij} (T_j^4 - T_i^4) \quad (4.6)$$

where  $\mathbf{q}_{rad,i}$  is the radiation heat flux from the neighbouring particles to particle  $i$ .  $\epsilon$ ,  $\sigma$ ,  $N$  and  $T$  are the particle emissivity, the Stefan-Boltzmann constant, the number of particles and the particle surface temperature,

respectively.  $F_{ij}$  is the view factor between particles  $i$  and  $j$ .

It is difficult, however, to implement Equation 4.6 in a simulation, as it requires a summation over all particles for each particle and the calculation of the view factor for each pair of particles. Therefore an appropriate spherical control volume  $\vartheta$  is defined around each target particle, see Figure 4.3. It is assumed that the target particle exchanges radiation with its surrounding control volume:

$$\mathbf{q}_{rad,i} = \epsilon\sigma F_{i\vartheta}(T_{\vartheta,i}^4 - T_i^4) \quad (4.7)$$

As the target particle is enclosed by the radiation control volume,  $F_{i\vartheta} = 1$ . The parameter  $T_{\vartheta,i}$  is the average temperature of particles and gas phase in the radiation control volume  $\vartheta$  given by [204]:

$$T_{\vartheta,i} = \epsilon T_{g,\vartheta} + (1 - \epsilon) \frac{1}{N_{\vartheta}} \sum_{j=1;\neq i}^{N_{\vartheta}} T_j \quad (4.8)$$

where  $\epsilon$ ,  $T_{g,\vartheta}$  and  $N_{\vartheta}$  are the bed porosity, the gas temperature and the number of particles located in the volume  $\vartheta$ , respectively. If the target

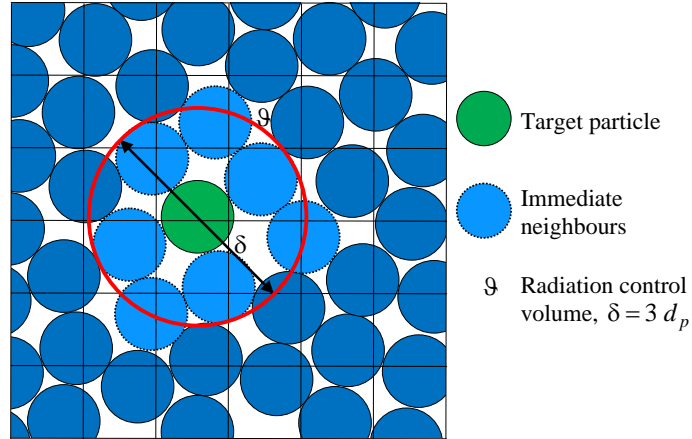


Figure 4.3: Radiation control volume and neighbouring particles in the packed bed radiation model

particle is close to a wall, some CFD cells in the radiation control volume are adjacent to the wall. Including the effect of walls on the radiation to the target particle,  $T_{\vartheta,i}$  turns out as:

$$T_{\vartheta,i} = (1 - \xi) \left[ \epsilon T_{g,\vartheta} + (1 - \epsilon) \frac{1}{N_{\vartheta}} \sum_{j=1; \neq i}^{N_{\vartheta}} T_j \right] + \xi \frac{1}{M_{\vartheta}} \sum_{j=1}^{M_{\vartheta}} T_{wall,j} \quad (4.9)$$

where  $M_{\vartheta}$  and  $T_{wall}$  are the number of cells in the radiation control volume adjacent to the wall and the wall temperature, respectively. The parameter  $\xi$  is a constant which represents the weight of wall temperatures on  $T_{\vartheta,i}$ . In this study  $\xi$  is set to 0.5 to achieve a plausible horizontal temperature profile in the packed bed near the walls.

Thermal radiation from the freeboard above the packed bed is one of the most important mechanisms of grate firing systems and is responsible for initiating the thermo-chemical processes. The average radiation temperature for the particles located at the top of the packed bed is calculated by:

$$T_{\vartheta,i} = 0.5 \left( \frac{\mathbf{q}_{rad}}{\sigma} \right)^{1/4} + 0.5 \left[ \epsilon T_{g,\vartheta} + (1 - \epsilon) \frac{1}{N_{\vartheta}} \sum_{j=1; \neq i}^{N_{\vartheta}} T_j \right] \quad (4.10)$$

where  $\mathbf{q}_{rad}$  is the radiation heat flux from the freeboard. It is calculated by simulating the gas phase combustion with ANSYS FLUENT.

The radiation model is applied as a sub-model to simulate a packed bed biomass combustion in *Paper V*.

# Chapter 5

## Homogeneous reactions

Biomass, has a higher volatile matter content compared to coal. The volatiles leave through the pores of the particle and mix with the surrounding air. Where this is an oxidising environment and the temperature is high enough the volatiles further react to  $\text{CO}_2$  and  $\text{H}_2\text{O}$ . Combustion of volatiles is an important process in packed bed biomass combustion, because it produces the energy required for heating, drying and pyrolysis of the fuel bed.

### 5.1 Reaction mechanisms

Thermodynamics determines the ideal end state of a reaction process. It does not tell us, however, how fast the reaction proceeds and whether, under a particular reaction condition, the reaction can proceed to the equilibrium state. Finding answers to these questions is the role of chemical kinetics.

The global reactions describe an overall process by which reactants are converted to anticipated products at the end of the process. They do not describe the actual physical process. Physically a global reaction is a very unlikely event, because it neglects the intermediate products and reactions. The elementary reactions are the reactions that actually take place. Unlike global reactions, all elementary reactions are reversible.

The detailed explanation at the molecular level of how a reaction proceeds is called the reaction mechanism. In general, a chemical reaction mechanism



is a collection of elementary reactions that describes the whole process, from the beginning to the end. The end state as determined by the reaction mechanism must be consistent with thermodynamic predictions for the end state of an overall reaction process.

In previous studies only global reactions have been considered, which may not be sufficiently accurate for a broad range of operating conditions. In this study detailed mechanisms are used for the homogeneous reactions. A famous comprehensive mechanism, GRI-Mech 2.11, is used in this study [205]. It is a compilation of 277 elementary chemical reactions and associated rate coefficient expressions and thermochemical parameters for the 49 species involved in the mechanism. GRI-Mech has been optimised for methane and natural gas. It includes reactions that are involved in the combustion of other hydrocarbon constituents of natural gas (e.g. ethane, propane, methanol, ethylene, and acetylene). Additionally, a reduced version of the GRI mechanism, DRM22 [206], is applied in order to evaluate the results and applicability of the reduced mechanism. It is a 22-species reaction set with 104 elementary reactions. The relatively large number of reactions involved in these mechanisms may be a limitation for their applicability for simulations of industrial biomass grate furnaces. Therefore the C-H-O subset of the skeletal Kilpinen97 mechanism [207, 208] is also applied in order to evaluate its results compared to the more detailed mechanisms. It is a mechanism with 12 species and 25 reactions.

Many different gas species are released during biomass pyrolysis. In order to use the detailed reaction mechanisms, the released gas species in the pyrolysis model must be compatible with the list of species considered in the mechanisms. The next section addresses the composition of volatiles.

## 5.2 Composition of volatiles

The volatile yield from pyrolysis includes a complex mixture which has been found to include several hydrocarbons. Numerous factors affect the composition of the pyrolysis products: temperature, heating rate, residence

time, reactor geometry, pressure as well as the chemical and physical properties of biomass are the chief parameters. Several studies have investigated the composition of the pyrolysis products. The most commonly detected gas species are CO, CO<sub>2</sub>, H<sub>2</sub>, H<sub>2</sub>O, CH<sub>4</sub>, C<sub>x</sub>H<sub>y</sub> (light hydrocarbons), CH<sub>m</sub>O<sub>n</sub> (tar) and other trace compounds. The yields of permanent gases as a function of pyrolysis temperature are provided in Figure 5.1, based on experimental data collected from [57–76, 81–88]. It contains data from various biomass and reactor types as well as experimental conditions. It gives an overview of measured product compositions from several woody biomass sources. Variations in the detected yields of individual species are often of the same order as the size of the detected fractions. This is due to a combination of uncertainties in the measurement methods, variations in the fuel composition and experimental conditions. It is worth pointing

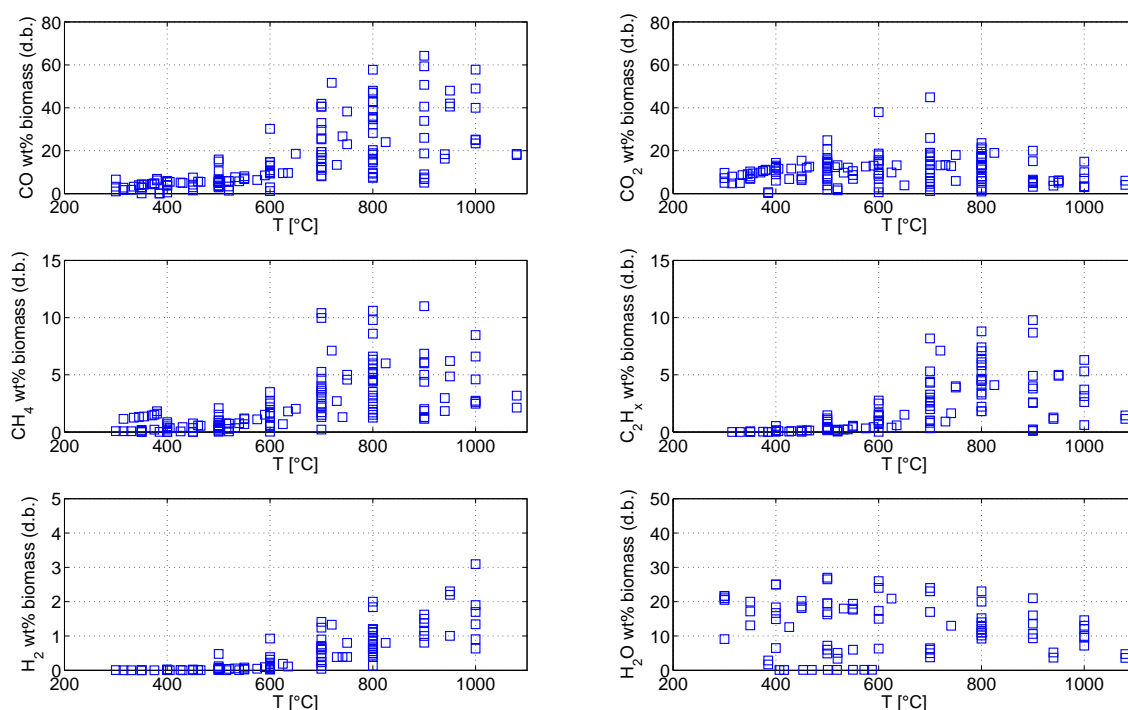


Figure 5.1: The yields of permanent gases as functions of pyrolysis temperature, data from [57–76, 81–88].

out that the reported data on product distribution is sometimes incomplete (for example, some investigations did not report the water yield). Hence, in Figure 5.1 the points in a given subplot sometimes do not have corresponding points in the other subplots.

The permanent gases consist mainly of CO, CO<sub>2</sub>, H<sub>2</sub>O, with lower amounts of CH<sub>4</sub>, C<sub>2</sub> hydrocarbons and H<sub>2</sub>. The yields of CO, CH<sub>4</sub>, C<sub>2</sub>H<sub>x</sub> and H<sub>2</sub> show an exponential increase in the temperature range of 300-1000°C. The CO<sub>2</sub> and H<sub>2</sub>O trends are different; they display almost constant values over the whole temperature range investigated. However, there is a slight decrease in the yields of CO<sub>2</sub> and H<sub>2</sub>O with temperature, starting from 800°C. It suggests that pyrolysis temperature has a minor effect on the yields of CO<sub>2</sub> and H<sub>2</sub>O.

At low temperatures, when the secondary reactions of volatiles are negligible, most of the permanent gases result from degradation of the solid biomass. At this temperature range, CO, CO<sub>2</sub> and H<sub>2</sub>O are the main permanent gas species with small quantities of CH<sub>4</sub>. Moreover, the collected literature data show a weak relationship between temperature and the production of gases within this temperature range.

As temperature increases, the yields of the combustible gases (CO, CH<sub>4</sub>, C<sub>2</sub>H<sub>x</sub> and H<sub>2</sub>) become a strong function of temperature. The increase of CO, CH<sub>4</sub> and C<sub>2</sub>H<sub>x</sub> is attributed to the decrease of the tar yields (see Figure 2.2). It is a clear indication that they are the major secondary products resulting from the tar conversions. This behaviour is in accordance with dedicated experiments [87–89, 92], in which it was observed that carbon monoxide is quantitatively the most important product from the homogeneous tar conversion, with over two-thirds of the tar lost at high temperatures. Corresponding methane and C<sub>2</sub> hydrocarbons each accounted for about 10 wt% of the converted tar.

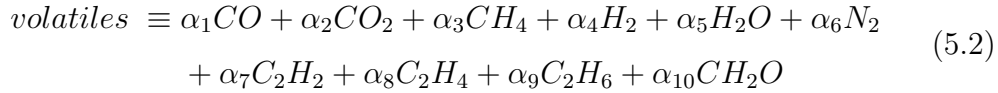
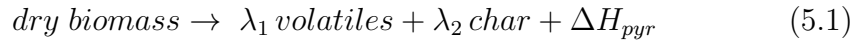
Since the volatile species must be compatible with the list of species considered by the kinetic mechanism, intersection species between each mechanism and the most commonly reported gas components in the literature

for biomass pyrolysis [57–76, 81–88] are considered in the pyrolysis model. The pyrolysis product compositions considered in the simulations with each mechanism are listed in Table 5.1.

Table 5.1: The volatile compositions considered in the simulations with different mechanisms.

GRI2.11:	CO	CO <sub>2</sub>	CH <sub>4</sub>	H <sub>2</sub>	H <sub>2</sub> O	N <sub>2</sub>	C <sub>2</sub> H <sub>2</sub>	C <sub>2</sub> H <sub>4</sub>	C <sub>2</sub> H <sub>6</sub>	CH <sub>2</sub> O
DRM22:	CO	CO <sub>2</sub>	CH <sub>4</sub>	H <sub>2</sub>	H <sub>2</sub> O	N <sub>2</sub>	C <sub>2</sub> H <sub>2</sub>	C <sub>2</sub> H <sub>4</sub>	C <sub>2</sub> H <sub>6</sub>	CH <sub>2</sub> O
Kilpinen97:	CO	CO <sub>2</sub>	CH <sub>4</sub>	H <sub>2</sub>	H <sub>2</sub> O	N <sub>2</sub>				

The pyrolysis reaction in the particle model turns out as:



Since there is no  $\text{C}_x\text{H}_y$  and  $\text{CH}_m\text{O}_n$  in the Kilpinen97 mechanism, it was not possible to consider them as pyrolysis products in the simulations with this mechanism. Therefore  $\alpha_7$  to  $\alpha_{10}$  for this case would be zero.

It is worth noting that the tars formed in the primary pyrolysis reaction are assumed to be fully converted into its main secondary products, e.g. CO, C<sub>2</sub>H<sub>2</sub>, C<sub>2</sub>H<sub>4</sub>. This is because the tar composition and chemical formula, as well as the rate of its secondary conversion, are unknown. However, it may affect the temperature and species profiles released from fuel beds. This assumption is plausible for large particles in packed bed conditions because it is known that tar is very reactive when in contact with a hot char layer and easily breaks down [53, 92, 93]. It is reported that a fraction amounting to as much as 35 wt% of the tar released during pyrolysis undergoes rapid conversion (residence time less than 2.5 ms) in the presence of fresh wood pyrolysis char [57, 59, 92]. Moreover, experiments on the homogeneous tar thermal cracking reactions indicated that these reactions are significant at temperatures above 500°C, even for a residence time of less than 0.2 s and they exhibit a strong increase with temperature [88, 93]. Morf et al. [89]

showed that a tar conversion rate of 88 wt% can be achieved at 990°C and a residence time of 0.12 s.

There are ten unknowns for the GRI2.11 and DRM22 mechanisms and six unknowns for the Kilpinen97 mechanism,  $\alpha_i$ , in Equation 5.2. The next section explains how they are determined.

### 5.2.1 Conservation of elements and enthalpy

The volatiles on the left hand side of Equation 5.2 can be expressed as  $CH_aO_bN_c$  and a, b, and c are determined from the fuel ultimate and proximate analyses. Char and volatile yields in wt %,  $\lambda_1$  and  $\lambda_2$ , on the right hand side of Equation 5.1 are determined from the biomass proximate analysis. Elemental balances for C, H, O and N provide four equations:

$$C : \quad \alpha_1 + \alpha_2 + \alpha_3 + 2\alpha_7 + 2\alpha_8 + 2\alpha_9 + \alpha_{10} = 1 \quad (5.3)$$

$$H : \quad 4\alpha_3 + 2\alpha_4 + 2\alpha_5 + 2\alpha_7 + 4\alpha_8 + 6\alpha_9 + 2\alpha_{10} = a \quad (5.4)$$

$$O : \quad \alpha_1 + 2\alpha_2 + \alpha_5 + \alpha_{10} = b \quad (5.5)$$

$$N : \quad 2\alpha_6 = c \quad (5.6)$$

The conservation of enthalpy can be expressed in terms of the heat of combustion. For Equation 5.1 it turns out as:

$$\Delta H_{c,dry\ wood}^\circ = \lambda_1 \Delta H_{c,volatiles}^\circ + \lambda_2 \Delta H_{c,char}^\circ + \Delta H_{pyr} \quad (5.7)$$

$\Delta H_{c,dry\ wood}^\circ$  is the high heating value (HHV) of the fuel. There are measured values for HHV of different biomass fuels and it can also be calculated with proximate analysis by empirical correlations such as the Gaur correlation [209]. The heat of pyrolysis,  $\Delta H_{pyr}$ , varies greatly depending on the type of material. Values found in literature range from zero to  $\pm 0.5$  MJ/kg [26, 210, 211]. In this study it is assumed that the heat of pyrolysis is zero. The reason will be explained at the end of this section. Since it is assumed that the heat of char combustion is equal to that of carbon,

$\Delta H_{c,volatiles}^\circ$  can be calculated from Equation 5.7.

The conservation of enthalpy for Equation 5.2 is:

$$\begin{aligned} & \alpha_1 M_{CO} \Delta H_{c,CO}^\circ + \alpha_3 M_{CH_4} \Delta H_{c,CH_4}^\circ + \alpha_4 M_{H_2} \Delta H_{c,H_2}^\circ + \\ & \alpha_7 M_{C_2H_2} \Delta H_{c,C_2H_2}^\circ + \alpha_8 M_{C_2H_4} \Delta H_{c,C_2H_4}^\circ + \alpha_9 M_{C_2H_6} \Delta H_{c,C_2H_6}^\circ + \\ & \alpha_{10} M_{CH_2O} \Delta H_{c,CH_2O}^\circ = M_{volatiles} \Delta H_{c,volatiles}^\circ \end{aligned} \quad (5.8)$$

There are five equations, 5.3-5.6 and 5.8, and ten (GRI2.11 and DRM22) or six (Kilpinen97) unknowns,  $\alpha_i$ , which means that the system is underdetermined. Such a system has an infinite number of solutions. In order to obtain a meaningful result, some additional constraints are needed. These can be derived from measurements. The experimental data presented in Figure 5.1 [57–76, 81–88] are used to calculate the mass ratios of CO, CH<sub>4</sub>, H<sub>2</sub> and H<sub>2</sub>O to CO<sub>2</sub> and C<sub>2</sub>H<sub>x</sub> to CH<sub>4</sub>, as illustrated in Figures 5.2 and 5.3. The collected data are a compilation of measured values using various fuels, reactors and operating conditions (heating rate, particle size, etc.). According to Figures 5.2 and 5.3, the following constraints can be concluded:

$$0.1 < \frac{\alpha_1 M_{CO}}{\alpha_2 M_{CO_2}} < 10 \quad (5.9)$$

$$0.1 < \frac{\alpha_3 M_{CH_4}}{\alpha_2 M_{CO_2}} < 1 \quad (5.10)$$

$$0.05 < \frac{\alpha_4 M_{H_2}}{\alpha_2 M_{CO_2}} < 0.4 \quad (5.11)$$

$$0.5 < \frac{\alpha_5 M_{H_2O}}{\alpha_2 M_{CO_2}} < 4 \quad (5.12)$$

$$0.1 < \frac{\alpha_7 M_{C_2H_2} + \alpha_8 M_{C_2H_4} + \alpha_9 M_{C_2H_6}}{\alpha_3 M_{CH_4}} < 1.5 \quad (5.13)$$

Therefore the set of Equations 5.3-5.6 and 5.8 is solved with the least square method in order to find the optimal solution and with the help of the additional constraints, 5.9-5.13, volatiles composition can be determined.

It is worth noting that Equations 5.7 and 5.8 are slightly temperature dependent, because the values of biomass HHV and heat of combustion are at

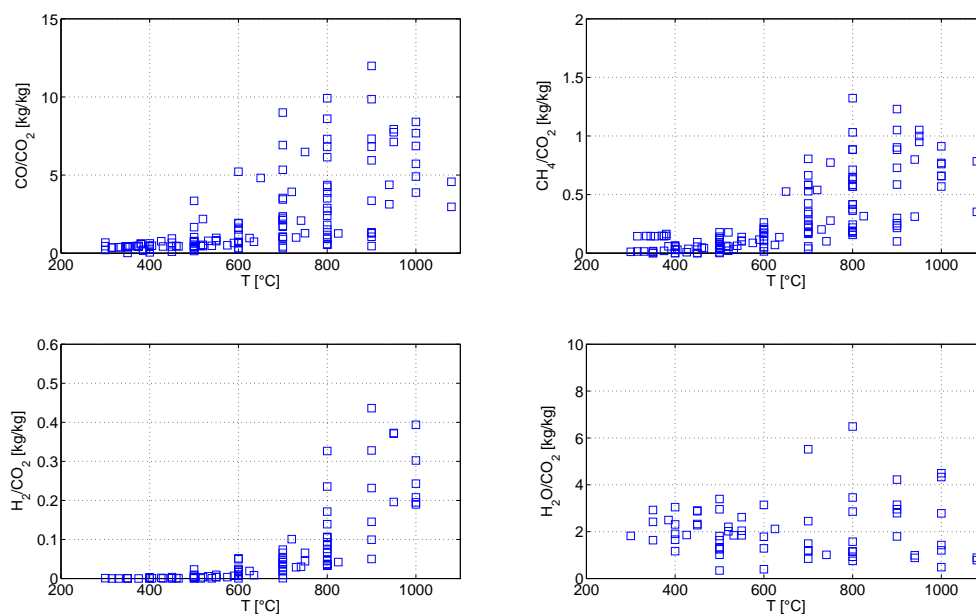


Figure 5.2: The mass ratios of CO, CH<sub>4</sub>, H<sub>2</sub> and H<sub>2</sub>O yields to CO<sub>2</sub> yield as functions of pyrolysis temperature, data from [57–76, 81–88].

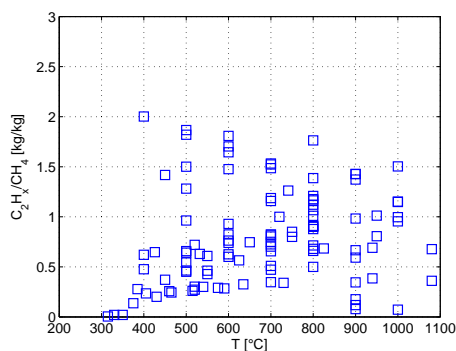


Figure 5.3: The mass ratio of C<sub>2</sub>H<sub>x</sub>=C<sub>2</sub>H<sub>2</sub>+C<sub>2</sub>H<sub>4</sub>+C<sub>2</sub>H<sub>6</sub> yields to CH<sub>4</sub> yield as a function of pyrolysis temperature, data from [57–76, 81–88].

standard conditions. Therefore using the volatiles composition obtained by solving the set of equations 5.3-5.6 and 5.8 for other temperatures results in a small deviation from zero for  $\Delta H_{pyr}$ . In other words, since the pyrolysis in

the particle model happens at temperatures higher than standard condition the effect of the sensible enthalpy on Equation 5.8 results to a small deviation from zero which can be interpreted as the heat of pyrolysis,  $\Delta H_{pyr}$ . Therefore, in the model the pyrolysis reaction will be slightly endothermic, which is in line with the previous findings [26, 210, 211]. However, there is a possibility in the particle model to set the heat of pyrolysis to zero or even to a reliable value from literature.

The results of the investigations on the effects of different kinetic mechanisms on the ignition time and formation of the flame in the freeboard, as well as on the species concentrations above the packed bed, are presented in *Paper V*.



# Chapter 6

## Summary and conclusion

In this work great effort was made to model the packed bed of biomass grate furnaces. The result was the development of a basic version of a 3D CFD model for packed bed combustion systems, the most relevant biomass combustion technology for small and medium scale applications.

The first step involved the development of a one-dimensional single particle model to simulate the thermal conversion of thermally thick particles by considering intra-particle gradients. The development of an appropriate particle model which can be coupled with available CFD tools was necessary in order to directly link the bed model with gas phase combustion models, and to simultaneously simulate the entire biomass grate furnace. In the layer model each particle is divided into four layers: wet (virgin) fuel, dry fuel, char residue and ash, corresponding to the four main stages of biomass thermal conversion. The sub-processes of thermal biomass conversion are considered using separate sub-models. Moisture evaporation is assumed to occur at a constant temperature, while biomass pyrolysis is modelled using three competing decomposition reactions for the pseudo-components, cellulose, hemicellulose and lignin. Char oxidation is kinetically and/or diffusionally controlled. The number of governing equations and grid points inside the particle were reduced to speed up the numerical calculations, without impairing the model accuracy. It was programmed in C/C++ and linked with ANSYS FLUENT to simultaneously resolve the mass and energy

balance equations for the particle and its surrounding gas phase during its thermal conversion. The layer model is validated under pyrolysis and combustion conditions with different particle sizes, shapes, and moisture contents. The model results are in good agreement with the experimental data. The results of the model validation are presented in *Paper I*.

The influence of the heating rate on the pyrolysis kinetic model and successively on the overall mass loss of biomass particles, raises the need to investigate the range of heating rates which may occur during pyrolysis. For this purpose the layer model was used to simulate the temperature profile inside biomass particles as well as particle mass loss during pyrolysis under various conditions. The average time derivative of the centre temperature of the pyrolysis layer, weighted by the volatiles release rate, was found to be an appropriate indicator for the heating rate in biomass particles during pyrolysis. The results clearly show the biomass fuels and combustion conditions for which the results of conventional TGA systems (typically with heating rates well below 50 K/min) can be applied, and when kinetic parameters derived from high heating rate experiments are needed. This distinction is of great importance because at present pyrolysis kinetic parameters derived from low heating rate TGA experiments are often used incorrectly. More information about the methodology and detailed results are available in *Paper II*.

As a next step in the development of the CFD packed bed combustion model, a novel approach was taken by coupling two separate multiphase models in ANSYS FLUENT - the Euler-granular model and the discrete phase model (DPM) which simulate hydrodynamics and thermal conversion of the solid particles in the packed bed, respectively. A user defined function (UDF) was programmed to calculate the particle trajectories based on the velocity field of the granular phase obtained by the Euler-granular model. The standard discrete phase model (DPM) was used to model the thermal conversion of the biomass particles. This method was used to predict the positions of the drying, pyrolysis, and char burnout zones in a small-scale underfeed stoker furnace. The results of this simulation are presented in *Paper III*.

The 3D packed bed combustion model was then further improved by solving the thermal conversion of the biomass particles with the layer model instead of the standard discrete phase model (DPM). The layer model enhances the packed bed model by considering the biomass particles as thermally thick. This means that the intra-particle species and temperature gradients are considered and the parallel progress of the thermal conversion sub-processes is taken into account. Moreover, the layer model considers the particles as cylinders. Pyrolysis is modelled using three competing decomposition reactions for the pseudo-components, cellulose, hemicellulose and lignin. Char oxidation is kinetically and/or diffusionally controlled. The char gasification reactions are included. The products of char oxidation are CO and CO<sub>2</sub>, and the ratio between these species changes depending on the particle temperature. The model was tested with the same small-scale underfeed stoker furnace and the results are presented in *Paper IV*. As it is mentioned in *Paper IV*, due to consideration of the particles as thermally thick the results are improved concerning the maximum predicted particle temperatures in the bed which implies that the particle temperatures are better predicted. This is of great advantage for a correct description of particle burnout and the release of gaseous and ash forming species.

The 3D CFD combustion model for biomass grate furnaces was further extended with models for the radiative heat transfer between the particles and for the gas phase combustion in the packed bed as well as the freeboard. Having an accurate model for homogeneous reactions is important for packed bed biomass combustion because it produces the energy required for heating, drying and pyrolysis of the fuel bed. Species concentrations are also affected by the model applied for the homogeneous reactions. Therefore, detailed kinetic mechanisms rather than global reactions were used for simulating the combustion of volatiles in the freeboard. To the author's knowledge a coupled packed bed and gas phase combustion simulation with detailed kinetic mechanisms and with the consideration of particle-particle radiation has not been reported yet. A full mechanism (GRI2.11), a reduced mechanism (DRM22) and a skeletal mechanism (Kilpinen97) were investigated and

their results compared. In order to validate the entire 3D packed bed model it was applied to simulate a laboratory-scale fixed bed reactor. The model performance was extensively validated with several experimental data, i.e. CO, CO<sub>2</sub>, CH<sub>4</sub>, H<sub>2</sub>, H<sub>2</sub>O and O<sub>2</sub> concentrations above the fuel bed, temperatures at different heights in the bed and in the freeboard, and the propagation rate of the ignition front. There is hardly any difference between the results of GRI2.11 and DRM22 and they are in good agreements with the experimental data. When compared to the measurements, the results of the Kilpinen97 mechanism are generally acceptable. However, considering that the Kilpinen97 mechanism has significantly less number of species and reactions than the two other mechanisms, it can be concluded that for industrial applications where reduction of the calculation time is important, the Kilpinen97 mechanism is preferable to the more detailed mechanisms. The results of the model validation with the experimental data are given in *Paper V*.

The 3D packed bed model presents certain advantages in terms of avoiding separation between the packed bed and the freeboard, considering biomass particles as thermally thick particles, and modelling the combustion chemistry by means of a comprehensive mechanism. Additionally, it allows the effect of particle-related parameters (e.g. size, physical properties and moisture content) as well as operating conditions (e.g. air distribution below the grate, flue gas recirculation and air staging conditions in a furnace) on the thermal conversion of the entire packed bed to be investigated.

## Outlook

The presented model has some limitations; for example, the tar secondary reactions are excluded, the effect of moving grate bars on the packed bed is not modelled, spherical shape of particles is assumed in the Euler-granular model, streak formation is not modelled and the release of nitrogen species and ash forming elements is excluded. These all need to be addressed in further developments of the model, to improve and extend its applicability

for the development and optimisation of biomass grate firing systems.

As a first step of model improvement the pyrolysis scheme should be improved and a mechanistic scheme, be capable of predicting yields of permanent gas and tar components, needs to be used, in order to predict the yields of pyrolysis products dependent on the pyrolysis temperature and severity. It reduces the input parameters of the model which have to be determined with empirical correlations as it is explained in section 5.2. Moreover, it makes it possible to consider the tar secondary reactions.

An appropriate gas-solid multiphase flow model for moving grates is needed to consider the effect of moving grate bars on the packed bed, and to avoid separation between the thermal conversion of the biomass particles and the hydrodynamics of the multiphase flow. First attempts have shown that Euler-granular model can not well predict mixing of particles and effect of moving grate bars. The discrete elements model (DEM) is a promising candidate, however it extremely increases the calculation time for industrial applications. An option would be to use GPU computing (Graphics Processing Unit) to accelerate the computation for industrial applications. Additionally, a hybrid model, i.e. combination of Eulerian and Lagrangian approaches, may also worth to try.

In order to consider streak formation, a mixing function based on the Reynolds number is needed. This mixing function gives information about the mixing quality of the volatiles and the primary air. In the positions where mixing is poor the rates of homogeneous reactions are damped which leads to have some streaks above the bed.

# Bibliography

- [1] Merrick D., “Mathematical models of the thermal decomposition of coal. 1. the evolution of volatile matter,” *Fuel*, vol. 62, no. 5, pp. 534–539, 1983.
- [2] Van Der Lans R.P., Pedersen L.T., Jensen A., Glarborg P., Dam-Johansen K., “Modelling and experiments of straw combustion in a grate furnace,” *Biomass and Bioenergy*, vol. 19, no. 3, pp. 199–208, 2000.
- [3] Vortmeyer D., Schaefer R.J., “Equivalence of one- and two-phase models for heat transfer processes in packed beds: one dimensional theory,” *Chemical Engineering Science*, vol. 29, no. 2, pp. 485–491, 1974.
- [4] Finlayson B.A., “Packed bed reactor analysis by orthogonal collocation,” *Chemical Engineering Science*, vol. 26, no. 7, pp. 1081–1091, 1971.
- [5] Hobbs M.L., Radulovic P.T., Smoot, L.D., “Modeling fixed-bed coal gasifiers,” *AIChE Journal*, vol. 38, no. 5, pp. 681–702, 1992.
- [6] Bryden K.M., Ragland K.W., “Numerical modeling of a deep, fixed bed combustor,” *Energy and Fuels*, vol. 10, no. 2, pp. 269–275, 1996.
- [7] Shin D., Choi S., “The combustion of simulated waste particles in a fixed bed,” *Combustion and Flame*, vol. 121, no. 1-2, pp. 167–180, 2000.
- [8] Blasi C.D., “Dynamic behaviour of stratified downdraft gasifiers,” *Chemical Engineering Science*, vol. 55, no. 15, pp. 2931–2944, 2000.

- [9] Cooper J., Hallett W.L.H., “A numerical model for packed-bed combustion of char particles,” *Chemical Engineering Science*, vol. 55, no. 20, pp. 4451–4460, 2000.
- [10] Liang X.H., Kozinski J.A., “Numerical modeling of combustion and pyrolysis of cellulosic biomass in thermogravimetric systems,” *Fuel*, vol. 79, no. 12, pp. 1477–1486, 2000.
- [11] Saastamoinen J.J., Taipale R., Horttanainen M., Sarkomaa P., “Propagation of the ignition front in beds of wood particles,” *Combustion and Flame*, vol. 123, no. 1-2, pp. 214–226, 2000.
- [12] Thunman H., Leckner B., “Ignition and propagation of a reaction front in cross-current bed combustion of wet biofuels,” *Fuel*, vol. 80, no. 4, pp. 473–481, 2001.
- [13] Yang Y.B., Goh Y.R., Zakaria R., Nasserzadeh V., Swithenbank J., “Mathematical modelling of {MSW} incineration on a travelling bed,” *Waste Management*, vol. 22, no. 4, pp. 369–380, 2002.
- [14] Collazo J., Porteiro J., Patio D., Granada E., “Numerical modeling of the combustion of densified wood under fixed-bed conditions,” *Fuel*, vol. 93, pp. 149–159, 2012.
- [15] Duffy N.T.M., Eaton J.A., “Investigation of factors affecting channelling in fixed-bed solid fuel combustion using CFD,” *Combustion and Flame*, 2013.
- [16] Hermansson S., Thunman H., “CFD modelling of bed shrinkage and channelling in fixed-bed combustion,” *Combustion and Flame*, vol. 158, no. 5, pp. 988–999, 2011.
- [17] Peters B., “Measurements and application of a discrete particle model (dpm) to simulate combustion of a packed bed of individual fuel particles,” *Combustion and Flame*, vol. 131, no. 1-2, pp. 132–146, 2002.

- [18] Simsek E., Brosch B., Wirtz S., Scherer V., Krll F., “Numerical simulation of grate firing systems using a coupled CFD/Discrete Element Method (DEM),” *Powder Technology*, vol. 193, no. 3, pp. 266–273, 2009.
- [19] Anca-Couce A., Zobel N., Jakobsen H.A., “Multi-scale modeling of fixed-bed thermo-chemical processes of biomass with the representative particle model: Application to pyrolysis,” *Fuel*, vol. 103, pp. 773–782, 2013.
- [20] Basu P., *Biomass Gasification and Pyrolysis: Practical Design*. Boston: Academic Press, 2010.
- [21] Demirbas A., “Biorefineries: Current activities and future developments,” *Energy Conversion and Management*, vol. 50, no. 11, pp. 2782–2801, 2009.
- [22] Grønli M., *A theoretical and experimental study of the thermal degradation of biomass*. PhD thesis, The Norwegian University of Science and Technology, Norway, 1996.
- [23] Bellais M., *Modelling of the pyrolysis of large wood particles*. PhD thesis, KTH - Royal Institute of Technology, Sweden, 2007.
- [24] Di Blasi C., “Multi-phase moisture transfer in the high-temperature drying of wood particles,” *Chemical Engineering Science*, vol. 53, no. 2, pp. 353–366, 1998.
- [25] Thunman H., Leckner B., Niklasson F., Johnsson F., “Combustion of wood particles - a particle model for eulerian calculations,” *Combustion and Flame*, vol. 129, no. 1-2, pp. 30–46, 2002.
- [26] Chan W.C.R., Kelbon M., Krieger B.B., “Modelling and experimental verification of physical and chemical processes during pyrolysis of a large biomass particle,” *Fuel*, vol. 64, no. 11, pp. 1505–1513, 1985.



- [27] Bryden K.M., Ragland K.W., Rutland C.J., “Modeling thermally thick pyrolysis of wood,” *Biomass and Bioenergy*, vol. 22, no. 1, pp. 41 – 53, 2002.
- [28] Bryden K.M. , Hagge M.J., “Modeling the combined impact of moisture and char shrinkage on the pyrolysis of a biomass particle,” *Fuel*, vol. 82, no. 13, pp. 1633–1644, 2003.
- [29] Sreekanth M. , Sudhakar D.R. , Prasad B.V.S.S.S. , Kolar A.K. , Leckner B., “Modelling and experimental investigation of devolatilizing wood in a fluidized bed combustor,” *Fuel*, vol. 87, no. 12, pp. 2698–2712, 2008.
- [30] Benkoussas B. , Consalvi J.L. , Porterie B. , Sardoy N. , Loraud J.C., “Modelling thermal degradation of woody fuel particles,” *International Journal of Thermal Sciences*, vol. 46, no. 4, pp. 319–327, 2007.
- [31] Ouelhazi N., Arnaud G., Fohr J.P., “A two-dimensional study of wood plank drying. the effect of gaseous pressure below boiling point,” *Transport in Porous Media*, vol. 7, no. 1, pp. 39–61, 1992.
- [32] Wurzenberger J.C., Wallner S., Raupenstrauch H., Khinast J.G., “Thermal conversion of biomass: Comprehensive reactor and particle modeling,” *AIChE Journal*, vol. 48, no. 10, pp. 2398–2411, 2002.
- [33] Zobel N., *The representative particle model*. PhD thesis, Technischen Universität Berlin, Germany, 2007.
- [34] Bruch C., Peters B., Nussbaumer T., “Modelling wood combustion under fixed bed conditions,” *Fuel*, vol. 82, no. 6, pp. 729–738, 2003.
- [35] Porteiro J., Míguez J.L., Granada E., Morán J.C., “Mathematical modelling of the combustion of a single wood particle,” *Fuel Processing Technology*, vol. 87, no. 2, pp. 169–175, 2006.
- [36] Porteiro J., Granada E., Collazo J., Patiño D., Morán J.C., “A model for the combustion of large particles of densified wood,” *Energy & Fuels*, vol. 21, no. 6, pp. 3151–3159, 2007.

- [37] Galgano A., Di Blasi C., “Coupling a CFD code with a solid-phase combustion model,” *Progress in Computational Fluid Dynamics*, vol. 6, no. 4-5, pp. 287–302, 2006.
- [38] Galgano A., Di Blasi C., “Modeling the propagation of drying and decomposition fronts in wood,” *Combustion and Flame*, vol. 139, no. 1-2, pp. 16–27, 2004.
- [39] Peters B., Bruch C., “Drying and pyrolysis of wood particles: Experiments and simulation,” *Journal of Analytical and Applied Pyrolysis*, vol. 70, no. 2, pp. 233–250, 2003.
- [40] Peters B., Schöder E., Bruch C., “Measurements and particle resolved modelling of the thermo-and fluid dynamics of a packed bed,” *Journal of Analytical and Applied Pyrolysis*, vol. 70, no. 2, pp. 211–231, 2003.
- [41] Peters B., *Thermal conversion of solid fuels*. Southampton: WIT Press, 2003.
- [42] Yang Y.B., Sharifi V.N., Swithenbank J., Ma L., Darvell L.I., Jones J.M., Pourkashanian M., Williams A., “Combustion of a single particle of biomass,” *Energy & Fuels*, vol. 22, no. 1, pp. 306–316, 2008.
- [43] Thunman H., Davidsson K., Leckner B., “Separation of drying and devolatilization during conversion of solid fuels,” *Combustion and Flame*, vol. 137, no. 1-2, pp. 242–250, 2004.
- [44] Bharadwaj A., Baxter L.L., Robinson A.L., “Effects of intraparticle heat and mass transfer on biomass devolatilization: Experimental results and model predictions,” *Energy & Fuels*, vol. 18, no. 4, pp. 1021–1031, 2004.
- [45] Saastamoinen, J.J., “Simplified model for calculation of devolatilization in fluidized beds,” *Fuel*, vol. 85, no. 17-18, pp. 2388–2395, 2006.
- [46] de Diego L. F., García-Labiano F., Abad A., Gayán P., Adánez J., “Modeling of the devolatilization of nonspherical wet pine wood

- particles in fluidized beds,” *Industrial and Engineering Chemistry Research*, vol. 41, no. 15, pp. 3642–3650, 2002.
- [47] Saastamoinen J., Richard J.R., “Simultaneous drying and pyrolysis of solid fuel particles,” *Combustion and Flame*, vol. 106, no. 3, pp. 288–300, 1996.
- [48] Bilbao R., Mastral J.F., Lana J.A., Ceamanos J., Aldea M.E., Betrán M., “A model for the prediction of the thermal degradation and ignition of wood under constant and variable heat flux,” *Journal of Analytical and Applied Pyrolysis*, vol. 62, no. 1, pp. 63–82, 2002.
- [49] Bilbao, R., Mastral, J.F., Ceamanos, J., Aldea, M.E., “Modelling of the pyrolysis of wet wood,” *Journal of Analytical and Applied Pyrolysis*, vol. 36, no. 1, pp. 81–97, 1996.
- [50] Alves S.S., Figueiredo J.L., “A model for pyrolysis of wet wood,” *Chemical Engineering Science*, vol. 44, no. 12, pp. 2861–2869, 1989.
- [51] Peters B., Schrder E., Bruch C., Nussbaumer T., “Measurements and particle resolved modelling of heat-up and drying of a packed bed,” *Biomass and Bioenergy*, vol. 23, no. 4, pp. 291–306, 2002.
- [52] Neves D., Thunman H., Matos A., Tarelho L., Gómez-Barea A., “Characterization and prediction of biomass pyrolysis products,” *Progress in Energy and Combustion Science*, vol. 37, no. 5, pp. 611–630, 2011.
- [53] Yin R., Liu R., Wu J., Wu X., Sun C., Wu C., “Influence of particle size on performance of a pilot-scale fixed-bed gasification system,” *Bioresource Technology*, vol. 119, pp. 15–21, 2012.
- [54] Nik-Azar M., Hajaligol M.R., Sohrabi M., Dabir, B., “Effects of heating rate and particle size on the products yields from rapid pyrolysis of beech-wood,” *Fuel Science and Technology International*, vol. 14, no. 4, pp. 479–502, 1996.

- [55] Diebold J.P., Bridgwater A.V., “Overview of fast pyrolysis of biomass for the production of liquid fuels,” in *Developments in Thermochemical Biomass Conversion* (Bridgwater A.V., Boocock D.G.B., ed.), pp. 5–27, Blackie Academic & Professional, 1997.
- [56] Neves D., Thunman H., Seemann M., Ideias P., Motas A., Tarelho L., Gómez-Barea A., “A database on biomass pyrolysis for gasification applications,” in *Proceedings of the 17<sup>th</sup> European Biomass Conference and Exhibition*, (Hamburg, Germany), 29 June - 3 July 2009.
- [57] Nunn T. R., Howard J. B., Longwell J. P., Peters W. A., “Product compositions and kinetics in the rapid pyrolysis of sweet gum hardwood,” *Industrial & Engineering Chemistry Process Design and Development*, vol. 24, no. 3, pp. 836–844, 1985.
- [58] Hajaligol M. R., Howard J. B., Longwell J. P., Peters W. A., “Product compositions and kinetics for rapid pyrolysis of cellulose,” *Industrial & Engineering Chemistry Process Design and Development*, vol. 21, no. 3, pp. 457–465, 1982.
- [59] Nunn T. R., Howard J. B., Longwell J. P., Peters W. A., “Product compositions and kinetics in the rapid pyrolysis of milled wood lignin,” *Industrial & Engineering Chemistry Process Design and Development*, vol. 24, no. 3, pp. 844–852, 1985.
- [60] Di Blasi C.D., Signorelli G., Portoricco G., “Countercurrent fixed-bed gasification of biomass at laboratory scale,” *Industrial and Engineering Chemistry Research*, vol. 38, no. 7, pp. 2571–2581, 1999.
- [61] Di Blasi C., Branca C., Santoro A., Gonzalez Hernandez E., “Pyrolytic behavior and products of some wood varieties,” *Combustion and Flame*, vol. 124, no. 1-2, pp. 165–177, 2001.
- [62] Di Blasi C., Signorelli G., Di Russo C., Rea G., “Product distribution from pyrolysis of wood and agricultural residues,” *Industrial and Engineering Chemistry Research*, vol. 38, no. 6, pp. 2216–2224, 1999.

- [63] Scott D. S. , Piskorz J., Radlein D., “Liquid products from the continuous flash pyrolysis of biomass,” *Industrial & Engineering Chemistry Process Design and Development*, vol. 24, no. 3, pp. 581–588, 1985.
- [64] Horne P.A., Williams P.T., “Influence of temperature on the products from the flash pyrolysis of biomass,” *Fuel*, vol. 75, no. 9, pp. 1051–1059, 1996.
- [65] Agblevor F.A., Besler S., Wiselogel A.E., “Fast pyrolysis of stored biomass feedstocks,” *Energy & Fuels*, vol. 9, no. 4, pp. 635–640, 1995.
- [66] Wang X., Kersten S.R.A., Prins W., van Swaaij W.P.M., “Biomass pyrolysis in a fluidized bed reactor. part 2: Experimental validation of model results,” *Industrial and Engineering Chemistry Research*, vol. 44, no. 23, pp. 8786–8795, 2005.
- [67] Zanzi R., Sjöström K., Björnbom E., “Rapid pyrolysis of agricultural residues at high temperature,” *Biomass and Bioenergy*, vol. 23, no. 5, pp. 357–366, 2002.
- [68] Fagbemi L., Khezami L., Capart R., “Pyrolysis products from different biomasses: Application to the thermal cracking of tar,” *Applied Energy*, vol. 69, no. 4, pp. 293–306, 2001.
- [69] Scott D.S., Piskorz J., Bergougnou M.A., Graham R., Overend R.P., “The role of temperature in the fast pyrolysis of cellulose and wood,” *Industrial and Engineering Chemistry Research*, vol. 27, no. 1, pp. 8–15, 1988.
- [70] Becidan M., Skreiberg Ø., Hustad J.E., “Products distribution and gas release in pyrolysis of thermally thick biomass residues samples,” *Journal of Analytical and Applied Pyrolysis*, vol. 78, no. 1, pp. 207–213, 2007.

- [71] de Jong W., Pirone V., Wójtowicz M.A., “Pyrolysis of miscanthus giganteus and wood pellets: Tg-ftir analysis and reaction kinetics,” *Fuel*, vol. 82, no. 9, pp. 1139 – 1147, 2003.
- [72] Dupont C., Commandré J.M., Gauthier P., Boissonnet G., Salvador S., Schweich D., “Biomass pyrolysis experiments in an analytical entrained flow reactor between 1073K and 1273K,” *Fuel*, vol. 87, no. 7, pp. 1155–1164, 2008.
- [73] Dupont C., Chen L., Cances J., Commandre J.M., Cuoci A., Pierucci S., Ranzi E., “Biomass pyrolysis: Kinetic modelling and experimental validation under high temperature and flash heating rate conditions,” *Journal of Analytical and Applied Pyrolysis*, vol. 85, no. 12, pp. 260 – 267, 2009.
- [74] Yu Q., Brage C., Chen G., Sjöström K., “Temperature impact on the formation of tar from biomass pyrolysis in a free-fall reactor,” *Journal of Analytical and Applied Pyrolysis*, vol. 40-41, pp. 481–489, 1997.
- [75] Beaumont O., Schwob Y., “Influence of physical and chemical parameters on wood pyrolysis,” *Industrial and Engineering Chemistry Process Design and Development*, vol. 23, no. 4, pp. 637–641, 1984.
- [76] Encinar J.M., González J.F., González J., “Fixed-bed pyrolysis of cynara cardunculus l. product yields and compositions,” *Fuel Processing Technology*, vol. 68, no. 3, pp. 209 – 222, 2000.
- [77] Chen G., Andries J., Luo Z., Spliethoff H., “Biomass pyrolysis/gasification for product gas production: the overall investigation of parametric effects,” *Energy Conversion and Management*, vol. 44, no. 11, pp. 1875 – 1884, 2003.
- [78] Dufour A., Girods P., Masson E., Rogaume Y., Zoulalian A., “Synthesis gas production by biomass pyrolysis: Effect of reactor temperature on product distribution,” *International Journal of Hydrogen Energy*, vol. 34, no. 4, pp. 1726 – 1734, 2009.

- [79] Bridgwater A.V., Meier D., Radlein D., “An overview of fast pyrolysis of biomass,” *Organic Geochemistry*, vol. 30, no. 12, pp. 1479–1493, 1999.
- [80] Williams P.T., Besler S., “The influence of temperature and heating rate on the slow pyrolysis of biomass,” *Renewable Energy*, vol. 7, no. 3, pp. 233–250, 1996.
- [81] González J.F., Ramiro A., González-García C.M., Gañán J., Encinar J.M., Sabio E., Rubiales J., “Pyrolysis of almond shells. energy applications of fractions,” *Industrial and Engineering Chemistry Research*, vol. 44, no. 9, pp. 3003–3012, 2005.
- [82] Wei L., Xu S., Zhang L., Zhang H., Liu C., Zhu H., Liu S., “Characteristics of fast pyrolysis of biomass in a free fall reactor,” *Fuel Processing Technology*, vol. 87, no. 10, pp. 863–871, 2006.
- [83] Aguado R., Olazar M., San José M.J., Aguirre G., Bilbao J., “Pyrolysis of sawdust in a conical spouted bed reactor. yields and product composition,” *Industrial and Engineering Chemistry Research*, vol. 39, no. 6, pp. 1925–1933, 2000.
- [84] Li S., Xu S., Liu S., Yang C., Lu Q., “Fast pyrolysis of biomass in free-fall reactor for hydrogen-rich gas,” *Fuel Processing Technology*, vol. 85, no. 8-10, pp. 1201–1211, 2004.
- [85] Couhert C., Commandre J.M., Salvador S., “Is it possible to predict gas yields of any biomass after rapid pyrolysis at high temperature from its composition in cellulose, hemicellulose and lignin?,” *Fuel*, vol. 88, no. 3, pp. 408–417, 2009.
- [86] Commandré J.M., Lahmidi H., Salvador S., Dupassieux N., “Pyrolysis of wood at high temperature: The influence of experimental parameters on gaseous products,” *Fuel Processing Technology*, vol. 92, no. 5, pp. 837–844, 2011.

- [87] Graham R.G., Bergougnou M.A., Overend R.P., “Fast pyrolysis of biomass,” *Journal of Analytical and Applied Pyrolysis*, vol. 6, no. 2, pp. 95–135, 1984.
- [88] Boroson M.L., Howard J.B., Longwell J.P., Peters W.A., “Product yields and kinetics from the vapor phase cracking of wood pyrolysis tars,” *AIChE Journal*, vol. 35, no. 1, pp. 120–128, 1989.
- [89] Morf P., Hasler P., Nussbaumer T., “Mechanisms and kinetics of homogeneous secondary reactions of tar from continuous pyrolysis of wood chips,” *Fuel*, vol. 81, no. 7, pp. 843–853, 2002.
- [90] Branca C., Giudicianni P., Di Blasi C., “GC/MS characterization of liquids generated from low-temperature pyrolysis of wood,” *Industrial and Engineering Chemistry Research*, vol. 42, no. 14, pp. 3190–3202, 2003.
- [91] Diebold J.P., Milne T.A., Czernik S., Osamaa A., Bridgwater A.V., Cuevas A., Gust S., Huffman D., Piskorz J., “Proposed specification for various grades of pyrolysis oils,” in *Developments in Thermochemical Biomass Conversion* (Bridgwater A.V., Boocock D.G.B., ed.), Blackie Academic & Professional, 1997.
- [92] Boroson M.L., Howard J.B., Longwell J.P., Peters W.A., “Heterogeneous cracking of wood pyrolysis tars over fresh wood char surfaces,” *Energy & Fuels*, vol. 3, no. 6, pp. 735–740, 1989.
- [93] Gilbert P., Ryu C., Sharifi V., Swithenbank J., “Tar reduction in pyrolysis vapours from biomass over a hot char bed,” *Bioresource Technology*, vol. 100, no. 23, pp. 6045–6051, 2009.
- [94] Shen J., Wang X.S., Garcia-Perez M., Mourant D., Rhodes M.J., Li C.Z., “Effects of particle size on the fast pyrolysis of oil mallee woody biomass,” *Fuel*, vol. 88, no. 10, pp. 1810–1817, 2009.



- [95] Thurner F., Mann U., “Kinetic investigation of wood pyrolysis,” *Industrial & Engineering Chemistry, Process Design and Development*, vol. 20, no. 3, pp. 482–488, 1981.
- [96] Wagenaar B.M., Prins W., van Swaaij W.P.M., “Flash pyrolysis kinetics of pine wood,” *Fuel Processing Technology*, vol. 36, no. 1-3, pp. 291–298, 1993.
- [97] Di Blasi C., “Modeling chemical and physical processes of wood and biomass pyrolysis,” *Progress in Energy and Combustion Science*, vol. 34, no. 1, pp. 47–90, 2008.
- [98] Miller R.S., Bellan J., “A generalized biomass pyrolysis model based on superimposed cellulose, hemicellulose and lignin kinetics,” *Combustion Science and Technology*, vol. 126, no. 1-6, pp. 97–137, 1997.
- [99] Branca C., Albano A., Di Blasi C., “Critical evaluation of global mechanisms of wood devolatilization,” *Thermochimica Acta*, vol. 429, no. 2, pp. 133–141, 2005.
- [100] Ward S.M., Braslaw J., “Experimental weight loss kinetics of wood pyrolysis under vacuum,” *Combustion and Flame*, vol. 61, no. 3, pp. 261–269, 1985.
- [101] Koufopoulos C. A., Lucchesi A., Maschio, G., “Kinetic modelling of the pyrolysis of biomass and biomass components,” *The Canadian Journal of Chemical Engineering*, vol. 67, no. 1, pp. 75–84, 1989.
- [102] Raveendran K., Ganesh A., Khilar K.C., “Pyrolysis characteristics of biomass and biomass components,” *Fuel*, vol. 75, no. 8, pp. 987–998, 1996.
- [103] Orfaõ J.J.M., Antunes F.J.A., Figueiredo J.L., “Pyrolysis kinetics of lignocellulosic materials - three independent reactions model,” *Fuel*, vol. 78, no. 3, pp. 349–358, 1999.

- [104] Belderok H.J.M., “Experimental investigation and modeling of the pyrolysis of biomass,” 2007. MSc thesis, Eindhoven University of Technology, The Netherland.
- [105] P. L. Manyá J.J., Velo E., “Kinetics of biomass pyrolysis: A reformulated three-parallel-reactions model,” *Industrial and Engineering Chemistry Research*, vol. 42, no. 3, pp. 434–441, 2003.
- [106] Becidan M., Várhegyi G., Hustad J.E., Skreiberg ø., “Thermal decomposition of biomass wastes. a kinetic study,” *Industrial and Engineering Chemistry Research*, vol. 46, no. 8, pp. 2428–2437, 2007.
- [107] Miranda R., Sosa-Blanco C., Bustos-Martínez D., Vasile C., “Pyrolysis of textile wastes. i. kinetics and yields,” *Journal of Analytical and Applied Pyrolysis*, vol. 80, no. 2, pp. 489–495, 2007.
- [108] Várhegyi G., Antal M.J., Jakab E., Szabó P., “Kinetic modeling of biomass pyrolysis,” *Journal of Analytical and Applied Pyrolysis*, vol. 42, no. 1, pp. 73–87, 1997.
- [109] Teng H., Wei Y.C., “Thermogravimetric studies on the kinetics of rice hull pyrolysis and the influence of water treatment,” *Industrial and Engineering Chemistry Research*, vol. 37, no. 10, pp. 3806–3811, 1998.
- [110] Grønli M.G., Várhegyi G., Di Blasi C., “Thermogravimetric analysis and devolatilization kinetics of wood,” *Industrial and Engineering Chemistry Research*, vol. 41, no. 17, pp. 4201–4208, 2002.
- [111] Antal M.J., Varhegyi G., “Cellulose pyrolysis kinetics: The current state of knowledge,” *Industrial and Engineering Chemistry Research*, vol. 34, no. 3, pp. 703–717, 1995.
- [112] Di Blasi C., “Combustion and gasification rates of lignocellulosic chars,” *Progress in Energy and Combustion Science*, vol. 35, no. 2, pp. 121–140, 2009.
- [113] Froment G. F., Bischoff K. B., *Chemical reactor analysis and design*. New York: John Wiley, 1990.

- [114] Gómez-Barea A., Leckner B., “Modeling of biomass gasification in fluidized bed,” *Progress in Energy and Combustion Science*, vol. 36, no. 4, pp. 444–509, 2010.
- [115] Laurendeau N.M., “Heterogeneous kinetics of coal char gasification and combustion,” *Progress in Energy and Combustion Science*, vol. 4, no. 4, pp. 221–270, 1978. cited By (since 1996) 247.
- [116] Hobbs M.L., Radulovic P.T., Smoot L.D., “Combustion and gasification of coals in fixed-beds,” *Progress in Energy and Combustion Science*, vol. 19, no. 6, pp. 505–586, 1993.
- [117] Bews I.M., Hayhurst A.N., Richardson S.M., Taylor S.G., “The order, arrhenius parameters, and mechanism of the reaction between gaseous oxygen and solid carbon,” *Combustion and Flame*, vol. 124, no. 1-2, pp. 231–245, 2001.
- [118] Hurt R.H., Calo J.M., “Semi-global intrinsic kinetics for char combustion modeling,” *Combustion and Flame*, vol. 125, no. 3, pp. 1138–1149, 2001.
- [119] Williams A., Pourkashanian M., Jones J.M., “Combustion of pulverised coal and biomass,” *Progress in Energy and Combustion Science*, vol. 27, no. 6, pp. 587–610, 2001.
- [120] Ollero P., Serrera A., Arjona R., Alcantarilla S., “Diffusional effects in tga gasification experiments for kinetic determination,” *Fuel*, vol. 81, no. 15, pp. 1989–2000, 2002.
- [121] Gómez-Barea A., Ollero P., Arjona R., “Reaction-diffusion model of tga gasification experiments for estimating diffusional effects,” *Fuel*, vol. 84, no. 12-13, pp. 1695–1704, 2005.
- [122] Gómez-Barea A., Ollero P., Fernández-Baco C., “Diffusional effects in co2 gasification experiments with single biomass char particles. 1. experimental investigation,” *Energy and Fuels*, vol. 20, no. 5, pp. 2202–2210, 2006.

- [123] Gómez-Barea A., Ollero P., Villanueva A., “Diffusional effects in co2 gasification experiments with single biomass char particles. 2. theoretical predictions,” *Energy and Fuels*, vol. 20, no. 5, pp. 2211–2222, 2006. cited By (since 1996) 5.
- [124] Bischoff K.B., “Accuracy of the pseudo steady state approximation for moving boundary diffusion problems,” *Chemical Engineering Science*, vol. 18, no. 11, pp. 711–713, 1963.
- [125] Bischoff K.B., “Further comments on the pseudo steady state approximation for moving boundary diffusion problems,” *Chemical Engineering Science*, vol. 20, no. 8, pp. 783–784, 1965.
- [126] Theofanous T.G., Lim H.C., “An approximate analytical solution for non-planar moving boundary problems,” *Chemical Engineering Science*, vol. 26, no. 8, pp. 1297–1300, 1971.
- [127] Johansson R., Thunman H., Leckner B., “Influence of intraparticle gradients in modeling of fixed bed combustion,” *Combustion and Flame*, vol. 149, no. 1-2, pp. 49–62, 2007.
- [128] Johnson M.F.L., Stewart W.E., “Pore structure and gaseous diffusion in solid catalysts,” *Journal of Catalysis*, vol. 4, no. 2, pp. 248–252, 1965.
- [129] Patisson F., François M.G., Ablitzer D., “A non-isothermal, non-equimolar transient kinetic model for gas-solid reactions,” *Chemical Engineering Science*, vol. 53, no. 4, pp. 697–708, 1998.
- [130] Lu H., Robert W., Peirce G., Ripa B., Baxter L.L., “Comprehensive study of biomass particle combustion,” *Energy and Fuels*, vol. 22, no. 4, pp. 2826–2839, 2008.
- [131] Bird R. B., Stewart W. E., Lightfoot E. N., *Transport phenomena*. New York: John Wiley, second ed., 2002.

- [132] Scala F., “Mass transfer around freely moving active particles in the dense phase of a gas fluidized bed of inert particles,” *Chemical Engineering Science*, vol. 62, no. 16, pp. 4159–4176, 2007.
- [133] Tamarin A.I., “Mass transfer between the gas and solid particles in a fluidized bed,” *Journal of Engineering Physics*, vol. 41, no. 6, pp. 1346–1350, 1981.
- [134] La Nauze R.D., Jung K., Kastl J., “Mass transfer to large particles in fluidised beds of smaller particles,” *Chemical Engineering Science*, vol. 39, no. 11, pp. 1623–1633, 1984.
- [135] Guedes De Carvalho J.R.F., Coelho M.A.N., “Comments on mass transfer to large particles in fluidized beds of smaller particles,” *Chemical Engineering Science*, vol. 41, no. 1, pp. 209–210, 1986.
- [136] Coelho M.A.N., Guedes De Carvalho J.R.F., “Transverse dispersion in granular beds. part ii. mass transfer from large spheres immersed in fixed or fluidised beds of small inert particles,” *Chemical Engineering Research and Design*, vol. 66, no. 2, pp. 178–189, 1988.
- [137] Agarwal P.K., Mitchell W.J., La Nauze R.D., “Transport phenomena in multi-particle systems-iii. active particle mass transfer in fluidized beds of inert particles,” *Chemical Engineering Science*, vol. 43, no. 9, pp. 2511–2521, 1988.
- [138] Guedes De Carvalho J.R.F., Pinto A.M.F.R., Pinho C.M.C.T., “Mass transfer around carbon particles burning in fluidised beds,” *Chemical Engineering Research and Design*, vol. 69, no. 1, pp. 63–70, 1991.
- [139] Guedes De Carvalho J.R.F., Alves M.A.M., “Mass transfer and dispersion around active sphere buried in a packed bed,” *AIChE Journal*, vol. 45, no. 12, pp. 2495–2502, 1999.
- [140] Hayhurst A.N., Parmar M.S., “Measurement of the mass transfer coefficient and sherwood number for carbon spheres burning in a

- bubbling fluidized bed,” *Combustion and Flame*, vol. 130, no. 4, pp. 361–375, 2002.
- [141] Hsiung T.H., Thodos G., “Mass transfer in gas-fluidized beds: measurement of actual driving forces,” *Chemical Engineering Science*, vol. 32, no. 6, pp. 581–592, 1977.
- [142] Prins W., Casteleijn T.P., Draijer W., van Swaaij W.P.M., “Mass transfer from a freely moving single sphere to the dense phase of a gas fluidized bed of inert particles,” *Chemical Engineering Science*, vol. 40, no. 3, pp. 481–497, 1985.
- [143] Palchenok G.I., Tamarin A.I., “Mass transfer at a moving particle in a fluidized bed of coarse material,” *Journal of Engineering Physics*, vol. 47, no. 2, pp. 916–922, 1984.
- [144] Tamarin A.I., Palchyonok G.I., Goryunov K.E., “Heat and mass transfer of model particles in a fluidized bed of inert material,” *Heat transfer. Soviet research*, vol. 17, no. 2, pp. 136–141, 1984.
- [145] Palchonok G. I., Dolidovich A. F., Andersson S., Leckner B., “Calculation of true heat and mass transfer coefficients between particles and a fluidized bed,” in *Fluidization VII* (Porter O. E., Nicklin D. J., ed.), p. 913920, New York: Engineering Foundation, 1992.
- [146] Joulie R., Rios G.M., “Theoretical analysis of heat and mass transfer phenomena during fluidized bed sublimation,” *Drying Technology*, vol. 11, no. 1, pp. 157–182, 1993.
- [147] Joulie R., Barkat M., Rios G.M., “Effect of particle density on heat and mass transfer during fluidized bed sublimation,” *Powder Technology*, vol. 90, no. 1, pp. 79–88, 1997.
- [148] Palchonok G. I., *Heat and mass transfer to a single particle in fluidized bed*. PhD thesis, Chalmers University of Technology, Sweden, 1998.

- [149] Hayhurst A.N., “The mass transfer coefficient for oxygen reacting with a carbon particle in a fluidized or packed bed,” *Combustion and Flame*, vol. 121, no. 4, pp. 679–688, 2000.
- [150] Paterson W.R., Hayhurst A.N., “Mass or heat transfer from a sphere to a flowing fluid,” *Chemical Engineering Science*, vol. 55, no. 10, pp. 1925–1927, 2000.
- [151] Scala F., “Calculation of the mass transfer coefficient for the combustion of a carbon particle,” *Combustion and Flame*, vol. 157, no. 1, pp. 137–142, 2010.
- [152] Dennis, J.S., Hayhurst, A.N., Scott, S.A., “The combustion of large particles of char in bubbling fluidized beds: The dependence of sherwood number and the rate of burning on particle diameter,” *Combustion and Flame*, vol. 147, no. 3, pp. 185–194, 2006.
- [153] Arthur J.R., “Reactions between carbon and oxygen,” *Transactions of the Faraday Society*, vol. 47, pp. 164–178, 1951.
- [154] Rossberg M., “Experimentelle ergebnisse uber die primarreaktionen bei der kohlenstoffverbrennung,” *Z. Elektrochem*, vol. 60, pp. 952–956, 1956.
- [155] Walker P.L., Rusinko F., Austin L.G., “Gas reactions of carbon,” *Advances in Catalysis*, vol. 11, no. C, pp. 133–221, 1959.
- [156] Otterbein M., Bonnetain L., “Combustion d’un carbone vitreux sous basses pressions d’oxygene,” *Carbon*, vol. 6, no. 6, pp. 877–885, 1968.
- [157] Mitchell R.E., Kee R.J., Glarborg P., Coltrin M.E., “The effect of co conversion in the boundary layers surrounding pulverized-coal char particles,” *Symposium (International) on Combustion*, vol. 23, no. 1, pp. 1169–1176, 1991.
- [158] Du Z., Sarofim A.F., Longwell J.P., Mims C.A., “Kinetic measurement and modeling of carbon oxidation,” *Energy & Fuels*, vol. 5, no. 1, pp. 214–221, 1991.

- [159] Linjewile T.M., Agarwal P.K., "The product co/co<sub>2</sub> ratio from petroleum coke spheres in fluidized bed combustion," *Fuel*, vol. 74, no. 1, pp. 5–11, 1995.
- [160] Linjewile T.M., Agarwal P.K., "The influence of product co/co<sub>2</sub> ratio on the ignition and temperature history of petroleum coke particles in incipiently gas-fluidized beds," *Fuel*, vol. 74, no. 1, pp. 12–16, 1995.
- [161] Tognotti L., Longwell J.P., Sarofim A.F., "The products of the high temperature oxidation of a single char particle in an electrodynamic balance," *Symposium (International) on Combustion*, vol. 23, no. 1, pp. 1207–1213, 1991.
- [162] Monson C.R., Germane G.J., Blackham A.U., Smoot L.D., "Char oxidation at elevated pressures," *Combustion and Flame*, vol. 100, no. 4, pp. 669–683, 1995.
- [163] Evans D.D., Emmons H.W., "Combustion of wood charcoal," *Fire Safety Journal*, vol. 1, no. 1, pp. 57–66, 1977.
- [164] Pedersen K., "The product ratio of co/co<sub>2</sub> in the oxidation of biomass char," 2003. MSc thesis, Technical University of Denmark, Denmark.
- [165] Bhagat P.M., "Wood charcoal combustion and the effects of water application," *Combustion and Flame*, vol. 37, no. 0, pp. 275–291, 1980.
- [166] Hayhurst A.N., Parmar M.S., "Does solid carbon burn in oxygen to give the gaseous intermediate co or produce co<sub>2</sub> directly? some experiments in a hot bed of sand fluidized by air," *Chemical Engineering Science*, vol. 53, no. 3, pp. 427–438, 1998.
- [167] Kulasekaran S., Linjewile T.M., Agarwal P.K., Biggs M.J., "Combustion of a porous char particle in an incipiently fluidized bed," *Fuel*, vol. 77, no. 14, pp. 1549–1560, 1998.
- [168] Linjewile T.M., Gururajan V.S., Agarwal P.K., "The co/co<sub>2</sub> product ratio from the combustion of single petroleum coke spheres in an



- incipiently fluidized bed,” *Chemical Engineering Science*, vol. 50, no. 12, pp. 1881–1888, 1995.
- [169] Biggs M.J., Agarwal P.K., “The co/co<sub>2</sub> product ratio for a porous char particle within an incipiently fluidized bed: A numerical study,” *Chemical Engineering Science*, vol. 52, no. 6, pp. 941–952, 1997.
- [170] Wang F.Y., Bhatia S.K., “A generalised dynamic model for char particle gasification with structure evolution and peripheral fragmentation,” *Chemical Engineering Science*, vol. 56, no. 12, pp. 3683–3697, 2001.
- [171] Prins W., *Fluidised bed combustion of a single carbon particle*. PhD thesis, University of Twente, The Netherlands, 1987.
- [172] Lu H., *Experimental and modelling investigation of biomass particle combustion*. PhD thesis, Brigham Young University, USA, 2006.
- [173] Lu H., Ip E., Scott J., Foster P., Vickers M., Baxter L.L., “Effects of particle shape and size on devolatilization of biomass particle,” *Fuel*, vol. 89, no. 5, pp. 1156–1168, 2010.
- [174] Ha M.Y. , Choi B. R., “A numerical study on the combustion of a single carbon particle entrained in a steady flow,” *Combustion and Flame*, vol. 97, no. 1, pp. 1–16, 1994. cited By (since 1996) 16.
- [175] Džiugys A., Peters B., “An approach to simulate the motion of spherical and non-spherical fuel particles in combustion chambers,” *Granular Matter*, vol. 3, no. 4, pp. 231–265, 2001.
- [176] Cundall P.A., Strack O.D.L., “Discrete numerical model for granular assemblies,” *Geotechnique*, vol. 29, no. 1, pp. 47–65, 1979. cited By (since 1996) 3370.
- [177] Hoomans B.P.B., Kuipers J.A.M., Briels W.J., Van Swaaij W.P.M., “Discrete particle simulation of bubble and slug formation in a two-dimensional gas-fluidised bed: A hard-sphere approach,” *Chemical Engineering Science*, vol. 51, no. 1, pp. 99–118, 1996.

- [178] Gidaspow D., *Multiphase flow and fluidization*. Boston: Academic Press, 1994.
- [179] Lun C.K.K., Savage S.B., Jeffrey D.J., Chepuruiy N., “Kinetic theories for granular flow: inelastic particles in couette flow and slightly inelastic particles in a general flowfield,” *Journal of Fluid Mechanics*, vol. 140, pp. 223–256, 1984. cited By (since 1996) 857.
- [180] Syamlal M., Rogers W., O’Brien T. J., “Mfix documentation: Theory guide,” tech. rep., U.S. Department of Energy, Morgantown Energy Technology Center, 1993.
- [181] Gidaspow D., Bezburuah R., Ding J., “Hydrodynamics of circulating fluidized beds, kinetic theory approach,” in *Fluidization VII* (Porter O. E., Nicklin D. J., ed.), pp. 75–82, New York: Engineering Foundation, 1992.
- [182] Ding J., Gidaspow D., “Bubbling fluidization model using kinetic theory of granular flow,” *AIChE Journal*, vol. 36, no. 4, pp. 523–538, 1990.
- [183] Agrawal K., Loezos P.N., Syamlal M., Sundaresan S., “The role of meso-scale structures in rapid gas-solid flows,” *Journal of Fluid Mechanics*, vol. 445, pp. 151–181, 2001.
- [184] Hjertager B.H., Solberg T., Ibsen C.H., Hansen K.G., “Multi-fluid CFD modelling of fluidized bed reactors,” *International Journal of Chemical Reactor Engineering*, vol. 2, 2004.
- [185] Wang W., Lu B., Zhang N., Shi Z., Li J., “A review of multiscale CFD for gas-solid CFB modeling,” *International Journal of Multiphase Flow*, vol. 36, no. 2, pp. 109–118, 2010.
- [186] Taghipour F., Ellis N., Wong C., “Experimental and computational study of gas-solid fluidized bed hydrodynamics,” *Chemical Engineering Science*, vol. 60, no. 24, pp. 6857–6867, 2005.

- [187] Wang S., Lu H., Li X., Yu L., Ding J., Zhao Y., “CFD simulations of bubbling beds of rough spheres,” *Chemical Engineering Science*, vol. 63, no. 23, pp. 5653–5662, 2008.
- [188] Popoff B., Braun M., “A lagrangian approach to dense particulate flows,” in *Proceedings of the 6<sup>th</sup> International Conference on Multiphase Flow (ICMF)*, (Leipzig, Germany), July 9 - 13 2007.
- [189] Ng B.H., Ding Y.L., Ghadiri M., “Modelling of dense and complex granular flow in high shear mixer granulator - A CFD approach,” *Chemical Engineering Science*, vol. 64, no. 16, pp. 3622–3632, 2009.
- [190] Botterill J.S.M., Salway A.G., Teoman Y., “The effective thermal conductivity of high temperature particulate beds. experimental determination,” *International Journal of Heat and Mass Transfer*, vol. 32, no. 3, pp. 585 – 593, 1989.
- [191] Achenbach E., “Heat and flow characteristics of packed beds,” *Experimental Thermal and Fluid Science*, vol. 10, no. 1, pp. 17–27, 1995.
- [192] Inaba H., Fukuda T., “Transient heat transfer behaviors in cylindrical porous beds at relatively large reynolds numbers,” *Wärme- und Stoffübertragung*, vol. 18, pp. 109–116, 1984.
- [193] Inaba H., Fukuda T., Saito H., Mayinger F., “Transient behavior of heat removal from a cylindrical heat storage vessel packed with spherical porous particles,” *Wärme- und Stoffübertragung*, vol. 22, pp. 325–333, 1988.
- [194] Khan J.A., Beasley D.E., Alatas B., “Evaporation from a packed bed of porous particles into superheated vapor,” *International Journal of Heat and Mass Transfer*, vol. 34, no. 1, pp. 267–280, 1991.
- [195] Gupta S.N., Chaube R.B., Upadhyay S.N., “Fluid-particle heat transfer in fixed and fluidized beds,” *Chemical Engineering Science*, vol. 29, no. 3, pp. 839–843, 1974.

- [196] Resnick H., *Simultaneous heat and mass transfer in a diffusion-controlled chemical reaction*. PhD thesis, MIT, USA, 1952.
- [197] Wakao N., Kaguei S., Funazkri T., “Effect of fluid dispersion coefficients on particle-to-fluid heat transfer coefficients in packed beds. correlation of nusselt numbers,” *Chemical Engineering Science*, vol. 34, no. 3, pp. 325–336, 1979.
- [198] Eckert E.R.G., Drake R.M.J., *Heat and Mass Transfer*. New York: McGraw-Hill, 1959.
- [199] Collier A.R., Hayhurst A.N., Richardson J.L., Scott S.A., “The heat transfer coefficient between a particle and a bed (packed or fluidised) of much larger particles,” *Chemical Engineering Science*, vol. 59, no. 21, pp. 4613–4620, 2004.
- [200] Denton W. H., “The heat transfer and flow resistance for fluid flow through randomly packed spheres,” in *The General Discussion on Heat Transfer*, pp. 370–373, Institute of Mechanical Engineers and ASME: London, 1951.
- [201] Scott S.A., Davidson J.F., Dennis J.S., Hayhurst A.N., “Heat transfer to a single sphere immersed in beds of particles supplied by gas at rates above and below minimum fluidization,” *Industrial and Engineering Chemistry Research*, vol. 43, no. 18, pp. 5632–5644, 2004.
- [202] Gnielinski V., “Gleichungen zur berechnung des wärme- und stoffaustausches in durchströmten ruhenden kugelschüttungen bei mittleren und grossen pecletzahlen,” *Verfahrenstechnik*, vol. 12, no. 6, pp. 363–366, 1978.
- [203] Martin H., “Low peclet number particle-to-fluid heat and mass transfer in packed beds,” *Chemical Engineering Science*, vol. 33, no. 7, pp. 913 – 919, 1978.

- [204] Zhou Z.Y., Yu A.B., Zulli P., “Particle scale study of heat transfer in packed and bubbling fluidized beds,” *AIChE Journal*, vol. 55, no. 4, pp. 868–884, 2009.
- [205] Bowman C.T., Hanson R.K., Davidson D.F., Gardiner W.C., Lissianski V., Smith G.P., Golden D.M., Frenklach M., Goldenberg M., “GRI-Mech 2.11.” [http://www.me.berkeley.edu/gri\\_mech/](http://www.me.berkeley.edu/gri_mech/).
- [206] Kazakov A., Frenklach M., “DRM22.” <http://www.me.berkeley.edu/drm/>.
- [207] Kilpinen P. available on address: [pia.kilpinen@uku.fi](mailto:pia.kilpinen@uku.fi) or [pia.kilpinen@abo.fi](mailto:pia.kilpinen@abo.fi).
- [208] Zahirovic S., Scharler R., Kilpinen P., Obernberger I., “A kinetic study on the potential of a hybrid reaction mechanism for prediction of nox formation in biomass grate furnaces,” *Combustion Theory and Modelling*, vol. 15, no. 5, pp. 645–670, 2011.
- [209] Gaur S., Reed TB., “An atlas of thermal data for biomass and other fuels.” <http://www.osti.gov/energycitations/servlets/purl/82384-DuRSmv/webviewable/82384.pdf>. National Renewable Energy Laboratory, USA.
- [210] Koufopoulos C.A. Papayannakos N., Maschio G., Lucchesi A., “Modelling of the pyrolysis of biomass particles. studies on kinetics, thermal and heat transfer effects,” *Canadian Journal of Chemical Engineering*, vol. 69, no. 4, pp. 907–915, 1991.
- [211] W. Park, A. Atreya, and H. Baum, “Experimental and theoretical investigation of heat and mass transfer processes during wood pyrolysis,” *Combustion and Flame*, vol. 157, no. 3, pp. 481–494, 2010.

# Paper I

Contents lists available at [SciVerse ScienceDirect](http://www.sciencedirect.com)

# Fuel Processing Technology

journal homepage: [www.elsevier.com/locate/fuproc](http://www.elsevier.com/locate/fuproc)

## A CFD model for thermal conversion of thermally thick biomass particles

Ramin Mehrabian<sup>a,b,\*</sup>, Selma Zahirovic<sup>a,b,c</sup>, Robert Scharler<sup>a,b,c</sup>, Ingwald Obernberger<sup>a,b,c</sup>, Stefan Kleditzsch<sup>d</sup>, Siegmart Wirtz<sup>e</sup>, Viktor Scherer<sup>e</sup>, Hong Lu<sup>f</sup>, Larry L. Baxter<sup>f</sup>

<sup>a</sup> BIOENERGY 2020+ GmbH, Inffeldgasse 21b, 8010 Graz, Austria

<sup>b</sup> Institute for Process and Particle Engineering, Graz University of Technology, Inffeldgasse 21b, 8010 Graz, Austria

<sup>c</sup> BIOS BIOENERGIESYSTEME GmbH, Inffeldgasse 21b, 8010 Graz, Austria

<sup>d</sup> ANSYS Germany GmbH, Birkenweg 14a, 64295 Darmstadt, Germany

<sup>e</sup> Department of Energy Plant Technology, Ruhr-Universität Bochum, Universitätsstrasse 150, D-44780 Bochum, Germany

<sup>f</sup> Department of Chemical Engineering, Brigham Young University, 350 CB, Provo, UT 84602, USA

### ARTICLE INFO

#### Article history:

Received 12 August 2011

Received in revised form 24 November 2011

Accepted 25 November 2011

Available online xxxx

#### Keywords:

Biomass  
Thermal conversion  
Thermally thick  
Modelling  
CFD

### ABSTRACT

A one-dimensional model for the thermal conversion of thermally thick biomass particles is developed for the simulation of the fuel bed of biomass grate furnaces. The model can be applied for cylindrical and spherical particles. The particle is divided into four layers corresponding to the main stages of biomass thermal conversion. The energy and mass conservation equations are solved for each layer. The reactions are assigned to the boundaries. The model can predict the intra-particle temperature gradient, the particle mass loss rate as well as the time-dependent variations of particle size and density, as the most essential features of particle thermal conversion. When simulating the fuel bed of a biomass grate furnace, the particle model has to be numerically efficient. By reducing the number of variables and considering the lowest possible number of grid points inside the particle, a reasonable calculation time of less than 1 min for each particle is achieved. Comparisons between the results predicted by the model and by the measurements have been performed for different particle sizes, shapes and moisture contents during the pyrolysis and combustion in a single-particle reactor. The results of the model are in good agreement with experimental data which implies that the simplifications do not impair the model accuracy.

© 2011 Elsevier B.V. All rights reserved.

### 1. Introduction

During the last two decades, the share of energy production by biomass combustion/gasification plants gradually increased, because biomass is a CO<sub>2</sub> neutral source of energy in a sustainable agriculture/forestry. Biomass grate furnaces are the most relevant biomass combustion technology for small- and medium-scale applications. The thermal conversion of biomass in grate furnaces occurs in a packed bed and the combustible volatiles burn in the combustion chamber. The optimisation of biomass grate furnaces is ongoing to improve the efficiency and further reduce emissions. In this respect it is very important to gain detailed information about the combustion process in the furnace and on the grate.

Computational fluid dynamics (CFD) are an efficient tool for the design and optimisation of biomass grate furnaces. They proved to be valuable to predict the flow field as well as the gas phase combustion. At present, however, simulating the packed bed combustion with reasonable accuracy and computational costs is difficult. Moreover, the existing bed models resolve the packed bed combustion separately

from the gas phase above it and produce heat and mass release profiles which serve as boundary conditions for gas phase simulation by a CFD code. Therefore, developing an appropriate particle model which can be coupled with available CFD tools is necessary in order to directly link the bed model with the gas phase combustion models and to simultaneously perform the simulation of the entire biomass grate furnace.

A combination of several sub-processes such as heat-up, drying, pyrolysis and char burnout represents the global process of thermo-chemical conversion of solid biomass particles. Depending on the size and physical properties of biomass particles, temperature and species gradients may develop inside the particles causing intra-particle transport processes. The group of particles with distinct gradient development and simultaneous progress of different conversion stages is called thermally thick. On the contrary, in case of thermally thin particles no gradients are present inside the particle and the conversion stages take place sequentially.

Several studies have been performed to describe the thermal conversion of a thermally thick biomass particle. Peters [1] and Bruch et al. [2] resolved the temperature and gas species inside the particle by solving a set of one-dimensional transient conservation equations for energy and mass of gaseous and solid phases inside the particle. They assumed the particle as sphere and neglected the char gasification reactions. Experimental mass loss profiles were utilised to validate the single particle model. Wurzenberger et al. [3] proposed

\* Corresponding author. Tel.: +43 316 8739232; fax: +43 316 8739202.  
E-mail address: [ramin.mehrabian@bioenergy2020.eu](mailto:ramin.mehrabian@bioenergy2020.eu) (R. Mehrabian).

another one-dimensional model for spherical particles. They solved the continuity equations of the gas phase in the particle pores, pressure change, species conservation equations and the energy balance in the radial direction. They applied the particle model to simulate an entire biomass packed bed with a 1-D bed model. The bed is assumed as a porous media and only the gradients in the primary air flow direction were considered. Experiments with single particles were used to evaluate the single particle model. They concluded that for a good agreement with experimental data, 20 grid points are needed for discretisation of a particle. This number of grids and solving several equations increased the computation time to several minutes for the simulation of a single particle. A simple approach has been proposed by Thunman et al. [4]. They resolved the temperature gradients inside a thermally thick particle by discretising the particle into four computational cells. Each cell corresponds to a stage of the biomass conversion process. They calculated the drying, pyrolysis, and combustion rates by a simple model for each sub-process. Additionally, Porteiro et al. [5,6] attempted to describe the thermal degradation of biomass particles. They used the Thunman discretisation scheme to treat a cylindrical particle with a one-dimensional model. However, they had to increase the number of grid points to achieve acceptable resolutions. The model validation was performed by using the reported experimental data in literatures, but they did not report the validity of the model regarding temperature predictions under combustion conditions. Recently, a comprehensive model that provides descriptions of particle mass and temperature changes for a single particle during combustion has been proposed by Lu et al. [7,8]. They investigated the influence of particle shape and size on biomass degradation [9]. They solved a set of one-dimensional equations, including the mass conservation equation for each species, 12 species, the momentum equation for the gas phase within the particle pores and the total energy equation. The particles can be geometrically represented as an infinite plate, an infinite cylinder or a sphere.

The aim of this work is to develop a model for the thermal conversion of thermally thick particles which can be used for the simulation of biomass grate furnaces. It means that it has to be numerically efficient with reasonable accuracy. Additionally, it has to be implemented in a CFD environment, in order to directly integrate the packed bed modelling into the available CFD tools for the simulations of turbulent reactive flow in combustion chambers of furnaces. For these purposes, the model uses a comparably small number of governing equations to describe the most essential characteristics of the thermal conversion of thermally thick biomass particles. The concept of layers is applied to discretise the biomass particle with the lowest possible number of layers (four) to fasten the numerical calculations. The particle model is programed in C/C++ and coupled to ANSYS FLUENT to simultaneously resolve the thermal conversion of the particles and the surrounding gases. The comparisons with experimental data have been performed under varying conditions and particle geometries. They indicate that despite the simplifications of the model, the results are in good agreement with the measurements. Additionally, a feasible calculation time has been achieved – less than 1 min for a single particle simulation – in order to make the application of the model in biomass grate furnace simulations possible.

## 2. Layer model

The layer model is proposed to account for intra-particle transport processes and simultaneous sub-processes of the thermal conversion of thermally thick solid biomass particles. The layer model treats the typical particle shapes (sphere and finite cylinders) of biomass in one dimension. The description of the particle thermal conversion with one-dimensional models is a usual simplification assumption to reduce the model complexities and calculation time [1–9]. The validity of this assumption was already addressed by Ha and Choi [10].

In order to apply the one-dimensional governing equations for the finite cylinder geometry, the Thunman approach [4] was selected to discretise the particles. This approach assumes that the particle boundary conditions are homogeneous and every point at a certain axial or radial distance from the particle surface has the same temperature and conversion state, see Fig. 1.

In the layer model the particle is divided into four layers, which correspond to the fuel conversion stages: wet fuel, dry fuel, char, and ash. Consequently, the boundaries between the layers are related to the conversion sub-processes drying, pyrolysis, and char burnout fronts, as illustrated in Fig. 1. The thickness of each layer is determined by the amount of wet fuel, dry fuel, char and ash in each time step and assuming a constant density for each layer. As the conversion proceeds the mass of each layer changes and boundaries move towards the particle centre. Therefore, the particle size and density vary during the thermal conversion.

The conservation equation of thermal energy is [11]:

$$\frac{\partial}{\partial t} \rho H = -\nabla \cdot \rho v H - \nabla \cdot q \quad (1)$$

where the left hand side of the equation is the accumulation rate of enthalpy per unit volume, the first term on the right hand side is the rate of enthalpy change by advection per unit volume and the second term represents the contribution of the conductive heat transfer per unit volume. The advection term in this equation can be interpreted as the energy transfer in/from each layer when the boundaries move towards the centre of the particle.

The internal energy equation is discretised into four layers by setting a temperature for every boundary and layer. In order to simplify the equation, the thermal energy per unit volume is replaced by the thermal energy of each layer, therefore the thermal energy balance of layer  $i$  is:

$$\frac{\partial}{\partial t} \sum_c m_{c,L_i} H_{c,L_i} = \sum_{c=in} \dot{m}_{c,B_{(i-1)}} H_{c,B_{(i-1)}} - \sum_{c=out} \dot{m}_{c,B_i} H_{c,B_i} + k_{L_i} \Delta x_{0,L_i} (T_{B_{(i-1)}} - T_{L_i}) - k_{L_i} \Delta x_{1,L_i} (T_{L_i} - T_{B_i}) \quad (2)$$

where  $\sum_c$  is the summation over all components (solid and gas) of the layer,  $\sum_{c=in}$  represents the summation over all components which enter the layer from the previous boundary and  $\sum_{c=out}$  is the summation over all components which leave the layer to the next boundary.  $m_{c,L_i}$

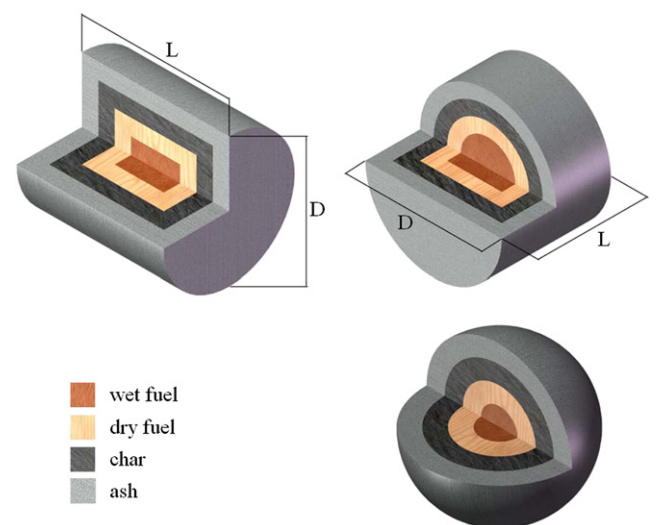


Fig. 1. Discretisation scheme for spherical and cylindrical particles with length (L) longer and shorter than the diameter (D).



and  $H_{c,L_i}$  are the mass and specific enthalpy of each component present in the layer  $L_i$ , respectively.  $\dot{m}_{c,B_i}$  and  $H_{c,B_i}$  are the mass flow rate and specific enthalpy of each component at the boundary  $B_i$ , respectively.  $K_{L_i}$  is the thermal conductivity of the layer  $L_i$ .  $\Delta x_{0,L_i}$  is the ratio of the area of the boundary  $B_{i-1}$  to half of the layer  $L_i$  thickness.  $\Delta x_{1,L_i}$  is the ratio of the area of the boundary  $B_i$  to half of the layer  $L_i$  thickness. Additionally,  $T_{L_i}$  and  $T_{B_i}$  are the temperature at the centre of the layer  $L_i$  and the temperature of the boundary  $B_i$ , respectively.

The conservation of mass of each layer reads:

$$\frac{\partial}{\partial t} \sum_c m_{c,L_i} = \sum_{c=in} \dot{m}_{c,B_{i-1}} - \sum_{c=out} \dot{m}_{c,B_i} \quad (3)$$

substituting Eq. (3) and  $dH = c_p dT$  into Eq. (2):

$$\sum_c (m_{c,L_i}, c_{p,c}) \frac{dT_{L_i}}{dt} = \sum_{c=in} [\dot{m}_{c,B_{i-1}} (H_{c,B_{i-1}} - H_{c,L_i})] - \sum_{c=out} [\dot{m}_{c,B_i} (H_{c,L_i} - H_{c,B_i})] + k_{L_i} \Delta x_{0,L_i} (T_{B_{i-1}} - T_{L_i}) - k_{L_i} \Delta x_{1,L_i} (T_{L_i} - T_{B_i}). \quad (4)$$

The enthalpy of each component at every layer or boundary is calculated by:

$$H_c(T) = \Delta H_{f,c}^0 + \int_{T_{ref}}^T c_{p,c} dT. \quad (5)$$

The boundary temperatures are calculated by writing the energy balance for each boundary:

$$k_{L_i} \Delta x_{1,L_i} (T_{L_i} - T_{B_i}) - k_{L_{i+1}} x_{0,L_{i+1}} (T_{B_i} - T_{L_{i+1}}) = \sum_{c=in} \dot{m}_{c,B_i} H_{c,B_i} - \sum_{c=out} \dot{m}_{c,B_i} H_{c,B_i}. \quad (6)$$

Since the reactions are assigned to the boundaries, the components which enter a certain boundary might be different from the components which leave that boundary. Hence, the right hand side of Eq. (6) represents the enthalpy difference between products and reactants of the reactions, i.e. the enthalpies of reactions. The reaction rates,  $\dot{m}_r$ , and stoichiometric coefficients of reactions,  $\eta_{r,c}$ , determine the mass flow rate of each component from one layer over the boundary into the next layer, which implicitly determines the velocity of each boundary towards the particle centre:

$$\dot{m}_{c,B_i} = \sum_r \dot{m}_r \eta_{r,c} \quad (7)$$

where  $\sum_r$  is the summation over all reactions of boundary  $i$ .

### 2.1. Drying model

There are different models in literature available to calculate the evaporation rate during fast drying. They can be sorted into three groups: thermal models, equilibrium models and kinetic rate models. The kinetic rate models consider the drying as a heterogeneous reaction and use an Arrhenius equation to calculate its rate [4,12–14]. The pre-exponential factor and activation energy are set so that the drying rate has a large increase at 373.15 K. This model shows the advantages of easy implementation and numerical stability. However, it is difficult to apply the given kinetic data to conditions different from those for which the data have been derived. The equilibrium models are based on the hypothesis that the liquid water and the water vapour in the gas phase are in thermodynamic equilibrium. Thus, the drying rate is proportional to the difference of the equilibrium concentration and the current vapour concentration in the gas phase. The equilibrium assumption is usual in low-temperature drying models [15], therefore the mass transfer coefficient, which is highly

depending on the particle permeability, needs to be adjusted with experimental data gained under fast drying conditions [3,16]. The thermal models are the most often used ones in literature [2,5,6,17–25]. This model is based on the assumption that drying occurs at a fixed boiling temperature (373.15 K). Therefore, any amount of heat flow above this temperature is consumed by the drying process. Indeed, drying acts as a heat sink.

In this paper the thermal model which was adapted to the layer model structure is used. The drying zone is reduced to an infinitely thin moving front which forms the boundary between the wet fuel and the dry fuel layers (see Fig. 1). The front separates the centre of the particle which retains its initial moisture and the outside region where the moisture content is zero. Such a steep drying front for the fast drying of biomass is reported almost by all drying models [26]. However, an infinitely thin drying front may not be acceptable for small particles, where the width of the drying zone is not negligible compared to the particle size. This does not affect the presented model, because the layer model is developed to apply for thermally thick particles.

In the layer model it is also presumed that there is no intra-particle flow resistance. Therefore the water vapour instantaneously leaves the particle. However, the enthalpy change of each layer by advection of gaseous species is considered (the first and second terms on the right hand side of Eq. (2)). The drying rate is then completely controlled by the heat transfer. In accordance to the model assumptions, if the temperature of boundary zero,  $T_{B_0}$ , is equal or bigger than the boiling temperature, the time derivative term in the energy equation is set to zero and the total heat flux which reaches the boundary is used to raise the temperature of the moist wood from  $T_{L_0}$  to  $T_{B_0}$  and to evaporate the water:

$$k_{L_1} \Delta x_{0,L_1} (T_{L_1} - T_{B_0}) = R_{dr} (H_{wv,B_0} - H_{wl,L_0}) + \alpha R_{dr} (H_{df,B_0} - H_{df,L_0}) \quad (8)$$

where  $R_{dr}$  is the drying rate.  $H_{wv,B_0}$  and  $H_{wl,L_0}$  are the specific enthalpy of water vapour at the boundary  $B_0$  and of liquid water at the layer  $L_0$ .  $H_{df,B_0}$  and  $H_{df,L_0}$  are the specific enthalpy of dry fuel at the boundary  $B_0$  and at the layer  $L_0$ , respectively. Additionally,

$$\alpha = \frac{1 - MC}{MC} \quad (9)$$

where  $MC$  is the moisture content related to wet base.

The size of woody biomass changes as it gains or loses moisture. It shrinks when losing the bound water from solid structure and swells when gaining moisture in the solid structure. The free water has a negligible effect on the dimension, it only changes density. Since particle shrinkage during drying is much lower compared to the shrinkage occurring during pyrolysis and charcoal combustion [27], it is postulated that during drying, the size of the particle remains constant and its density decreases. However, during pyrolysis and char burnout, both shrinkage and change of density are considered in the layer model.

### 2.2. Pyrolysis model

Extensive surveys of pyrolysis models are available in literature [28–31]. The studies dealt with particle modelling, generally, use the one-component mechanism, proposed by Shafizadeh and Chin [32]. This model is based on three parallel reactions for the formation of gas, tar and char. The kinetic constants have to be determined experimentally and usually empirical data obtained by Chan et al. [12], Thurner and Mann [33], and Wagenaar et al. [34] are used. The advantage of implementing a one-component pyrolysis mechanism into particle conversion models is that both product yield and decomposition rate can be predicted. However, simplifying biomass fuels as one-component, produces inaccuracies in the results. The dependency of the product yields on temperature, specially the char yield, is not well predicted in this model [28,35]. Moreover, the one-component

mechanism fails to describe thermogravimetric curves of biomass pyrolysis, at least regarding the correct prediction of conversion time and the maximum pyrolysis rate [36].

In the present work, biomass pyrolysis is described in terms of decomposition of its three major components: hemicellulose, cellulose, and lignin. This model implicitly assumes the hypothesis of an independent decomposition of these three constituents. An Arrhenius equation is used to describe the pyrolysis of each major component. The kinetic parameters are determined by fitting to experimental results (e.g. TGA) concerning the mass loss rate versus temperature. The analysis of experimental data shows that the decomposition of hemicellulose and cellulose are associated with the shoulder and the peak of the mass loss curves, respectively. Lignin decomposes slowly over a broad range of temperature and forms the tail of the mass loss curves in the high temperature region.

In addition to kinetic constants, the mass shares of these components in a specific biomass fuel have to be determined in the three-component model. They also estimated like the kinetic parameters by fitting to experimental results. Assuming first-order reactions in respect to mass fraction for the decomposition of each major component leads to the following equations for the mass loss of a particle during pyrolysis:

$$\frac{dm_{df}}{dt} = - \sum_{i=1}^3 R_i \quad (10)$$

$$R_i = A_i \exp\left(\frac{-E_i}{RT}\right) a_i m_{df} \quad (11)$$

This model was subject to extensive experimental validation and the predictions from this model comply with the experimental thermogravimetric curves during the pyrolysis of several biomass fuels [37–43].

Several studies investigated the effect of heating rates on the characteristics of thermogravimetric curves, for example see [31,36–38]. They indicated that by increasing the heating rate the pyrolysis reactions take place at higher temperatures. Moreover, the hemicellulose shoulder and lignin tail become less visible, therefore the overlap between the pyrolysis of the three major biomass components increases. This means that the kinetic parameters and the mass fractions of the components obtained by the slow heating rate experiments (i.e. typically below 50 K/min) are not valid for fast heating rate conditions. Hence, a database for the empirical constants needed in the pyrolysis model was prepared from the fast heating rate experiments reported in literature. It was linked to the layer model and depending on the fuel type applied, the layer model chooses the proper values.

The three-component mechanism describes the pyrolysis rate, but the product yields cannot be predicted. As already mentioned, the one-component mechanism also cannot correctly predict the product yields, especially for large particles, because the final yield depends on temperature and there are great temperature differences occurring inside a large particle. Therefore, the final char yield should be defined according to measurements performed (if possible) or using available empirical correlations such as the one proposed by Saastamoinen and Richard [24]. Since the empirical correlations have been obtained under specified conditions, here, the result of the biomass proximate analysis is used to determine the product yields.

The volatile yield from pyrolysis includes a complex mixture and several hydrocarbons have been found in it [44,45]. Numerous factors affect the pyrolysis product distribution. Temperature, heating rate, residence time, reactor geometry, and pressure as well as chemical and physical properties of biomass are the chief parameters. This complex mixture mainly consists of CO, CO<sub>2</sub>, H<sub>2</sub>O, H<sub>2</sub>, light hydrocarbons and heavy hydrocarbons (tar) [46]. To simplify the combustion behaviour of the volatiles, the light and heavy hydrocarbons are lumped together and the chemical and physical properties of methane are assigned to this lumped hydrocarbon. The mass fraction of

each species, following the work of Thunman [46], is determined by closure of the elemental and energy balances. Since the residence time of the volatiles inside the particle is too short, the homogeneous reactions of the volatile components in the particle pores are neglected. The homogeneous reactions of the volatiles around the particle are considered as it is explained in Section 3. Therefore, the reaction enthalpies of the homogeneous reactions implicitly raise the particle temperature by radiation and convection. The heterogeneous reactions of CO<sub>2</sub>, H<sub>2</sub>O, and H<sub>2</sub>, while they are crossing the char layer, are considered as explained in the next section.

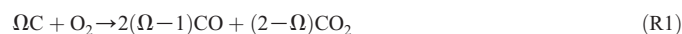
### 2.3. Char conversion model

Char conversion models are more complicated than biomass pyrolysis models, as they are heterogeneous reactions for which both intrinsic kinetic and transport phenomena are important. As the char conversion proceeds, depending on the char type and operating conditions, the density and/or size of the char particle decreases due to the mass loss. The classical uniform char conversion model assumes that the reaction occurs uniformly throughout the entire particle and temperature and species fields inside the particle are flat. The reaction rate in this model can be evaluated by the char intrinsic reactivity, this model is applicable for low temperature or low rate reactions [47].

Apart from the classical model, the char models based on reaction place can be classified into surface reaction models and zone reaction models. In the surface reaction models the reaction is fast and it occurs at a surface, as soon as the reactant gas reaches the reaction surface. As the reactions proceed, the reaction surface moves towards the centre of the particle. In this case the reaction rates are correlated to the area of the reaction surface. In the zone reaction models, the reactions take place in a region inside the particle which grows and travels inwards the particle during the conversion [47–49]. Therefore the reaction rates are a function of available contact area in the reaction zone.

Additionally, based on the ash behaviour, two different char conversion models can be distinguished. The ash remaining from the char conversion may leave the particle as soon as it is produced or it can build up an additional layer surrounding the char particle. The former case is called shrinking particle and the later shrinking core. In the shrinking particle models, the particle size change is proportional to the conversion rate. However, in the shrinking core models, the particle size is related to the char conversion and also ash density and porosity. Furthermore, in the shrinking core models, the ash layer increases the resistance to mass and heat transfer.

It has been experimentally verified that the char combustion is such a rapid reaction that it occurs in a very thin layer [48]. Additionally, since the surface reaction models are more compatible with the structure of the layer model, the char conversion reactions are assumed to occur at the interface between char and ash layer. The char oxidation with O<sub>2</sub> and gasification with CO<sub>2</sub>, H<sub>2</sub>O and H<sub>2</sub> are considered as the char conversion reactions:



The reaction of char with oxygen is much faster than char gasifications with carbon dioxide, water vapour and hydrogen for most of the practical applications [48,50]. Hence, where the oxygen is depleted, these gasification reactions become important. The fundamental kinetic analysis of carbonaceous solid conversion can be found in [50,51].

Apart from kinetics of the reactions, they always involve a mass transport rate because the process of a heterogeneous reaction may be divided into the following steps:

- i. transport of oxidising/gasifying agent to the particle surface
- ii. diffusion through the ash layer
- iii. adsorption on the reaction surface
- iv. chemical reaction
- v. desorption of products from the surface
- vi. diffusion of products through the ash layer
- vii. transport of products from the particle surface back to the ambient.

Except the chemical reaction, the remaining are mass transport steps. Hence, two main regimes can be introduced in char conversion [50]: the kinetic controlled regime for low temperatures and so small char particles that the mass transport rate is much faster than the chemical reaction, and the transport controlled regime for high temperatures and bigger particles, where the intra-particle and/or external mass transfer rates become lower than the kinetic rate of the chemical reaction, leading to a limited penetration of gas species into the char particle.

In this work, the rate of char conversion reactions is a function of both kinetic rate at the reaction surface and mass transfer rate to/from the reaction surface. Assuming a global reaction rate of order one with respect to the concentration of oxidising/gasifying agent, leads to the char conversion rate as:

$$\frac{dm_{ch}}{dt} = - \sum_{i=1}^4 \frac{\Omega_i M_c}{\frac{1}{k_{c,i} A_{B_2}} + \frac{1}{h_m A_{B_3}} + \frac{1}{D_e} \int_{r_{B_3}}^{r_{B_2}} \frac{dr}{A(r)}} X_{\infty,i} \quad (12)$$

where  $i = 1$  to 4 corresponds to reactions R1–R4, respectively.  $\Omega_i$  is the stoichiometric ratio of moles of carbon per mole of oxidising/gasifying agent in the corresponding reaction.  $M_c$ ,  $A$ ,  $k_{c,i}$ ,  $h_m$  and  $X_{\infty,i}$  are the carbon molecular weight, the surface area, the constant rate of reaction  $i$ , the mass transfer coefficient and the molar concentration of oxidising/gasifying agent of reaction  $i$  at the bulk flow, respectively. The reaction rate constants of reactions R1–R4,  $k_{c,i}$ , are listed in Table 1.  $D_e$  is the effective diffusivity of the ash layer, which depends on the ash porosity,  $\epsilon$ , the tortuosity,  $\tau$ , and the molecular diffusivity of the penetrating gaseous component,  $D_a$ :

$$D_e = \frac{\epsilon}{\tau} D_a \quad (13)$$

The tortuosity can be replaced by the inverse of the porosity, which is often a reasonable approximation [47,53]:

$$D_e = \epsilon^2 D_a \quad (14)$$

The molecular diffusivity of the reactive agent in the ash layer pores can be written as [8,47]:

$$\frac{1}{D_a} = \frac{1}{D_{ab}} + \frac{1}{D_{Ka}} \quad (15)$$

The binary diffusivity,  $D_{ab}$ , is calculated by the Chapman–Enskog kinetic theory [11]. For simplicity, the mixture in the ash layer pores is

assumed to be air and the binary diffusivity of the oxidising/gasifying agent in air is calculated. The Knudsen diffusivity is given by:

$$D_{Ka} = \frac{2}{3} d_{pore} \sqrt{\frac{2RT}{\pi M_a}} \quad (16)$$

where  $M_a$  is the molecular weight of the diffusing species and  $d_{pore}$  is the pore diameter. This equation was derived assuming random collisions of the gas molecules with the walls, which is reasonable when the pore size is larger than the molecular dimensions and much smaller in comparison with the mean free path [47].

The mass transfer coefficient of reactant species in the boundary layer around the particle,  $h_m$  in Eq. (12), is obtained by the Sherwood number:

$$Sh = \frac{h_m d_p}{D_{ab}} \quad (17)$$

There are several experimental and theoretical investigations to determine the Sherwood number for a reacting particle. Scala [54] investigated many of empirical/theoretical correlations available for Sherwood. He showed that almost all the theoretical correlations failed to predict a Sherwood number comparable to his experimental data of a freely moving active particle in the dense phase of a fluidised bed. However, a semi-empirical correlation proposed by Hayhurst and Parmar [55] among several empirical correlations excellently fits his experimental data. Hayhurst and Parmar measured the temperature of freely moving single graphite spheres and coal char particles during their combustion in a fluidised bed as well as outlet gas concentrations to calculate the burning rate. By estimating the CO/CO<sub>2</sub> ratio as combustion products, they suggested a Frössling-type expression:

$$Sh = 2\epsilon_{bed} + 0.69 (Re/\epsilon_{bed})^{1/2} Sc^{1/3} \quad (18)$$

where  $\epsilon_{bed}$  is the bed voidage.

It should be mentioned that this correlation for  $Sh$  holds for the case of equimolar counter diffusion, albeit in reactions R1–R4 the diffusion of reactants towards the reaction surface and of products away from it are not equimolar and even for the oxidation reaction, the molar flux of products is temperature dependent. Hayhurst [56], Paterson and Hayhurst [57] and Scala [58] proved that assuming CO as the only product of reaction R1, which represents the biggest deviation from equimolar counter diffusion condition, leads to an error less than 10%. If CO and CO<sub>2</sub> are considered as products, the error is even less. Therefore this error can be neglected in comparison to other uncertainties such as the determination of  $D_e$ , and experimental errors during the calculation of the Sherwood number [59].

The CO/CO<sub>2</sub> product ratio in reaction R1 has been the subject of many experimental and modelling studies, since it has a great effect on the particle temperature as well as the char oxidation rate. According to the work of Tognotti et al. [60] there is almost no doubt that both CO and CO<sub>2</sub> are primary products of char oxidation. They heated single char particles by laser irradiation and avoided CO oxidation to CO<sub>2</sub> in the particle boundary layer by maintaining the surrounding gas at room temperature. Their results clearly indicate that at high temperatures both CO and CO<sub>2</sub> are primary products of char oxidation.

Table 2 summarises empirical correlations for CO/CO<sub>2</sub> product ratios available in the literature so far. Measurement data have been correlated in all of them using an Arrhenius relation and the product ratio increases by temperature. Only Linjewile and Agarwal [67,68] reported a decrease in the product ratio at particle temperatures between 970 K and 1220 K. The product ratio has a local maximum of 0.5 at 970 K and decreases to 0.2 at 1220 K, at higher temperatures it increases again. The CO/CO<sub>2</sub> ratios obtained by correlations in Table 2 have little agreement. This is probably due to different types

**Table 1**  
Heterogeneous reaction rate constants (R1–R4).

$k_{c,R1} = 1.715^a \times T_{B_2} \exp(-9000^b/T_{B_2})$	[52]
$k_{c,R2} = k_{c,R3} = 3.42^a \times T_{B_2} \exp(-15600^b/T_{B_2})$	[52]
$k_{c,R4} = 3.42e^{-3} \times T_{B_2} \exp(-15600^b/T_{B_2})$	[52]

<sup>a</sup>[m.s<sup>-1</sup>.K<sup>-1</sup>].

<sup>b</sup>[K].

**Table 2**  
CO/CO<sub>2</sub> product ratios.

CO/CO <sub>2</sub>	Temperature (K)	Carbonaceous material	Size (mm)	Oxygen (vol.%)	Reference
$10^{3.4}e^{(-6240/T)}$	730–1170	Coal char, graphite	0.85–2.41	5–25	[61]
$1860e^{(-7200/T)}$	790–1690	Electrode carbon	Cylinders: 12.1 o.d., 8.3 i.d., 10 long	3–21	[62]
$170e^{(-3220/T)}$	800–950	Graphon	Fine particles	1–26	[63]
$25.7e^{(-2000/T)}$	770–920	Vitreous carbon		3–15	[64]
$8.5 \times 10^9 e^{(-33,200/T)}$	1500–1800	Coal char		6–12	[65]
$120e^{(-3200/T)}$	670–890	Soot particles		5–100	[66]
$1336e^{(-7643/T)}$	850–970				
$4.72 \times 10^{-3} e^{(4539/T)}$	970–1220	Petroleum coke	3–11	21	[67,68]
$12.41e^{(-5063/T)}$	850–970				
$94e^{(-2980/T)}$				5	
$70e^{(-3070/T)}$	670–1670	Spherocharb char	0.18–0.24	20	[60]
$50e^{(-3070/T)}$				100	
$3 \times 10^8 e^{(-33,237/T)}$	1400–2100	Utah coal char	0.07	5–21	[69]
$4.3e^{(-3390/T)}$	1000–1370	Wood charcoal	Cylinders: 27 o.d., 114 long	21	[70]
$12e^{(-3300/T)}$		Biomass charcoal			[71]

of fuels used which lead to different morphologies, porosities, pore sizes and internal surface areas. Moreover, different experimental procedures and conditions may be another parameter. The suggested correlations by Linjewile and Agarwal [67,68] and Evans and Emmons [70] are the only ones that have nearly the same values for CO/CO<sub>2</sub>, although Evans and Emmons [70] did not report two local extrema at 970 K and 1220 K.

The correlation of Evans and Emmons [70] has been selected in this study, because two independent measurements concede it. Furthermore, there are enough evidences, that show at high temperatures, approaching 1400 K, CO rapidly oxidises to CO<sub>2</sub> so close to the particle surface that it gives its heat of combustion to the particle [72–76]. Therefore the CO/CO<sub>2</sub> ratio at high temperatures should be one or even smaller than one as reported by several measurements [67,70,77,78]. Only the correlations of Linjewile and Agarwal [67,68] as well as of Evans and Emmons [70] are able to predict the acceptable CO/CO<sub>2</sub> ratio at high temperatures.

#### 2.4. Boundary conditions

The external surface of the particle exchanges heat and mass with the surroundings. The Neumann boundary condition of the energy equation, Eq. (4), at the particle surface with known emissivity,  $\epsilon_{rad}$ , and radiation,  $T_{rad}$ , as well as convection,  $T_{conv}$ , temperatures is:

$$-k_{L_3} \Delta x_{1,L_3} (T_{L_3} - T_{B_3}) = \epsilon_{rad} \sigma A_{B_3} (T_{rad}^4 - T_{B_3}^4) + h A_{B_3} (T_{conv} - T_{B_3}) \quad (19)$$

where  $\sigma$  is the Stefan–Boltzmann constant.  $h$  is the convective heat transfer coefficient and is determined by an appropriate correlation for the Nusselt number. For spherical particles the Ranz–Marshall correlation is used [79]:

$$Nu = 2.0 + 0.6 Re^{1/2} Pr^{1/3} \quad (20)$$

and for cylindrical particles the correlation proposed by Churchill and Bernstein is applied [79]:

$$Nu = 0.3 + \frac{0.62 Re^{1/2} Pr^{1/3}}{[1 + (0.4/Pr)^{2/3}]^{1/4}} \left[ 1 + \left( \frac{Re}{282000} \right)^{5/8} \right]^{4/5} \quad (21)$$

Additionally, the symmetry boundary condition is applied for the energy equation, at the particle centre which leads to zero heat flux. The boundary condition equations require some variables from the gas layer adjacent to the particle. They are the gas phase temperature and radiation temperature in Eq. (19), the gas phase velocity and

physical properties needed to calculate Re and Pr, as well as the species concentrations around the particle which are used in the char conversion model. By coupling the layer model with ANSYS FLUENT these variables are calculated in each time step by the gas phase simulation performed in ANSYS FLUENT and introduced to the layer model as input, instead of using the constant values of initial conditions. All these variables correspond to the current cell where the particle is located.

#### 2.5. Solution strategy

The mass of the components and the temperature of each layer are solved as the principal variables. The nonlinear partial differential energy equation is solved by the finite difference method with an explicit fifth-order Runge–Kutta scheme with six-stage step size control [80]. This method is very efficient when the solution has a sharp front, as in our case. The sharp front leads to very large derivatives of the solution for a part of the region of integration. In such a condition the assumption that the local truncation error is changing smoothly is invalid, therefore any step choosing algorithm most probably produces an unacceptable step. This Runge–Kutta scheme computes solutions at several different orders to detect sharp fronts before all six function evaluations have been computed, therefore the calculation time for rejecting a step is greatly reduced.

After obtaining the new mass and temperature of the layers, the radius of each layer is computed by assuming a constant density for each component during the life-time of each layer. If the thickness of a layer is smaller than 1  $\mu\text{m}$ , it is deactivated and the conservation equations are not solved for that layer. Afterwards, thermal conductivity, heat capacity and enthalpy of each active layer are updated. Temperature and heat flux of the boundaries are computed by using the layer temperature from the previous step. Reaction rates are updated to calculate the mass fluxes. Finally by computing the derivatives of the principal variables, the mass and temperature of the layers for the next step are obtained. As mentioned before, the time step is set dynamically but it cannot be larger than 0.01 s.

### 3. Gas phase model

There is a strong interaction between gas and solid phases during the thermal conversion of biomass particles. The gas phase model provides the variables which are used for the boundary conditions of the layer model. Therefore, accurate gas phase modelling successively leads to reliable results of the layer model. On the other hand the layer model calculations provide the mass, energy, and momentum sources/sinks for the gas phase governing equations. ANSYS



FLUENT is utilised to resolve the flow field, temperature distribution and species concentrations in the gas phase. The layer model is coupled with ANSYS FLUENT as a user defined function (UDF) and the trajectories of particles are calculated by the discrete phase model (DPM). The realizable  $k$ - $\epsilon$  model describes the turbulent flow. An eddy-break-up approach is used to represent the combustion of the turbulent reactive flow. It takes the time scales of reaction kinetic rates and species mixing by turbulence into consideration. Thus, the reaction rate is limited by the slowest of these processes. The species conservation equations for the volatiles  $\text{CH}_4$ ,  $\text{CO}$ ,  $\text{CO}_2$ ,  $\text{H}_2$ ,  $\text{H}_2\text{O}$  and  $\text{O}_2$  are solved. A global 4-step mechanism considering all the species describes the gas phase combustion [81,82]. The radiation which is an important part in combustion simulations is calculated by the Discrete Ordinates Model.

#### 4. Model validation

To validate the layer model, the experimental data of the work of Lu et al. [7,8] have been utilised. They used a single-particle reactor to measure particle surface temperature, centre temperature and mass loss during thermal conversion of cylindrical particles under non-oxidising and oxidising conditions. Fig. 2 schematically illustrates the experimental setup. The reactor has an inner diameter (ID) of 0.15 m and a height of 0.5 m. Four heating elements heat both the reactor and the particle. Air or nitrogen is heated in the pre-heater before it enters the reactor from the bottom and exits from the top. A type K thermocouple monitors the centre gas temperature. The actual gas temperature was corrected for radiative and other losses from the thermocouple bead based on the wall temperature, bulk gas velocity, and the thermocouple bead size. This resulted in a gas temperature of 1050 K. The reactor wall temperature is not uniform in the axial direction due to reactor configurations, so an average wall temperature measured by an imaging pyrometer (1276 K) is used for modelling.

They performed several test runs for various particle sizes and moisture contents. In this study, each test run is simulated by using the layer model coupled to ANSYS FLUENT in order to compare the measurements and model predictions. Table 3 summarises the physical and chemical properties used in the simulations of the single particle reactor.

#### 4.1. Results and discussions

In Fig. 3 the contours of gas temperature and  $\text{H}_2\text{O}$ ,  $\text{CO}$ , and  $\text{CO}_2$  molar concentrations along a vertical cross section of the single-particle reactor are presented. These results are related to the combustion of a cylindrical particle with  $d_p = 9.5$  mm,  $l_p = 9.5$  mm and  $MC = 40\%$  w.b. The comparison between the predicted and measured data during the combustion of this cylindrical particle is presented in Fig. 4.

The measured particle surface and centre temperatures in Fig. 4 are well predicted by the model. There is a small discrepancy at the end of the char burnout between the simulated and measured centre temperatures. The model predicted higher temperatures which might be attributed to the physical properties of the ash layer in the simulation. A small thermal conductivity or the prediction of a larger thickness of the ash layer leads to higher resistance against the heat transfer and thus increases the particle centre temperature. As it is shown in Fig. 4, the predicted particle mass loss is in consistence with the measurements.

Both experimental data and model predictions show that during the char combustion stage the particle temperature rises gradually and declines sharply after the peak value is reached. This supports theoretical descriptions of combustion mechanisms of large particles. The oxidiser diffusion rate primarily controls the char combustion rate. The char burning rate slows down as the available surface area decreases with decreasing particle size, as it can be seen in Eq. (12). However, the decrease of the particle mass compensates it and the particle temperature increases slowly. Once the char is completely consumed, the particle, i.e. ash, cools rapidly towards the convective gas temperature, depending on the radiative environment.

The gas temperature around the particle in Fig. 3, slightly decreases at the beginning. It is due to particle heat-up and the endothermic evaporation. When volatile components start to release, the exothermic homogeneous reactions around the particle sharply rise the gas temperature. By approaching the end of pyrolysis, the rate of pyrolysis slows down which decreases the gas phase temperature gradually. At the end of pyrolysis the flame surrounding the particle disappears. During char burnout the particle surface temperature increases and heats up the gas phase by convective heat transfer. Additionally, the oxidation of  $\text{CO}$  (a product of the char burnout) increases the gas phase temperature to about 150 K above the gas inlet temperature during char conversion.

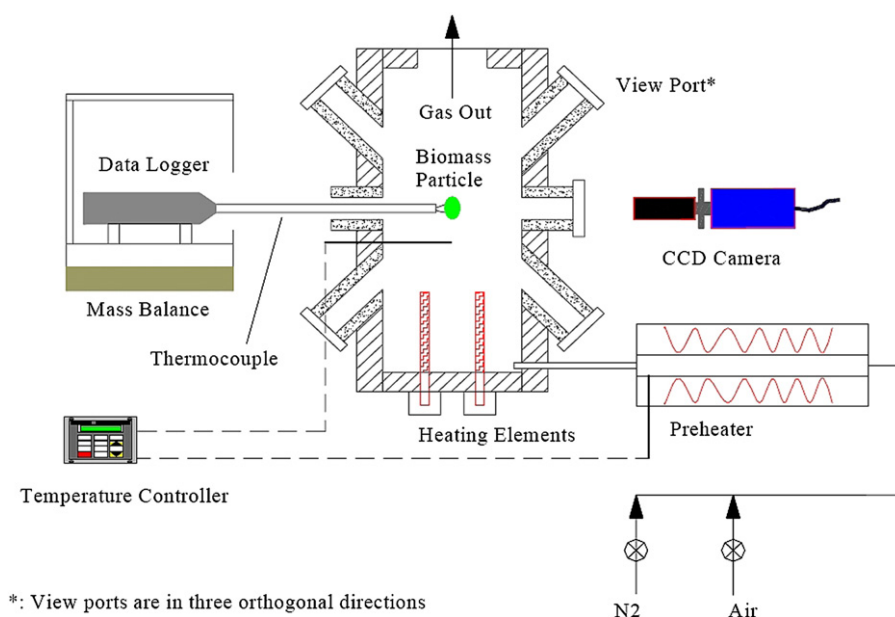


Fig. 2. Schematic diagram of the single-particle reactor [7].

**Table 3**  
Parameters used in the single-particle reactor simulations.

Proximate analysis			
C	48.1	wt.% d.b.	
H	5.77	wt.% d.b.	
O	45.53	wt.% d.b.	
N	0.1	wt.% d.b.	
Ultimate analysis			
Water	6 and 40	wt.% w.b.	
Volatiles	90	wt.% d.b.	
Char	9.5	wt.% d.b.	
Ash	0.5	wt.% d.b.	
Density			
Dry wood	545	kg.m <sup>-3</sup>	[7]
Char	200	kg.m <sup>-3</sup>	[83]
Ash	300	kg.m <sup>-3</sup>	
Heat capacity			
Dry wood	1500 + T	J.kg <sup>-1</sup> .K <sup>-1</sup>	[42]
Char	420 + 2.09 T + 6.85 × 10 <sup>-4</sup> T <sup>2</sup>	J.kg <sup>-1</sup> .K <sup>-1</sup>	[42]
Ash	420 + 2.09 T + 6.85 × 10 <sup>-4</sup> T <sup>2</sup>	J.kg <sup>-1</sup> .K <sup>-1</sup>	[42]
Thermal conductivity			
Dry wood	0.056 + 2.6 × 10 <sup>-4</sup> T	W.m <sup>-1</sup> .K <sup>-1</sup>	[7]
Char	0.071	W.m <sup>-1</sup> .K <sup>-1</sup>	[7]
Ash	1.2	W.m <sup>-1</sup> .K <sup>-1</sup>	[7]
Particle emissivity			
Particle emissivity	ε = 0.85	–	
Pyrolysis model			
Hemicellulose	A = 2.527 × 10 <sup>11</sup>	s <sup>-1</sup>	[36]
	E = 147	kJ.mol <sup>-1</sup>	[36]
	a = 0.26	–	[36]
Cellulose	A = 1.379 × 10 <sup>14</sup>	s <sup>-1</sup>	[36]
	E = 193	kJ.mol <sup>-1</sup>	[36]
	a = 0.64	–	[36]
Lignin	A = 2.202 × 10 <sup>12</sup>	s <sup>-1</sup>	[36]
	E = 181	kJ.mol <sup>-1</sup>	[36]
	a = 0.10	–	[36]
Char conversion model			
Pore diameter	100	μm	[14]
Porosity of ash layer	0.9		

The water vapour release is quick at the beginning and declines close to the end of the drying phase. However, there is a small fraction of water around the particle during pyrolysis which is due to the combustion of volatiles and the assumption that the volatile species include water vapour. The concentration of CO<sub>2</sub> around the particle is higher than CO which might be due to the oxidation of CO and CH<sub>4</sub> close to the particle surface. Additionally, the CO/CO<sub>2</sub> product ratio of char oxidation implies that the amount of CO produced is less than CO<sub>2</sub>.

The gas and solid phase calculations are strongly coupled. The layer model calculates the energy and mass sources which are used in the gas phase governing equations. The gas phase calculations obtain several parameters which are used as boundary conditions for the layer model. These parameters are temperature, species concentrations and velocity of the gas layer adjacent to the particle surface, as well as the radiation temperature. As it can be seen the temperature and species concentrations around the particle are time dependent. In particular, they are significantly different from the inlet conditions and are strongly affected by the mass sources generated from the solid conversion. Therefore, using the constant initial values of these parameters in the boundary conditions of the particle model leads to some inconsistencies as the gas temperature influences the particle heating rate and the heterogeneous reactions R1–R4 are affected by the species concentrations.

Fig. 5 compares the predicted centre temperature during combustion of a cylindrical particle with  $d_p = 6.35$  mm,  $l_p = 21.44$  mm and  $MC = 6\%$  w.b. with the experimental data. It is extremely hard to

determine surface temperature with thermocouples correctly, because during devolatilisation volatiles burn around the particle, which affects the thermocouple reading. Additionally, during char oxidation the particle starts to shrink and the thermocouple wire cannot track the shrinking surface, hence the bead becomes exposed to the surrounding flame. The measured surface temperature in this experiment was not reliable to be reported. The predicted centre temperatures are in good qualitative agreement with the measured ones. The rapid temperature increase of the measured centre temperature in the beginning might be due to the conduction through the thermocouple wire. The mass profile covers well the measured values (see Fig. 5).

To evaluate the layer model under non-oxidising conditions, the measured surface and centre temperatures as well as the normalised particle mass of four different experiments are compared with the simulation results.

The results of an experiment with a cylindrical particle of  $d_p = 9.5$  mm,  $l_p = 9.5$  mm and  $MC = 6\%$  w.b. during pyrolysis in nitrogen are illustrated in Fig. 6. The particle surface and centre temperature predictions generally agree with experimental data. Measured centre temperature increases faster at the beginning which might be caused by the thermal conduction effects through the wire. Both the simulated and experimental results show a distinct difference between particle surface and centre temperatures which confirms the need for consideration of intra-particle gradients in biomass thermal conversion modelling.

During the simulation the boundary of each layer approaches to the particle centre, until it disappears once its thickness becomes less than 1 μm. When the most inner layer disappears, the temperature of the next layer is assigned as the particle centre temperature. Due to the coarse discretisation of each particle into four layers, the disappearance of the layers might lead to some discontinuities in the centre temperature curves. The discontinuity at the end of the drying process, e.g. disappearance of the drying layer, is more visible because the assumption of constant temperature,  $T_{B_0} = 373.15$ , during the drying process magnifies the effect of the layer disappearance. As an example, in Fig. 6 two discontinuities are seen in the predicted centre temperature curve, when the wet layer and dry layer disappear at the end of the drying and pyrolysis process, respectively. They can be smoothed by increasing the number of layers, however, it costs computational time.

The particle mass predicted by the model decreases faster than the measured one at the beginning. This discrepancy is believed to be due to coarse spatial discretisation and the empirical constants used in the pyrolysis model. The coarse spatial discretisation might lead to an overprediction of the temperature of the boundary between dry fuel and char layers, where the pyrolysis is assumed to occur. Consequently, the pyrolysis rate model which is an exponential function of temperature, overvalues the particle mass loss rate. Furthermore, the empirical constants of the pyrolysis model are obtained under certain conditions. Therefore, any changes in these conditions, might impact the validity of the pyrolysis empirical constants.

In Fig. 7 the measurements and simulated results of the same particle with higher moisture content,  $MC = 40\%$  w.b., during pyrolysis in nitrogen are compared. Both the measured data and the model prediction show that the particle centre temperature rises to the water boiling point and then stays constant until the particle dries, then it rises again. The effect of vaporisation on the centre temperature is more pronounced in comparison to Fig. 6 due to higher moisture content and it appears as a temperature plateau. The model predictions for particle centre and surface temperature as well as the particle mass loss profile agree well with experiments.

Temperature and normalised mass profiles during pyrolysis of longer cylindrical particles,  $l_p = 38$  mm, with two different moisture contents, 6% and 40% w.b., are illustrated in Figs. 8 and 9. All the predicted surface and centre temperatures as well as the particle mass history are in good agreement with experimental data, except the

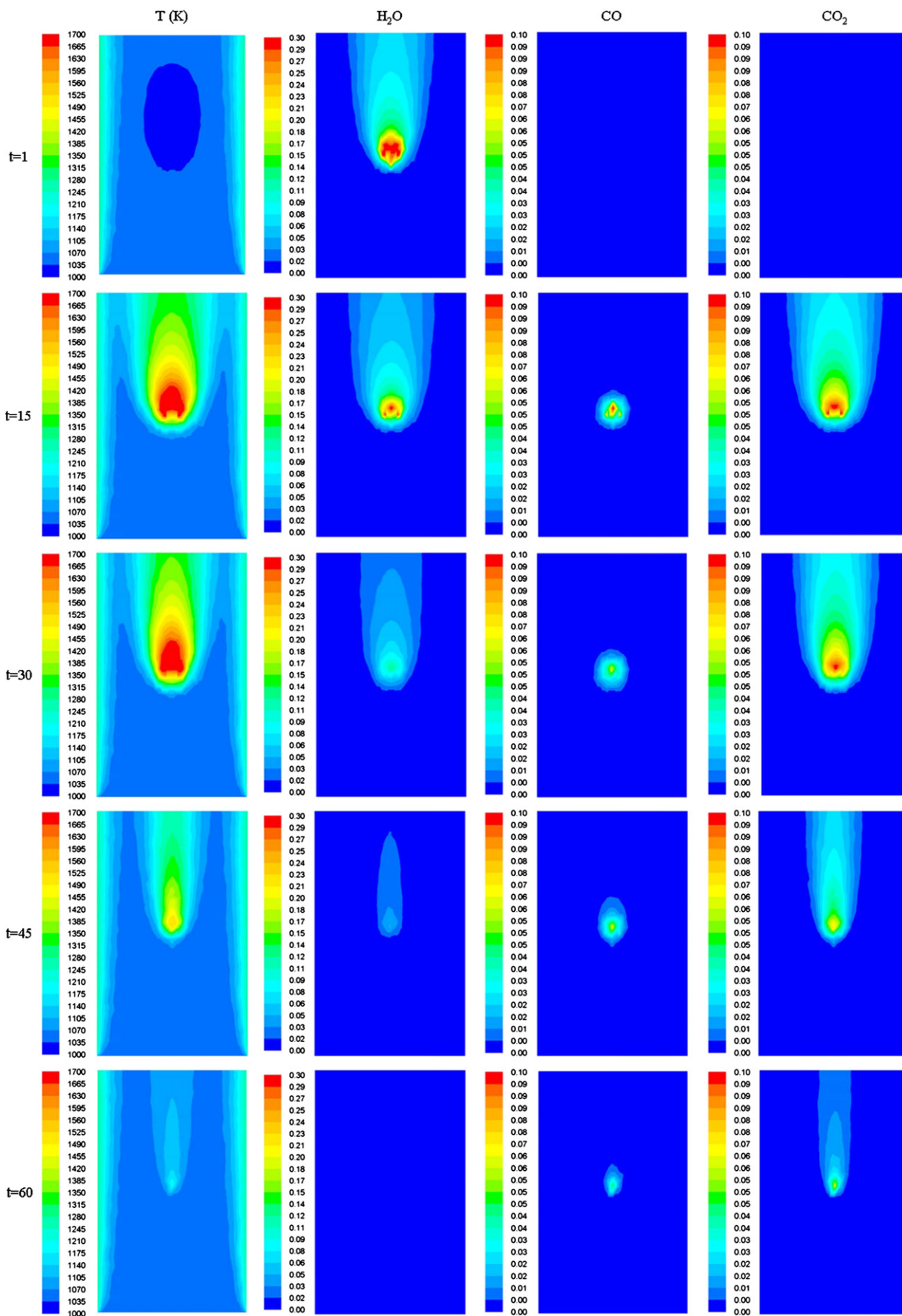


Fig. 3. Contours of gas phase temperature and H<sub>2</sub>O, CO as well as CO<sub>2</sub> mole fractions at a vertical cross section of the single-particle reactor during combustion of a cylindrical poplar wood particle;  $d_p = 9.5$  mm,  $l_p = 9.5$  mm, MC = 40% w.b.; time is given in seconds.



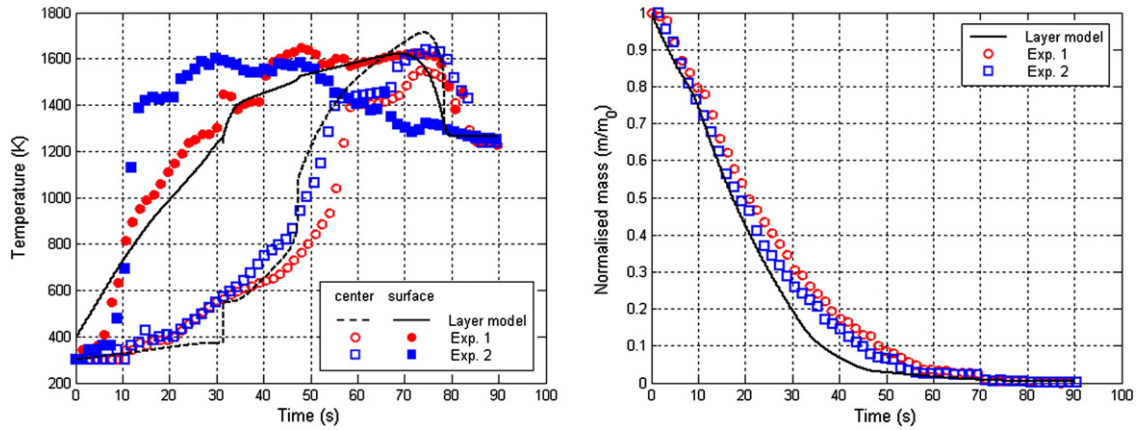


Fig. 4. Comparison between simulated and measured temperatures and normalised mass profiles during combustion of a cylindrical poplar wood particle;  $d_p = 9.5$  mm,  $l_p = 9.5$  mm,  $MC = 40\%$  w.b.

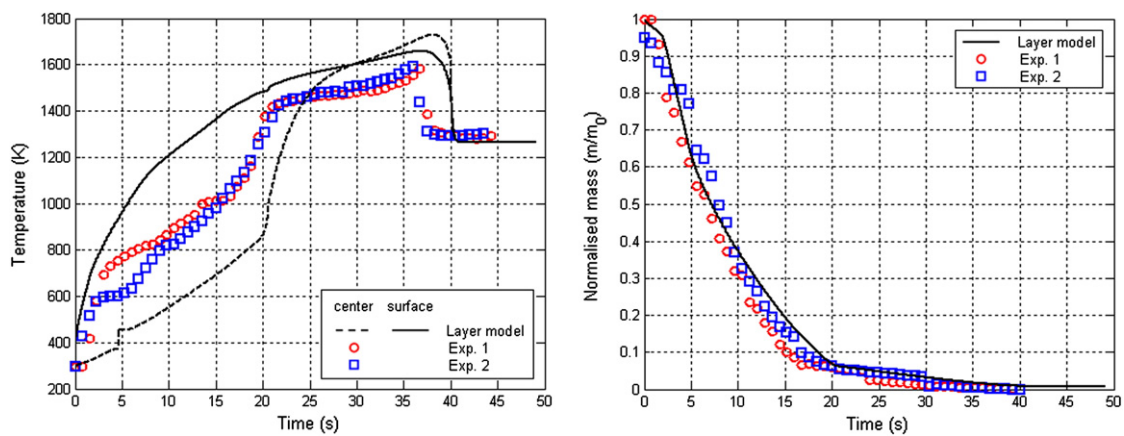


Fig. 5. Comparison between simulated and measured temperatures and normalised mass profiles during combustion of a cylindrical poplar wood particle;  $d_p = 6.35$  mm,  $l_p = 21.44$  mm,  $MC = 6\%$  w.b.

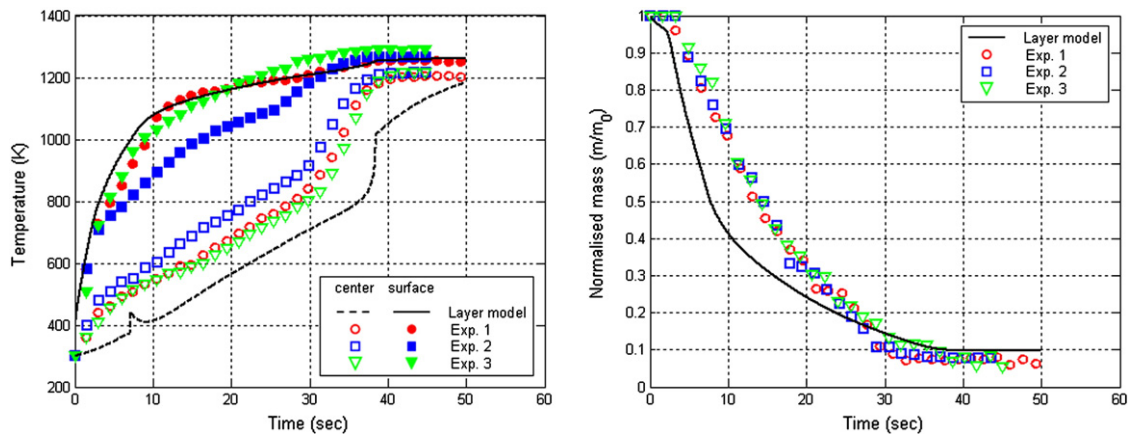


Fig. 6. Comparison between simulated and measured temperatures and normalised mass profiles during pyrolysis of a cylindrical poplar wood particle;  $d_p = 9.5$  mm,  $l_p = 9.5$  mm,  $MC = 6\%$  w.b.

normalised mass profile of the particle with  $MC = 6\%$  w.b., Fig. 8. The discrepancy is most probably attributed to the empirical constants used in the hemicellulose pyrolysis rate model because the predicted mass loss rate is faster than measurements at the beginning of the pyrolysis process and it is known that the hemicellulose pyrolysis takes place sooner than the other biomass components.

In all the simulated and measured results under pyrolysis conditions, the centre temperature rises faster at the end of the pyrolysis process and during heating up of the remaining char. This is due to

a considerable decrease of particle mass and also particle shrinkage during pyrolysis. As it can be seen in Eq. (4), the variation of the particle temperature is a function of particle mass and size.

The particle shape has a significant influence on the thermal conversion of biomass particles. Among the particles with the same mass but different shapes, the particle with the higher sphericity has the lowest mass loss rate, because the higher sphericity means a smaller surface area to mass ratio. Since heat and mass transfer are scaled with the surface area, it leads to lower heat and mass transfer rates to/from the



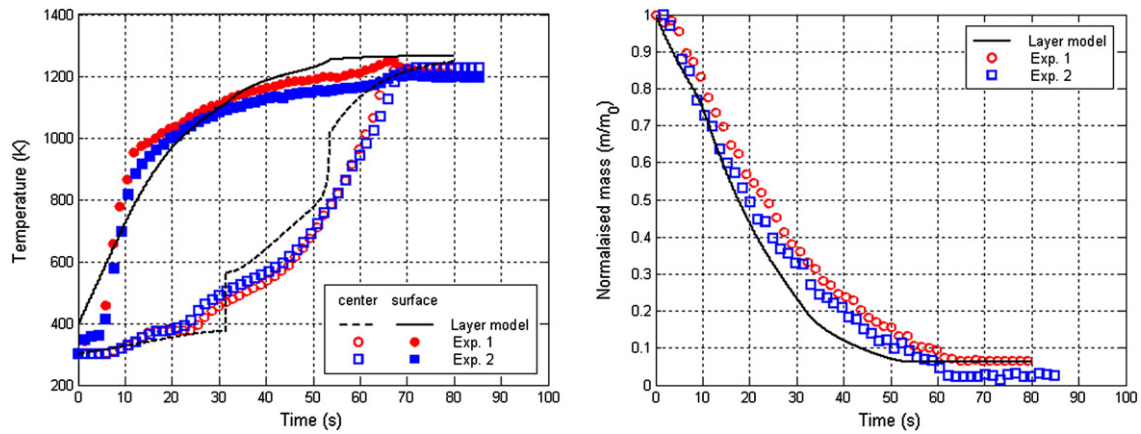


Fig. 7. Comparison between simulated and measured temperatures and normalised mass profiles during pyrolysis of a cylindrical poplar wood particle;  $d_p = 9.5$  mm,  $l_p = 9.5$  mm,  $MC = 40\%$  w.b.

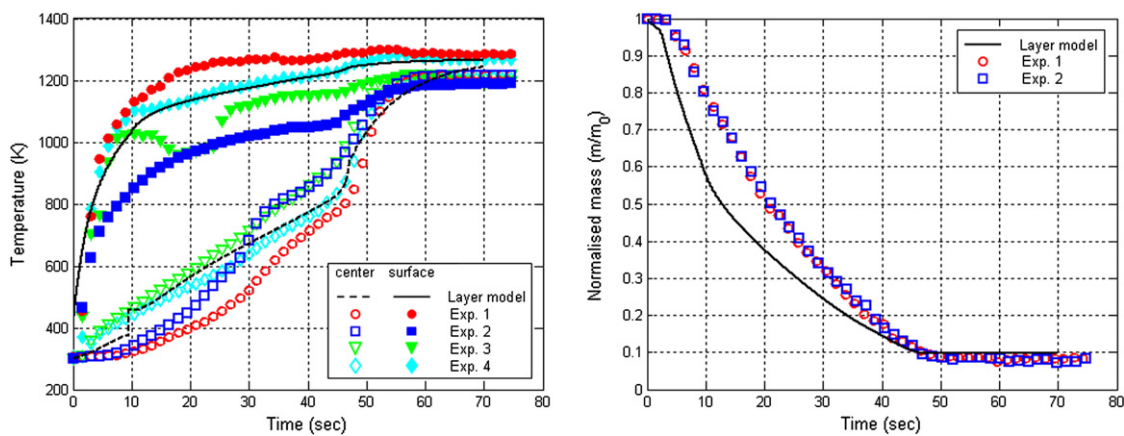


Fig. 8. Comparison between simulated and measured temperatures and normalised mass profiles during pyrolysis of a cylindrical poplar wood particle;  $d_p = 9.5$  mm,  $l_p = 38$  mm,  $MC = 6\%$  w.b.

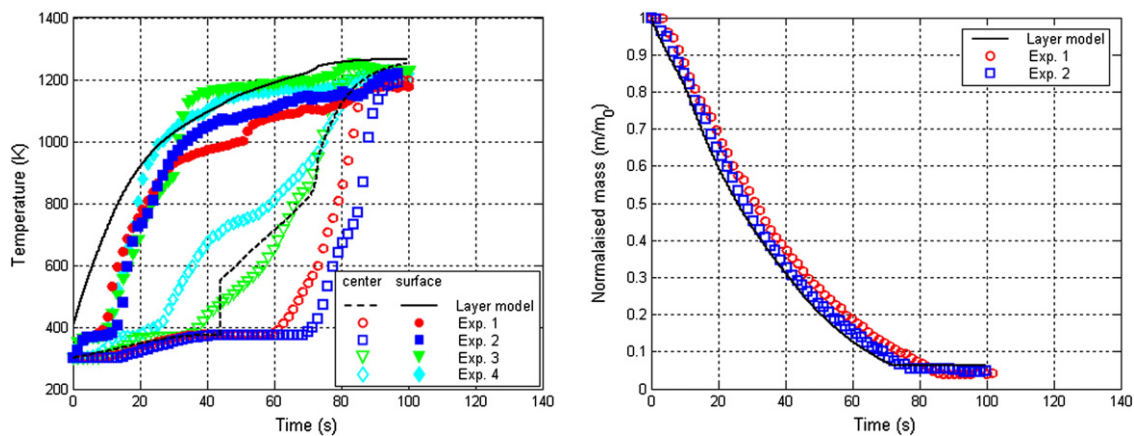


Fig. 9. Comparison between simulated and measured temperatures and normalised mass profiles during pyrolysis of a cylindrical poplar wood particle;  $d_p = 9.5$  mm,  $l_p = 38$  mm,  $MC = 40\%$  w.b.

particle. Therefore, assuming spherical shape for non-spherical particles would lead to a substantial error in the prediction of their combustion behaviour [9]. In the layer model a shape factor, which is the area of the control surface at each boundary, is used to describe different shapes. This shape factor appears as  $\Delta x$  in Eq. (2). Since  $\Delta x$  is directly proportional to the surface area, it increases with the particle aspect ratio. It consequently leads to faster heat transfer and reaction rates. The results of the validation simulations for different particle geometries indicate that the effect of the particle shape is correctly considered in the layer model.

The layer model can be directly compared with the sophisticated model of Lu et al. [7,8], because the variations of the particle mass and temperature were simulated in the same experiments as in this study. In some cases the model of Lu et al. predicts the measured data better (Figs. 6 and 8) and in some other cases the layer model does (Figs. 4, 7 and 9). At this point it should be mentioned that in the model of Lu et al. a set of fourteen governing equations is solved, while the layer model contains only an energy equation. Additionally, in the layer model the lowest possible number of grid points is

considered to discretise biomass particles. Therefore, the layer model is considerably faster than the model of Lu et al. and as it is mentioned before they have the same level of accuracy. Furthermore, the layer model is coupled to ANSYS FLUENT, which is of a great advantage for its further application in grate furnace simulations [84].

## 5. Summary and conclusions

A one-dimensional single particle model was developed to simulate the thermal conversion of thermally thick particles by considering intra-particle gradients. The particle is divided into four layers: wet (virgin) fuel, dry fuel, char residue and ash which correspond to the four main stages of biomass thermal conversion. The sub-processes of thermal biomass conversion are treated by separate sub-models. Moisture evaporation is assumed to occur at a constant temperature, while biomass pyrolysis is modelled through three competing decomposition reactions. Char oxidation is kinetically and/or diffusionally controlled. The model can be applied for the packed bed simulations. Therefore, the number of governing equations and grid points inside the particle were reduced to fasten the numerical calculations, without impairing the model accuracy. The model was programmed in C/C++ and linked with ANSYS FLUENT to simultaneously resolve the mass and energy balance equations for the particle and its surrounding gas phase during its thermal conversion. The validation simulations were performed with different particle sizes, shapes, and moisture contents under pyrolysis and combustion conditions. The model results are in good agreement with experimental data, which indicates that the model accuracy was not affected by the simplifications of the model. Moreover, the model performs the particle simulations rather quickly, in a minute. The level of information, accuracy and numerical efforts of the layer model are found to be sufficient to apply it in the next step for biomass grate furnace simulations. There each particle in the packed-bed will be treated by the layer model, whereas the gas phase combustion in the voids as well as above the fuel bed will be calculated by existing gas phase combustion models. Moreover, a model to describe the influence of the particle–particle interactions on the particle movements on the grate should also be considered. In this way an overall simulation model for fixed bed biomass combustion applications will be achieved.

## Nomenclature

$A$	area [ $\text{m}^2$ ]
$\mathbf{A}$	pre-exponential factor [ $\text{s}^{-1}$ ]
$a$	mass fraction of each biomass component [–]
$c_p$	specific heat capacity [ $\text{J.kg}^{-1}.\text{K}^{-1}$ ]
$\mathcal{D}_a$	ordinary gas molecular diffusivity [ $\text{m}^2.\text{s}^{-1}$ ]
$\mathcal{D}_{ab}$	binary diffusivity [ $\text{m}^2.\text{s}^{-1}$ ]
$\mathcal{D}_e$	effective diffusivity [ $\text{m}^2.\text{s}^{-1}$ ]
$\mathcal{D}_{Ka}$	Knudsen diffusivity [ $\text{m}^2.\text{s}^{-1}$ ]
$d$	diameter [m]
$\mathbf{E}$	activation energy [ $\text{kJ.mol}^{-1}$ ]
$H$	specific enthalpy [ $\text{J.kg}^{-1}$ ]
$\Delta H_f^\circ$	standard enthalpy of formation [ $\text{J.kg}^{-1}$ ]
$h$	convective heat transfer coefficient [ $\text{W.m}^{-2}.\text{K}^{-1}$ ]
$h_m$	mass transfer coefficient [ $\text{m.s}^{-1}$ ]
$k$	thermal conductivity [ $\text{W.m}^{-1}.\text{K}^{-1}$ ]
$k_c$	reaction rate constants [ $\text{m.s}^{-1}$ ]
$l$	length [m]
$m$	mass [kg]
$MC$	moisture content, wet based [ $\text{kg}_{\text{water}}/\text{kg}_{\text{wetfuel}}$ ]
$M_c$	carbon molecular weight [ $\text{kg.kmol}^{-1}$ ]
$\dot{m}$	mass flow rate [ $\text{kg.s}^{-1}$ ]
$Nu$	Nusselt number [–]
$Pr$	Prandtl number [–]
$\mathbf{q}$	heat flux [ $\text{W.m}^{-2}$ ]
$R$	reaction rate [ $\text{kg.s}^{-1}$ ]
$\mathbf{R}$	universal gas constant [ $\text{kJ.mol}^{-1}.\text{K}^{-1}$ ]

$Re$	Reynolds number [–]
$Sc$	Schmidt number [–]
$Sh$	Sherwood number [–]
$T$	temperature [K]
$t$	time [s]
$\mathbf{v}$	velocity [ $\text{m.s}^{-1}$ ]
$X$	molar concentration of gas species [ $\text{mol.m}^{-3}$ ]
$\Delta x_0$	ratio between area of a layer left boundary to the half of the layer thickness [m]
$\Delta x_1$	ratio between area of a layer right boundary to the half of the layer thickness [m]

## Greek symbols

$\epsilon$	porosity [–]
$\epsilon$	emissivity [–]
$\eta$	stoichiometric coefficient of reactions [–]
$\rho$	density [ $\text{kg.m}^{-3}$ ]
$\sigma$	Stefan–Boltzmann constant [ $\text{W.m}^{-2}.\text{K}^{-4}$ ]
$\tau$	tortuosity [–]
$\Omega$	stoichiometric ratio of moles of carbon per mole of oxidising/gasifying agent in corresponding reaction [–]

## Subscripts

$B$	boundary
$c$	component (solid and gas)
$ch$	char
$dr$	drying
$df$	dry fuel
$L_i$	layer ( $L_0$ : wet fuel layer, $L_1$ : dry fuel layer, $L_2$ : char layer, $L_3$ : ash layer)
$p$	particle
$r$	reaction
$rad$	radiative
$wl$	water liquid
$wv$	water vapour
$\infty$	ambient condition

## References

- [1] B. Peters, Measurements and application of a discrete particle model (DPM) to simulate combustion of a packed bed of individual fuel particles, *Combustion and Flame* 131 (2002) 132–146.
- [2] C. Bruch, B. Peters, T. Nussbaumer, Modelling wood combustion under fixed bed conditions, *Fuel* 82 (2003) 729–738.
- [3] J.C. Wurzenberger, S. Wallner, H. Raupenstrauch, J.G. Khinast, Thermal conversion of biomass: comprehensive reactor and particle modeling, *AIChE Journal* 48 (2002) 2398–2410.
- [4] H. Thunman, B. Leckner, F. Niklasson, F. Johnsson, Combustion of wood particles—a particle model for Eulerian calculations, *Combustion and Flame* 129 (2002) 30–46.
- [5] J. Porteiro, J.L. Miguez, E. Granada, J.C. Moran, Mathematical modelling of the combustion of a single wood particle, *Fuel Processing Technology* 87 (2006) 169–175.
- [6] J. Porteiro, E. Granada, J. Collazo, D. Patiño, J.C. Morán, A model for the combustion of large particles of densified wood, *Energy & Fuels* 21 (2007) 3151–3159.
- [7] H. Lu, Experimental and modelling investigation of biomass particle combustion, PhD thesis, Brigham Young University, 2006.
- [8] H. Lu, W. Robert, G. Peirce, B. Ripa, L.L. Baxter, Comprehensive study of biomass particle combustion, *Energy & Fuels* 22 (2008) 2826–2839.
- [9] H. Lu, E. Ip, J. Scott, P. Foster, M. Vickers, L.L. Baxter, Effects of particle shape and size on devolatilization of biomass particle, *Fuel* 89 (2010) 1156–1168.
- [10] M.Y. Ha, B.R. Choi, A numerical study on the combustion of a single carbon particle entrained in a steady flow, *Combustion and Flame* 97 (1994) 1–16.
- [11] R.B. Bird, W.E. Stewart, E.N. Lightfoot, *Transport Phenomena*, second ed. John Wiley & Sons, New York, 2002.
- [12] W.C.R. Chan, M. Kelbon, B.B. Krieger, Modelling and experimental verification of physical and chemical processes during pyrolysis of a large biomass particle, *Fuel* 64 (1985) 1505–1513.
- [13] K.M. Bryden, M.J. Hagge, Modeling the combined impact of moisture and char shrinkage on the pyrolysis of a biomass particle, *Fuel* 82 (2003) 1633–1644.

- [14] M. Srekanth, D.R. Sudhakar, B.V.S.S.S. Prasad, A.K. Kolar, B. Leckner, Modelling and experimental investigation of devolatilizing wood in a fluidized bed combustor, *Fuel* 87 (2008) 2698–2712.
- [15] N. Ouelhazi, G. Arnaud, J.P. Fohr, A two-dimensional study of wood plank drying. The effect of gaseous pressure below boiling point, *Transport in Porous Media* 7 (1992) 39–91.
- [16] N. Zobel, The representative particle model, PhD thesis, Technischen Universität Berlin, 2007.
- [17] A. Galgano, C. Di Blasi, Modeling the propagation of drying and decomposition fronts in wood, *Combustion and Flame* 39 (2004) 16–27.
- [18] B. Peters, E. Schröder, C. Bruch, Measurements and particle resolved modelling of the thermo- and fluid dynamics of a packed bed, *Journal of Analytical and Applied Pyrolysis* 70 (2003) 211–231.
- [19] B. Peters, *Thermal Conversion of Solid Fuels*, WIT Press, Southampton, 2003.
- [20] Y.B. Yang, V.N. Sharifi, J. Swithenbank, L. Ma, L.I. Darvell, J.M. Jones, M. Pourkashanian, A. Williams, Combustion of a single particle of biomass, *Energy & Fuels* 22 (2008) 306–316.
- [21] H. Thunman, K. Davidsson, B. Leckner, Separation of drying and devolatilization during conversion of solid fuels, *Combustion and Flame* 137 (2004) 242–250.
- [22] A. Bharadwaj, L.L. Baxter, A.L. Robinson, Effects of intraparticle heat and mass transfer on biomass devolatilization: experimental results and model predictions, *Energy & Fuels* 18 (2004) 1021–1031.
- [23] J.J. Saastamoinen, Simplified model for calculation of devolatilization in fluidized beds, *Fuel* 85 (2006) 2388–2395.
- [24] J. Saastamoinen, J.R. Richard, Simultaneous drying and pyrolysis of solid fuel particles, *Combustion and Flame* 106 (1996) 288–300.
- [25] R. Bilbao, J.F. Mastral, J.A. Lana, J. Ceamanos, M.E. Aldea, M. Betrán, A model for the prediction of the thermal degradation and ignition of wood under constant and variable heat flux, *Journal of Analytical and Applied Pyrolysis* 62 (2002) 63–82.
- [26] C. Di Blasi, Multi-phase moisture transfer in the high-temperature drying of wood particles, *Chemical Engineering Science* 53 (1998) 353–366.
- [27] R.R. Kumar, A.K. Kolar, B. Leckner, Shrinkage characteristics of Casuarina wood during devolatilization in a fluidized bed combustor, *Biomass and Bioenergy* 30 (2006) 153–165.
- [28] C. Di Blasi, Modeling chemical and physical processes of wood and biomass pyrolysis, *Progress in Energy and Combustion Science* 34 (2008) 47–90.
- [29] B. Moghtaderi, The state-of-the-art in pyrolysis modelling of lignocellulosic solid fuels, *Fire and Materials* 30 (2006) 1–34.
- [30] S.R.A. Kersten, X. Wang, W. Prins, W.P.M. Van Swaaij, Biomass pyrolysis in a fluidized bed reactor. Part 1: literature review and model simulations, *Industrial and Engineering Chemistry Research* 44 (2005) 8773–8785.
- [31] M.J. Antal, G. Várhegyi, Cellulose pyrolysis kinetics: the current state of knowledge, *Industrial and Engineering Chemistry Research* 34 (1995) 703–717.
- [32] F. Shafizadeh, P.P.S. Chin, Thermal deterioration of wood, *ACS Symposium Series* 43 (1977) 57–81.
- [33] F. Thurner, U. Mann, Kinetic investigation of wood pyrolysis, *Industrial and Engineering Chemistry Process Design and Development* 20 (1981) 482–488.
- [34] B.M. Wagenaar, W. Prins, W.P.M. Van Swaaij, Flash pyrolysis kinetics of pine wood, *Fuel Processing Technology* 36 (1994) 291–302.
- [35] R.S. Miller, J. Bellan, A generalized biomass pyrolysis model based on superimposed cellulose, hemicellulose and lignin kinetics, *Combustion Science and Technology* 126 (1996) 97–137.
- [36] C. Branca, A. Albano, C. Di Blasi, Critical evaluation of wood devolatilization mechanisms, *Thermochimica Acta* 429 (2005) 133–141.
- [37] G. Várhegyi, M.J. Antal, E. Jakab, P. Szabo, Kinetic modeling of biomass pyrolysis, *Journal of Analytical and Applied Pyrolysis* 42 (1996) 73–78.
- [38] H. Teng, Y.C. Wei, Thermogravimetric studies on the kinetics of rice hull pyrolysis and the influence of water treatment, *Industrial and Engineering Chemistry Research* 37 (1998) 3806–3811.
- [39] H.J.M. Belderok, Experimental investigation and modeling of the pyrolysis of biomass, MSc thesis, Eindhoven University of Technology, 2007.
- [40] R. Miranda, C. Sosa-Blanco, D. Bustos-Martínez, C. Vasile, Pyrolysis of textile wastes I. Kinetics and yields, *Journal of Analytical and Applied Pyrolysis* 80 (2007) 489–495.
- [41] J.J.M. Orfao, F.J.A. Antunes, J.L. Figueiredo, Pyrolysis kinetics of lignocellulosic materials – three independent reactions model, *Fuel* 78 (1999) 349–358.
- [42] M.G. Grønli, A theoretical and experimental study of the thermal degradation of biomass, PhD thesis, The Norwegian University of Science and Technology, 1996.
- [43] M.G. Grønli, G. Várhegyi, C. Di Blasi, Thermogravimetric analysis and devolatilization kinetics of wood, *Industrial and Engineering Chemistry Research* 41 (2002) 4201–4208.
- [44] R. Zanzi, K. Sjöström, E. Björnbo, Rapid high-temperature pyrolysis of biomass in a free-fall reactor, *Fuel* 75 (1996) 545–550.
- [45] C. Di Blasi, C. Branca, A. Santoro, E.G. Hernandez, Pyrolytic behavior and products of some wood varieties, *Combustion and Flame* 124 (2001) 165–177.
- [46] H. Thunman, F. Niklasson, F. Johnsson, B. Leckner, Composition of volatile gases and thermochemical properties of wood for modeling of fixed or fluidized beds, *Energy & Fuels* 15 (2001) 1488–1497.
- [47] G.F. Froment, K.B. Bischoff, *Chemical Reactor Analysis and Design*, John Wiley & Sons, New York, 1990.
- [48] A. Gómez-Barea, B. Leckner, Modelling of biomass gasification in fluidized bed, *Progress in Energy and Combustion Science* 36 (2010) 444–509.
- [49] M.L. de Souza-Santos, *Solid Fuels Combustion and Gasification*, second ed. CRC Press, 2010.
- [50] C. Di Blasi, Combustion and gasification rates of lignocellulosic chars, *Progress in Energy and Combustion Science* 35 (2009) 121–140.
- [51] I.M. Bews, A.N. Hayhurst, S.M. Richardson, S.G. Taylor, The order, Arrhenius parameters, and mechanism of the reaction between gaseous oxygen and solid carbon, *Combustion and Flame* 124 (2001) 231–245.
- [52] R. Johansson, H. Thunman, B. Leckner, Influence of intraparticle gradients in modeling of fixed bed combustion, *Combustion and Flame* 149 (2007) 49–62.
- [53] F. Patisson, M.G. Francois, D. Ablitzer, A non-isothermal, non-equimolar transient kinetic model for gas–solid reactions, *Chemical Engineering Science* 53 (1998) 97–708.
- [54] F. Scala, Mass transfer around freely moving active particles in the dense phase of a gas fluidized bed of inert particles, *Chemical Engineering Science* 62 (2007) 4159–4176.
- [55] A.N. Hayhurst, M.S. Parmar, Measurement of the mass transfer coefficient and Sherwood number for carbon spheres burning in a bubbling fluidized bed, *Combustion and Flame* 130 (2002) 361–375.
- [56] A.N. Hayhurst, The mass transfer coefficient for oxygen reacting with a carbon particle in a fluidized or packed bed, *Combustion and Flame* 121 (2000) 679–688.
- [57] W.R. Paterson, A.N. Hayhurst, Mass or heat transfer from a sphere to a flowing fluid, *Chemical Engineering Science* 55 (2000) 1925–1927.
- [58] F. Scala, Calculation of the mass transfer coefficient for the combustion of a carbon particle, *Combustion and Flame* 157 (2010) 137–142.
- [59] J.S. Dennis, A.N. Hayhurst, S.A. Hayhurst, The combustion of large particles of char in bubbling fluidized beds: the dependence of Sherwood number and the rate of burning on particle diameter, *Combustion and Flame* 147 (2006) 185–194.
- [60] L. Tognotti, J.P. Longwell, A.F. Sarofim, The products of the high temperature oxidation of a single char particle in an electrodynamic balance, *Proceedings of the Combustion Institute* 23 (1990) 1207–1213.
- [61] J.A. Arthur, Reactions between carbon and oxygen, *Transactions of the Faraday Society* 47 (1951) 164–178.
- [62] M. Rossberg, Experimentelle Ergebnisse über die Primärreaktionen bei der Kohlenstoffverbrennung, *Zeitschrift für Elektrochemie* 60 (1956) 952–956.
- [63] P.L. Walker, F. Rusinko, L.G. Austin, Gas reactions of carbon, *Advanced Catalysis* 11 (1959) 133–221.
- [64] M. Otterbein, L. Bonnetain, Combustion d'un carbone vitreux sous basses pressions d'oxygene, *Carbon* 6 (1968) 877–885.
- [65] R.E. Mitchell, R.J. Kee, P. Glarborg, M.E. Coltrin, The effect of CO conversion in the boundary layers surrounding pulverized-coal char particles, *Proceedings of the Combustion Institute* 23 (1990) 1169–1176.
- [66] Z.Y. Du, A.F. Sarofim, J.P. Longwell, C.A. Mires, Kinetic measurement and modeling of carbon oxidation, *Energy & Fuels* 5 (1991) 214–221.
- [67] T.M. Linjewile, P.K. Agarwal, The product CO/CO<sub>2</sub> ratio from petroleum coke spheres in fluidized bed combustion, *Fuel* 74 (1995) 5–11.
- [68] T.M. Linjewile, P.K. Agarwal, The product CO/CO<sub>2</sub> ratio from petroleum coke spheres in fluidized bed combustion, *Fuel* 74 (1995) 12–16.
- [69] C.R. Monson, G.J. Germane, A.U. Blackham, L.D. Smoot, Char oxidation at elevated pressures, *Combustion and Flame* 100 (1995) 669–683.
- [70] D.D. Evans, H.W. Emmons, Combustion of wood charcoal, *Fire Safety Journal* 1 (1977) 57–66.
- [71] K. Pedersen, The product ratio of CO/CO<sub>2</sub> in the oxidation of biomass char, MSc thesis, Technical University of Denmark, 2003.
- [72] A.N. Hayhurst, M.S. Parmar, Does solid carbon burn in oxygen to give the gaseous intermediate CO or produce CO<sub>2</sub> directly? Some experiments in a hot bed of sand fluidized by air, *Chemical Engineering Science* 53 (1998) 427–438.
- [73] S. Kulasekaran, T.M. Linjewile, P.K. Agarwal, M.J. Biggs, Combustion of a porous char particle in an incipiently fluidized bed, *Fuel* 77 (1998) 1549–1560.
- [74] T.M. Linjewile, V.S. Gururajan, P.K. Agarwal, The CO/CO<sub>2</sub> product ratio from the combustion of single petroleum coke spheres in an incipiently fluidized bed, *Chemical Engineering Science* 50 (1995) 1881–1888.
- [75] M.J. Biggs, P.K. Agarwal, The CO/CO<sub>2</sub> product ratio for a porous char particle within an incipiently fluidized bed: a numerical study, *Chemical Engineering Science* 52 (1997) 941–952.
- [76] F.Y. Wang, S.K. Bhatia, A generalised dynamic model for char particle gasification with structure evolution and peripheral fragmentation, *Chemical Engineering Science* 56 (2001) 3683–3697.
- [77] P. Basu, J. Broughton, D.E. Elliott, *Proc. Fluidized Combust. Inst. Fuel Symp. Ser.*, London, 1, 1975, pp. A3.1–A3.10.
- [78] W. Prins, Fluidised bed combustion of a single carbon particle, PhD thesis, University of Twente, 1987.
- [79] F.P. Incropera, D.P. De Witt, *Introduction to Heat Transfer*, second ed. John Wiley & Sons, New York, 1990.
- [80] J.R. Cash, A.H. Krap, A variable order Runge–Kutta method for initial value problems with rapidly varying right-hand sides, *ACM Transactions on Mathematical Software* 16 (1990) 201–222.
- [81] R. Scharler, T. Fleckl, I. Obernberger, Modification of a Magnussen constant of the eddy dissipation model for biomass grate furnaces by means of hot gas in-situ FT-IR absorption spectroscopy, *Progress in Computational Fluid Dynamics* 3 (2003) 102–111.
- [82] R. Scharler, I. Obernberger, Numerical optimisations of biomass grate furnaces, *Proc. 5th INFUB*, Portugal, 2000.
- [83] D. Bergström, S. Israelsson, M. Öhman, S. Dahlqvist, R. Gref, C. Boman, I. Wåsterlund, Effects of raw material particle size distribution on the characteristics of Scots pine sawdust fuel pellets, *Fuel Processing Technology* 89 (2008) 1324–1329.
- [84] R. Mehrabian, S. Stangl, R. Scharler, I. Obernberger, CFD simulation of biomass grate furnaces with a comprehensive 3D packed bed model, *Proc. 25th German Flame Day*, Germany, 2011.

# Paper II





Contents lists available at SciVerse ScienceDirect

Fuel

journal homepage: [www.elsevier.com/locate/fuel](http://www.elsevier.com/locate/fuel)

# Effects of pyrolysis conditions on the heating rate in biomass particles and applicability of TGA kinetic parameters in particle thermal conversion modelling

Ramin Mehrabian<sup>a,b,\*</sup>, Robert Scharler<sup>a,b,c</sup>, Ingwald Obernberger<sup>a,b,c</sup>

<sup>a</sup> BIOENERGY 2020+ GmbH, Inffeldgasse 21b, 8010 Graz, Austria

<sup>b</sup> Institute for Process and Particle Engineering, Graz University of Technology, Inffeldgasse 21b, 8010 Graz, Austria

<sup>c</sup> BIOS BIOENERGIESYSTEME GmbH, Inffeldgasse 21b, 8010 Graz, Austria

## ARTICLE INFO

### Article history:

Received 14 January 2011

Received in revised form 30 June 2011

Accepted 27 September 2011

Available online 12 October 2011

### Keywords:

Biomass

Pyrolysis

TGA

Heating rate

## ABSTRACT

A one-dimensional single particle model is utilised to investigate the effects of radiation temperature, moisture content, particle size and biomass physical properties on the heating rate in biomass particles during pyrolysis. The model divides the particle into four layers – drying, pyrolysis, char and ash layer – corresponding to the four main stages of biomass thermal conversion. The average of the time derivative of the pyrolysis layer centre temperature weighted by the pyrolysis rate is introduced as an appropriate indicator for the heating rate in the particle during pyrolysis. The influencing parameters on the heating rate are summarised in the Biot number and the thermal time constant, to make the investigation of their effects easier. The heating rate is inversely proportional to the thermal time constant. The effect of a variation of the Biot number on the heating rate is negligible in comparison to the thermal time constant. Therefore, the thermal time constant can be sufficiently used to specify the heating rate regimes during pyrolysis. It is found that for thermal time constants of more than 50 s, pyrolysis takes place in a low heating rate regime, i.e. less than 50 K/min. Additionally, the heating rate during pyrolysis of various biomass types under a wide range of thermal conversion conditions has been examined, in order to classify the heating rate regime of pyrolysis in state-of-the-art combustion/gasification plants. The pyrolysis of wood dust and wood pellets is found to happen always in high heating rate regimes. Therefore, the kinetic parameters obtained by conventional TGA systems (typically with heating rates lower than 50 K/min) are not applicable for them. On the contrary, the pyrolysis of wood logs always happens in low heating rate regimes, which indicates that kinetic parameters obtained by conventional TGA systems can be applied. However, pyrolysis of wood chips can undergo low or high heating rate regimes depending on their particle size. Concerning the moisture content, it can be stated that it does not strongly influence the heating rate regime of certain biomass particles.

© 2011 Elsevier Ltd. All rights reserved.

## 1. Introduction

Due to the importance of modelling the thermal conversion of biomass particles for the design and optimisation of biomass combustion systems, several studies have been performed to describe the thermo-chemical conversion of biomass fuels [1–9]. Since, a combination of several sub-processes such as heat-up, drying, pyrolysis, and char burnout represents the global process of thermal conversion of solid biomass particles, all the presented models include a sub-model for pyrolysis. Usually the rate of biomass pyrolysis is described by an Arrhenius equation. The results of

TGA experiments are used to determine the empirical constants of the Arrhenius equation.

Most of the TGA experiments have been performed under low heating rate conditions, e.g. less than 50 K/min, because high heating rate TGA measurements are rather complex. However, it is known that heating rates of the TGA experiments influence the characteristics of thermogravimetric curves [10–13]. Indeed, the pyrolysis rate is affected by the heating rate in the particle and it leads to different kinetic parameters. Therefore, it is crucial to know under which conditions pyrolysis occurs in low/high heating rate regimes, in order to apply the appropriate TGA kinetic parameters.

In this paper, a numerical model for the thermal conversion of thermally thick particles has been used to study the influence of different parameters on the heating rate during pyrolysis. The influencing parameters on the heating rate are summarised in

\* Corresponding author at: BIOENERGY 2020+ GmbH, Inffeldgasse 21b, 8010 Graz, Austria. Tel.: +43 (0) 316 8739232; fax: +43 (0) 316 8739202.

E-mail address: [ramin.mehrabian@bioenergy2020.eu](mailto:ramin.mehrabian@bioenergy2020.eu) (R. Mehrabian).

**Nomenclature**

$A$	pre-exponential factor ( $s^{-1}$ )	$\beta$	heating rate ( $K s^{-1}$ )
$Bi$	Biot number (-)	$\delta_{ash}$	thickness of ash layer (m)
$c_i$	biomass pseudo-component contributions (-)	$\epsilon$	emissivity (-)
$c_p$	specific heat capacity ( $J kg^{-1} K^{-1}$ )	$\phi$	porosity (-)
$D$	diameter (m)	$\eta$	tortuosity (-)
$\mathcal{D}$	diffusivity ( $m^2 s^{-1}$ )	$\lambda$	thermal conductivity ( $W m^{-1} K^{-1}$ )
$E$	activation energy ( $kJ mol^{-1}$ )	$\rho$	density ( $kg m^{-3}$ )
$h$	heat transfer coefficient ( $W m^{-2} K^{-2}$ )	$\sigma$	Stefan–Boltzmann constant ( $W m^{-2} K^{-4}$ )
$h_m$	mass transfer coefficient ( $m s^{-1}$ )	$\tau$	thermal time constant (s)
$k$	kinetic rate constant ( $s^{-1}$ )	$\Omega$	stoichiometric ratio of moles of carbon per mole of oxidising/gasifying agent in corresponding reaction (-)
$L_c$	characteristic length scale (m)		
$m$	mass (kg)		
$M_c$	carbon molecular weight ( $kg kmol^{-1}$ )	<b>Subscripts</b>	
$MC$	moisture content, wet based (%)	0	initial condition
$Nu$	Nusselt number (-)	conv	convection
$R$	universal gas constant ( $kJ mol^{-1} K^{-1}$ )	$e$	effective
$S$	surface area ( $m^2$ )	$f$	final condition
$t$	time (s)	$g$	gas
$T$	temperature (K)	$p$	particle
$T_m$	temperature at maximum conversion rate (K)	$pl$	pyrolysis layer
$X_\infty$	molar concentration of gas species at bulk flow ( $mol m^{-3}$ )	$rad$	radiation
		$s$	solid
<b>Greek symbols</b>			
$\alpha_i$	conversion of each biomass pseudo-component (-)		

two characteristic numbers, the Biot number and the thermal time constant. Based on the characteristic numbers a method is proposed to distinguish between pyrolysis at low and high heating rate conditions for biomass fuels used in state-of-the-art combustion plants. By these means, the application ranges of low and high heating rate TGA experiments are clearly determined.

**2. Particle model**

In order to investigate the effect of the boundary conditions on the heating rate in a biomass particle during pyrolysis, an in-house code for modelling thermal conversion of thermally thick particles was used. The layer model accounts for intra-particle transport processes and simultaneous sub-processes of thermal conversion of thermally thick solid biomass particles. To reduce the model complexities and calculation time, only the radial temperature gradient in the particle is considered. This is an usual simplification assumption. Its validity was already addressed by Ha and Choi [14].

To apply the one-dimensional model for a finite cylindrical geometry (as an approximation for the biomass particle shape), Thunman's discretisation [3] approach has been applied. This approach assumes that the particle boundary conditions are homogeneous and every point in the particle at a certain distance from the particle surface has the same temperature and conversion state. The particle is divided into four layers: drying layer, pyrolysis layer, char and ash layer. The boundaries between the layers are related to the conversion sub-processes: drying, pyrolysis and char burnout fronts. At the beginning of the thermal conversion process only drying is of relevance. Due to heating up, moisture starts to get released from the particle. The pyrolysis layer consists of dry biomass and is located around the drying layer as the drying front moves towards the particle centre. When pyrolysis commences, the dry biomass converts to char and volatiles. Volatiles leave the particle and char builds a layer around the pyrolysis layer. Finally, char burnout also creates another layer which contains only ash and surrounds the char layer. As the conversion of the fuel particle proceeds, drying,

pyrolysis and char burnout fronts move from the surface to the centre of the particle. Fig. 1 shows the scheme of the layer model for a cylindrical thermally thick particle at a certain time when all the sub-processes of thermal conversion are existing.

The conversion of each layer is simulated by separate sub-models. It is assumed that drying occurs at a fixed boiling temperature in an infinitely thin zone that separates the wet and the dry part of the particle. Such a steep drying front for the fast drying of biomass is reported almost by all drying models [15]. The drying process acts as a heat sink, it means that any amount of heat flow above the boiling temperature is consumed by the drying process. This approach to calculate the evaporation rate is the most often used model in literature, for instance [4–6,16–20]. It is assumed that there is no resistance to mass transfer, and therefore the water vapour instantaneously leaves the particle. However, the cooling effect of the water vapour transfer through the particle is considered. Therefore the drying rate is controlled by heat transfer.

Biomass pyrolysis is described by decomposition of its three pseudo-components hemicellulose, cellulose, and lignin. This model implicitly assumes the hypothesis of an independent decomposition of these three constituents. An Arrhenius equation is used to describe the pyrolysis of each pseudo-component. It represents the dependence of the kinetic rate constant  $k$  on the absolute temperature  $T$ :

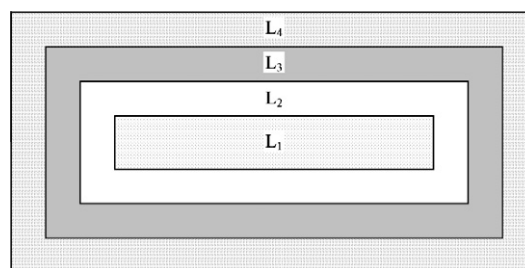


**Fig. 1.** Scheme of the layer model;  $L_1$ ... drying layer;  $L_2$ ... pyrolysis layer;  $L_3$ ... char layer;  $L_4$ ... ash layer.

$$k = A \exp\left(-\frac{E}{RT}\right) \quad (1)$$

A is the pre-exponential factor, E is the activation energy and R is the universal gas constant.

The overall mass loss rate of a particle during pyrolysis is given as:

$$-\frac{dm}{dt} = \sum_{i=1}^3 c_i \frac{d\alpha_i}{dt} \quad (2)$$

where *i* is related to each pseudo-component,  $c_i = m_{0,i} - m_{f,i}$  is a measure of the contribution of the partial decomposition processes to the overall mass loss  $m_0 - m_f$ . The conversion of each pseudo-component  $\alpha_i$  can be expressed by:

$$\alpha_i = \frac{m_{0,i} - m_i}{m_{0,i} - m_{f,i}} \quad (3)$$

The pseudo-components are all assumed to decompose individually according to a first-order reaction, therefore the conversion rate of each pseudo-component is given by:

$$\frac{d\alpha_i}{dt} = A_i \exp\left(-\frac{E_i}{RT}\right)(1 - \alpha_i) \quad (4)$$

Char conversion models are more complicated than biomass pyrolysis models, as they are based on heterogeneous reactions for which both intrinsic kinetic and transport phenomena are important. It has been experimentally verified that char combustion is such a rapid reaction that it occurs in a very thin layer [21]. Due to the structure of the layer model, the char conversion reactions are assumed to occur at the interface between char and ash layer. Char oxidation with O<sub>2</sub> and gasification with CO<sub>2</sub>, H<sub>2</sub>O and H<sub>2</sub> are considered as char conversion reactions. The heterogeneous reaction rate constants are listed in Table 1. The rate of char conversion reactions is a function of both kinetic rate at the reaction surface and mass transfer rate to/from the reaction surface. Assuming a global reaction rate of first order with respect to the oxidising/gasifying agent concentration at the reaction surface, leads to char conversion rate as:

$$\frac{dm_{ch}}{dt} = - \sum_{i=1}^4 \frac{\Omega_i M_c}{\frac{1}{k_i S} + \frac{1}{h_m S} + \int_{\delta_{ash}} \frac{dr}{D_e} S(r)} X_{\infty,i} \quad (5)$$

where *i* = 1–4 corresponds to the heterogeneous reactions in Table 1 and  $\Omega_i$  is the stoichiometric ratio of moles of carbon per mole of oxidising/gasifying agent in the corresponding reaction.  $M_c$ ,  $S$ ,  $k_i$ ,  $\delta_{ash}$  and  $X_{\infty,i}$  are the carbon molecular weight, the surface area of the char burnout front, the kinetic rate constant of heterogeneous reaction *i*, the thickness of the ash layer and the molar concentration of oxidising/gasifying agent of reaction *i* at the bulk flow, respectively.

The mass transfer coefficient of reactant species in the boundary layer around the particle  $h_m$ , is obtained by the Sherwood number. The effective diffusivity of the ash layer  $D_e$ , depends on the ash porosity  $\phi$ , the tortuosity  $\eta$ , and the molecular diffusivity of the penetrating gaseous component  $D_a$ :

$$D_e = \frac{\phi}{\eta} D_a \quad (6)$$

**Table 1**  
Heterogeneous reaction kinetic rate constants [22].

$\Omega C + O_2 \rightarrow 2(\Omega - 1)CO + (2\Omega)CO_2$	$k_c = 1.715 T \exp(-9000/T)$ $\Omega = \frac{2(1+4.3 \exp(-3390/T))}{2+4.3 \exp(-3390/T)}$
$C + CO_2 \rightarrow 2CO$	$k_c = 3.42 T \exp(-15,600/T)$
$C + H_2O \rightarrow CO + H_2$	$k_c = 3.42 T \exp(-15,600/T)$
$C + 2H_2 \rightarrow CH_4$	$k_c = 3.42 \times 10^{-3} T \exp(-15,600/T)$

The tortuosity can be replaced by the inverse of the porosity, which is often a reasonable approximation [23–25]:

$$D_e = \phi^2 D_a \quad (7)$$

Since particle shrinkage during drying is much lower compared to that occurring during pyrolysis and charcoal combustion [26], it is postulated that during drying, the size of the particle remains constant and its density decreases. However, both shrinkage and density change during the pyrolysis and char burnout are considered in the layer model.

The external surface of the particle exchanges heat and mass with the surroundings. Boundary conditions are required to complete the system of equations. The symmetry boundary condition is applied for the energy equation, at the particle centre which leads to zero heat flux. The Neumann boundary condition is used at the particle surface with known emissivity,  $\epsilon$ , and radiation,  $T_{rad}$ , as well as convection,  $T_{conv}$ , temperatures:

$$\lambda \left(\frac{\partial T}{\partial r}\right)_{r=R} = \epsilon \sigma (T_{rad}^4 - T_{r=R}^4) + h_{conv}(T_{conv} - T_{r=R}) \quad (8)$$

where  $\sigma$  is the Stefan–Boltzmann constant.  $h_{conv}$  is the convective heat transfer coefficient and is determined by an appropriate correlation for the Nusselt number. For spherical particles the Ranz–Marshall correlation and for cylindrical particles the correlation proposed by Churchill and Bernstein are applied [27].

To validate the layer model, experimental data of a single-particle reactor reported by Lu et al. [7] were utilised. Measured particle surface temperatures, centre temperatures and mass loss during thermal conversion of cylindrical particles under oxidising and non-oxidising conditions were compared with the predictions of the layer model. Table 2 summarises the physical and chemical properties used in the simulations of the single particle reactor. Some of the results of validation simulations are presented in Figs. 2 and 3. The model predictions for particle centre and surface temperature as well as the particle mass loss profile agree well with experiments. A detailed description of the layer model and its application for the simulation of an underfeed stoker furnace are presented in [9].

In this study the validated layer model is applied to calculate the heating rate in different biomass particles under various pyrolysis conditions.

### 3. Pyrolysis mass loss function

The mass loss rate of each pseudo-component, Eq. (4), for constant heating rate experiments  $T = \beta t + T_0$ , can be rearranged to:

$$\frac{d\alpha_i}{dT} = \frac{A_i}{\beta} \exp(1 - \alpha_i) \quad (9)$$

If one looks for the temperature at which the maximum conversion rate of each pseudo-component occurs  $T_m$ , the second derivative of  $\alpha_i$  in respect to temperature is required:

$$\frac{d^2\alpha_i}{dT^2} = \frac{A_i}{\beta} \exp\left(-\frac{E_i}{RT}\right) \left[\frac{E_i}{RT^2}(1 - \alpha_i) - \frac{d\alpha_i}{dT}\right] \quad (10)$$

The extrema of the conversion rate of each pseudo-component are the roots of equation  $d^2\alpha_i/dT^2 = 0$ . Considering Eqs. (10) and (9) results in:

$$\frac{E_i}{RT} - \ln\left(\frac{RA_i}{E_i\beta} T^2\right) = 0 \quad (11)$$

Eq. (11) might have only one root. According to the DTG curves this root corresponds to the temperature  $T_m$  for each pseudo-component. This equation was also applied as a characteristic pyrolysis temperature by Saastamoinen [19].

**Table 2**  
Parameters used in the simulations.

Proximate analysis (wt.% d.b.)				Ultimate analysis (wt.% d.b.)			
	Poplar	Spruce	Beech		Poplar	Spruce	Beech
C	48.1	52.04	48.3	Volatiles	90	81.2	78.1
H	5.77	6.07	6.0	Char	9.5	18.3	21.29
O	45.53	40.99	44.99	Ash	0.5	0.5	0.61
N	0.1	0.4	0.1				
		Density (kg m <sup>-3</sup> )		Conductivity [7] (W m <sup>-1</sup> K <sup>-1</sup> )		Heat capacity [34] (J kg <sup>-1</sup> K <sup>-1</sup> )	
Dry wood		545 <sup>a</sup> [7]		0.14 + 6.5 × 10 <sup>-4</sup> T		1500 + T	
Char		200 [28]		0.071		420 + 2.09T + 6.85 × 10 <sup>-4</sup> T <sup>2</sup>	
Ash		300		1.2		420 + 2.09T + 6.85 × 10 <sup>-4</sup> T <sup>2</sup>	
Water		998.2		0.6		4182	
Particle emissivity (-)		ε = 0.85					
Bulk flow velocity (m/s)		1					
		Hemicellulose		Cellulose		Lignin	
<i>Pyrolysis model [10]</i>							
A (s <sup>-1</sup> )		2.527 × 10 <sup>11</sup>		1.379 × 10 <sup>14</sup>		2.202 × 10 <sup>12</sup>	
E (kJ mol <sup>-1</sup> )		147		193		181	
<i>Char conversion model</i>							
Pore diameter (μm)		100 [29]					
Porosity of ash layer		0.9					

<sup>a</sup> Poplar wood.

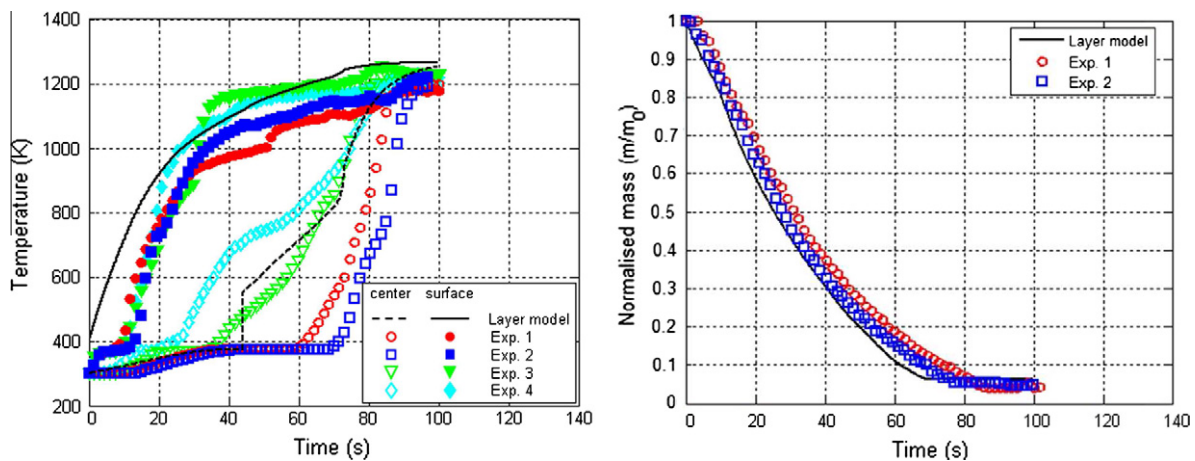


**Fig. 2.** Comparison between simulated and measured temperature and normalised mass profiles during pyrolysis of a cylindrical poplar wood particle;  $D = 9.5$  mm,  $L = 38$  mm,  $MC = 40\%$  w.b.,  $T_{rad} = 1276$  K; the experimental data are from Lu et al. [7].

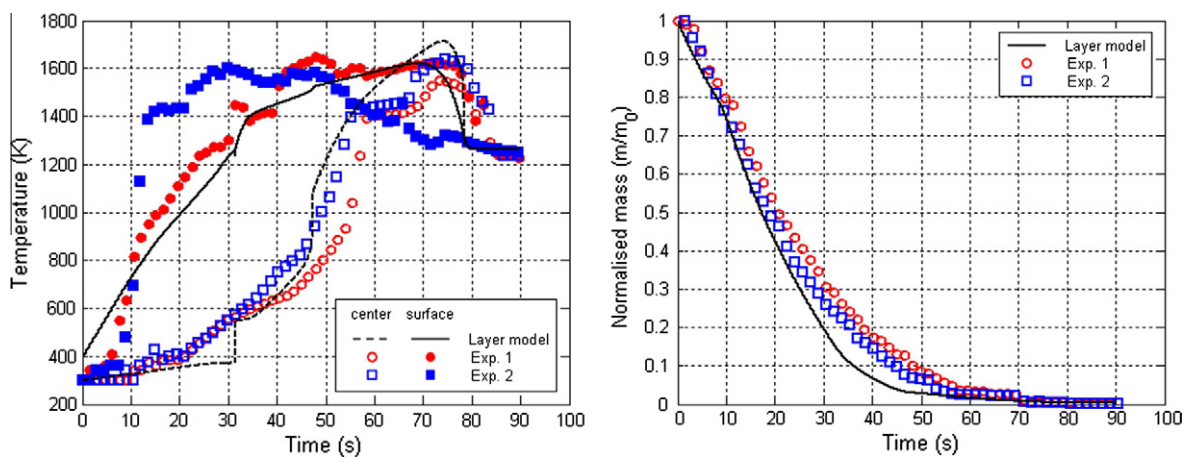


**Fig. 3.** Comparison between simulated and measured temperature and normalised mass profiles during combustion of a cylindrical poplar wood particle;  $D = 9.5$  mm,  $L = 9.5$  mm,  $MC = 40\%$  w.b.,  $T_{rad} = 1276$  K; the experimental data are from Lu et al. [7].



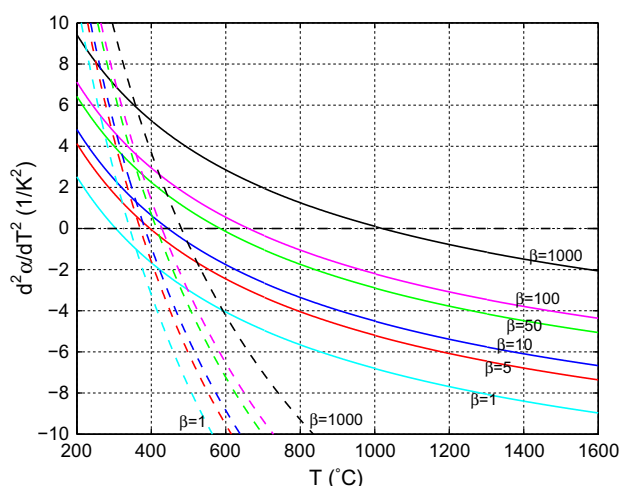


**Fig. 4.** Effect of the heating rate on the root of Eq. (11),  $\beta$  is given in (K/min). Solid lines are related to kinetic data obtained at 5 (K/min):  $A = 3.98$  (1/s),  $E = 46$  (kJ/mol) [30] and dashed lines are related to kinetic data obtained at 80 (K/min):  $A = 2.202 \times 10^{12}$  (1/s),  $E = 181$  (kJ/mol) [10].

Several experimental results [10–13,31–33] confirm that increasing the heating rate moves the DTG curves towards higher temperatures. This lateral shift or delayed decomposition might be attributed to the residence time of the sample. Since a higher heating rate means shorter exposure to a certain temperature or temperature domain, the sample needs to reach higher temperatures to have enough time for completion of the overall decomposition.

As it can be seen the second term of Eq. (11) is a function of the heating rate  $\beta$ . For a given set of kinetic parameters, i.e.  $A_i$  and  $E_i$ , any changes in the heating rate alert  $T_m$  and successively lead to a lateral shift of the DTG curve. In other words, as the heating rate increases, the DTG curves as well as the temperature  $T_m$  move towards higher temperatures. Fig. 4 illustrates the effect of the heating rate on the root of Eq. (11). In this figure the kinetic data for the decomposition of beech lignin at low and high heating rates (5 and 80 K/min) were applied [10,30]. The temperature  $T_m$  increases in both sets of kinetic data, when the heating rate raises from 1 to 1000 K/min.

Accordingly, the pyrolysis mass loss function is able to predict the lateral shift of DTG curves by changing the heating rate. However, applying low heating rate kinetic parameters overestimates the increase of  $T_m$ . It can be explained by the ratio of the pre-exponential factor to the activation energy. As it is seen in Eq. (11), if this ratio is small, the temperature for the maximum conversion rate drastically changes by variations of the heating rate. Almost in all TGA experiments at low heating rate the ratio of the pre-exponential factor to the activation energy is small enough to result in an unrealistic  $T_m$ , particularly for lignin.

Fig. 5 shows the effect of applying high and low heating rate kinetic parameters for the simulation of pyrolysis of a poplar particle under high heating rate conditions. As it can be seen the simulation results obtained by applying the high heating rate kinetic parameters are in agreement with the experimental data. At the end of pyrolysis (attributed to pyrolysis of lignin), there is a deviation between the simulation results obtained by applying the low heating rate kinetic parameters and the measured values. It indicates that applying the low heating rate kinetic parameters for the simulation of a high heating rate case leads to much slower mass loss rate during the pyrolysis of lignin in comparison to the measurements as well as the results of the simulation with the high heating rate kinetic parameters. It means that the pyrolysis

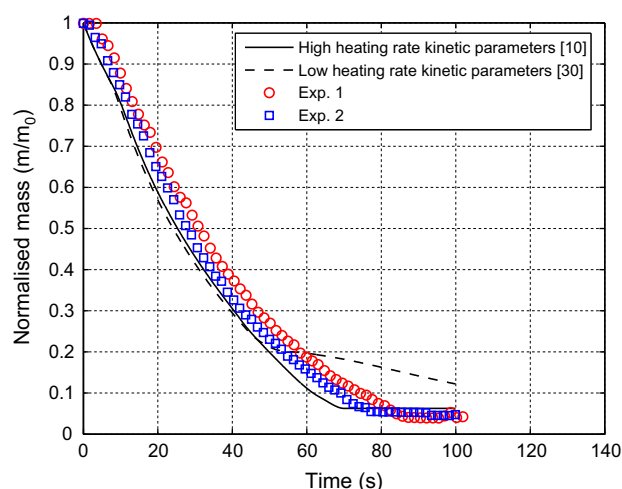


**Fig. 5.** Effect of applying high and low heating rate kinetic parameters for the simulation of pyrolysis of a poplar particle under high heating rate conditions; the pyrolysis conditions are the same as in Fig. 2; the experimental data are from Lu et al. [7].

of lignin in the case of applying the low heating rate kinetic parameters begins at higher temperatures. Hence, as it is shown in Fig. 4, the increase of  $T_m$  has been over-predicted by applying the low heating rate kinetic parameters.

Therefore, using kinetic parameters measured at low heating rate TGA experiments for the simulation of pyrolysis in high heating rate regime leads to an unrealistic shape of the DTG curves. It, successively, impairs the overall mass loss profile during pyrolysis.

#### 4. Influencing parameters on the heating rate

The rate of variation of temperature distribution inside a bio-mass particle over time as it is exposed to an external heat flux, depends on the particle density  $\rho$ , specific heat capacity  $c_p$ , size, thermal conductivity  $\lambda_s$  as well as the heat flux itself. The moisture content also indirectly affects the heating rate. It changes the particle density, heat capacity and thermal conductivity. To generalise the investigation of the effects of these parameters on the heating rate, they are summarised in the Biot number and the thermal time constant:

$$Bi = \frac{h_e L_c}{\lambda_s} \quad (12)$$

$$\tau = \frac{\rho_s c_p L_c}{h_e} \quad (13)$$

where  $h_e$  is the effective heat transfer coefficient and  $L_c$  is the particle characteristic length which is the ratio of the particle volume to its surface area. Such a definition for the characteristic length facilitates its calculation for particles with various shapes. The effective heat transfer coefficient can be defined as:

$$h_e = h_{rad} + h_{conv} = \epsilon \sigma (1 + \theta + \theta^2 + \theta^3) T_{rad}^3 + \frac{\lambda_g Nu}{L_c} \quad (14)$$

where  $\theta = \frac{T_p}{T_{rad}}$ .

The Biot number gives a measure of the ratio between the heat transfer resistances inside and at the surface of the particle. The thermal time constant shows the respond of the particle to changes in its thermal environment. In other words, a big thermal time constant means that the particle temperature changes slowly over time.

Since the particle size and physical properties as well as the external heat flux change during the thermal conversion of a particle, the Biot number and thermal time constant of a particle depend on the degree of conversion. However, one can consider a certain state of the particle conversion and calculate these two characteristic numbers based on the reference state. Therefore, in this study, the Biot number and thermal time constant based on the initial condition are used to classify the particle pyrolysis conditions. Additionally, for calculating the effective heat transfer coefficient (Eq. (14)), the physical properties of air at the corresponding radiation temperature are used. The Ranz–Marshall correlation is applied for the Nusselt number.

### 5. Results and discussion

The layer model simulation results of the pyrolysis of a spruce pellet with 8% w.b. moisture content, 6 mm diameter and 3 cm length which is exposed to 700 °C radiation temperature in an oxidising environment, are presented in Fig. 6. The particle surface temperature and the temperature at the centre of the pyrolysis layer at the beginning are the same and they increase with different slopes. Due to the drying process the boundary between the drying layer and the pyrolysis layer moves towards the particle centre. Therefore, the thickness of the pyrolysis layer increases which results in a deviation of the pyrolysis layer centre temperature from the particle surface temperature. When the char burnout starts (after about 25 s), the particle surface temperature sharply increases which results in a big deviation from the pyrolysis layer centre temperature. Approaching the end of pyrolysis, this difference declines because the pyrolysis layer thickness decreases as a result of dry wood decomposition. At the end of the pyrolysis process the pyrolysis layer vanishes and the char and ash layer remain.

Since pyrolysis happens in the pyrolysis layer, the time derivative of its centre temperature is an indicator for the heating rate at which pyrolysis takes place. The time derivative of the pyrolysis layer centre temperature is presented in Fig. 7. Moreover, the released volatiles over time, expressed as percentage of the total amount of the volatiles is shown in Fig. 7. It can be seen that at the beginning the heating rate dramatically decreases from a large value to about 340 K/min and it remains constant for some seconds. There is a local minimum at time about 15 s. It is due to the end of the drying process. The end of drying means that the drying layer disappears which results in some numerical instabilities in the layer model.

The heating rate of the pyrolysis layer is directly proportional to the temperature difference between the surface temperature and the pyrolysis layer centre temperature, the thermal conductivity and the inverse of the distance between the particle surface and the centre of the pyrolysis layer. As it is shown in Fig. 6, the fast increase of the particle surface temperature at the beginning of char burnout results in a large difference between the surface temperature and the temperature at the centre of the pyrolysis layer. Therefore, the heating rate of the pyrolysis layer increases between 25 and 30 s.

Afterwards, the increasing rate of the particle surface temperature declines and stays constant. At the same time, the pyrolysis layer centre temperature gradually increases. Hence, the difference between this temperature and the particle surface temperature declines. Additionally, conversion of dry wood to charcoal during pyrolysis decreases the thermal conductivity, because the conductivity of charcoal is less than that of dry wood [34]. Therefore, the heating rate gradually decreases between 30 and 55 s. Then, it raises, because the distance between the particle surface and the centre of the pyrolysis layer rapidly declines. The rate of decrease

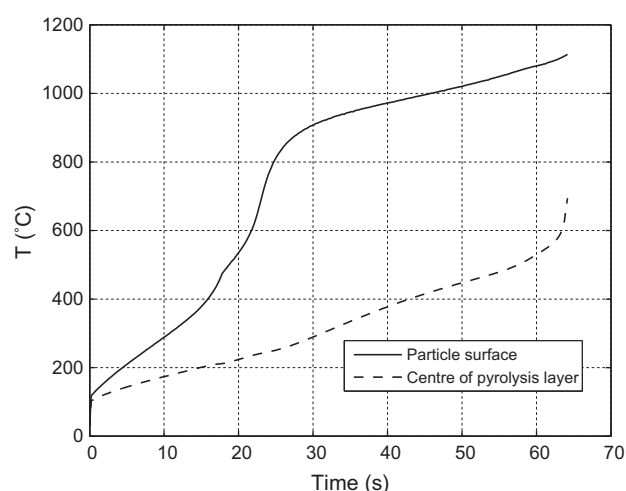


Fig. 6. Simulated temperatures of the particle surface and of the centre of the pyrolysis layer for a spruce pellet with  $D = 6$  mm,  $L = 30$  mm and  $MC = 8\%$  w.b. exposed to  $T_{rad} = 700$  °C during pyrolysis in an oxidising environment.

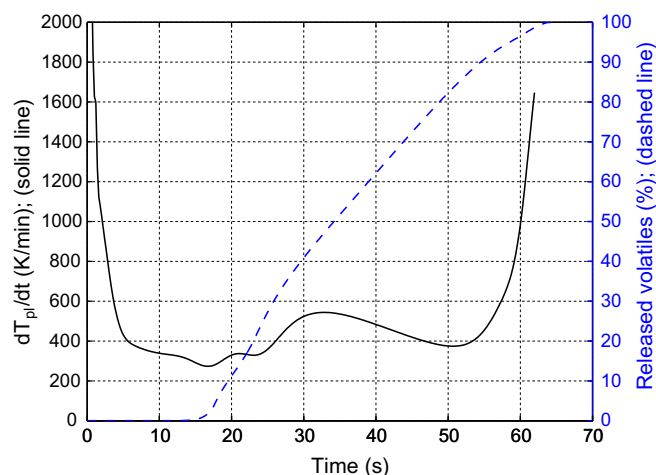


Fig. 7. Time derivative of the centre temperature of the pyrolysis layer presented in Fig. 6 and percentage of volatiles released during the pyrolysis of the spruce pellet.

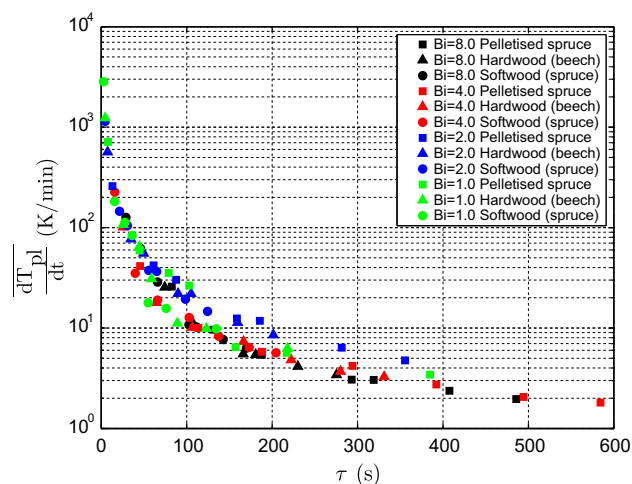


Fig. 8. Volatiles release rate weighted average of the heating rate of the pyrolysis layer vs. thermal time constant for various Biot numbers and different biomass fuels (data according to Table 3).

**Table 3**

Average of the heating rate of the pyrolysis layer centre temperature weighted by pyrolysis rate in dependence of the Biot number, the thermal time constant and biomass particle density as presented in Fig. 8.

Case	T (°C)	MC (%w.b.)	D (m)	L (m)	Pelletised spruce $\rho_p = 1200$ (kg/m <sup>3</sup> )		Hardwood (beech) $\rho_p = 680$ (kg/m <sup>3</sup> )		Softwood (spruce) $\rho_p = 420$ (kg/m <sup>3</sup> )	
					$\tau$ (s)	$\frac{dT_{pl}}{dt}$ (K/min)	$\tau$ (s)	$\frac{dT_{pl}}{dt}$ (K/min)	$\tau$ (s)	$\frac{dT_{pl}}{dt}$ (K/min)
<i>Bi = 8.0</i>										
1	1326	8	0.050	0.080	82.65	25.86	46.83	60.51	28.93	1.26e <sup>2</sup>
2	1192	8	0.060	0.120	1.31e <sup>2</sup>	9.63	74.37	25.46	45.93	62.21
3	1100	8	0.070	0.100	1.88e <sup>2</sup>	5.42	1.07e <sup>2</sup>	11.47	65.8	28.74
4	1004	10	0.085	0.210	2.93e <sup>2</sup>	3.06	1.66e <sup>2</sup>	5.52	1.03e <sup>2</sup>	10.77
5	982	10	0.084	0.300	3.19e <sup>2</sup>	3.04	1.81e <sup>2</sup>	5.43	1.12e <sup>2</sup>	10.24
6	923	10	0.093	0.400	4.08e <sup>2</sup>	2.37	2.30e <sup>2</sup>	4.15	1.43e <sup>2</sup>	7.68
7	880	10	0.100	0.500	4.86e <sup>2</sup>	1.96	2.75e <sup>2</sup>	3.42	1.70e <sup>2</sup>	6.31
<i>Bi = 4.0</i>										
1	1214	8	0.025	0.050	45.53	41.42	25.80	1.01e <sup>2</sup>	15.93	2.25e <sup>2</sup>
2	998	10	0.040	0.070	1.14e <sup>2</sup>	10.03	64.43	17.91	39.80	35.07
3	872	10	0.050	0.100	1.88e <sup>2</sup>	5.81	1.07e <sup>2</sup>	10.11	65.85	18.95
4	845	20	0.055	0.145	2.94e <sup>2</sup>	4.20	1.67e <sup>2</sup>	7.34	1.03e <sup>2</sup>	12.70
5	777	20	0.065	0.150	3.92e <sup>2</sup>	2.74	2.22e <sup>2</sup>	4.82	1.37e <sup>2</sup>	8.31
6	801	30	0.070	0.130	4.94e <sup>2</sup>	2.06	2.80e <sup>2</sup>	3.70	1.73e <sup>2</sup>	6.41
7	762	30	0.075	0.150	5.84e <sup>2</sup>	1.81	3.31e <sup>2</sup>	3.27	2.05e <sup>2</sup>	5.67
<i>Bi = 2.0</i>										
1	1206	8	0.009	0.024	13.08	2.59e <sup>2</sup>	7.41	5.66e <sup>2</sup>	4.58	1.14e <sup>3</sup>
2	832	8	0.019	0.060	61.23	42.03	34.70	76.96	21.43	1.45e <sup>2</sup>
3	737	8	0.022	0.090	87.59	30.24	49.64	55.43	30.66	1.05e <sup>2</sup>
4	710	20	0.030	0.060	1.59e <sup>2</sup>	12.44	89.97	22.06	55.57	37.48
5	672	20	0.031	0.080	1.86e <sup>2</sup>	11.80	1.05e <sup>2</sup>	22.00	64.96	36.58
6	577	20	0.040	0.080	2.81e <sup>2</sup>	6.37	1.60e <sup>2</sup>	11.36	98.52	19.35
7	527	20	0.045	0.090	3.56e <sup>2</sup>	4.76	2.02e <sup>2</sup>	8.53	1.24e <sup>2</sup>	14.63
<i>Bi = 1.0</i>										
1	900	8	0.005	0.013	7.90	7.11e <sup>2</sup>	4.56	1.24e <sup>3</sup>	2.76	2.84e <sup>3</sup>
2	477	8	0.012	0.030	45.05	59.22	25.75	1.07e <sup>2</sup>	15.77	1.82e <sup>2</sup>
3	467	20	0.015	0.030	78.89	35.32	44.70	64.88	27.61	1.13e <sup>2</sup>
4	510	30	0.016	0.035	1.03e <sup>2</sup>	26.43	58.79	30.83	36.07	83.46
5	397	30	0.020	0.035	1.57e <sup>2</sup>	6.44	89.15	11.17	55.06	17.81
6	427	40	0.020	0.050	2.17e <sup>2</sup>	5.65	1.23e <sup>2</sup>	9.88	75.98	15.71
7	387	50	0.025	0.050	3.85e <sup>2</sup>	3.43	2.18e <sup>2</sup>	6.25	1.35e <sup>2</sup>	9.83

of pyrolysis layer thickness at the end of pyrolysis is significantly higher than at the beginning of pyrolysis, because of the gradual increase in pyrolysis layer temperature during pyrolysis and the fact that the pyrolysis rate is an exponential function of temperature.

The main outcome of Fig. 7 is that the heating rate during the release of volatiles varies between 300 and more than 1000 K/min for the spruce pellet under the given conditions. However, most of the volatiles are released at heating rates between 300 and 550 K/min. It shows that in order to define a value which is an appropriate indicator for the heating rate during pyrolysis both the heating rate and the release rate of volatiles at that heating rate have to be considered. Therefore, the volatiles release rate weighted average of the heating rate is introduced as:

$$\overline{\frac{dT_{pl}}{dt}} = \frac{\sum_{i=1}^n \left(\frac{dT_{pl}}{dt}\right)_i \cdot \left(\frac{dm_{vol}}{dt}\right)_i}{\sum_{i=1}^n \left(\frac{dm_{vol}}{dt}\right)_i} \quad (15)$$

where  $i$  is related to each time step during the pyrolysis.  $\overline{\frac{dT_{pl}}{dt}}$  for Fig. 7 is 461 K/min.

The volatiles release rate weighted average of the heating rate of the pyrolysis layer versus the thermal time constant for different Biot numbers and biomass fuels are presented in Fig. 8. For each Biot number several cases with various radiation temperatures, moisture contents and particle sizes were taken into account (they can be seen in Table 3 and by the markers in Fig. 8). Since the Biot number is independent of density, for each Biot number three

different particle densities, 420, 680 and 1200 kg/m<sup>3</sup> are considered for softwood (spruce), hardwood (beech) and pelletised spruce, respectively. The physical properties used in Eqs. (12) and (13) are reported in Table 2. As already mentioned the Biot number and the thermal time constant are calculated based on the initial condition. Therefore, the physical properties are related to the moist fuel and the effect of the moisture content is considered by using the mass weighted mixing law:

$$X_{moistfuel} = (1 - MC)X_{dryfuel} + MCX_{water} \quad (16)$$

where  $X$  denotes the physical properties, e.g. density, specific heat and thermal conductivity and  $MC$  is the fuel moisture content.

An increase in density at a constant Biot number increases the thermal time constant which can be simply explained by Eq. (13). The comparison between different biomass fuels (densities) for a certain case indicates that the heating rate decreases by an increase in density, because the particles with higher density need more thermal energy for a certain change in their temperature over time.

According to Fig. 8, the heating rate exponentially declines by increasing the thermal time constant. This can be explained by the definition of the thermal time constant, i.e. the tendency of the particle to retain its temperature while its thermal environment has been changed. The variation of the Biot number has only a negligible effect on the heating rate in comparison to the variation of thermal time constant.

In addition, since each Biot number can result in both high and low heating rate regimes between 1000 K/min and less than 10 K/

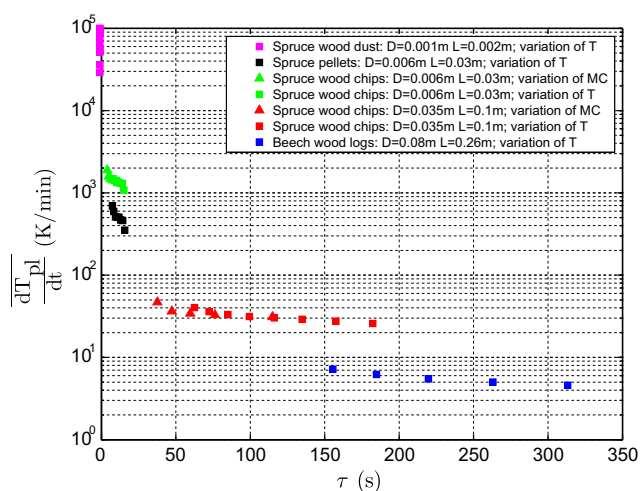


**Fig. 9.** Volatiles release rate weighted average of the heating rate of the pyrolysis layer vs. thermal time constant for different biomass fuels used in state-of-the-art combustion plants (data according to Table 4).

min, the Biot number cannot be used to specify the heating rate regime during pyrolysis. However, the thermal time constant can determine the heating rate regime. As it can be seen in Fig. 8, the cases with thermal time constants higher than 50 s indicate a low heating rate regime, i.e.  $\frac{dT_{pl}}{dt} < 50$  K/min.

Additionally, the pyrolysis rate weighted average of the heating rate of different biomass fuels applied in state-of-the-art combustion/gasification plants versus the thermal time constant are shown in Fig. 9. Pellets, wood chips, wood dust and wood logs have been chosen to cover most biomass combustion applications. Pellets according to the Austrian standard (ÖNORM M7135) typically show a moisture content of 8% w.b. as well as a diameter of 0.006 m and a length of 0.03 m. Regarding wood chips two different sizes were considered, one particle size class similar to pellets (small wood chips) and another one with a diameter of 0.035 m

and a length of  $L = 0.1$  m (large wood chips). The moisture content of wood chips has been varied between 10 and 55% w.b. Additionally, wood logs according to the Austrian standard (ÖNORM CEN/TS 14961) with a moisture content of 12% w.b. (M20), a diameter of 0.08 m and a length of 0.26 m (P250) have been considered. Since the layer model is applicable for cylindrical and spherical shapes, the wood log is assumed to be cylindrical. The diameter and length of an equivalent cylindrical wood log were calculated by keeping the volume and surface area constant. Wood dust was considered to be cylindrical with a moisture content of 10% w.b., a diameter of 0.001 m and a length of 0.002 m.

Pellets, wood logs and wood dust typically show a rather constant moisture content, therefore, only the effect of radiation temperature on the heating rate was investigated for these biomass fuels. However, for wood chips the effects of both radiation temperature and moisture content were examined, due to the possible big variations in moisture contents. Radiation temperature varied between 600 and 1300 °C for all biomass types, except for wood dust, where radiation temperatures up to 1500 °C have been considered. In Table 4 the corresponding data shown in Fig. 9 are listed. By these variations concerning biomass type and combustion conditions all typical applications like stoves, fixed and fluidised bed combustion/gasification systems as well as dust combustion plants are considered.

Fig. 9 indicates that wood dust and wood pellet pyrolysis always occur in high heating rate regimes. On the other hand wood log pyrolysis happens in a low heating rate regime. For wood chips the heating rate regime depends on the particle size. The effect of density can also be seen in Fig. 9 by comparison between spruce pellets and spruce wood chips of the same size. The higher the density the lower the heating rate (in agreement with the results of Fig. 8). A comparison between the effects of moisture content and radiation temperature on the heating rates of wood chips shows that radiation temperature has a bigger influence, particularly for small wood chips. It can be stated that moisture content does not strongly influence the heating rate regime of a certain biomass particles.

**Table 4**  
Biot number, thermal time constant and heating rate of different biomass fuels as presented in Fig. 9 in dependence of radiation temperature and moisture content.

T (°C)	Spruce wood dust $D = 0.001$ m, $L = 0.002$ m				Spruce pellets $D = 0.006$ m, $L = 0.03$ m				Beech wood logs $D = 0.08$ m, $L = 0.26$ m			
	MC (%w.b.)	Bi (-)	$\tau$ (s)	$\frac{dT_{pl}}{dt}$ (K/min)	MC (%w.b.)	Bi (-)	$\tau$ (s)	$\frac{dT_{pl}}{dt}$ (K/min)	MC (%w.b.)	Bi (-)	$\tau$ (s)	$\frac{dT_{pl}}{dt}$ (K/min)
600	10	0.49	0.21	2.83e <sup>4</sup>	8	0.87	15.61	3.53e <sup>2</sup>	12	3.55	3.13e <sup>2</sup>	4.58
700	10	0.52	0.20	3.48e <sup>4</sup>	8	0.95	14.29	4.61e <sup>2</sup>	12	4.23	2.62e <sup>2</sup>	5.02
800	10	0.56	2.71	4.96e <sup>4</sup>	8	1.05	12.95	4.68e <sup>2</sup>	12	5.06	2.19e <sup>2</sup>	5.48
900	10	0.59	0.19	5.41e <sup>4</sup>	8	1.15	11.81	5.04e <sup>2</sup>	12	6.02	1.85e <sup>2</sup>	6.21
1000	10	0.64	0.18	6.30e <sup>4</sup>	8	1.28	10.61	5.07e <sup>2</sup>	12	7.16	1.55e <sup>2</sup>	7.18
1100	10	0.70	0.16	7.40e <sup>4</sup>	8	1.43	9.45	5.10e <sup>2</sup>	-	-	-	-
1200	10	0.78	0.15	8.27e <sup>4</sup>	8	1.64	8.28	5.95e <sup>2</sup>	-	-	-	-
1300	10	0.84	0.14	8.51e <sup>4</sup>	8	1.83	7.42	6.93e <sup>2</sup>	-	-	-	-
1400	10	0.90	0.13	9.58e <sup>4</sup>	-	-	-	-	-	-	-	-
1500	10	0.96	0.11	9.61e <sup>4</sup>	-	-	-	-	-	-	-	-
	Spruce wood chips $D = 0.006$ m, $L = 0.03$ m				Spruce wood chips $D = 0.035$ m, $L = 0.1$ m							
1000	10	1.26	3.89	1.89e <sup>3</sup>	10	3.88	37.64	46.89				
1000	20	1.17	4.88	1.58e <sup>3</sup>	20	3.61	47.30	36.31				
1000	30	1.10	6.16	1.49e <sup>3</sup>	30	3.38	59.71	34.25				
1000	40	1.03	7.87	1.42e <sup>3</sup>	40	3.18	76.26	32.86				
1000	55	0.95	11.86	1.34e <sup>3</sup>	55	2.91	1.15 <sup>2</sup>	31.01				
600	50	0.66	51.10	1.08e <sup>3</sup>	50	1.64	1.82e <sup>2</sup>	25.87				
700	50	0.72	13.83	1.30e <sup>3</sup>	50	1.89	1.58e <sup>2</sup>	27.56				
800	50	0.80	12.54	1.32e <sup>3</sup>	50	2.21	1.35e <sup>2</sup>	29.01				
900	50	0.87	11.42	1.34e <sup>3</sup>	50	2.57	1.16e <sup>2</sup>	30.27				
1000	50	0.97	10.27	1.34e <sup>3</sup>	50	3.00	99.43	31.42				
1100	50	1.09	9.14	1.42e <sup>3</sup>	50	3.51	85.01	33.20				
1200	50	1.25	8.01	1.47e <sup>3</sup>	50	4.12	72.36	36.07				
1300	50	1.39	7.18	1.48e <sup>3</sup>	50	4.77	62.54	40.41				

## 6. Summary and conclusions

The influence of the heating rate on the pyrolysis kinetic model and successively on the overall mass loss of biomass particles, raises the demand to investigate the range of heating rates which may occur during pyrolysis. For this purpose a one-dimensional single particle model was utilised to simulate the temperature profile inside biomass particles as well as the particles mass loss during pyrolysis under various conditions. The average of the time derivative of the pyrolysis layer centre temperature weighted by the volatiles release rate was found to be an appropriate indicator for the heating rate in biomass particles during pyrolysis.

It was shown that the heating rate is mainly affected by the radiation temperature and the particle size. Moreover, the density of the biomass particles has a relevant influence. Compared to the other parameters, the moisture content shows only small influences. The influencing parameters on the heating rate were summarised in the Biot number and the thermal time constant, in order to generalise the investigations. It has been found that the heating rate exponentially decreases as the thermal time constant increases. The variation of the Biot number has only a negligible effect on the heating rate. Therefore, to specify the heating rate regime the thermal time constant is sufficient. The results show that if the thermal time constant is more than 50 s, pyrolysis happens in a low heating rate regime, i.e.  $\frac{dT_{pl}}{dt} < 50$  K/min.

Additionally, the heating rate during pyrolysis of different biomass fuels applied in state-of-the-art combustion plants was examined. A broad range of biomass types and thermal conversion conditions were considered to cover all typical biomass combustion applications. It was found that pyrolysis of wood dust and wood pellets always occur in high heating rate regimes. Furthermore, wood log pyrolysis always takes place in a low heating rate regime. However, the heating rate regime during pyrolysis of wood chips is dependent on the particle size.

The results clearly show for which biomass fuels and combustion conditions the results of conventional TGA systems (typically with heating rates well below 50 K/min) can be applied and when kinetic parameters derived from high heating rate experiments are needed. This distinguishment is of great importance, because at present in many cases pyrolysis kinetic parameters derived from low heating rate TGA experiments are incorrectly used.

## References

- [1] Peters B. Measurements and application of a discrete particle model (DPM) to simulate combustion of a packed bed of individual fuel particles. *Combust Flame* 2002;131:132–46.
- [2] Wurzenberger JC, Wallner S, Raupenstrauch H, Khinast JG. Thermal conversion of biomass: comprehensive reactor and particle modeling. *AIChE J* 2002;48:2398–410.
- [3] Thunman H, Leckner B, Niklasson F, Johnsson F. Combustion of wood particles – a particle model for Eulerian calculations. *Combust Flame* 2002;129:30–46.
- [4] Bruch C, Peters B, Nussbaumer T. Modelling wood combustion under fixed bed conditions. *Fuel* 2003;82:729–38.
- [5] Porteiro J, Miguez JL, Granada E, Morán JC. Mathematical modelling of the combustion of a single wood particle. *Fuel Process Technol* 2006;87:169–75.
- [6] Porteiro J, Granada E, Collazo J, Patiño D, Morán JC. A model for the combustion of large particles of densified wood. *Energy Fuels* 2007;21:3151–9.
- [7] Lu H, Robert W, Peirce G, Ripa B, Baxter LL. Comprehensive study of biomass particle combustion. *Energy Fuels* 2008;22:2826–39.
- [8] Lu H, Ip E, Scott J, Foster P, Vickers M, Baxter LL. Effects of particle shape and size on devolatilization of biomass particle. *Fuel* 2010;89:1156–68.
- [9] Mehrabian R, Stangl S, Scharler R, Obernberger I. CFD simulation of biomass grate furnaces with a comprehensive 3D packed bed model. In: 25th German flame day conference, Karlsruhe, Germany; September 2011.
- [10] Branca C, Albano A, Di Blasi C. Critical evaluation of wood devolatilization mechanisms. *Thermochim Acta* 2005;429:133–41.
- [11] Antal MJ, Várhegyi G. Cellulose pyrolysis kinetics: the current state of knowledge. *Ind Eng Chem Res* 1995;34:703–17.
- [12] Várhegyi G, Antal MJ, Jakab E, Szabo P. Kinetic modeling of biomass pyrolysis. *J Anal Appl Pyrol* 1996;42:73–8.
- [13] Teng H, Wei YC. Thermogravimetric studies on the kinetics of rice hull pyrolysis and the influence of water treatment. *Ind Eng Chem Res* 1998;37:3806–11.
- [14] Ha MY, Choi BR. A numerical study on the combustion of a single carbon particle entrained in a steady flow. *Combust Flame* 1994;97:1–16.
- [15] Di Blasi C. Multi-phase moisture transfer in the high-temperature drying of wood particles. *Chem Eng Sci* 1998;53:353–66.
- [16] Galgano A, Di Blasi C. Modeling the propagation of drying and decomposition fronts in wood. *Combust Flame* 2004;139:16–27.
- [17] Yang YB, Sharifi VN, Swithenbank J, Ma L, Darvell LI, Jones JM, et al. Combustion of a single particle of biomass. *Energy Fuels* 2008;22:306–16.
- [18] Thunman H, Davidsson K, Leckner B. Separation of drying and devolatilization during conversion of solid fuels. *Combust Flame* 2004;137:242–50.
- [19] Saastamoinen JJ. Simplified model for calculation of devolatilization in fluidized beds. *Fuel* 2006;85:2388–95.
- [20] Bilbao R, Mastral JF, Lana JA, Ceamanos J, Aldea ME, Betrán M. A model for the prediction of the thermal degradation and ignition of wood under constant and variable heat flux. *J Anal Appl Pyrol* 2002;62:63–82.
- [21] Gómez-Barea A, Leckner B. Modelling of biomass gasification in fluidized bed. *Prog Energy Combust Sci* 2010;36:444–509.
- [22] Johansson R, Thunman H, Leckner B. Influence of intraparticle gradients in modeling of fixed bed combustion. *Combust Flame* 2007;149:49–62.
- [23] Froment GF, Bischoff KB. *Chemical reactor analysis and design*. New York: John Wiley & Sons; 1990.
- [24] Johnson MFL, Stewart WE. Pore structure and gaseous diffusion in solid catalysts. *J Catal* 1965;4:248–52.
- [25] Patisson F, Francois MG, Ablitzer D. A non-isothermal, non-equimolar transient kinetic model for gas–solid reactions. *Chem Eng Sci* 1998;53:97–708.
- [26] Kumar RR, Kolar AK, Leckner B. Shrinkage characteristics of Casuarina wood during devolatilization in a fluidized bed combustor. *Biomass Bioenergy* 2006;30:153–65.
- [27] Incropera FP, De Witt DP. *Introduction to heat transfer*. 2nd ed. New York: John Wiley & Sons; 1990.
- [28] Bergström D, Israelsson S, Öhman M, Dahlqvist S, Gref R, Boman C, et al. Effects of raw material particle size distribution on the characteristics of Scots pine sawdust fuel pellets. *Fuel Process Technol* 2008;89:1324–9.
- [29] Sreekanth M, Sudhakar DR, Prasad BVSSS, Kolar AK, Leckner B. Modelling and experimental investigation of devolatilizing wood in a fluidized bed combustor. *Fuel* 2008;87:2698–712.
- [30] Grønli MG, Várhegyi G, Di Blasi C. Thermogravimetric analysis and devolatilization kinetics of wood. *Ind Eng Chem Res* 2002;41:4201–8.
- [31] Williams PT, Besler S. The influence of temperature and heating rate on the slow pyrolysis of biomass. *Renew Energy* 1996;7:233–50.
- [32] Biagini E, Fantei A, Tognotti L. Effect of the heating rate on the devolatilization of biomass residues. *Thermochim Acta* 2008;472:55–63.
- [33] Mani T, Murugan P, Abedi J, Mahinpey N. Pyrolysis of wheat straw in a thermogravimetric analyzer: effect of particle size and heating rate on devolatilization and estimation of global kinetics. *Chem Eng Res Des* 2010;88:952–8.
- [34] Grønli M. A theoretical and experimental study of the thermal degradation of biomass. PhD thesis, Norway: The Norwegian University of Science and Technology; 1996.

# Paper III



## OPTIMISATION OF BIOMASS GRATE FURNACES WITH A NEW 3D PACKED BED COMBUSTION MODEL - ON EXAMPLE OF A SMALL-SCALE UNDERFEED STOKER FURNACE

Mehrabian, R.<sup>1,2,\*</sup>, Scharler, R.<sup>1,2,3</sup>, Weissinger, A.<sup>4</sup>, Obernberger, I.<sup>1,2,3</sup>

<sup>1</sup>BIOENERGY 2020+ GmbH, Inffeldgasse 21b, 8010 Graz, Austria

Tel.: +43 (0)316 8739232; Fax: +43 (0)316 8739202; E-mail: [ramin.mehrabian@bioenergy2020.eu](mailto:ramin.mehrabian@bioenergy2020.eu)

<sup>2</sup>Institute for Process and Particle Engineering, Graz University of Technology, Inffeldgasse 21b, A-8010 Graz, Austria

<sup>3</sup>BIOS BIOENERGIESYSTEME GmbH, Inffeldgasse 21b, A-8010 Graz, Austria

<sup>4</sup>KWB - Kraft und Wärme aus Biomasse GmbH, Industriestrasse 235, A-8321 St. Margarethen, Austria

**ABSTRACT:** The design and optimisation of a biomass grate furnace requires accurate and efficient models for the combustion process on the grate as well as the turbulent reactive flow in the combustion chamber. Computational Fluid Dynamics (CFD) have been successfully applied for gas phase combustion. However, no numerical models for the biomass packed bed combustion, which can be used as engineering design tools, are commercially available at present. This paper presents an innovative 3D CFD model for biomass packed bed combustion consisting of an Euler-Granular model for hydrodynamics of gas-particle multiphase flow and a thermally thin particle model for combustion of biomass particles. Modelling the particle trajectories and the thermal conversion of each particle in the bed constitutes the simulation of the entire bed combustion. The simulation of a small-scale underfeed stoker furnace of KWB has been successfully performed by the application of the new packed bed combustion model. The positions of the drying, pyrolysis and char burnout zones in the fuel bed as well as the temperature distribution among the particles seem to be plausible and could be confirmed by observations. Furthermore, a good qualitative agreement concerning the flue gas temperatures measured by thermocouples at different positions in the combustion chamber, and CO emissions measured at boiler outlet could be achieved. The new packed bed model provides the advantages of considering the release profiles of species and energy from the fuel bed close to reality and enables to consider the chemical compositions, size and physical properties of the fuel particles as well as the influence of primary air distribution and grate motion on the particle trajectories.

**Keywords:** biomass, combustion, fixed bed, CFD, modelling.

### 1 INTRODUCTION AND OBJECTIVES

CFD simulation techniques are an efficient tool for the design and optimisation of biomass grate furnaces. They have demonstrated to be valuable to predict the flow and the gas phase combustion in furnaces [1-4]. However, at present there is a lack of reasonably accurate and computationally efficient simulation tools for packed bed biomass combustion.

The main problems encountered in modelling biomass packed bed combustion are the hydrodynamics of the gas-solid multiphase flow and thermal conversion of the biomass particles. There are various simulation methods applicable to the dense gas-solid multiphase flows (granular flows). Generally they can be classified into two approaches: the discrete element methods (DEM) based on the molecular dynamics and the continuum mechanics methods or two-fluid model (TFM) based on the assumption that the gas and particulate phases form two inter-penetrating continua [5].

The discrete element method is fully based on the Lagrangian framework, i.e. the motion of each particle is defined by classical Newtonian mechanics and contact mechanics of deformation. The particle-particle collision is modelled by the soft sphere method [6] or hard sphere method [7]. In general, discrete models are powerful and they are able to predict the rotation and velocity of each particle. Moreover, they allow the investigation of the effect of individual physical particle properties in the granular flow. The limiting parameter in the DEM is the number of particles. Hence, in most cases, the calculation time is too high for industrial scale systems.

The Euler/Euler two-fluid model assumes that the particulate phase behaves as a fluid. Therefore, the continuity and momentum equations with jump conditions for phase interfaces are solved for both gas and particulate phases. In this approach all the particles

are assumed to be identical, specified by their mean diameter and density. Therefore handling a poly-disperse system, i.e. a system with different particle sizes, requires several solid phases corresponding to the number of particle diameter classes. Hjertager reported a quadratical increase of computational effort with the number of phases [8]. Additionally, the modelling of particle-particle collisions in this approach is rather complicated. It has been implemented in the momentum equation of solid phase by the viscosity and normal stress tensor of the solid phase. There are several correlations for the solid viscosity term and the solid normal stress tensor [9-14]. They have been driven by making an analogy between the particle-particle collisions and the kinetic theory of gases [15]. The concept of granular temperature is defined to represent the kinetic energy of random particle fluctuations around their mean velocities. A conservation energy equation is formulated for this kinetic fluctuation energy in which the kinetic energy is produced by shear and fluid turbulence and dissipated by inelastic collisions and interaction with the fluid. The collisions between the particles are assumed to be a function of this kinetic fluctuation energy. The capability of the TFM for simulation of granular systems has been proven by its numerous applications, see [16] and its references.

In the present work the commercial CFD software, ANSYS FLUENT 12, has been utilised to simulate the hydrodynamics of the packed bed granular flow. Among the available gas-solid multiphase models in ANSYS FLUENT the Euler-Granular model has been selected because it is based on the kinetic theory of granular flows and allows the consideration of inter-particle interactions which are of key importance in modelling of packed beds. This model has been successfully used for predicting the hydrodynamic behaviour of a bubbling fluidised bed [17-19]. In this study the Euler-Granular

model was applied for an underfeed stoker grate furnace for the first time.

As already mentioned, the thermal conversion of the biomass particles is another challenge in modelling of biomass packed bed combustion. A realistic approach is to consider the packed bed as an ensemble of finite representative particles, where each of these particles undergoes a sequence of processes such as heat-up, drying, pyrolysis, and oxidation. The Euler-Granular model opted for tracing the particle trajectories in the packed bed does not allow considering these processes for each individual particle. Therefore, the modelling of particles thermal conversion was performed by the ANSYS FLUENT discrete phase model (DPM). Although the DPM is not suitable for particle tracking under packed bed conditions, because it ignores the volume of particles and particle-particle collisions, its combustible particle model provides a powerful tool to simulate the thermal conversion of each biomass particle and in turn the entire packed bed.

In this study a 3D packed bed model based on the combination of Euler-Granular model for predicting the hydrodynamics of the packed bed and the discrete phase model for the thermal conversion of the packed bed is presented. Then the model was applied for the first time to simulate the fixed bed combustion in an underfeed stoker furnace.

## 2 METHODOLOGY

Packed bed modelling was divided into two parts, hydrodynamics of the packed bed multiphase flow, and thermal conversion of the biomass particles. The Euler-Granular model was selected to simulate the former and the later was predicted by the discrete phase model (DPM). In order to combine these two models in ANSYS FLUENT a simulation with non-reacting flow based on the Euler-Granular model with appropriate granular viscosity (empirically determined) was performed and the simulated velocity field of the granular phase was stored as user defined memory (UDM). Then these data were used to prescribe the particle velocities in the DPM simulation by means of a user defined function (UDF).

In the DPM simulation, as a first approach, the particles are assumed to be thermally thin, i.e. temperature is uniform inside the particles. Moreover, the convection and radiation heat transfer between the particle-gas as well as particle-particle radiation is considered. The standard DPM drying and pyrolysis models describe the release rates of the water vapour and volatile components. The standard DPM diffusion limited char burnout model was modified, in order to consider the effect of particle-gas relative velocity on the rate of particle heterogeneous oxidation reaction. The turbulent reactive flow in the combustion chamber above the packed bed was described by the following models: the Realizable  $k-\epsilon$  model for turbulence; the Eddy Dissipation Model with modified Magnussen constants [1] for turbulence-chemistry interaction, a global 4-steps mechanism considering volatiles,  $\text{CH}_4$ ,  $\text{CO}$ ,  $\text{CO}_2$ ,  $\text{H}_2$ ,  $\text{H}_2\text{O}$ , and  $\text{O}_2$  for gas phase combustion, and the Discrete Ordinate Model for radiation.

In the next sections the governing equations for both parts of the packed bed model are explained.

### 2.1 Hydrodynamics of the packed bed

The Euler-Granular model treats the gas-solid multiphase flow as interpenetrating continua. It incorporates the concept of the volume fraction. The volume fraction represents the space occupied by each phase and they are assumed to be continuous functions of space and time and their sum is equal to one:

$$\sum_{i=1}^n \alpha_i = 1 \quad (1)$$

Conservation equations for solid and gas phase are derived to obtain a set of equations. They have similar structure for both phases because of the same Eulerian treatment. The mass balance for phase  $k$  yields

$$\frac{\partial}{\partial t}(\alpha_k \rho_k) + \nabla \cdot (\alpha_k \rho_k \vec{u}_k) = \sum_{\substack{i=g,s \\ i \neq k}} (\dot{m}_{ik} - \dot{m}_{ki}) \quad (2)$$

where  $\rho$  is the density [ $\text{kg.m}^{-3}$ ] and  $\vec{u}$  is the velocity vector [ $\text{m.s}^{-1}$ ].  $\dot{m}_{ik}$  characterises the mass transfer [ $\text{kg.s}^{-1}.\text{m}^{-3}$ ] from the  $i^{\text{th}}$  to the  $k^{\text{th}}$  phase and  $\dot{m}_{ki}$  characterises the mass transfer from the  $k^{\text{th}}$  to the  $i^{\text{th}}$  phase.

The momentum conservation equation for gas and solid phase are:

$$\begin{aligned} \frac{\partial}{\partial t}(\alpha_g \rho_g \vec{u}_g) + \nabla \cdot (\alpha_g \rho_g \vec{u}_g \vec{u}_g) = \\ -\alpha_g \nabla p + \nabla \cdot \vec{\tau}_g + \alpha_g \rho_g \vec{g} \\ + (K_{gs} \cdot (\vec{u}_s - \vec{u}_g) + \dot{m}_{sg} \vec{u}_s - \dot{m}_{gs} \vec{u}_g) \end{aligned} \quad (3)$$

$$\begin{aligned} \frac{\partial}{\partial t}(\alpha_s \rho_s \vec{u}_s) + \nabla \cdot (\alpha_s \rho_s \vec{u}_s \vec{u}_s) = \\ -\alpha_s \nabla p - \nabla p_s + \nabla \cdot \vec{\tau}_s + \alpha_s \rho_s \vec{g} \\ + (K_{gs} (\vec{u}_g - \vec{u}_s) + \dot{m}_{gs} \vec{u}_g - \dot{m}_{sg} \vec{u}_s) \end{aligned} \quad (4)$$

where  $K_{gs}$  is the interphase momentum exchange coefficient [ $\text{kg.s}^{-1}.\text{m}^{-3}$ ].

The constitutive equations are required to close the governing equations.

- Gas phase Newtonian viscous stress tensor:

$$\vec{\tau}_g = \alpha_g \mu_g \left[ (\nabla \vec{u}_g + \nabla \vec{u}_g^T) - \frac{2}{3} \nabla \cdot \vec{u}_g \vec{I} \right] \quad (5)$$

where  $\mu_g$  is the molecular viscosity [ $\text{N.s.m}^{-2}$ ],  $\vec{I}$  is the identity matrix, and the second term on the right hand side is for the effect of compressibility.

- Solid phase stress tensor:

$$\vec{\tau}_s = \alpha_s \mu_s (\nabla \vec{u}_s + \nabla \vec{u}_s^T) + \alpha_s \left( \lambda_s - \frac{2}{3} \mu_s \right) \nabla \cdot \vec{u}_s \vec{I} \quad (6)$$

where  $\mu_s$  is the solid shear viscosity [ $\text{N.s.m}^{-2}$ ] and  $\lambda_s$  is the solid bulk viscosity [ $\text{N.s.m}^{-2}$ ].

- Solid phase pressure:

$$p_s = \alpha_s \rho_s T_G + 2\rho_s (1+e) \alpha_s^2 g_0 T_G \quad (7)$$

where  $T_G$  is the granular temperature [ $\text{m}^2.\text{s}^{-2}$ ],  $e$  is the particle-particle restitution coefficient and  $g_0$  is the radial distribution function. The first term on the right hand side of Equation 7 is the kinetic term and the second term is due to particle collisions. The granular temperature is associated with the kinetic energy of the



fluctuating particle motion and is introduced as:

$$T_G = \frac{1}{3} \bar{u}'^2 \quad (8)$$

where  $\bar{u}'$  is the deviation of particle instantaneous velocity from mean particle velocity, like the Reynolds decomposition in turbulence modelling. In the derivation of Equation 8 it is assumed that deviations of particle velocity from mean velocity in all spatial directions are equal. It can be shown that the conservation equation for particle kinetic fluctuation energy reads [11]:

$$\frac{3}{2} \left[ \frac{\partial}{\partial t} (\alpha_s \rho_s T_G) + \nabla \cdot (\alpha_s \rho_s \bar{u}' T_G) \right] = (\bar{\tau}_s - p_s I) : \nabla \bar{u}'_s + \nabla \cdot (\kappa \nabla T_G) - \gamma - 3K_{gs} T_G \quad (9)$$

The first term on the right hand side is production of fluctuations by shear, the second term is diffusion of fluctuation energy, the third term is dissipation due to inelastic collisions, and the last term is dissipation by interaction with gas phase. According to Gidaspow et. al. [9] the diffusion coefficient for kinetic fluctuation energy is:

$$\kappa = \frac{150 d_s \rho_s \sqrt{T_G \pi}}{384(1+e) g_0} \left[ 1 + \frac{6}{5} \alpha_s g_0 (1+e) \right]^2 + 2 d_s \rho_s \alpha_s^2 g_0 (1+e) \sqrt{\frac{T_G}{\pi}} \quad (10)$$

and collisional kinetic energy dissipation is represented by the expression derived by Lun et. al. [10]:

$$\gamma = \frac{12}{d_s \sqrt{\pi}} \rho_s \alpha_s^2 g_0 (1-e^2) T_G^{3/2} \quad (11)$$

The radial distribution function in Equations 7, 10 and 11 is a correction factor that modifies the probability of collisions between grains when the volume fraction of the solid phase increases up to its maximum value. A form successfully used by Ding and Gidaspow [20] is:

$$g_0 = \left[ 1 - \left( \frac{\alpha_s}{\alpha_{s,\max}} \right)^{1/3} \right]^{-1} \quad (12)$$

where  $\alpha_{s,\max}$  is the maximum solid volume fraction or packing limit. For uniform spheres  $\alpha_{s,\max} = \frac{\pi}{3\sqrt{2}}$  [11].

It can be seen in Equations 3 and 4 that momentum exchange between the gas and solid phase is based on the value of the interphase momentum exchange coefficient,  $K_{gs}$ . It can be written in the following general form:

$$K_{gs} = \frac{\alpha_g \alpha_s \rho_s f}{\tau_s} \quad (13)$$

where  $f$  is the drag function and is differently defined in the various momentum exchange coefficient models.  $\tau_s$  is the particle relaxation time [s] which is defined as

$$\tau_s = \frac{\rho_s d_s^2}{18 \mu_g} \quad (14)$$

where  $d_s$  is the diameter [m] of the granular material.

In the simulation of the KWB underfeed stoker furnace, the Syamlal-O'Brien [21] model was used to model the drag function:

$$f = \frac{\text{Re}}{24 \nu^2} \left( 0.63 + \frac{4.8}{\sqrt{\text{Re}/\nu}} \right)^2 \quad (15)$$

Re denotes the relative particle Reynolds number:

$$\text{Re} = \frac{\rho_g |\bar{u}'_s - \bar{u}'_g| d_s}{\mu_g} \quad (16)$$

and  $\nu$  is called terminal velocity and is given by:

$$\nu = 0.5 \left( A - 0.06 T \text{Re} + \sqrt{(0.06 \text{Re})^2 + 0.12 \text{Re} (2B - A) + A^2} \right) \quad (17)$$

where

$$A = \alpha_g^{4.14} \quad (18)$$

$$B = \begin{cases} 0.8 \alpha_g^{1.28} & \alpha_g \leq 0.85 \\ \alpha_g^{2.65} & \alpha_g > 0.85 \end{cases} \quad (19)$$

Additionally, there are two parameters left in Equation 6 which need to be modelled: solid shear viscosity  $\mu_s$  and solid bulk viscosity  $\lambda_s$ . The flow behaviour of the granular phase is determined by the solid stress tensor, particularly its viscosity terms. There are some equations to model the viscosity terms and in all of them they are proportional to the radial distribution function [9-13]. As it can be seen in Equation 12, by approaching the solid volume fraction to its maximum value (packing limit), the radial distribution function goes to infinity. Hence the bulk and shear viscosities calculated by these equations for packed bed condition tends to infinity, because the solid volume fraction is most of the time near the packing limit. Therefore, these models mostly provide unrealistic results for packed bed simulations. Moreover, it is worth to mention that the existing models for the bulk and shear viscosities are mainly assessed under fluidized bed conditions and by changing them the results are not valid anymore.

In this work, the viscosity terms are roughly determined by performing several simulations with different values for the bulk and shear viscosities, in order to obtain realistic simulation results concerning packed bed shape and flow behaviour qualitatively agreeing with observations.

## 2.2 Thermal conversion of particles

As mentioned, the second relevant part of fuel bed simulation is the thermal conversion of the particles. The modelling of particle thermal conversions is performed by the discrete phase model (DPM). In this study, as the first attempt, the standard combustible particle model of DPM is used to simulate particle thermal conversions based on the thermally thin particle assumption. This assumption neglects the intra-particle temperature gradient and simplifies the partial differential energy equation of the particles to the following ordinary differential equation [22]:

$$m_p c_p \frac{dT_p}{dt} = h A_p (T_\infty - T_p) + \varepsilon_p A_p \sigma (T_R^4 - T_p^4) + Q_s \quad (20)$$

where  $m_p$ ,  $A_p$ ,  $c_p$  and  $\varepsilon_p$  are mass [kg], surface area [m<sup>2</sup>], heat capacity [J.kg<sup>-1</sup>.K<sup>-1</sup>] and emissivity of the particle, respectively.  $h$  is the heat transfer coefficient [W.m<sup>-2</sup>.K<sup>-1</sup>],  $T_\infty$  is ambient temperature [K],  $\sigma$  is the Stefan-Boltzmann constant [W.m<sup>-2</sup>.K<sup>-4</sup>],  $T_R$  is the radiation temperature [K] and  $Q_s$  is the energy source/sink term [W] originating from drying, pyrolysis

and char combustion processes.

The processes of particle thermal conversion are modelled by the available DPM sub-models for drying, pyrolysis and char burnout. Drying is modelled by two subsequent steps, according to the vaporisation law and the boiling law of the DPM.

The vaporisation law is applied when the particle temperature is between the vaporisation temperature and boiling temperature. The vaporisation temperature is a model parameter and has no physical significance. The rate of vaporisation is governed by diffusion and it is related to the difference in vapour concentrations at the particle surface and bulk gas as well as the mass transfer coefficient which is calculated from the Sherwood number. Afterwards the particle temperature is updated according to the Equation 20 and replacing the following sink term:

$$Q_s = -\dot{m}_{vap} h_{fg} \quad (21)$$

where  $\dot{m}_{vap}$  is the vaporisation rate [ $kg.s^{-1}$ ] and  $h_{fg}$  is the latent heat [ $J.kg^{-1}$ ].

Once the particle temperature reaches the boiling temperature, the boiling law is initiated. Throughout the boiling law, the temperature of the particle is assumed to remain constant at boiling temperature. Hence, the boiling rate is limited by the heat transfer rate and derived from Equation 20:

$$\dot{m}_{boil} h_{fg} = h A_p (T_\infty - T_p) + \varepsilon_p A_p \sigma (T_R^4 - T_p^4) \quad (22)$$

where  $\dot{m}_{boil}$  is the boiling rate [ $kg.s^{-1}$ ].

Several models for biomass pyrolysis are reported in the literatures. There is not a meaningful difference between their results under the combustion conditions where the heating rate is high. Therefore, in this study in order to decrease the computational effort a simple and sufficiently accurate pyrolysis model was applied. The mechanism of the pyrolysis reaction considered to be single-step and the release rate of the volatiles assumed to be first order depending on the amount of volatiles remaining in the particle,

$$\dot{m}_{py} = -k \left[ m_p - (1 - Y_{v,0}) (1 - Y_{w,0}) m_{p,0} \right] \quad (23)$$

where  $Y_{v,0}$ ,  $Y_{w,0}$  and  $m_{p,0}$  are volatile fraction, water fraction and mass of the particle at initial condition, respectively. The kinetic rate of this single-step reaction,  $k$ , is calculated from an Arrhenius equation:

$$k = A \exp\left(-\frac{E}{RT}\right) \quad (24)$$

$A$  is the pre-exponential factor and  $E$  is the activation energy.  $A = 2.5 \times 10^8 [s^{-1}]$  and  $E = 125 [kJ.mol^{-1}]$  are used for the simulation of the KWB underfeed stoker furnace [23]. Because these values are for the pyrolysis of softwood and the fuel in the KWB underfeed stoker furnace is softwood pellets. The temperature of the particle during the pyrolysis is calculated from Equation 20. The heat of pyrolysis reaction is neglected in comparison with heat of drying and combustion reactions [23, 24].

After the volatiles of the particle are completely released, the char oxidation surface reaction starts to consume the char of the particle. The product of this heterogeneous reaction was assumed to be carbon monoxide. This assumption is justified by the equilibrium of the Boudouard heterogeneous reaction, because at

particle temperatures under combustion conditions mainly carbon monoxide is released during char burnout [25]. The rate of the char burnout reaction is assumed to be diffusion limited, such as in several studies [26-29]. According to the fact that the oxygen mass is conserved in the particle boundary layer, i.e. quasi-steady state assumption, the char oxidation rate is derived by assuming that the oxygen consumption at the particle surface is equal to the diffusion of oxygen across the particle boundary layer. The mass transfer rate of the oxygen from the bulk to the surface of the particle is obtained from the Sherwood number. It can be shown that in the DPM standard diffusion limited char burnout model, a constant Sherwood number equal to 2.0 is assumed. The Sherwood number equal to 2.0 is valid only for the stagnation conditions where the particle-gas relative velocity is equal to zero. Therefore, for the cases with the significant particle-gas relative velocity, as for the KWB underfeed stoker furnace, this model underpredicts the rate of char oxidation. Because it neglects the effect of the particle-gas relative velocity on the oxygen mass transfer from the bulk to the surface of the particle.

In order to overcome this shortcoming, the following equation was applied for the char burnout rate:

$$\dot{m}_{comb} = -2\pi d_p Sh D_{AB} \frac{Y_{o_2} T_\infty \rho_g}{s(T_p + T_\infty)} \quad (25)$$

where  $\dot{m}_{comb}$  is the char burnout rate [ $kg.s^{-1}$ ],  $D_{AB}$  is the binary diffusion coefficient [ $m^2.s^{-1}$ ],  $Y_{o_2}$  is the bulk oxygen mass fraction,  $s$  is the ratio between mass of oxygen to the mass of char in the char oxidation reaction and  $Sh$  is Sherwood number calculated from Ranz-Marshall correlation [30]:

$$Sh = 2 + 0.6 Re^{1/2} Sc^{1/3} \quad (26)$$

where  $Sc$  is the Schmidt number and  $Re$  is the Reynolds number based on the particle-gas relative velocity, see Equation 16.

It can be assumed that during the char burnout reaction the particle-gas relative velocity and flue gas temperature are nearly constant. Therefore, the average particle-gas relative velocity and flue gas temperature during the char oxidation reaction, obtained from the simulations, are used to calculate the Reynolds and Schmidt numbers in the Sherwood number correlation. This modification leads to an improvement of the prediction accuracy concerning char burnout rate, since it provides a more realistic description of the mass transfer coefficient than the standard DPM model.

### 3 INVESTIGATED GRATE SYSTEM

The grate of the KWB underfeed stoker furnace is shown in Figure 1. The fuel, softwood pellets, is fed on the grate from below and is transported towards the outer edge of the grate. Primary air is supplied through the grate from nozzles at the bottom which form a concentric ring with the fuel feeding tube in the centre. In the simulation the primary air nozzles are represented by three concentric rings as it is shown in Figure 1.

Since wood pellets are a very homogeneous biomass fuel, it is realistic to assume an average biomass size and physical properties to characterise them. Therefore, in the Euler-Granular model the solid phase was represented

only by one particle size class, i.e. one solid phase. As it mentioned before, it considerably reduces the calculation time. Moreover, the pellets are assumed to have spherical forms and their average diameter is calculated based on the equivalent volume. The fuel analysis and operating conditions and other input parameters used in the simulation of the KWB underfeed stoker grate furnace are listed in Table I.

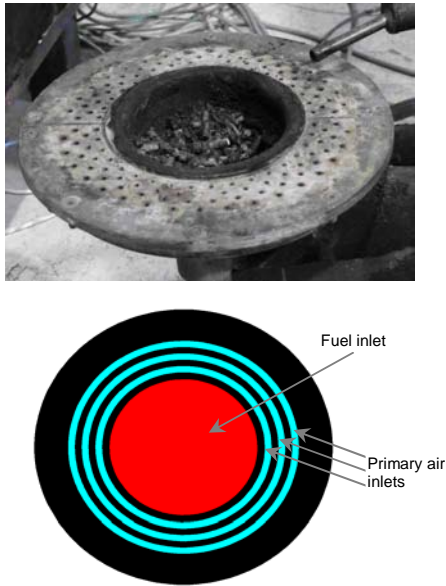


**Figure 1:** Top: grate of the KWB underfeed stoker furnace; bottom: scheme of the grate used for simulations

**Table I:** Fuel analysis, operating conditions and particle physical properties used in the simulation

Ultimate Analysis		
C	wt% d.b.	50.1
H	wt% d.b.	5.7
O	wt% d.b.	43.72
N	wt% d.b.	0.12
Ash	wt% d.b.	0.36
Proximate Analysis		
Moisture content	wt% w.b.	8.12
Volatiles	wt% d.b.	77.1
Fixed carbon	wt% d.b.	22.54
Net calorific value	MJ/kg w.b.	17.244
Total air ratio	-	1.58
Primary air ratio	-	0.64
Particle Physical Properties		
Average diameter	mm	6
Average density	kg.m <sup>-3</sup>	1120
Specific heat	J.kg <sup>-1</sup> .K <sup>-1</sup>	1500 + T
Thermal conductivity	W.m <sup>-1</sup> .K <sup>-1</sup>	0.173

Since the plant technology investigated is restricted Know-How of the company KWB-Kraft und Wärme aus Biomasse GmbH, only selected results, relevant concerning 3D packed bed combustion model development, are presented in the next part.

#### 4 RESULTS AND DISCUSSION

The positions of the drying, pyrolysis, and char burnout zone inside the fuel bed are illustrated in Figure

2, Figure 3 and Figure 4, respectively by means of the particle tracks on the grate coloured by drying, pyrolysis and char burnout rates as well as the contours of these rates along a vertical cross section through the grate axis. As it is shown in these figures, the three sub-processes of particle thermal conversion sequentially happen with an overlap between each other. Drying takes place in the centre of the bed above the fuel inlet. Afterwards particles start to release volatiles along their radial path to the outer edge of the grate. According to the simulation, the main part of the pyrolysis happens at a ring around the drying zone. The remaining char mainly reacts with oxygen above the outer primary air injection region.

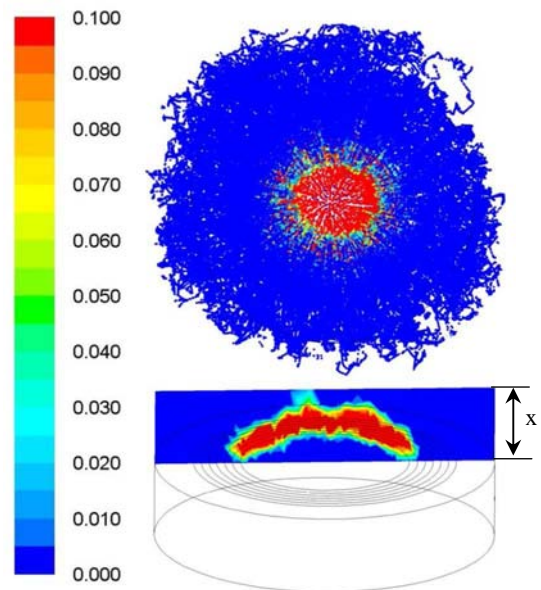


**Figure 2:** Top: particle tracks on the grate coloured by drying rates [mg/s]; bottom: contours of drying rate [mg/s] at a vertical cross section through the grate axis; x= 5cm

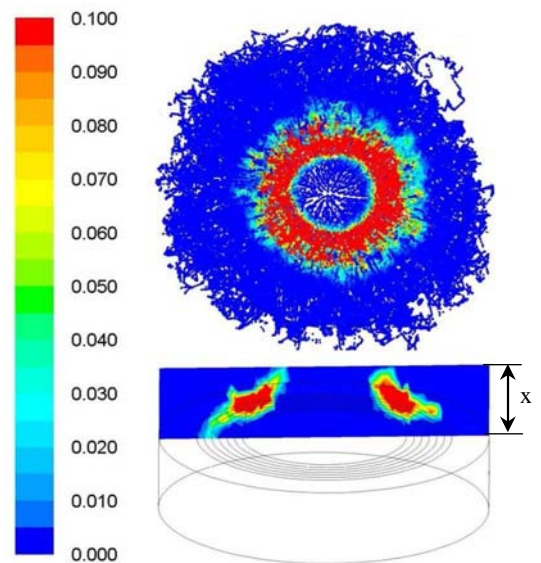


**Figure 3:** Top: particle tracks on the grate coloured by pyrolysis rates [mg/s]; bottom: contours of pyrolysis rate [mg/s] at a vertical cross section through the grate axis; x= 5cm



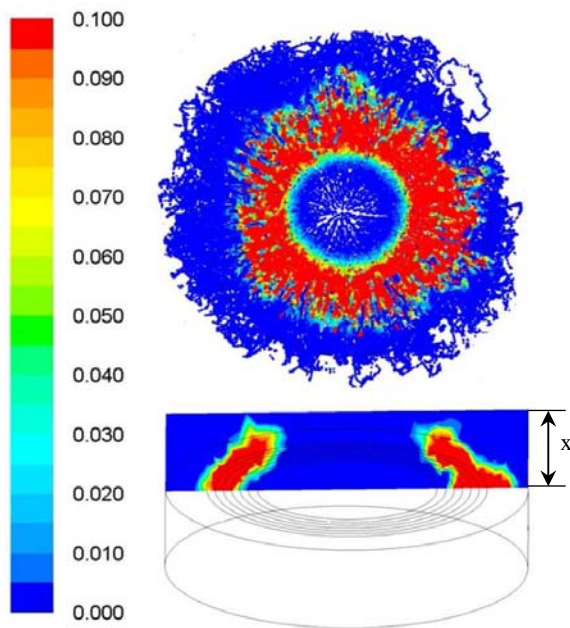


**Figure 4:** Top: particle tracks on the grate coloured by char burnout rates [mg/s]; bottom: contours of char burnout rate [mg/s] at a vertical cross section through the grate axis;  $x= 5\text{cm}$

The particle tracks coloured by the simulated particle temperatures are shown in Figure 5. The flue gas temperatures along the vertical cross section of the combustion chamber as well as a horizontal cross section close to the surface of the fuel bed are shown in Figure 6. Additionally, a picture taken from a window at the top of the furnace is enclosed in Figure 6 for comparison. However, from the picture the entire bed can not be seen, due to a reduction of diameter at the position where the secondary air is injected.

The predicted locations of the fuel conversion stages in the fuel bed are an explanation of the simulated particle temperatures in Figure 5 and also the flue gas temperatures along the horizontal cross section close to the surface of the fuel bed in Figure 6. It can be seen, that at the surface of the fuel bed, the lowest particle and flue gas temperatures occur in the centre, which is due to the fact that drying takes place there. After the drying region the particle temperatures increase due to radiation and the volatile components of the particles are released. A fraction of the volatile components burns at the surface of the fuel bed, therefore the flue gas temperatures along the horizontal cross section shown in Figure 6 have their highest value right above the pyrolysis region. The highest particle temperatures occur at the outer primary air inlet region due to char oxidation. Outside the primary air injection rings, both the flue gas and particle temperatures are reduced, because almost no homogeneous gas phase reactions happen in this region and also the energy release due to char burnout is low due to the comparatively small amount of char. The results regarding to the variations of the particle temperatures, Figure 5, and the flue gas temperatures along the horizontal cross section close to the surface of the fuel bed, Figure 6, are in good agreement with the picture taken from the top of the furnace, shown in Figure 6.

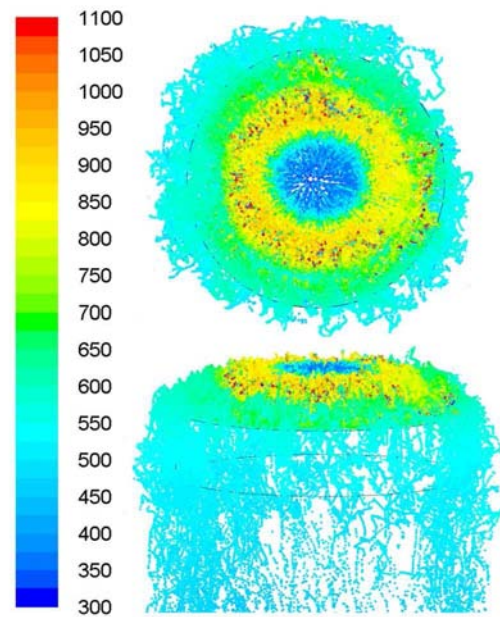


**Figure 5:** Particle tracks on the grate coloured by particle temperatures (K)

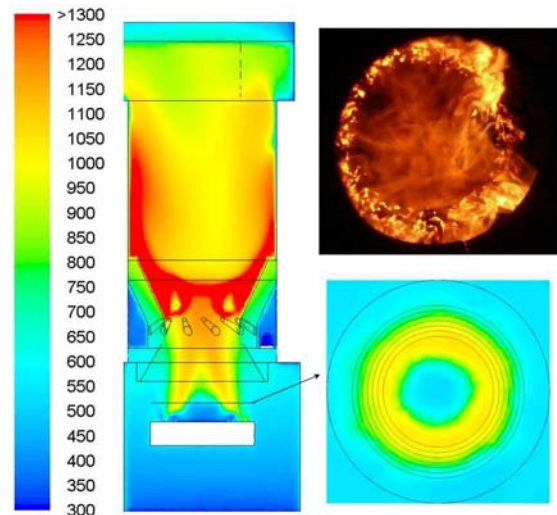


**Figure 6:** Contours of flue gas temperatures (K); left: along the vertical cross section of the combustion chamber; right top: visual observation from a window at the top of the furnace; right bottom: along a horizontal cross section close to the surface of the fuel bed (4cm above the grate, shown in the vertical cross section)

In Figure 7 to Figure 10 the contours of  $\text{O}_2$ ,  $\text{H}_2\text{O}$ ,  $\text{CH}_4$ , and  $\text{CO}$  close to the surface of the fuel bed are shown, respectively. The distribution of these species can be explained by the positions of the thermal conversion sub-processes. These figures pronounce that the release profiles of the species from the fuel bed are dependent on the radial as well as angular positions on the grate. Hence, modelling the release of volatile components from the fuel bed to the gas phase with 1D profiles as the boundary conditions for the gas phase simulation may lead to some inconsistencies.

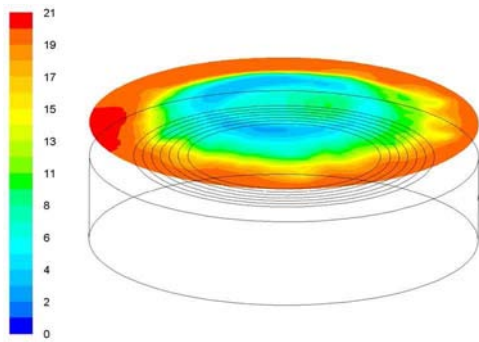


**Figure 7:** Contours of  $O_2$  concentrations approximately at the surface of the fuel bed [vol%-dry]

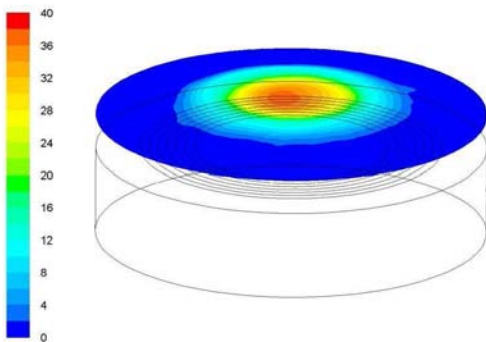


**Figure 8:** Contours of  $H_2O$  concentrations approximately at the surface of the fuel bed [vol%]

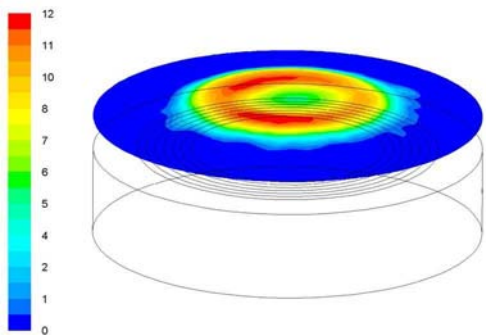


**Figure 9:** Contours of  $CH_4$  concentrations approximately at the surface of the fuel bed [vol%-dry]

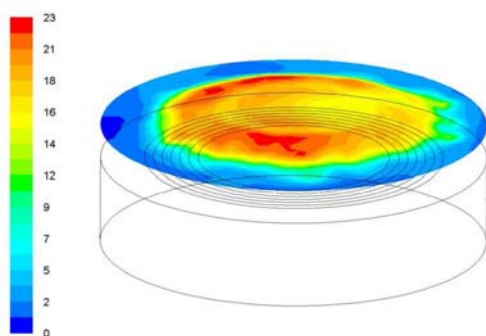


**Figure 10:** Contours of  $CO$  concentrations approximately at the surface of the fuel bed [vol%-dry]

## 5 CONCLUSIONS

In order to design and optimise biomass grate furnaces, a CFD based packed bed combustion model has been developed. The model is based on the kinetic theory of granular flow for the prediction of the hydrodynamics of the packed bed and the thermally thin particle model with a set of sufficiently accurate transient models for the thermal conversion of individual biomass particles. The thermal conversion of the entire bed is simulated by predicting the trajectories and the thermal conversion of the particles in the bed.

The model has been successfully applied to simulate KWB underfeed stoker grate furnace. The maximum predicted particle temperatures in the bed are relatively lower than the previous experiments of a lab-scale batch reactor. It implies that the products of the char oxidation reaction can not be only carbon monoxide and a fraction of carbon monoxide should also be considered. However, the modified char burnout model predicts the unburned char to be less than 1 wt.%, which is in good agreement regarding the burnout quality of the grate ash. Moreover, the results regarding variations of the particle and flue gas temperatures at the bed surface and the locations of the fuel conversion stages are in qualitative agreements with visual observations of the packed bed.

Hence, the new 3D packed bed model provides the following advantages for the simulation of grate furnaces:

- The effect of particle related parameters, e.g. size, physical properties and chemical compositions, on the thermal conversion of the entire packed bed can be investigated
- Modelling the hydrodynamics of the packed bed by the granular kinetic theory allows to model the particle movements on the grate under consideration of particle-particle collisions
- The applied hydrodynamics model allows to study the influence of grate motion and primary air distribution below the bed on the particle trajectories
- The influence of primary air distribution on the thermal conversion of the packed beds can be investigated
- Better prediction of the profiles of species and energy released from the fuel bed, as important input data for the simulation of gas phase combustion.

As next steps of model improvement, the development of an enhanced heat transfer model for the packed bed, the utilisation of a thermally thick model for particle conversion and the application of a new hybrid Euler-Euler/Euler-Lagrange model for the coupled simulation of particle movement and thermal conversion are foreseen.

## 6 REFERENCES

- [1] Scharler R., Fleckl, T., Obernberger, I, 2003: Modification of a Magnussen Constant of the Eddy Dissipation Model for biomass grate furnaces by means of hot gas in-situ FT-IR absorption spectroscopy. Progress in Computational Fluid dynamics, Vol. 3, pp. 102-111.
- [2] Scharler R., Obernberger I., 2000: Numerical optimisations of biomass grate furnaces.

- Proceedings of the 5<sup>th</sup> European Conference on Industrial Furnaces and Boilers INFUB, Portugal.
- [3] Scharler R., Zahirovic S., Schulze K., Kleditzsch S. Obernberger I., 2006: Simulationsgestützte Auslegung und Optimierung von Biomassefeuerungs- und Kesselanlagen – Einsatzmöglichkeiten, Stand der Technik und innovative Methoden. Österreichische Ingenieur- und Architektenzeitung, Vol. 10-12, pp. 296-309.
- [4] Scharler, R., 2001: Entwicklung und Optimierung von Biomasse-Rostfeuerungen durch CFD-Analyse. Ph.D. thesis, Graz University of Technology, Austria.
- [5] Dziugys A., Peters B., 2001: An approach to simulate the motion of spherical and non-spherical fuel particles in combustion chambers. Granular Matter, Vol. 3, pp. 231-265.
- [6] Cundall P. A., Strack O. D. L., 1979: Discrete numerical model for granular assemblies. Geotechnique, Vol. 29, pp. 47-65.
- [7] Hoomans B. p. B., Kuipers J. A. M. Briels W. J. van Swaij W. P. M., 1996: Discrete particle simulation of bubble and slug formation in a two-dimensional gas fluidized bed: a hard sphere approach, Chemical Engineering Science, Vol. 51, pp. 99-118.
- [8] Hjertager B. H., Solberg T., Ibsen C. H., Hansen K. G., 2003: Multi-Fluid CFD modelling of fluidised bed reactors. Invited Presentation Computational Fluid Dynamics in Chemical Engineering III, Davos, Switzerland.
- [9] Gidaspow D., Bezburuah R., Ding J., 1992: Hydrodynamics of Circulating Fluidized Beds, Kinetic Theory Approach. In O. E. Potter and D. J. Nicklin, Eds., Fluidization VII, Engineering Foundation, pp. 75-82.
- [10] Lun C. K. K., Savage S. B., Jeffrey D. J., Chepurniy N., 1984: Kinetic theories for granular flow: inelastic particles in Couette flow and slightly inelastic particles in a general flow field. J. Fluid Mech., Vol. 140, pp. 223-256.
- [11] Gidaspow D., 1994: Multiphase flow and fluidization. Academic Press, Boston.
- [12] Syamlal M., Rogers W., O'Brien T. J., 1993: MFIX Documentation: Volume 1, Theory Guide. National Technical Information Service, Springfield, VA, DOE/METC-9411004, NTIS/DE9400087.
- [13] Gidaspow D., Jayaswal U. K., Ding J., 1991: Navier-Stokes Equation Model for Liquid-Solid Flows Using Kinetic Theory. Liquid Solid Flows, Vol. 118, New York: ASME, pp. 165-178.
- [14] Sinclair J. L., Jackson R., 1989: Gas-particle flow in a vertical pipe with particle-particle interactions. AIChE Journal, Vol. 35, pp. 1473-1486.
- [15] Chapman S., Cowling T.G., 1970: The mathematical theory of non-uniform gases. Cambridge University Press, Cambridge.
- [16] Wang W., Lu B., Zhang N., Shi Z., Li J., 2010: A review of multiscale CFD for gas-solid CFB modelling. Int J Multiphase Flow, Vol. 36, pp. 109-118.
- [17] Taghipour F., Ellis N., Wong C., 2005: Experimental and computational study of gas-solid fluidized bed hydrodynamics. Chemical Engineering Science, Vol. 60, pp. 6857-6867.
- [18] Boemer, A., 1996: Euler/Euler-Simulation der Fluidodynamik blasenbildender Wirbelschichten. PhD Thesis, University of Aachen, Germany.
- [19] Popoff B., Braun M., 2007: A Lagrangian Approach to Dense Particulate Flows. 6th International Conference on Multiphase Flow (ICMF), Leipzig, Germany.
- [20] Ding J., Gidaspow D., 1990: A Bubbling Fluidization Model Using Kinetic Theory of Granular Flow. AIChE J., Vol. 36, pp. 523-538.
- [21] Syamlal M., O'Brien T. J., 1989: Computer Simulation of Bubbles in a Fluidized Bed. AIChE Symp. Series, Vol. 85, pp. 22-31.
- [22] ANSYS FLUENT 12.0, Theory Guide.
- [23] Gronli M., 1996: A theoretical and experimental study of the thermal degradation of biomass. Ph.D. thesis, The Norwegian University of Science and Technology, Norway.
- [24] Zahirovic S., Scharler R., Obernberger I., 2004: Advanced CFD modelling of pulverised biomass combustion. Proceeding of the 6<sup>th</sup> International Conference Science in Thermal and Biomass Conversion, Victoria, Canada, Vol. 1, pp. 267-284.
- [25] Mathieu P., Dubuisson R., 2002: Performance analysis of a biomass gasifier. Energy Conversion and Management, Vol. 43, pp. 1291-1299.
- [26] Bruch C., Peters B., Nussbaumer T., 2003: Modelling wood combustion under fixed bed combustion. Fuel, Vol. 82, pp. 729-738.
- [27] Wu C., 2006: Fuel-NOx formation during low-grade fuel combustion in a swirling-flow burner. Ph.D thesis, Brigham Young University, USA.
- [28] Porteiro J., Miguez J. L., Granada E., Moran J. C., 2006: Mathematical modelling of the combustion of a single wood particle. Fuel Processing Technology, Vol. 87, pp. 169-175.
- [29] Meesri C., Moghtaderi B., 2003: Experimental and numerical analysis of sawdust-char combustion reactivity in a drop tube reactor. Combustion Science and Technology, Vol. 175, pp. 793-823.
- [30] Bird R. B., Stewart W. E., Lightfoot E. N., 2002: Transport phenomena, John Wiley & Sons.

## 7 ACKNOWLEDGEMENTS

We gratefully acknowledge the Austrian *Kplus* program of the Federal Government of Austria, the State Government of Styria as well as the State Government of Lower Austria for funding the work presented in this paper.

## 8 LOGO SPACE

bioenergy2020+





**BIOENERGIESYSTEME GmbH**  
Inffeldgasse 21b, A-8010 Graz



## Paper IV



# CFD simulation of biomass grate furnaces with a comprehensive 3D packed bed model

Ramin Mehrabian<sup>1,2,\*</sup>, Stefan Stangl<sup>1</sup>, Robert Scharler<sup>1,2,3</sup>, Ingwald Obernberger<sup>1,2,3</sup>, Alexander Weissinger<sup>4</sup>

<sup>1</sup>BIOENERGY 2020+ GmbH, Inffeldgasse 21b, 8010 Graz, Austria

<sup>2</sup>Institute for Process and Particle Engineering, Graz University of Technology, Inffeldgasse 21b, A-8010 Graz, Austria

<sup>3</sup>BIOS BIOENERGIESYSTEME GmbH, Inffeldgasse 21b, A-8010 Graz, Austria

<sup>4</sup>KWB - KRAFT UND WÄRME AUS BIOMASSE GmbH, Industriestrasse 235, A-8321 St. Margarethen/Raab, Austria

## Abstract

A 3D CFD model for biomass packed bed combustion has been developed at BIOENERGY 2020+ in co-operation with BIOS BIOENERGIESYSTEME and KWB in a previous work [1]. It consists of an Euler-Granular model for hydrodynamics of gas-particle multiphase flow and a thermally thin particle model for combustion of biomass particles. In this paper, this model has been improved by the implementation of a layer model for thermally thick particles. The new packed bed model provides the advantages of considering the intra-particle species and temperature gradients and, accordingly, allows for parallel progress of the thermal conversion sub-processes. Moreover, the layer model considers a more realistic shape for biomass particles, e.g. cylinders. Enhanced models for pyrolysis and char oxidation are applied and char gasification reactions are included. Additionally, the products of char oxidation are CO and CO<sub>2</sub>, whereas the ratio between these species changes depending on the particle temperature. The simulation of a small-scale underfeed stoker furnace has been successfully performed by the application of the new packed bed combustion model. The positions of the drying, pyrolysis and char burnout zones in the fuel bed as well as the temperature distribution among the particles seem to be plausible and could be confirmed by observations. Furthermore, a good qualitative agreement concerning the flue gas temperatures measured by thermocouples at different positions in the combustion chamber and CO emissions measured at boiler outlet could be achieved.

## 1. Introduction and objectives

CFD simulation techniques are an efficient tool for the design and optimisation of biomass grate furnaces. They have successfully been applied to predict the turbulent reactive flow in combustion chambers of furnaces [2-5]. However, at present there is a lack of reasonably accurate and computationally efficient simulation tools for packed bed biomass combustion, which directly integrate the packed bed modelling into the available models for the turbulent reactive flow.

A combination of several sub-processes such as heat-up, drying, pyrolysis and char burnout represents the thermal conversion of solid biomass particles. Depending on the size and the physical properties of the biomass particles, temperature and species gradients may develop inside the particles causing intra-particle transport processes. The group of particles with gradients inside the particle and simultaneous progress of the different conversion stages is called thermally thick particles. The biomass particles in grate furnaces typically belong to this group. Several studies have been performed to describe the thermal conversion of a single thermally thick biomass particle [6-11].

In this work the packed bed is considered as an ensemble of representative particles, where each of these particles undergoes thermal conversion processes. The conversion of these particles is modelled by a thermally thick particle model. The layer model is able to describe the most essential characteristics of the thermal conversion of the thermally thick biomass particles, such as the intra-

---

\* Corresponding author: Tel: +43 316 873 9232; email: ramin.mehrabian@bioenergy2020.eu

particle temperature gradient, the overall mass loss, the particle shrinkage and the change of physical properties during conversion. The layer model is applicable for cylindrical as well as spherical shapes. The particle model is implemented into ANSYS FLUENT as a User Defined Function (UDF) to perform the simulations of the entire biomass grate furnace. The hydrodynamics of the packed bed granular flow are modelled by the Euler-Granular model of ANSYS FLUENT. This model is based on the kinetic theory of granular flows and allows the consideration of inter-particle interactions which are of key importance when modelling packed beds.

Therefore, a new 3D packed bed model based on a combination of the Euler-Granular model for tracing the particle trajectories and the layer model for the thermal conversion of the thermally thick particles is presented. Then the model is applied to simulate the packed bed combustion in an underfeed stoker furnace.

## 2. Methodology

Packed bed modelling is divided into two parts, the hydrodynamics of the packed bed multiphase flow, and the thermal conversion of the biomass particles. The Euler-Granular model of ANSYS FLUENT is selected to simulate the packed bed multiphase flow. However, the Euler-Granular model does not enable the implementation of the layer model for the simulation of the thermal conversion of the particles via UDF. On the other hand, the Discrete Phase Model (DPM) of ANSYS FLUENT is not suitable for particle tracking under packed bed conditions, because it ignores the particle-particle collisions. However, its multi-component particle model provides a possibility to hook the layer model to ANSYS FLUENT. Therefore, a simulation with non-reacting flow based on the Euler-Granular model was performed and the simulated velocity field of the granular phase was stored as a User Defined Memory (UDM). Then, these data were used to prescribe the particle velocities in the DPM simulations by means of a UDF. Since the Euler-Granular simulation is without reactions, the effect of particle shrinkage on their movements is not considered.

As mentioned, the layer model considers the intra-particle species and temperature gradients and, accordingly, allows to consider the parallel progress of the thermal conversion sub-processes. Moreover, the layer model provides the advantages of considering a more realistic shape for biomass particles, e.g. finite cylinders, in contrast to the former packed bed model, where particles were approximated as spherical. Drying occurs at a fixed boiling temperature and its progress is limited by the transport of heat inside the particle. Pyrolysis is modelled by three independent competitive reactions for cellulose, hemicellulose, and lignin. The char oxidation and gasification reactions are assumed to be limited by the kinetic rate as well as the mass transport rate, which is calculated based on Sherwood correlations for cylindrical particles. The products of char oxidation are CO and CO<sub>2</sub>, whereas the ratio between these species changes depending on the particle temperature. In the next sub-sections, both parts of the packed bed model are explained.

The turbulent reactive flow in the combustion chamber above the packed bed is described by the following models: the Realizable  $k-\epsilon$  model for turbulence; the Eddy Dissipation Model with modified Magnussen constants [2] for turbulence-chemistry interaction, a global 4-step mechanism considering volatiles, CH<sub>4</sub>, CO, CO<sub>2</sub>, H<sub>2</sub>, H<sub>2</sub>O, and O<sub>2</sub> for gas phase combustion [2-3], and the Discrete Ordinates Model for radiation.

### 2.1. Hydrodynamics of the packed bed

In the Euler-Granular model all the particles are assumed to be identical, specified by their mean diameter (spherical shape) and density. Therefore handling a poly-disperse system, i.e. a system with different particle sizes, requires several solid phases corresponding to the number of particle diameter classes. In this approach the gas-solid multiphase flow is considered as interpenetrating continua. It incorporates the concept of the volume fraction. The volume fraction represents the space occupied by

each phase and they are assumed to be continuous functions of space and time and their sum is equal to one. The conservation equations for solid and gas phase have a similar structure because of the same Eulerian treatment. The solid phase momentum equation is similar to that of the gas phase with some additional terms, i. e. solid pressure ( $p_s$ ), solid stress-strain tensor ( $\bar{\tau}_s$ ) and inter-phase momentum exchange coefficient ( $K_{gs}$ ), accounting for the solid phase behaviour:

$$\frac{\partial}{\partial t}(\alpha_s \rho_s \bar{u}_s) + \nabla \cdot (\alpha_s \rho_s \bar{u}_s \bar{u}_s) = -\alpha_s \nabla p - \nabla p_s + \nabla \cdot \bar{\tau}_s + \alpha_s \rho_s \bar{g} + (K_{gs}(\bar{u}_g - \bar{u}_s) + \dot{m}_{gs} \bar{u}_g - \dot{m}_{sg} \bar{u}_s) \quad (1)$$

where  $\rho_s$  is the density of the solid phase [ $kg.m^{-3}$ ],  $\bar{u}$  is the velocity vector [ $m.s^{-1}$ ] and  $\alpha_s$  is the volume fraction of the solid phase [-].  $\dot{m}_{gs}$  and  $\dot{m}_{sg}$  characterise the mass transfer [ $kg.s^{-1}.m^{-3}$ ] from the gas to the solid phase and contrariwise, respectively.

There are several correlations for these additional terms [12-17]. They have been driven by making an analogy between the particle-particle collisions and the kinetic theory of gases [18]. The concept of granular temperature is defined to represent the kinetic energy of random particle fluctuations around their mean velocities. A conservation energy equation is formulated for this kinetic fluctuation energy in which the kinetic energy is produced by shear stress and turbulence and dissipated by inelastic collisions and interaction with the fluid. The collisions between the particles are assumed to be a function of this kinetic fluctuation energy. A detailed description of the Euler-Granular model is presented in [1].

## 2.2. Thermal conversion of particles (layer model)

As mentioned, the second part of the packed bed model is the thermal conversion of the particles. It is performed by an in-house code (layer model). The layer model accounts for intra-particle transport processes and the simultaneous progress of the thermal conversion sub-processes.

To reduce the model complexities and calculation time, only the radial temperature gradient in the particle is considered. This is a usual simplifying assumption. Its validity was already addressed by Ha and Choi [19]. To apply the one-dimensional model for a finite cylindrical geometry, Thunman's discretisation approach [9] has been applied. This approach assumes that the particle boundary conditions are homogeneous and every point in the particle at a certain distance from the particle surface has the same temperature and conversion state. The particle is divided into four layers: drying layer, pyrolysis layer, char and ash layer. The boundaries between the layers are related to the conversion sub-processes: drying, pyrolysis and char burnout fronts. At the beginning of the thermal conversion process only drying is of relevance. Due to heating up, moisture starts to get released from the particle. The pyrolysis layer consists of dry biomass and is located around the drying layer as the drying front moves towards the particle centre. When pyrolysis commences, the dry biomass converts to char and volatiles. The volatiles leave the particle and the char builds a layer around the pyrolysis layer. Finally, char burnout also creates another layer which contains only ash and surrounds the char layer. As the conversion of the fuel particle proceeds, drying, pyrolysis and char burnout fronts move from the surface to the centre of the particle. Figure 1 shows the scheme of the layer model for a cylindrical particle at a certain time when all the sub-processes of thermal conversion are occurring.

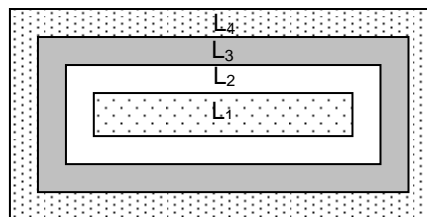


Figure 1: Scheme of the layer model; L<sub>1</sub>...drying layer; L<sub>2</sub>...pyrolysis layer; L<sub>3</sub>...char layer; L<sub>4</sub>...ash layer.

The conversion of each layer is simulated by separate sub-models. It is assumed that drying occurs at a fixed boiling temperature in an infinitely thin zone that separates the wet and the dry part of the particle. Such a steep drying front for the fast drying of biomass is reported almost by all drying models [20]. The drying process acts as a heat sink. It means that any amount of heat flow above the boiling temperature is consumed by the drying process. This approach to calculate the evaporation rate is the most often used model in literature, for instance [7, 10]. It is assumed that there is no resistance to mass transfer, and therefore the water vapour instantaneously leaves the particle. However, the cooling effect of the water vapour transfer through the particle is considered. Therefore the drying rate is controlled by the heat transfer.

Biomass pyrolysis is described by the decomposition of its three pseudo-components hemicellulose, cellulose, and lignin. This model implicitly assumes the hypothesis of an independent decomposition of these three constituents. An Arrhenius equation is used to describe the pyrolysis of each pseudo-component. The overall mass loss rate of a particle during pyrolysis is given as:

$$-\frac{dm}{dt} = \sum_{i=1}^3 c_i \frac{da_i}{dt} \quad (2)$$

where  $i$  is related to each pseudo-component,  $c_i = m_{0,i} - m_{f,i}$  is a measure of the contribution of the partial decomposition processes to the overall mass loss  $m_0 - m_f$ . The conversion of each pseudo-component  $a_i$  can be expressed by:

$$a_i = \frac{m_{0,i} - m_i}{m_{0,i} - m_{f,i}} \quad (3)$$

where  $m_{0,i}$  and  $m_{f,i}$  are the initial and the final mass [kg] of the  $i^{\text{th}}$  pseudo-component, respectively.  $m_i$  is the actual mass [kg] of the  $i^{\text{th}}$  pseudo-component.

The pseudo-components are all assumed to decompose individually according to a first-order reaction, therefore the conversion rate of each pseudo-component is given by:

$$\frac{da_i}{dt} = A_i \exp\left(-\frac{E_i}{RT}\right)(1 - a_i) \quad (4)$$

where  $A$  is the pre-exponential factor [ $s^{-1}$ ],  $E$  is the activation energy [ $kJ.mol^{-1}$ ] and  $R$  is the universal gas constant [ $kJ.mol^{-1}.K^{-1}$ ]. The empirical constants needed in the pyrolysis model are obtained from the fast heating rate experiments reported by Branca et al. [21].

The volatiles yielded from pyrolysis include a complex mixture and several hydrocarbons have been found in it. This complex mixture mainly consists of CO, CO<sub>2</sub>, H<sub>2</sub>O, H<sub>2</sub>, light hydrocarbons and heavy hydrocarbons (tar). To simplify the combustion behaviour of the volatiles, the light and heavy hydrocarbons are lumped together and the chemical and physical properties of methane are assigned to this lumped hydrocarbon.

Char conversion models are more complicated than biomass pyrolysis models, as they are based on heterogeneous reactions for which both intrinsic kinetic and transport phenomena are important. It has been experimentally verified that char combustion is such a rapid reaction that it occurs in a very thin layer [22]. Due to the structure of the layer model, the char conversion reactions are assumed to occur at the interface between the char and the ash layer. Char oxidation with O<sub>2</sub> and gasification with CO<sub>2</sub>, H<sub>2</sub>O and H<sub>2</sub> are considered as char conversion reactions. There is clear evidence that both CO and CO<sub>2</sub> are primary products of char oxidation [23]. The ratio of CO to CO<sub>2</sub> production changes with temperature [24]. The heterogeneous reaction rate constants as well as the CO/CO<sub>2</sub> product ratio are listed in Table 1. The rate of char conversion reactions is a function of both kinetic rate at the reaction surface and mass transfer rate to/from the reaction surface. Assuming a global reaction rate of first order with respect to the oxidising/gasifying agent concentration leads to char conversion rate as:

$$\frac{dm_{ch}}{dt} = - \sum_{i=1}^4 \frac{\Omega_i M_c}{\frac{1}{k_i S} + \frac{1}{h_m S} + \frac{1}{\int_{\delta_{ash}} \frac{dr}{D_e S(r)}}} X_{\infty, i} \quad (5)$$

where  $i = 1$  to 4 corresponds to the heterogeneous reactions in Table 1 and  $\Omega$  is the stoichiometric ratio of moles of carbon per mole of oxidising/gasifying agent in the corresponding reaction.  $M_c$ ,  $S$ ,  $k_i$ ,  $\delta_{ash}$  and  $X_{\infty, i}$  are the carbon molecular weight [ $kg.kmol^{-1}$ ], the surface area of the char burnout front [ $m^2$ ], the kinetic rate constant of heterogeneous reaction  $i$  [ $m.s^{-1}$ ], the thickness of the ash layer [ $m$ ] and the molar concentration of oxidising/gasifying agent of reaction  $i$  at the bulk flow [ $kmol.m^{-3}$ ], respectively.

The mass transfer coefficient of reactant species in the boundary layer around the particle  $h_m$  [ $m.s^{-1}$ ], is obtained by the Sherwood number. The effective diffusivity of the ash layer  $D_e$  [ $m^2.s^{-1}$ ], depends on the ash porosity  $\phi$  [-], the tortuosity  $\eta$  [-], and the molecular diffusivity of the penetrating gaseous component  $D_a$  [ $m^2.s^{-1}$ ]:

$$D_e = \frac{\phi}{\eta} D_a \quad (6)$$

The tortuosity can be replaced by the inverse of the porosity [26, 27]:

$$D_e = \phi^2 D_a \quad (7)$$

Table 1: Heterogeneous reaction rate constants [25]

$\Omega C + O_2 \rightarrow 2(\Omega - 1)CO + (2 - \Omega)CO_2$	$k = 1.715T \exp(-9000/T)$ $\Omega = \frac{2[1 + 4.3 \exp(-3390/T)]}{2 + 4.3 \exp(-3390/T)}$
$C + CO_2 \rightarrow 2CO$	$k = 3.42T \exp(-15600/T)$
$C + H_2O \rightarrow CO + H_2$	$k = 3.42T \exp(-15600/T)$
$C + 2H_2 \rightarrow CH_4$	$k = 3.42 \times 10^{-3} T \exp(-15600/T)$

Since particle shrinkage during drying is much lower compared to that occurring during pyrolysis and charcoal combustion [28], it is postulated that during drying, the size of the particle remains constant and its density decreases. However, during the pyrolysis and char burnout, due to the particle mass loss and consideration of different densities for dry wood, char and ash, both shrinkage and density change are considered in the layer model.

The external surface of the particle exchanges heat and mass with the surroundings. Boundary conditions are required to complete the system of equations. The symmetry boundary condition is applied for the energy equation at the particle centre which leads to zero heat flux. The specified gradient boundary condition is used at the particle surface:

$$\lambda \frac{dT}{dr} \Big|_{r=\frac{d}{2}} = \varepsilon \sigma (T_{rad}^4 - T_{r=\frac{d}{2}}^4) + h_{conv} (T_{conv} - T_{r=\frac{d}{2}}) \quad (8)$$

where  $d$  is the actual diameter of the particle [ $m$ ].  $\lambda$ ,  $\varepsilon$  and  $\sigma$  are the thermal conductivity [ $W.m^{-1}.K^{-1}$ ], emissivity (0.85) [-] and Stefan-Boltzmann constant [ $W.m^{-2}.K^{-4}$ ], respectively.  $h_{conv}$  is the convective heat transfer coefficient [ $W.m^{-2}.K^{-1}$ ]. It is determined by an appropriate correlation for the Nusselt number. For spherical particles the Ranz-Marshall correlation and for cylindrical particles the correlation proposed by Churchill and Bernstein are applied [29].

### 3. Investigated grate system and fuel applied

The grate of the KWB underfeed stoker furnace is shown in Figure 2. The fuel, softwood spruce pellets, is fed on the grate from below and is transported towards the outer edge of the grate. Primary air is supplied through the grate from nozzles at the bottom which form a concentric ring with the fuel feeding tube in the centre. In the simulation the primary air nozzles are represented by three concentric rings as it is shown in Figure 2.

Since wood pellets are a very homogeneous biomass fuel, it is realistic to assume an average biomass size and average physical properties to characterise them. Therefore, based on the average size of the pellets, a length and a diameter are used in the calculations of the layer model. Moreover, in the Euler-Granular model the solid phase was represented only by one particle size class, i.e. one solid phase. It considerably reduces the calculation time. Hjertager reported a quadratical increase of computational effort with the number of phases [30]. However, the particles in the Euler-Granular model can only be represented as spherical particles. Thus the average diameter of the pellets is calculated based on the equivalent volume. The fuel analysis and operating conditions and other input parameters used in the simulations of the KWB underfeed stoker grate furnace are listed in Table 2.

Since the plant technology investigated is restricted know how of the company KWB-Kraft und Wärme aus Biomasse GmbH, only selected results, relevant concerning the 3D packed bed combustion model development, are presented in the next part.

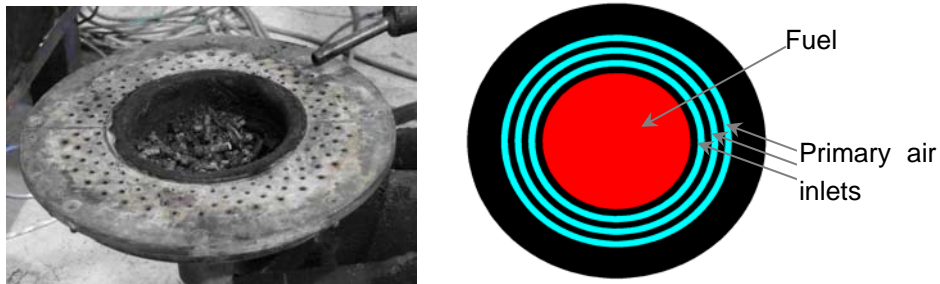


Figure 2: Left: grate of the KWB underfeed stoker furnace; right: scheme of the grate used for simulations

Table 2: Parameters used in the simulations

Ultimate Analysis [wt% d.b.]		Proximate Analysis [wt% d.b.]	
C	50.1	Moisture content [w.b.]	8.12
H	5.7	Volatiles	77.1
O	43.72	Fixed carbon	22.54
N	0.12	Ash	0.36
Total air ratio	1.58	Average diameter [m]	0.006
Primary air ratio	0.64	Average length [m]	0.018
Nominal power [kW]	20.0	Fuel feed rate [kg/h]	5.023
	$\rho$ [kg.m <sup>-3</sup> ]	$c_p$ [J.kg <sup>-1</sup> .K <sup>-1</sup> ]	$\lambda$ [W.m <sup>-1</sup> .K <sup>-1</sup> ]
Dry wood	1120	1500+T	0.14+6.5e <sup>-4</sup> T
Char	200	420+2.09T+6.85e <sup>-4</sup> T <sup>2</sup>	0.071
Ash	300	420+2.09T+6.85e <sup>-4</sup> T <sup>2</sup>	1.2
Water	998.2	4182	0.6
	Hemicellulose	Cellulose	Lignin
A [s <sup>-1</sup> ]	2.527e11	1.379e14	2.202e12
E [kJ.mol <sup>-1</sup> ]	147	193	181
C [-]	0.26	0.64	0.10
	Magnussen empirical constants		
A [-]	0.8	B [-]	0.5

#### 4. Results and discussion

Figure 3 shows the contours of the release rates of H<sub>2</sub>O, volatiles, CO and CO<sub>2</sub> along a vertical cross section through the grate axis. CO and CO<sub>2</sub> are the products of char oxidation. Here, the positions of the drying, pyrolysis, and char burnout zones inside the fuel bed are illustrated. In addition, the particle tracks on the grate coloured by the release rates of these species are presented in Figure 4. As it is shown in these figures, the three sub-processes of particle thermal conversion sequentially happen with an overlap between each other, particularly between pyrolysis and char burnout. Drying takes place in the centre of the bed above the fuel inlet. As it is shown in Figure 4, drying ends before the pellets reach the fuel bed surface. Afterwards, particles start to release volatiles along their radial path to the outer edge of the grate. The remaining char mainly reacts with oxygen above the outer primary air injection region.

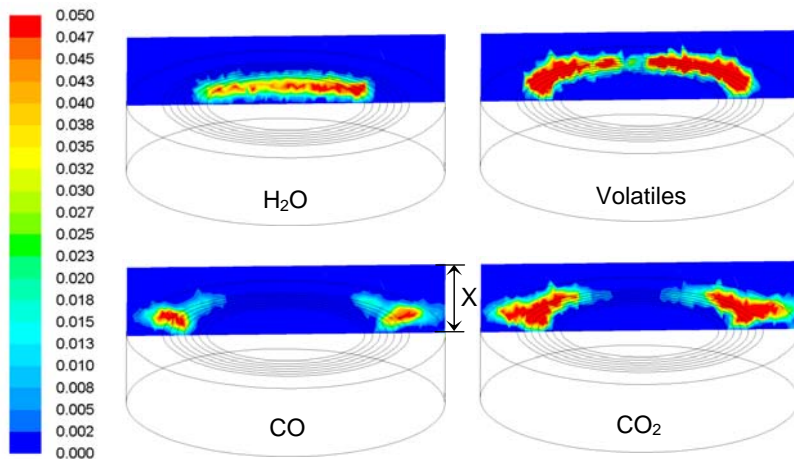


Figure 3: Contours of release rates of different species during the thermal conversion of the pellets [mg/s] at a vertical cross section through the grate axis;  $x= 5\text{cm}$

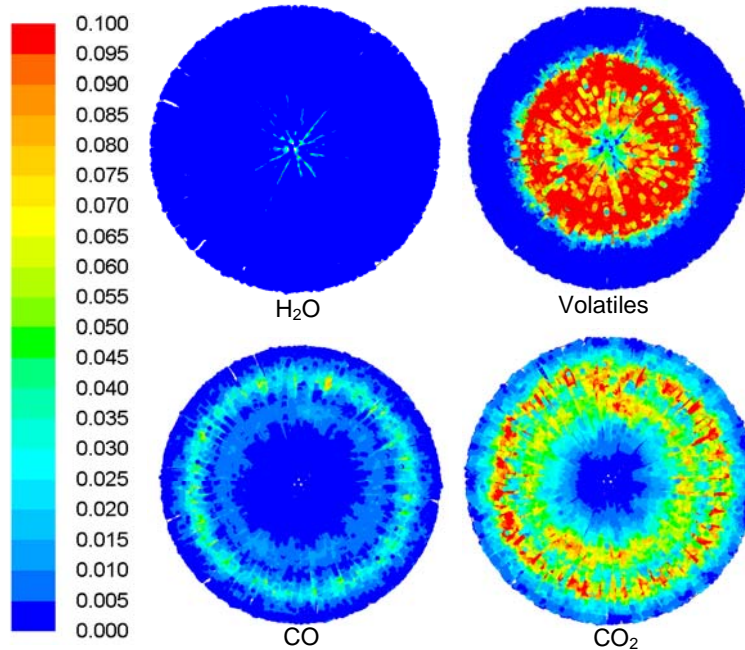


Figure 4: Particle tracks on the grate coloured by release rates of different species [mg/s]

According to the simulation results, less than 1.2 wt.% of the fixed carbon is consumed by the gasification reactions. It is due to their much slower reaction rates in comparison with the rate of the oxidation reaction. Using the CO/CO<sub>2</sub> product ratio in dependence of particle temperature, as in Table 1, results in an average value of about 0.48 for this ratio. It means the char oxidation produces more CO<sub>2</sub> than CO. It is attributed to the fact that at high temperatures most of the produced CO rapidly oxidises to CO<sub>2</sub> in the pores of the particles as well as in a layer so close to the particle surface that it gives its heat of combustion to the particle [31, 32]. Therefore, it is plausible to assume this produced CO<sub>2</sub> as the product of the heterogeneous char oxidation reaction.

The flue gas temperatures along a vertical cross section of the combustion chamber as well as the particle tracks coloured by the simulated particle temperatures are shown in Figure 5. Additionally, a picture taken from a window at the top of the furnace is enclosed in Figure 5 for comparison. However, from this picture the entire bed can not be seen, due to a reduction of diameter at the position where the secondary air is injected. The dashed line in Figure 5-b approximately represents the part of the bed which can be seen from the window at the top.

The predicted locations of the fuel conversion stages in the fuel bed are an explanation of the simulated particle temperatures in Figure 5. It can be seen that at the surface of the fuel bed, the lowest particle temperatures occur in the centre, which is due to the fact that drying takes place there. Afterwards, the particle temperatures increase due to the external heat flux and the volatile components of the particles are released. Char oxidation further increases the particle temperatures. The highest particle temperatures at the surface of the fuel bed occur at the outer primary air inlet region, due to the higher rate of char oxidation and the comparatively small size of the particles. Afterwards, the temperatures of the ash particles sharply decrease at the outer edge of the grate. The maximum predicted particle temperatures in the bed (1400 K) show an improvement in comparison with former simulations (1100 K) [1], because the new results are in good agreement with previous experiments performed in a lab-scale batch reactor [33]. It implies that both carbon monoxide and carbon dioxide have to be considered as the products of the char oxidation reaction. The results regarding to the variations of the particle temperatures are in good agreement with the picture taken from the top of the furnace.

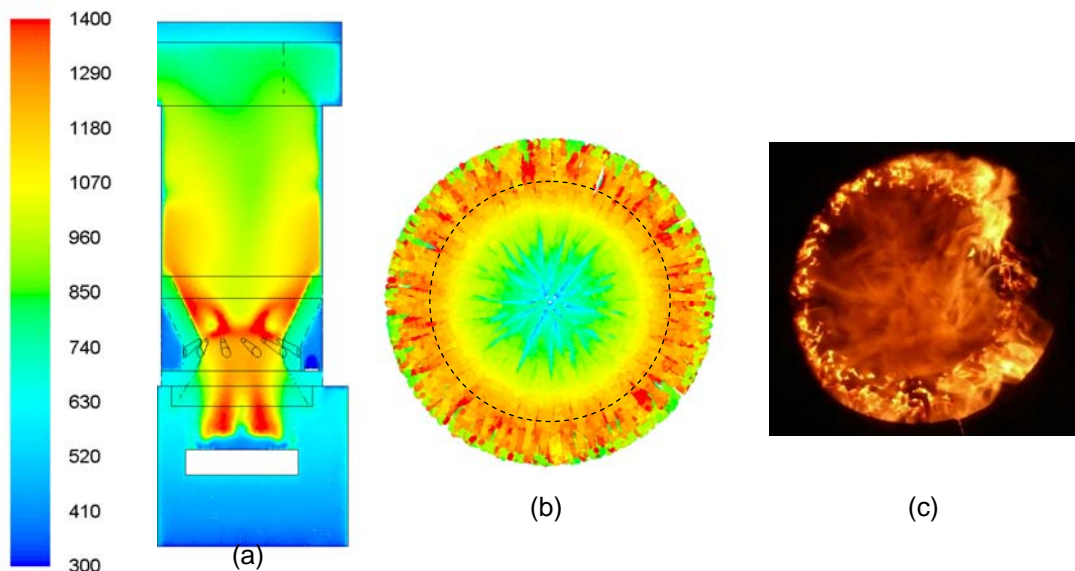


Figure 5: a) Contours of flue gas temperatures (K) along a vertical cross section of the combustion chamber; b) Particle tracks on the grate coloured by particle temperatures (K); c) Visual observation from a window at the top of the furnace.



## 5. Conclusion

The previous 3D CFD based packed bed combustion model [1] has been improved. In the new model, in contrast to the former one, the biomass particles are considered as thermally thick, i.e. the intra-particle species and temperature gradients are considered. Therefore, the parallel progress of the thermal conversion sub-processes is accounted for. Moreover, the layer model considers the particles as cylinders. The char burnout and pyrolysis models are more comprehensive than in the former model. The char gasification reactions are included. The products of char oxidation are CO and CO<sub>2</sub>, whereas the ratio between these species changes depending on the particle temperature.

The model has been successfully applied to simulate a 20 kW KWB underfeed stoker grate furnace. The maximum predicted particle temperatures in the bed are in agreement with values from experiments at a lab-scale batch reactor. Hence, the new 3D packed bed model can better predicate the particle temperatures and also burnout conditions. This is of great advantage for a correct description of particle burnout and the release of gaseous and ash forming species. The char burnout model predicts the unburned char to be less than 1 wt.%, which is in good agreement with experiences concerning the burnout quality of the grate ash. Moreover, the results regarding variations of the particle temperatures at the bed surface and the locations of the fuel conversion stages are in qualitative agreement with visual observations of the packed bed. Hence, the new 3D packed bed model provides the following advantages for the simulation of grate furnaces:

- The effect of particle related parameters, e.g. size, physical properties and moisture content, as well as operating conditions, e.g. air distribution below the grate and air staging conditions in a furnace, on the thermal conversion of the entire packed bed can be investigated.
- Modelling the hydrodynamics of the packed bed by the granular kinetic theory allows to approximate the particle movements on the grate under consideration of particle-particle collisions.
- Due to consideration of the particles as thermally thick, the particle temperatures and consequently the mass loss rate during the thermal conversion of the particles can be better predicted. Hence, the predicted release profiles of species and energy from the fuel bed are closer to reality.

As next steps of model improvement, the development of an enhanced heat transfer model inside the packed bed and the application of an appropriate gas-solid multiphase model to avoid the separate simulation for the dynamics of the particle movement in the bed are foreseen.

## 6. References

- [1] Mehrabian R., Scharler R., Weissinger A., Obernberger I., 2010: Optimisation of biomass grate furnaces with a new 3D packed bed combustion model - on example of a small-scale underfeed stoker furnace. Proceedings of the 18<sup>th</sup> European Biomass Conference, Lyon, France, pp. 1175-1183.
- [2] Scharler R., Fleckl, T., Obernberger, I., 2003: Modification of a Magnussen Constant of the Eddy Dissipation Model for biomass grate furnaces by means of hot gas in-situ FT-IR absorption spectroscopy. Progress in Computational Fluid dynamics, Vol. 3, pp. 102-111.
- [3] Scharler R., Obernberger I., 2000: Numerical optimisations of biomass grate furnaces. Proceedings of the 5<sup>th</sup> European Conference on Industrial Furnaces and Boilers INFUB, Portugal.
- [4] Scharler R., Zahirovic S., Schulze K., Kleditzsch S. Obernberger I., 2006: Simulationsgestützte Auslegung und Optimierung von Biomassefeuerungs- und Kesselanlagen – Einsatzmöglichkeiten, Stand der Technik und innovative Methoden. Österreichische Ingenieur- und Architektenzeitung, Vol. 10-12, pp. 296-309.
- [5] Scharler, R., 2001: Entwicklung und Optimierung von Biomasse-Rostfeuerungen durch CFD-Analyse. Ph.D. thesis, Graz University of Technology, Austria.
- [6] Peters B., 2002: Measurements and application of a discrete particle model (DPM) to simulate combustion of a packed bed of individual fuel particles. Combustion and Flame, Vol.131, pp. 132-146.
- [7] Bruch C., Peters B., Nussbaumer T., 2003: Modelling wood combustion under fixed bed conditions. Fuel, Vol. 82, pp. 729-738.
- [8] Wurzenberger J.C., Wallner S., Raupenstrauch H., Khinast J.G., 2002: Thermal conversion of biomass: Comprehensive reactor and particle modeling. AIChE J , Vol. 48, pp. 2398-2410.

- [9] Thunman H., Leckner B., Niklasson F., Johnsson F., 2002: Combustion of wood particles - a particle model for eulerian calculations. *Combustion and Flame*, Vol. 129 pp. 30-46.
- [10] Porteiro J., Granada E., Collazo J., Patino D., Moran J.C., 2007: A Model for the combustion of large particles of densified wood. *Energy & Fuels*, Vol. 21, pp. 3151-3159.
- [11] Lu H., Robert W., Peirce G., Ripa B., Baxter L.L., 2008: Comprehensive Study of Biomass Particle Combustion. *Energy & Fuels*, Vol. 22, pp. 2826-2839.
- [12] Gidaspow D., Bezburuah R., Ding J., 1992: Hydrodynamics of Circulating Fluidized Beds, Kinetic Theory Approach. In O. E. Potter and D. J. Nicklin, Eds., *Fluidization VII*, Engineering Foundation, pp. 75-82.
- [13] Lun C. K. K., Savage S. B., Jeffrey D. J., Chepurniy N., 1984: Kinetic theories for granular flow: inelastic particles in Couette flow and slightly inelastic particles in a general flow field. *J. Fluid Mech.*, Vol. 140, pp. 223–256.
- [14] Gidaspow D., 1994: *Multiphase flow and fluidization*. Academic Press, Boston.
- [15] Syamlal M., Rogers W., O'Brien T. J., 1993: *MFIX Documentation: Volume 1, Theory Guide*. National Technical Information Service, Springfield, VA, DOE/METC-9411004, NTIS/DE9400087.
- [16] Gidaspow D., Jayaswal U. K., Ding J., 1991: Navir-Stokes Equation Model for Liquid-Solid Flows Using Kinetic Theory. *Liquid Solid Flows*, Vol. 118, New York: ASME, pp. 165-178.
- [17] Sinclair J. L., Jackson R., 1989: Gas–particle flow in a vertical pipe with particle–particle interactions. *AIChE Journal*, Vol. 35, pp. 1473–1486.
- [18] Chapman S., Cowling T.G., 1970: *The mathematical theory of non-uniform gases*. Cambridge University Press, Cambridge.
- [19] Ha M.Y., Choi B.R., 1994: A numerical study on the combustion of a single carbon particle entrained in a steady flow. *Combustion and Flame*, Vol. 97, pp. 1-16.
- [20] Di Blasi C., 1998: Multi-phase moisture transfer in the high-temperature drying of wood particles. *Chemical Engineering Science*, Vol. 53, pp. 353-366.
- [21] Branca C., Albano A., Di Blasi C., 2005: Critical evaluation of wood devolatilization mechanisms. *Thermochim Acta*, Vol. 429, pp. 133-141.
- [22] Gomez-Barea A., Leckner B., 2010: Modelling of biomass gasification in fluidized bed. *Prog. Energy Combustion Science*, Vol. 36, pp. 444-509.
- [23] Tognotti L., Longwell J.P., Sarofim A.F., 1990: The products of the high temperature oxidation of a single char particle in an electrodynamic balance. *Proc. Combustion Inst.*, Vol. 23, pp. 1207–1213.
- [24] Evans D.D., Emmons H.W., 1977: Combustion of wood charcoal. *Fire Saf J*, Vol1, pp. 57–66.
- [25] Johansson R., Thunman H., Leckner B., 2007: Influence of intraparticle gradients in modeling of fixed bed combustion. *Combustion and Flame*, Vol. 149, pp. 49-62.
- [26] Froment G.F., Bischoff K.B., 1990: *Chemical reactor analysis and design*. New York: John Wiley & Sons.
- [27] Patisson F., Francois M.G., Ablitzer D., 1998: A non-isothermal, non-equimolar transient kinetic model for gas-solid reactions. *Chem. Eng. Sci.*, Vol. 53, pp. 97-708.
- [28] Kumar R.R., Kolar A.K., Leckner B., 2006: Shrinkage characteristics of Casuarina wood during devolatilization in a fluidized bed combustor. *Biomass Bioenergy*, Vol. 30, pp. 153-165.
- [29] Incropera F.P., De Witt D.P., 1990: *Introduction to heat transfer*. 2<sup>nd</sup> ed. New York: John Wiley & Sons.
- [30] Hjertager B. H., Solberg T., Ibsen C. H., Hansen K. G., 2003: Multi-Fluid CFD modelling of fluidised bed reactors. Invited Presentation *Computational Fluid Dynamics in Chemical Engineering III*, Davos, Switzerland.
- [31] Hayhurst A.N., Parmar M.S., 1998: Does solid carbon burn in oxygen to give the gaseous intermediate CO or produce CO<sub>2</sub> directly? Some experiments in a hot bed of sand fluidized by air. *Chem. Eng. Sci.*, Vol. 53, pp. 427-438.
- [32] Wang F.Y., Bhatia S.K., 2001: A generalised dynamic model for char particle gasification with structure evolution and peripheral fragmentation. *Chem. Eng. Sci.*, Vol. 56, pp. 3683-3697.
- [33] Dahl J., Obernberger I., 2004: Evaluation of the combustion characteristic of four perennial energy crops. *Proceedings of the 2<sup>nd</sup> world conference and exhibition on biomass for energy*, Rome, Italy.

# Paper V

# Multi-physics modelling of packed bed biomass combustion

Ramin Mehrabian<sup>a,b,\*</sup>, Ali Shiehnejadhesar<sup>a,b</sup>, Robert Scharler<sup>a,b,c</sup>, Ingwald Obernberger<sup>a,b,c</sup>

<sup>a</sup>*BIOENERGY 2020+ GmbH, Inffeldgasse 21b, 8010 Graz, Austria*

<sup>b</sup>*Institute for Process and Particle Engineering, Graz University of Technology, Inffeldgasse 21b, 8010 Graz, Austria*

<sup>c</sup>*BIOS BIOENERGIESYSTEME GmbH, Inffeldgasse 21b, 8010 Graz, Austria*

---

## Abstract

A transient 3D model for two main zones, namely the fuel bed and the freeboard, of biomass packed bed combustion systems was developed. It integrates the models for the biomass conversion sub-processes and solves the governing equations for the gas and solid phase and their interactions. The intra-particle gradients are included by considering the biomass particles as thermally thick particles. The shrinkage of the packed bed and the variations of the bed porosity due to the uneven consumption of the fuel are taken into account. Detailed kinetic mechanisms are used for the simulation of homogeneous gas phase reactions. To verify the model and to increase the understanding of packed bed combustion, laboratory-scale fixed-bed batch experiments have been performed in a reactor with 9.5 cm diameter and 10 cm length. The model performance was extensively validated with gas phase measurements (CO, CO<sub>2</sub>, CH<sub>4</sub>, H<sub>2</sub>, H<sub>2</sub>O and O<sub>2</sub>) above the fuel bed, temperatures at different heights in the bed and in the freeboard, and the propagation rate of reaction front. The simulation results are in a good agreement with the measured values.

## Keywords:

biomass, packed bed, combustion, modelling, CFD, experimental validation

---

\*Corresponding author. Tel: +43 (0) 316 8739232, Fax: +43 (0) 316 8739202.

Email address: [ramin.mehrabian@bioenergy2020.eu](mailto:ramin.mehrabian@bioenergy2020.eu) (Ramin Mehrabian)

## 1. Introduction

Among the applied biomass combustion technologies grate-firing is one of the most widely spread, because it can handle a wide range of fuels of varying quality and moisture contents and requires less fuel pretreatment. However, the bed inhomogeneity due to the inhomogeneity of the biomass fuel and insufficient mixing in the fuel bed, causes non-uniform combustion on the grate. This may reduce the efficiency of the plant and increase the emissions. Dealing with these deficiencies requires an improved understanding of the combustion processes in the fuel bed.

Due to the limited accessibility and inhomogeneity inside the packed bed, it is difficult and complex to obtain information by measurements about the conversion processes in the packed bed. As a result, there are few experimental investigations on packed bed biomass furnaces which include a complete set of measurements. Ryu et al. [1] measured temperatures, species and mass loss profiles of four different biomass types in a fixed bed under fuel-rich conditions. The combustion of straw in a fixed bed was experimentally investigated by van der Lans et al. [2]. They measured temperatures in the packed bed at different heights and species concentrations above the bed. Porteiro et al. [3, 4] measured the propagation rates of the reaction front in a fixed bed combustor.

The review of elaborations on packed bed modeling published in literature shows a broad variety of different model approaches to describe entire packed bed systems. The main distinctive features are homogeneous and heterogeneous models. The difference between them lies in the calculation of the energy equation. In homogeneous models the temperature of the gas and of the solid phase are assumed to be equal and one overall energy balance equation is applied [2, 5]. The physical properties which appear as constants in the energy equation are described by their effective values over the entire bed. In heterogeneous models the gas phase and the solid phase have individual energy equations [6–8]. They have different temperatures, and heat and mass transfer between the two phases are described by means of Nusselt and Sherwood correlations. When the temperature difference between the gas and solid is not negligible, which is the case for packed bed combustion, heterogeneous modelling is recommended.

Based on the treatment of the solid phase in the heterogeneous models, they can be classified into continuous models [9–12] and discrete particle mod-

els [13–16]. Continuous heterogeneous models treat both phases as if they are distributed continuously over the whole spacial domain. At each point in space both phases exist with distinguished properties. The common restriction of continuous packed bed models is that the intra-particle effects cannot be described sufficiently. Additionally, it is very difficult to model the inter-particle interactions in the packed bed with continuous models. The discrete particle models enhance the packed bed modelling by considering the packed bed as an ensemble of representative particles, where each of these particles undergoes thermal conversion processes. In this way the inter-particle effects, e.g. momentum and energy exchanges, can be fully described.

However, there is a limitation in almost all existing models, with the exception of [11], that they consider the packed bed and the freeboard separately, although there is a strong interaction between them. The conversion of the packed bed provides the temperatures and species as inlet conditions for gas phase modelling. Additionally, the published models are validated only to a certain extent, typically using either propagation rates of the reaction front or species profiles. This can be attributed to the fact that experimental data which include complete sets of measurements with a detailed information about the boundary conditions are scarce.

The objectives of this paper are to present a fully coupled three-dimensional model for the combustion of biomass packed beds which includes both the freeboard and the packed bed as well as detailed experimental data for model validation. A validated comprehensive single particle model [17] for the combustion of thermally thick biomass particles is applied to model the conversion of particles in the packed bed. The size and the position as well as the conversion state of each particle is determined at every time step. The packed bed shrinkage and local porosity of the bed are calculated in each time step. The interaction between the gas phase and particles is considered by an iterative procedure. The radiative heat transfer between the particles and the walls is updated at the beginning of each time step. With these results, the conservation equations of the entire bed are integrated. The homogeneous gas phase reactions are modelled with a detailed kinetic mechanism, instead of applying global reactions. To validate the coupled packed bed/gas phase model, an experimental setup under known conditions has been simulated and the temperature profiles at different heights in the packed bed and in the freeboard, several species concentrations above the fuel bed as well as the propagation of the reaction front are compared with measurements.

## 2. Experimental setup

The laboratory-scale reactor is a discontinuously operated pot furnace, see Figure 1. It consists of a cylindrical retort (height 0.35 m, i.d. 0.12 m), heated electrically by two separated PID controlled heating circuits. The biomass is put into a cylindrical sample holder (0.100 m height and 0.095 m i.d.) which is located inside the cylindrical retort. The retort and pot are made of fibre-reinforced SiC ceramics. The retort is surrounded by a thick wall of insulated firebricks. The pot rests on a weight balance to measure the mass loss during conversion. Air is introduced through a porous plate at the bottom of the fuel bed. Five thermocouples are installed inside the fuel bed according to Figure 1. Thermocouples are placed above the sample holder to measure the temperature of the flue gas in the free board. In order to avoid the penetration of false air, the reactor is sealed with thermal oil. The flue gas is extracted from above the fuel bed using a heated suction probe and introduced into an Emerson NGA 2000 to measure O<sub>2</sub> (paramagnetism), CO, CO<sub>2</sub> (NDIR) and H<sub>2</sub> (heat conductivity). Additionally a FT-IR (Ansyco) has been applied to measure H<sub>2</sub>O and CH<sub>4</sub>. Furthermore, the difference between ambient and reactor pressure is detected for the purpose of correcting the data gained by the weight measurements (causing additional forces acting on the balance). A detailed description of the laboratory-scale reactor was given in previous publications [18].

The experimental conditions for test runs performed and relevant fuel data are summarised in Table 1. The experiment was repeated three times with the same conditions to check the repeatability of the test runs.

## 3. Methodology

### 3.1. Particle model

The particle model accounts for intra-particle transport processes and simultaneous sub-processes of thermal conversion of thermally thick solid biomass particles. To reduce the model complexities and calculation time, only the radial temperature gradient in the particle is considered. This is an usual simplification assumption.

To apply the one-dimensional model for a finite cylindrical geometry (as an approximation for the biomass particle shape), Thunman's discretisation [19] approach has been applied. This approach assumes that the particle boundary conditions are homogeneous and every point in the particle at a certain

distance from the particle surface has the same temperature and conversion state. The particle is divided into four layers: drying layer, pyrolysis layer, char and ash layer. The boundaries between the layers are related to the conversion sub-processes: drying, pyrolysis and char burnout fronts. At the beginning of the thermal conversion process only drying is of relevance. Due to heating up, moisture starts to get released from the particle. The pyrolysis layer consists of dry biomass and is located around the drying layer as the drying front moves towards the particle centre. When pyrolysis commences, the dry biomass converts to char and volatiles. Volatiles leave the particle and char builds a layer around the pyrolysis layer. Finally, char burnout also creates another layer which contains only ash and surrounds the char layer. As the conversion of the fuel particle proceeds, drying, pyrolysis and char burnout fronts move from the surface to the centre of the particle.

The conversion of each layer is simulated by separate sub-models. It is assumed that drying occurs at a fixed boiling temperature in an infinitely thin zone that separates the wet and the dry part of the particle. The drying process acts as a heat sink, it means that any amount of heat flow above the boiling temperature is consumed by the drying process. It is assumed that there is no resistance to mass transfer, and therefore the water vapour instantaneously leaves the particle. However, the cooling effect of the water vapour transfer through the particle is considered.

Biomass pyrolysis is described by the decomposition of its three pseudo-components hemicellulose, cellulose, and lignin. This model implicitly assumes the hypothesis of an independent decomposition of these three constituents. An Arrhenius equation is used to describe the pyrolysis of each pseudo-component. It represents the dependence of the kinetic rate constant  $k$  on the absolute temperature  $T$ :

$$k = A \exp\left(-\frac{E}{RT}\right) \quad (1)$$

$A$  is the pre-exponential factor,  $E$  is the activation energy and  $R$  is the universal gas constant.

The overall mass loss rate of a particle during pyrolysis is given as:

$$-\frac{dm}{dt} = \sum_{i=1}^3 c_i \frac{d\alpha_i}{dt} \quad (2)$$



where  $i$  is related to each pseudo-component,  $c_i = m_{0,i} - m_{f,i}$  is a measure of the contribution of the partial decomposition processes to the overall mass loss  $m_0 - m_f$ . The conversion of each pseudo-component  $\alpha_i$  can be expressed by:

$$\alpha_i = \frac{m_{0,i} - m_i}{m_{0,i} - m_{f,i}} \quad (3)$$

The pseudo-components are all assumed to decompose individually according to a first-order reaction, therefore the conversion rate of each pseudo-component is given by:

$$\frac{d\alpha_i}{dt} = A_i \exp\left(-\frac{E_i}{RT}\right) (1 - \alpha_i) \quad (4)$$

Char conversion models are more complicated than biomass pyrolysis models, as they are based on heterogeneous reactions for which both intrinsic kinetic and transport phenomena are important. Due to the structure of the particle model, the char conversion reactions are assumed to occur at the interface between char and ash layer. Char oxidation with  $O_2$  and gasification with  $CO_2$ ,  $H_2O$  and  $H_2$  are considered as char conversion reactions. The rate of char conversion reactions is a function of both kinetic rate at the reaction surface and mass transfer rate to/from the reaction surface. Assuming a global reaction rate of first order with respect to the oxidising/gasifying agent concentration at the reaction surface, leads to a char conversion rate as:

$$\frac{dm_{ch}}{dt} = - \sum_{i=1}^4 \frac{\Omega_i M_c}{\frac{1}{k_{e,i} S} + \frac{1}{h_m S} + \int_{\delta_{ash}} \frac{dr}{\mathcal{D}_e S(r)}} X_{\infty,i} \quad (5)$$

where  $i = 1$  to 4 corresponds to the heterogeneous reactions in Table 2 and  $\Omega_i$  is the stoichiometric ratio of moles of carbon per mole of oxidising/gasifying agent in the corresponding reaction.  $M_c$ ,  $S$ ,  $k_i$ ,  $\delta_{ash}$  and  $X_{\infty,i}$  are the molecular weight of carbon, the surface area of the char burnout front, the kinetic rate constant of heterogeneous reaction  $i$ , the thickness of the ash layer and the molar concentration of oxidising/gasifying agent of reaction  $i$  in the bulk flow, respectively.

The mass transfer coefficient of reactants in the boundary layer around the particle  $h_m$ , is obtained by the Sherwood number. The effective diffusivity of the ash layer  $\mathcal{D}_e$ , depends on the ash porosity and the molecular diffusivity of the penetrating gaseous component [17].

Since particle shrinkage during drying is much lower compared to that occurring during pyrolysis and charcoal combustion [20], it is postulated that during drying, the size of the particle remains constant and its density decreases. However, both shrinkage and density change during pyrolysis and char burnout are considered in the particle model. The physical properties and parameters used in the particle model are summarised in Table 2. A detailed description of the particle model and its validation are given in [17].

### 3.2. Bed shrinkage

The consumption of the fuel influences two parameters of the packed bed: one is the shrinkage of the fuel bed and the second one is the bed porosity. Usually it is assumed that the bed continuously shrinks [6–8, 26]. However, experimental data show that the shrinkage of the fuel bed is not smooth and the porosity varies within the bed [9]. It may be attributed to uneven fuel consumption across the fuel bed.

One of the main features of the particle model is the calculation of the particle shrinkage during its thermal conversion. It allows to model the shrinkage of the bed based on the shrinkage of individual particles. Biomass particles are assumed to be always in contact with beneath particles. Therefore, shrinkage of the bed depends on the fuel conversion. In this way, the uneven fuel consumption in the packed bed causes discontinues shrinkage (bed collapse) and cavities at the surface of the fuel bed. Moreover, local bed porosity is calculated based on the volume fraction of solid in each computational cell in the packed bed at every time step. Hence, the effects of the fuel consumption and the bed shrinkage on the local bed porosity are considered. As it is explained in the next section, the calculated bed porosity is used to determine the gas phase pressure drop in the packed bed.

### 3.3. Bed pressure loss

The resistance to the gas flow is considered as a source term in the momentum equation of the continuous phase. The source term is calculated using the Ergun equation [27]:

$$\Delta S_i = - \left( \frac{\mu}{C_1} u_i + C_2 \rho_g u_i^2 \right) \quad (6)$$

where  $\mu$ ,  $u$  and  $\rho_g$  are the viscosity, the gas velocity and the gas density, respectively. The permeability,  $C_1$ , and inertial loss coefficient,  $C_2$ , for packed

beds are functions of the mean particle diameter,  $d_p$ , and bed porosity,  $\phi$ :

$$C_1 = \frac{d_p^2 \phi^3}{150(1 - \phi)^2} \quad (7)$$

$$C_2 = \frac{3.5(1 - \phi)}{d_p \phi^3} \quad (8)$$

The grate in the lab-reactor is a screen. It is represented as a uniformly porous medium to consider the resistance to gas flow. To model the pressure loss through a screen or perforated plate the permeability term can be eliminated:

$$\Delta S_i = -C_2 \rho_g u_i^2 \quad (9)$$

The inertial loss coefficient for a screen is tabulated as a function of Reynolds number and free area of the screen in [28].

### 3.4. Heat transfer

The mathematical description of the heat transfer in the packed bed requires some assumptions and simplifications, due to the complexity and irregular arrangement of the packed bed. As radiation is the dominant mechanism of heat transfer in combustion systems, the radiative heat transfer has to be considered. It is known that the conduction mechanism is important, if the temperature in the packed bed is below 450 K [29]. Therefore, among the possible conduction routs, only the conduction inside each particle is considered, as it is already explained in the particle model section 3.1. In addition, gas-particle convective heat transfer is also considered in the calculations. In the following sub-sections the convection and radiation mechanisms are explained.

#### 3.4.1. Convection

In the literature a variety of experimental and theoretical investigations have been published that address the problem of the convective heat transfer in a packed bed. Most of the articles describe a correlation of the mean Nusselt number as a function of the mean Reynolds number. A successful semi-empirical method to calculate the heat transfer rate inside a bed was introduced by [30]:

$$Nu_{lam} = 0.664 Pr^{1/3} (Re/\phi)^{1/2} \quad (10)$$

$$Nu_{turb} = \frac{0.037Pr(Re/\phi)^{0.8}}{1 + 2.443(Pr^{2/3} - 1)(Re/\phi)^{-0.1}} \quad (11)$$

$$Nu_p = 2 + (Nu_{lam}^2 + Nu_{turb}^2)^{1/2} \quad (12)$$

2 in this equation is the asymptotic solution for  $Re \rightarrow 0$ .

$Nu_p$  can now be used to calculate the mean Nusselt number for the packed bed:

$$Nu = f(\phi)Nu_p \quad (13)$$

where  $f(\phi)$  is an empirical factor which depends on the porosity of the bed:

$$f(\phi) = 1 + 1.5(1 - \phi) \quad (14)$$

A comparison between the correlations in literature and Equation 13 is shown in Figure 2. The empirical correlations from literature depict a scattering of the results due to non-uniformities in the void fraction distributions across the bed which leads to cold bypass flows as reported by [30, 31]. However, the important message of Figure 2 is that Equation 13 plausibly correlates the mean Nusselt number to the Reynolds number in packed beds.

#### 3.4.2. Radiation

Each particle in the packed bed emits radiation, which is absorbed by neighbouring particles. The influence of the neighbouring particles on radiative heat transfer is considered by changing the boundary condition on the particle surface:

$$q_{rad,i} = \sum_{j=1}^{NP} \epsilon\sigma F_{ij}(T_j^4 - T_i^4) \quad (15)$$

where  $q_{rad,i}$  is the radiation heat flux from the neighbouring particles to the particle  $i$ .  $\epsilon$ ,  $\sigma$ ,  $N$  and  $T$  are the particle emissivity, the Stefan-Boltzmann constant, the number of particles and the particle surface temperature, respectively.  $F_{ij}$  is the view factor between particle  $i$  and  $j$ .

It is difficult, however, to implement Equation 15 in a simulation, as it requires a summation over all particles for each particle and the calculation of the view factor for each pair of particles. Therefore, an appropriate spherical control volume  $\vartheta$  is defined around each target particle, see Figure 3. It is

assumed that the target particle exchanges radiation with its surrounding control volume:

$$q_{rad,i} = \epsilon\sigma F_{i\vartheta}(T_{\vartheta,i}^4 - T_i^4) \quad (16)$$

Since the target particle is enclosed by the radiation control volume,  $F_{i\vartheta} = 1$ . The parameter  $T_{\vartheta,i}$  is the average temperature of particles and gas phase in the radiation control volume  $\vartheta$  given by [42]:

$$T_{\vartheta,i} = \phi T_{g,\vartheta} + (1 - \phi) \frac{1}{NP_{\vartheta}} \sum_{j=1;\neq i}^{NP_{\vartheta}} T_j \quad (17)$$

where  $\phi$ ,  $T_{g,\vartheta}$  and  $NP_{\vartheta}$  are, respectively, the bed porosity, the gas temperature, and the number of particles located in the volume  $\vartheta$ .

If the target particle is close to a wall, some CFD cells in the radiation control volume are adjacent to the wall. Including the effect of walls on the radiation to the target particle,  $T_{\vartheta,i}$  turns out as:

$$T_{\vartheta,i} = (1 - \xi) \left[ \phi T_{g,\vartheta} + (1 - \phi) \frac{1}{NP_{\vartheta}} \sum_{j=1;\neq i}^{NP_{\vartheta}} T_j \right] + \xi \frac{1}{NC_{\vartheta}} \sum_{j=1}^{NC_{\vartheta}} T_{wall,j} \quad (18)$$

where  $NC_{\vartheta}$  and  $T_{wall}$  are the number of cells in the radiation control volume adjacent to the wall and the wall temperature, respectively. The parameter  $\xi$  is a constant which adds weight of the wall temperatures to  $T_{\vartheta,i}$ . In this study  $\xi$  is assumed to be 0.5 to achieve a plausible horizontal temperature profile in the packed bed near the walls.

Thermal radiation from the freeboard above the packed bed is one of the most important mechanisms of grate firing systems. It is responsible for the initiation of the thermo-chemical processes. The average radiation temperature for the particles located at the top of the packed bed is calculated by:

$$T_{\vartheta,i} = 0.5 \left( \frac{q_{rad}}{\sigma} \right)^{1/4} + 0.5 \left[ \phi T_{g,\vartheta} + (1 - \phi) \frac{1}{NP_{\vartheta}} \sum_{j=1;\neq i}^{NP_{\vartheta}} T_j \right] \quad (19)$$

where  $q_{rad}$  is the radiation heat flux from the freeboard. It is calculated by the simulation of the gas phase combustion with ANSYS FLUENT [27].

### 3.5. Gas phase model

Accurate modelling of the system chemistry is critical. In previous studies, mostly global reactions were considered. The global reactions describe an overall process by which reactants are converted to anticipated products at the end of the process. Therefore, they may not be sufficiently accurate for a broad range of operating conditions. The accurate description of the reaction kinetics is of high relevance, since they have a considerable impact on the simulation results. Therefore, in this study detailed mechanisms are used for the homogeneous reactions. A well-known comprehensive reduced mechanism, DRM22, is utilised in this study [43]. It is a 22 species reaction set with 104 elementary reactions reduced from GRI-Mech [44]. The full detailed GRI mechanism version 2.11 [45] has also been applied to evaluate the difference between the full mechanism and the reduced one. It consists of 49 species and 277 reversible reactions. Additionally, the C-H-O subset of the skeletal Kilpinen97 mechanism [46, 47], has been applied in order to evaluate the results and applicability of this mechanism for the simulation of biomass grate furnaces. It is a mechanism with 12 species and 25 reactions.

Many different gas species are released during biomass pyrolysis. Several studies investigated the composition of the product gaseous. Most commonly detected gas species are CO, CO<sub>2</sub>, H<sub>2</sub>, H<sub>2</sub>O, CH<sub>4</sub>, C<sub>x</sub>H<sub>y</sub>, CH<sub>m</sub>O<sub>n</sub> and other trace compounds. In order to use detailed reaction mechanisms, the released gas species in the pyrolysis model must be compatible with the species considered in the mechanisms. Therefore, the products of the pyrolysis reaction in simulations with GRI2.11, DRM22 and Kilpinen97 mechanisms are the intersection of the available species in each mechanism and the most reported gas components in literature. The pyrolysis product compositions considered in simulations with each mechanism are listed in Table 3. Later it is explained how the compositions are calculated. Since there is no C<sub>x</sub>H<sub>y</sub> and CH<sub>m</sub>O<sub>n</sub> in the Kilpinen97 mechanism, it was not possible to consider them as pyrolysis products in the simulations with this mechanism.

It is worth noting that the formed tars in the primary pyrolysis reaction are assumed to be fully converted into its main secondary products, e.g. CO, CH<sub>4</sub>, C<sub>2</sub>H<sub>x</sub>. This is due to the fact that the tar composition and chemical formula as well as the rate of its secondary conversion are unknown. This assumption is in line with the dedicated experiments [48, 49], in which it was observed that the carbon monoxide is quantitatively the most important product from the homogeneous tar conversion. Over two-thirds of the tar

lost at high temperatures forms carbon monoxide. Corresponding methane and C<sub>2</sub> hydrocarbons each account for about 10 wt% of the tar converted. This assumption is plausible for large particles in packed bed condition, because it is known that tar is very reactive when it is in contact with a hot char layer and it easily breaks down.

Conservation equations for C, H, O and N as well as enthalpy provide five equations in order to determine the composition of pyrolysis products. Since the number of equations are less than unknowns, i.e. 10 and 6 unknowns for DRM22 (GRI2.11) and Kilpinen97 mechanisms respectively, the system can have an infinite number of solutions. In order to obtain a meaningful result, some additional constraints are needed. They can be derived from measurements. The experimental data from literature [48–68] are used to calculate the mass ratios of CO, CH<sub>4</sub>, H<sub>2</sub> and H<sub>2</sub>O to CO<sub>2</sub> and C<sub>2</sub>H<sub>x</sub> to CH<sub>4</sub>. They are illustrated in Figure 4 and 5. The collected data are a compilation of measured values using various fuels, reactors and operating conditions (heating rates, particle sizes, etc.). According to Figure 4 and 5, the constraints needed can be gained. They are listed in Table 4.

The flow regime in the lab-reactor experiment is laminar ( $Re < 2300$ ). Therefore no turbulence model is required. It highlights the importance of the chemistry model, because the reaction rates are determined by the kinetic mechanism. The radiation which is an important part in combustion simulations is calculated by the Discrete Ordinate Model (DOM) together with the Weighted Sum of Gray Gases (WSGG) method to calculate the radiative absorption and emission coefficients. Mass diffusion coefficients are required whenever species transport equations in multi-component flows are solved. For reacting flows with low turbulence conditions the influence of molecular diffusion on mixing becomes comparable to the contribution of the turbulent diffusion. Hence, the molecular diffusion of each gas species in the mixture was calculated by the kinetic theory [35] instead of using a constant value.

### 3.6. Boundary conditions

The simulation domain consists of the cylindrical sample holder, the cylindrical retort, the air inlet tube and the exhaust tube. Since the outer walls are well insulated, the adiabatic boundary condition is used, except for the walls where the heating elements are located. The heating elements are surrounded by insulation material and controlled separately by two PID controllers to keep their assigned temperatures, i.e. 750°C for the upper part

and 450°C for the lower part. For the heated wall sections, a temperature dependent boundary condition is needed. If the wall temperature in each section is lower than the assigned temperature, the radiation boundary condition is applied. Once the temperature of the retort wall is higher than the temperatures of the heating elements, there is no heat flux from the heating elements to the retort wall and the insulation avoids any heat loss from the retort wall. Therefore, the adiabatic boundary condition is applied.

### *3.7. Solution strategy*

The pressure based segregated algorithm of ANSYS FLUENT is used as the basis for the computation of the continuous phase and it has been combined with the models describing the conversion of the particles and the packed bed. In each flow time step, the fluid properties are updated, then the conservation equations are solved to update the mass fluxes, pressure and velocities. Afterwards, species and energy equations are solved. These steps are repeated in each flow time step until a converged state is achieved. The converged state of the gas phase serves as boundary condition for the particle model. Discretisation of the differential equations of the flow field is performed in time with the first-order implicit scheme and in space with the second-order upwind scheme.

In the particle model, an adaptive particle time step is used which is smaller than the flow time step. In each particle time step, the boundary temperature, time derivatives of the particle layer temperatures and mass flow rates from each layer are calculated. The Runge-Kutta scheme is used to solve the system of equations. If the relative changes of mass and temperature of each layer are within a tolerance level of  $10^{-3}$ , the particle time step is acceptable, otherwise it is reduced. When the acceptable particle time step is achieved, the mass and temperatures of each layer as well as the particle size and the reaction rates are calculated and the particle state is advanced in time. This procedure is repeated until the flow time is reached. Thereafter, the particle energy and species source terms are returned to the flow solver. A more detailed overview of the particle model solution method is available in [17].

In the packed bed level, once the particles and flow have the same time, the local porosity of each cell inside the bed as well as the bed shrinkage are calculated. Additionally, the radiation temperature and the convective heat transfer coefficient for each particle in the packed bed are calculated.



#### 4. Results and discussion

Comparisons between the measured and predicted temperatures in the fuel bed are illustrated in Figure 6. The positions of thermocouples in the fuel bed are according to Figure 1. Axisymmetry conditions have been applied to simulate the experimental setup, thus P2a and P2c are corresponding to one point in the simulation domain. In Figure 7 measured and predicted molar concentrations of  $O_2$ ,  $CO$ ,  $CO_2$ ,  $CH_4$ ,  $H_2O$  and  $H_2$  above the fuel bed (11 cm) are presented. In this section, the results with DRM22 are compared to the experimental data and later the effect of different reaction mechanisms is discussed.

In both experimental and simulation results ignition of volatiles can be recognized, indicated by an abrupt decrease of  $O_2$  concentrations and sharp increases of  $CO$ ,  $CO_2$ ,  $H_2O$  and  $H_2$  concentrations. Afterwards, the thermal conversion of the packed bed accelerates. After the ignition, the simulated species concentrations depict similar trends as the measured values, except  $H_2O$ . In the simulation, in contrast to the experimental data,  $H_2O$  declines. The main reason for the sharp increase of  $H_2O$ , once the ignition occurs, is combustion in the gas phase. When oxygen depletes,  $H_2O$  mole fraction reduces to 0.1. Afterwards, it follows the trend of the experiments, however, with lower concentration. The reason of this deviation can be a lower concentration of water vapour in the composition of volatiles than the experiments. It is worth noting that in this study the composition of volatiles is determined by mass and energy balances. Most probably a mechanistic pyrolysis scheme, where the composition of volatiles is temperature dependent, could improve the results concerning  $H_2O$ .

The volatiles combustion front propagates downwards in the packed bed. Once the combustion front reaches a thermocouple, the temperature sharply increases. The steep increase in temperature occurs first at P1 then at P2 and finally at P3. The measured temperatures at P2a and P2c rise almost simultaneously, except the second test run (Exp2). The temperature rise at P2b occurs slightly after P2a and P2c. The model predicts well the first peak temperatures and their sequences. The temperature at each point inside the packed bed decreases after the combustion front has passed by. However, it remains relatively high, because the hot flue gas passes through the bed. The simulation results at P1, P2a and P2c comply with the experimental data concerning the gradual decline of temperatures. The model predicts

lower temperatures at P2b after the first temperature peak in comparison to the measured values. In addition, the steep increase in temperature at P3 is slightly delayed in comparison to the measured values. It implies that in the simulation the heat diffusion in the packed bed and the conversion rate is slower than in the experiments. This might be attributed to the heat transfer model inside the packed bed and also uncertainties of the physical properties, i.e. thermal conductivity.

Measured and modelled  $O_2$  concentrations above the fuel bed show that the entire oxygen is consumed by the combustion of pyrolysis products during the devolatilisation step. Therefore, the biomass char remains mostly unreacted behind the combustion front. As the combustion front reaches the grate, after about 25 min in the simulation, the temperature at P3 abruptly rises and concentrations of  $H_2O$ ,  $H_2$  and  $CH_4$  sharply decline which indicates the end of the pyrolysis process. At the end of pyrolysis, both model and experimental data show the same behavior, except CO and  $CO_2$  concentrations which deviate from the experimental data. In the model CO decreases, while the first and the second test runs (Exp1 and Exp2) show a gradual increase and the third one (Exp3) a slight decrease. The predicted  $CO_2$  concentrations rise while the experiments depict a decrease of  $CO_2$  at the end of pyrolysis and beginning of char burnout.

Sharp decrease of  $CO_2$  in the experiments at the beginning of char burnout can be attributed to the fact that  $CO_2$  produced by the char oxidation reaction is consumed by gasification reactions. However, there are some reasons for increase of  $CO_2$  and decrease of CO in the simulation at the beginning of char burnout. First, the correlations for the CO to  $CO_2$  product ratio for the char oxidation reaction predict more  $CO_2$  than CO at low temperatures, i.e. beginning of char oxidation. Second, at the beginning of char burnout the temperatures predicted at P2 and P3 are lower than the measured values. This leads to a lower gasification reaction rate in the simulation. Lastly, it may also be attributed to an over-prediction of the CO conversion by the water-gas shift reaction in the simulation because of lower temperatures in the simulation at the beginning of char burnout. By increasing temperature in the simulation more CO than  $CO_2$  is produced by the char oxidation reaction and the rate of gasification reactions increases. Hence, in the simulation  $CO_2$  starts to decrease and CO rises, as it can be seen in Figure 7.

Char burnout happens close to the grate, since the air is introduced from

below. During char oxidation, the oxygen is consumed near the grate. Once char oxidation starts, the bed temperatures at P1 and P2 start to gradually rise. It attributes to the heat generated by char combustion. Approaching the end of char burnout, the air to fuel ratio increases which promotes the homogeneous CO oxidation reaction. It results in sharp peaks in the CO<sub>2</sub> concentrations and temperatures at all thermocouple locations, particularly at P1 and P2, in both simulation and experimental data.

To evaluate the predicted propagation rate of the reaction front, the time difference between the first temperature peaks at P1, P2b and P3 have to be compared with the measured values. This comparison shows that the model predicts a slower propagation rate, 0.08 [kg.m<sup>-2</sup>s<sup>-1</sup>], while the propagation rate according to the experiments ranges from 0.09 to 0.12 [kg.m<sup>-2</sup>s<sup>-1</sup>]. The calculated propagation rate is comparable with the measured values of Porteiro et al. [3] for the combustion of wood pellets in a fixed bed reactor.

Some previous works reported a secondary reaction front, i.e. the char burnout front, propagating upwards towards the top of the packed bed and burning the char previously formed. This is true when the bed does not collapse and it retains its original structure. However, if biomass has a low ash content which forms a thin ash layer on a grate, it is more plausible that the char burnout front stays close to the grate and the biomass char particles on the grate are replaced by the upper particles when they are completely burned. The simulation results confirm this hypothesis. According to the simulations, char burnout happens on the grate in a region with a height of about 2-3 times of the initial particle size and above this region O<sub>2</sub> concentrations are zero, almost for the entire char oxidation process.

Moreover, the predicted flue gas temperature has been compared with the experimental data in Figure 8. The thermocouples are located 7.5 cm above the initial surface of the packed bed and 4 cm away from the wall of the reactor, see Figure 1. Both thermocouples measured rather similar temperature profiles. Since the reactor geometry has been modelled axisymmetrically, the predicted flue gas temperatures at these positions have been compared to the average values of the two thermocouple temperatures in each test run. Both measured and simulation results show the same trends concerning the flue gas temperature. The first temperature peak corresponds to the ignition of the pyrolysis products and the second peak is related to the end of char burnout where the air to fuel ratio increases. The deviation in the temperature peaks

between experiments and simulations might be due to the limitations of measuring flue gas temperature with thermocouples (the colder retort wall affects the thermocouple measurements by radiation).

The mass loss profile of the fuel bed over time is also shown in Figure 8. Three different periods can be distinguished based on the mass loss curves. The first one is the drying period in combination with pyrolysis without ignition of volatiles. Once ignition of volatiles happens most of the volatiles are released and the mass of the packed bed sharply declines with almost constant rate. After the end of the pyrolysis period, the remaining mass in the reactor is the same for all experiments and simulation results, about 50 g. During the char oxidation period the mass of the packed bed gradually decreases, as the char burnout rate is slower than the pyrolysis rate. According to the experiments the final remaining mass after char burnout is between 0.9 and 1.4 [g], the model prediction is 1.1 [g].

Both experimental and simulation results depict the same combustion behavior in the packed bed. The predicted trends of the species concentrations and the temperature profiles are similar to the experimental data. However, there are deviations from the experiments regarding H<sub>2</sub>O concentrations right after the ignition of volatiles and CO and CO<sub>2</sub> concentrations at the end of pyrolysis and the beginning of char burnout. The positions and the amounts of the peaks concerning the species concentrations as well as temperatures are well predicted, except for the maximum flue gas temperature. The conversion of the packed bed in the model lasts slightly longer than in the experiments. Some further developments may eliminate the current drawbacks of the model, such as improvements of the packed bed heat transfer model as well as a more enhanced pyrolysis scheme (e.g. a mechanistic scheme).

#### *4.1. Effect of the gas phase reaction mechanism*

In order to investigate the influence of the mechanism applied for modelling the reaction chemistry the results of the full mechanism (GRI2.11), the reduced mechanism (DRM22) and the skeletal mechanism (Kilpinen97) have been compared. There is hardly any difference between the results of GRI2.11 and DRM22. Therefore, in Figure 9 and Figure 10, only the results of DRM22 and Kilpinen97 are compared.

As it has already been mentioned, the Kilpinen97 mechanism includes no C<sub>x</sub>H<sub>y</sub> and CH<sub>m</sub>O<sub>n</sub> species. Hence, the composition of volatiles in the simulation with this mechanism consists of a lower number of species in com-

parison to DRM22 and they cannot have similar composition. Therefore, in the calculations of the volatiles composition for Kilpinen97 the mass ratios of  $\text{CO}/\text{CO}_2$ ,  $\text{CH}_4/\text{CO}_2$  and  $\text{H}_2/\text{CO}_2$  are considered to be as similar as possible to the corresponding ratios in the simulation with DRM22. In this way, the input parameters of the simulations with DRM22 and Kilpinen97 are better comparable. The comparison depicts that the skeletal mechanism Kilpinen97 with a considerably lower number of reactions and species than GRI2.11 and DRM22 can predict the species and temperature profiles as well as the mass loss evolution with acceptable accuracy for engineering applications. It is worth noting that the application of Kilpinen97 reduces the calculation time by about 17% in comparison to DRM22.

#### *4.2. Bed shrinkage and porosity*

As an indication of the bed shrinkage, a change of the normalised height of the fuel bed over time is shown in Figure 11. The surface of the fuel bed is not flat during the conversion of the packed bed because of the uneven consumption of the fuel. Therefore, in Figure 11 always the highest point of the surface of the bed has been considered. As it can be seen shrinkage starts with pyrolysis, because in the particle model it is postulated that during drying, the size of the particles remains constant, which is a plausible assumption [20]. The height of the fuel bed at the end of pyrolysis amounts to about 61% of the initial height. This is in line with previous findings of Kumar et al. [20], who reported a volume loss variation of 35% to 55%. As char burnout initiates, the decrease in bed height is not smooth anymore. The discontinuous local shrinkage can be interpreted as a bed collapse. However, by employing specific models for the bed collapse, such as [9], the results may be further improved.

Since the movement of the particles is only considered in gravity direction, it leads to an unrealistic shape of the ash layer on the grate at the end of char burnout. Therefore, it is assumed that as soon as a particle only contains ash and it reaches the grate it will be excluded from the calculation. As a consequence of this assumption the calculated bed height approaches to zero at the end of char burnout, see Figure 11. This is an acceptable assumption, because the ash content of wood pellets is very low. Moreover, as it can be seen in Figure 11, in the test runs at the end of char burnout an ash layer with a height of only a few millimeters and mass of about 0.9 to 1.4 grams was remained.

The local porosity inside the fuel bed influences the heat transfer and the flow field in the bed. The local porosity is affected by the bed shrinkage and the uneven consumption of fuel. Figure 12 shows the calculated local porosity inside the fuel bed. The bed porosity at the beginning is assumed to be constant and equal to 0.55 - a value derived from the bulk and particle density of the fuel used. The initial constant porosity of the bed changes, due to the uneven consumption of fuel particles and bed shrinkage. Due to the shrinkage of the bed, the upper part of the sample holder becomes empty and its porosity turns to one. Moreover, the uneven surface of the fuel bed can be seen in Figure 12. According to the simulations, the conversion of the biomass particles in the center of the sample holder is faster, particularly during char burnout. This can be attributed to the heat transfer to the wall of the sample holder from the particles near the wall which reduces particle temperatures.

## 5. Summary and conclusions

An unsteady three-dimensional model for the combustion of biomass packed beds is presented. The calculations of the freeboard region and the packed bed are combined. The model is able to capture the smooth shrinkage of the bed as well as the discontinuous shrinkage (bed collapse). The interactions between the gas and solid phases as well as the radiative heat transfer between the particles are considered. The biomass particles in the packed bed are modelled as thermally thick particles. Experimental results were obtained under fuel rich conditions with a laboratory-scale fixed bed reactor in order to validate the model and to obtain a better understanding of the combustion processes. The experimental data include gas species concentrations above the bed, bed temperatures, flue gas temperatures in the freeboard and mass loss evolution.

The packed bed model has been extensively validated concerning the temperature profiles at different heights in the packed bed and above the bed, several species concentrations in the freeboard as well as the propagation of the reaction front in the packed bed. The results of the model are in good agreement with the experimental data.

An accurate model for the combustion chemistry in the freeboard is of importance, due to its strong interactions with the packed bed. Hence, three combustion chemistry mechanisms have been investigated. The GRI2.11 and

DRM22 mechanisms gave almost identical results. The predicted flue gas temperature and species concentrations in the freeboard with the Kilpinen97 mechanism are acceptable. However, considering the fact that the skeletal Kilpinen97 mechanism has a considerably lower number of species and reactions than the two other mechanisms, it can be concluded that for engineering applications where the reduction of calculation time is important, the Kilpinen97 mechanism is preferable to the more detailed mechanisms. Additionally, the mechanisms investigated, especially DRM22 and GRI2.11, predict the ignition time and formation of the flame in the gas phase well.

The presented model covers certain advantages/improvements concerning the avoidance of the separation between packed bed and freeboard modelling, the consideration of biomass particles as thermally thick and the consideration of bed shrinkage. Models already published typically cover only one of these features. The present version of the model with a priori particle trajectories is currently being used to simulate biomass grate furnaces within a feasible calculation time. However, the model has some limitations: the movement of the particles is only considered in gravity direction and the effect of moving grate bars on the packed bed needs to be modeled. These issues need to be addressed in further developments of the model, to improve and extend its applicability to a wider range of biomass grate firing systems.

## 6. References

- [1] Ryu C, Yang YB, Khor A, Yates NE, Sharifi VN, Swithenbank J. Effect of fuel properties on biomass combustion: Part I. Experiments fuel type, equivalence ratio and particle size. *Fuel* 2006;85:1039-46.
- [2] van der Lans RP, Pedersen LT, Jensen A, Glarborg P, Dam-Johansen K. Modelling and experiments of straw combustion in a grate furnace. *Biomass & Bioenergy* 2000;19:199–208.
- [3] Porteiro J, Patino D, Collazo J, Granada E, Moran J, Miguez JL. Experimental analysis of the ignition front propagation of several biomass fuels in a fixed-bed combustor. *Fuel* 2010;89:26-35.
- [4] Porteiro J, Patino D, Miguez JL, Granada E, Moran J, Collazo J. Study of the reaction front thickness in a counter-current fixed-bed combustor of a pelletised biomass. *Combust. & Flame* 2012;159:1296-02.

- [5] Merrick D. Mathematical models of the thermal decomposition of coal. 1. The evolution of volatile matter. *Fuel* 1983;62:534–9.
- [6] Shin D, Choi S. The combustion of simulated waste particles in a fixed bed. *Combust. & Flame* 2000;121:167–80.
- [7] Di Blasi C. Dynamic behaviour of stratified downdraft gasifiers. *Chem. Eng. Sci.* 2000;55:2931–44.
- [8] Saastamoinen JJ, Taipale R, Horttanainen M, Sarkomaa P. Propagation of the ignition front in beds of wood particles. *Combust. & Flame*, 2000;123:214–26.
- [9] Hermansson S, Thunman H. CFD modelling of bed shrinkage and channelling in fixed-bed combustion. *Combust. & Flame* 2011;158:988-99.
- [10] Yang YB, Goh YR, Zakaria R, Nasserzadeh V, Swithenbank J. Mathematical modelling of MSW incineration on a travelling bed. *Waste Manage* 2002;22:369-80.
- [11] Collazo J, Porteiro J, Patino D, Granada E, Numerical modeling of the combustion of densified wood under fixed-bed conditions. *Fuel* 2012;93:149–59.
- [12] Duffy NT, Eaton JA. Investigation of factors affecting channelling in fixed-bed solid fuel combustion using CFD. *Combust. & Flame* 2013;106:2204-20.
- [13] Peters B. Measurements and application of a discrete particle model (DPM) to simulate combustion of a packed bed of individual fuel particles. *Combust. & Flame* 2002;131:132–46.
- [14] Mehrabian R, Stangl S, Scharler R, Obernberger I, Weissinger A. CFD simulation of biomass grate furnaces with a comprehensive 3D packed bed model. In: *Proc. of 25th German Flame Day, Karlsruhe, Germany, 2011.*
- [15] Simsek E, Brosch B, Wirtz S, Scherer V, Krll F. Numerical Simulation of Grate Firing Systems using a Coupled CFD / Discrete Element Method (DEM). *Powder Technol* 2009;193:266–73.



- [16] Anca-Couce A, Zobel N, Jakobsen HA. Multi-scale modeling of fixed-bed thermo-chemical processes of biomass with the representative particle model: Application to pyrolysis. *Fuel* 2013;103:773–782.
- [17] Mehrabian R, Zahirovic S, Scharler R, Obernberger I, Kleditzsch S, Wirtz S, Scherer V, Lu H, Baxter LL. A CFD model for thermal conversion of thermally thick biomass particles. *Fuel Process. Technol* 2012;95:96-108.
- [18] Stubenberger G, Scharler R, Zahirovic S, Obernberger I. Experimental investigation of nitrogen species release from different solid biomass fuels as a basis for release models. *Fuel* 2008;87:793-06.
- [19] Thunman H, Leckner B, Niklasson F, Johnsson F. Combustion of wood particles a particle model for eulerian calculations. *Combust. Flame* 2002;129:30–46.
- [20] Kumar RR, Kolar AK, Leckner B. Shrinkage characteristics of Casuarina wood during devolatilization in a fluidized bed combustor. *Biomass & Bioenergy* 2006;30:153–65.
- [21] Bergström D, Israelsson S, Öhman M, Dahlqvist S, Gref R, Boman C, Wästerlund I. Effects of raw material particle size distribution on the characteristics of Scots pine sawdust fuel pellets. *Fuel Process Technol* 2008;89:1324–9.
- [22] Grønli MG. A theoretical and experimental study of the thermal degradation of biomass. PhD thesis, The Norwegian University of Science and Technology, 1996.
- [23] Lu H. Experimental and modelling investigation of biomass particle combustion. PhD thesis, Brigham Young University, 2006.
- [24] Branca C, Albano A, Di Blasi C. Critical evaluation of wood devolatilization mechanisms. *Thermochim. Acta* 2005;429:133–41.
- [25] Srekanth M, Sudhakar DR, Prasad BVSSS, Kolar AK, Leckner B. Modelling and experimental investigation of devolatilizing wood in a fluidized bed combustor. *Fuel* 2008;87:2698–12.

- [26] Johansson R, Thunman H, Leckner B. Influence of intraparticle gradients in modeling of fixed bed combustion. *Combust. & Flame* 2007;149:49–62.
- [27] ANSYS Inc., ANSYS Fluent Theory Guide, Release 14.5, 2012.
- [28] Idelchik IE. *Handbook of Hydraulic Resistance*. 3rd edition, Begell House, 1996.
- [29] Botterill JSM, Salway AG, Teoman Y. The effective thermal conductivity of high temperature particulate bedsI. Experimental determination. *Int J Heat & Mass Transf* 1989;32:585–93.
- [30] Gnielinski V. Gleichungen zur Berechnung des Wärme- und Stoffaustausches in durchströmten ruhenden Kugelschüttungen bei mittleren und grossen Pecletzahlen. *Verfahrenstechnik* 1978;12:363–66.
- [31] Gupta SN, Chaube RB, Upadhyay SN. Fluid-particle heat transfer in fixed and fluidized beds. *Chem Eng Sci* 1974;29:839–43.
- [32] Denton WH. The heat transfer and flow Resistance for fluid flow through randomly packed spheres. In: *The General Discussion on Heat Transfer*, London: Institute of Mechanical Engineers and ASME; 1951, p. 370–373.
- [33] Resnick H. Simultaneous heat and mass transfer in a diffusion-controlled chemical reaction. PhD thesis, MIT, USA, 2006.
- [34] Eckert ERG, Drake RMJ. *Heat and Mass Transfer*. New York: McGraw-Hill; 1959.
- [35] Bird RB, Stewart WE, Lightfoot EN. *Transport Phenomena*. New York: John Wiley & Sons; 2002.
- [36] Wakao N, Kagueli S, Funazkri T. Effect of fluid dispersion coefficients on particle-to-fluid heat transfer coefficients in packed beds: Correlation of Nusselt numbers. *Chem Eng Sci* 1979;34:325–36.
- [37] Inaba H, Fukuda T, Saito H, Mayinger F. Transient behavior of heat removal from a cylindrical heat storage vessel packed with spherical porous particles. *Wärme- und Stoffübertragung* 1988;22:325–33

- [38] Khan JA, Beasley DE, Alatas B. Evaporation from a packed bed of porous particles into superheated vapor. *Int J Heat & Mass Transfer* 1991;34:267–80
- [39] Achenbach E. Heat and flow characteristics of packed beds. *Exp Thermal & Fluid Sci* 1995;10:17–27.
- [40] Collier AR, Hayhurst AN, Richardson JL, Scott SA. The heat transfer coefficient between a particle and a bed (packed or fluidised) of much larger particles. *Chem Eng Sci* 2004;59:4613–20
- [41] Scott SA, Davidson JF, Dennis JS, Hayhurst AN. Heat transfer to a single sphere immersed in beds of particles supplied by gas at rates above and below minimum fluidization. *Ind Eng Chem Res* 2004;43:5632–44
- [42] Zhou ZY, Yu AB, Zulli P. Particle scale study of heat transfer in packed and bubbling fluidized beds. *AIChE J* 2009;55:868–84.
- [43] Kazakov A, Frenklach M. <http://www.me.berkeley.edu/drm/>
- [44] Frenklach M, Wang H, Yu CL, Goldenberg M, Bowman CT, Hanson RK, Davidson DF, Chang EJ, Smith GP, Golden DM, Gardiner WC, Lissianski V. <http://www.me.berkeley.edu/gri-mech/>
- [45] Bowman CT, Hanson RK, Davidson DF, Gardiner WC, Lissianski V, Smith GP, Golden DM, Frenklach M, Goldenberg M. <http://www.me.berkeley.edu/gri-mech/>
- [46] Kilpinen P, available on address: [pia.kilpinen@uku.fi](mailto:pia.kilpinen@uku.fi) or [pia.kilpinen@abo.fi](mailto:pia.kilpinen@abo.fi)
- [47] Zahirovic S, Scharler R, Kilpinen P, Obernberger I. A kinetic study on the potential of a hybrid reaction mechanism for prediction of NO<sub>x</sub> formation in biomass grate furnaces. *Combust Theory & Model* 2011;15:645–70.
- [48] Boroson ML, Howard JB, Longwell JP, Peters WA. Product yields and kinetics from the vapor phase cracking of wood pyrolysis tars. *AIChE J* 1989;35:120–8.
- [49] Graham RG, Bergougnou MA, Overend RP. Fast pyrolysis of biomass. *J Anal Appl Pyr* 1984;6:95–135.

- [50] Nunn TR, Howard JB, Longwell JP, Peters WA. Product compositions and kinetics in the rapid pyrolysis of sweet gum hardwood. *Ind Eng Chem Process Des Dev* 1985;24:836–44.
- [51] Hajaligol MR, Howard JB, Longwell JP, Peters WA. Product compositions and kinetics for rapid pyrolysis of cellulose. *Ind Eng Chem Process Des Dev* 1982;21:457–65.
- [52] Di Blasi C, Signorelli G, Di Russo C, Rea G. Product Distribution from Pyrolysis of Wood and Agricultural Residues. *Ind Eng Chem Res* 1999;38:2216–24.
- [53] Di Blasi C, Branca C, Santoro A, Gonzalez HE. Pyrolytic behavior and products of some wood varieties. *Combust. & Flame* 2001;124:165–77.
- [54] Horne PA, Williams PT. Influence of temperature on the products from the flash pyrolysis of biomass. *Fuel* 1996;75:1051–9.
- [55] Agblevor FA, Besler S, Wiseloge AE. Fast Pyrolysis of Stored Biomass Feedstocks. *Energy & Fuels* 1995;9:635–40.
- [56] Wang X, Kersten SRA, Prins W, van Swaaij WPM. Biomass Pyrolysis in a Fluidized Bed Reactor Part 2: Experimental Validation of Model Results. *Ind Eng Chem Res* 2005;44:8786–95.
- [57] Fagbemi L, Khezami L, Capart R. Pyrolysis products from different biomasses: Application to the thermal cracking of tar. *Appl Energy* 2001;69:293–306.
- [58] Scott DS, Piskorz J, Bergougnou MA, Graham R, Overend RP. The role of temperature in the fast pyrolysis of cellulose and wood. *Ind Eng Chem Res* 1988;27:8–15.
- [59] Becidan M, Skreiberg Ø, Hustad JE. Products distribution and gas release in pyrolysis of thermally thick biomass residues samples. *J Anal Appl Pyr* 2007;78:207–13.
- [60] de Jong W, Pirone V, Wójtowicz MA. Pyrolysis of *Miscanthus Giganteus* and wood pellets: TG-FTIR analysis and reaction kinetics. *Fuel* 2003;82:1139–47.

- [61] Dupont C, Commandré JM, Gauthier P, Boissonnet G, Salvador S, Schweich D. Biomass pyrolysis experiments in an analytical entrained flow reactor between 1073K and 1273K. *Fuel* 2008;87:1155–64.
- [62] Dupont C, Chen L, Cances J, Commandre JM, Cuoci A, Pierucci S, Ranzi E. Biomass pyrolysis: Kinetic modelling and experimental validation under high temperature and flash heating rate conditions. *J Anal Appl Pyr* 2009;85:260–7.
- [63] Beaumont O, Schwob Y. Influence of physical and chemical parameters on wood pyrolysis. *Ind Eng Chem Process Des Dev* 1984;23:637-41.
- [64] Encinar JM, González JF, González J. Fixed-bed pyrolysis of *Cynara cardunculus* L. Product yields and compositions. *Fuel Process Technol* 2000;68:209–22.
- [65] Wei L, Xu S, Zhang L, Zhang H, Liu C, Zhu H, Liu S. Characteristics of fast pyrolysis of biomass in a free fall reactor. *Fuel Process Technol* 2006;87:863–71.
- [66] Aguado R, Olazar M, San José MJ, Aguirre G, Bilbao J. Pyrolysis of sawdust in a conical spouted bed reactor. Yields and product composition. *Ind Eng Chem Res* 2000;39:1925–33.
- [67] Li S, Xu S, Liu S, Yang C, Lu Q. Fast pyrolysis of biomass in free-fall reactor for hydrogen-rich gas. *Fuel Process Technol* 2004;85:1201–11.
- [68] Commandré JM, Lahmidi H, Salvador S, Dupassieux N. Pyrolysis of wood at high temperature: The influence of experimental parameters on gaseous products. *Fuel Process Technol* 2011;92:837–44.

## Nomenclature

$A$	pre-exponential factor [ $s^{-1}$ ]
$c_i$	biomass pseudo-component contributions [-]
$C_1$	permeability [ $m^2$ ]
$C_2$	inertial loss coefficient [ $m^{-1}$ ]
$D$	diffusivity [ $m^2.s^{-1}$ ]
$E$	activation energy [ $kJ.mol^{-1}$ ]
$F$	view factor
$h_m$	mass transfer coefficient [ $m.s^{-1}$ ]
$k$	kinetic rate constant [ $s^{-1}$ ]
$k_c$	reaction rate constants, char conversion [ $m.s^{-1}$ ]
$m$	mass [ $kg$ ]
$M_c$	molecular weight of carbon [ $kg.kmol^{-1}$ ]
$n$	mole [-]
$NC$	number of cells
$NP$	number of particles
$Nu$	Nusselt number [-]
$Pr$	Prandtl Number [-]
$q$	heat flux
$R$	universal gas constant [ $kJ.mol^{-1}.K^{-1}$ ]
$Re$	Reynolds Number [-]
$S$	surface area [ $m^2$ ]
$\Delta S$	momentum source term [ $kg.m^{-2}.s^{-2}$ ]
$t$	time [ $s$ ]
$T$	temperature [ $K$ ]
$u$	velocity [ $m.s^{-1}$ ]
$X_\infty$	molar concentration of gas species at bulk flow [ $kmol.m^{-3}$ ]

### Greek symbols

$\alpha_i$	conversion of each biomass pseudo-component [-]
$\delta_{ash}$	thickness of ash layer [ $m$ ]
$\epsilon$	emissivity [-]
$\phi$	porosity [-]
$\eta$	tortuosity [-]
$\mu$	viscosity [ $kg.m^{-1}.s^{-1}$ ]
$\rho$	density [ $kg.m^{-3}$ ]
$\sigma$	Stefan-Boltzmann constant [ $W.m^{-2}.K^{-4}$ ]
$\Omega$	stoichiometric ratio of moles of carbon per mole of oxidising/gasifying agent in corresponding reaction [-]

Subscripts

$0$	initial condition
$ch$	char
$e$	effective
$f$	final condition
$g$	gas
$lam$	laminar
$p$	particle
$rad$	radiation
$turb$	turbulent
$\vartheta$	radiation control volume

Table 1: Experimental conditions and relevant data of the biomass used in the laboratory-scale reactor tests.

Fuel	Oxidising medium	Air flow rate [Nl/min]	Temperature of heated walls		Sample wet mass [g]
			upper [°C]	lower [°C]	
Spruce pellets	Air	30	750	450	410
C [wt% d.b.]	H [wt% d.b.]	O [wt% d.b.]	N [wt% d.b.]	Ash [wt% d.b.]	MC [wt% w.b.]
49.5	6.1	44.05	0.05	0.3	7.1

Table 2: Parameters used in the particle model.

Particle density [21]		
biomass (wet)	1220	kg.m <sup>-3</sup>
char	250	kg.m <sup>-3</sup>
ash	300	kg.m <sup>-3</sup>
Heat capacity [22]		
biomass	1500 + T	J.kg <sup>-1</sup> .K <sup>-1</sup>
char	420 + 2.09T + 6.85×10 <sup>-4</sup> T <sup>2</sup>	J.kg <sup>-1</sup> .K <sup>-1</sup>
ash	420 + 2.09T + 6.85×10 <sup>-4</sup> T <sup>2</sup>	J.kg <sup>-1</sup> .K <sup>-1</sup>
Thermal conductivity [23]		
biomass	0.056 + 2.6×10 <sup>-4</sup> T	W.m <sup>-1</sup> .K <sup>-1</sup>
char	0.071	W.m <sup>-1</sup> .K <sup>-1</sup>
ash	1.2	W.m <sup>-1</sup> .K <sup>-1</sup>
Particle emissivity	ε = 0.85	-
Pyrolysis model [24]		
Hemicellulose	<b>A</b> = 2.527 × 10 <sup>11</sup>	s <sup>-1</sup>
	<b>E</b> = 147	kJ.mol <sup>-1</sup>
	<i>a</i> = 0.26	-
Cellulose	<b>A</b> = 1.379 × 10 <sup>14</sup>	s <sup>-1</sup>
	<b>E</b> = 193	kJ.mol <sup>-1</sup>
	<i>a</i> = 0.64	-
Lignin	<b>A</b> = 2.202 × 10 <sup>12</sup>	s <sup>-1</sup>
	<b>E</b> = 181	kJ.mol <sup>-1</sup>
	<i>a</i> = 0.10	-
Char conversion model		
Pore diameter	100 [25]	μm
Porosity of ash layer	0.9	
$\Omega C + O_2 \longrightarrow 2(\Omega - 1)CO + (2 - \Omega)CO_2$	$k_c = 1.715 T \exp(-9000/T)$ [26]	m.s <sup>-1</sup>
	$\Omega = \frac{2[1+4.3\exp(-3390/T)]}{2+4.3\exp(-3390/T)}$ [26]	m.s <sup>-1</sup>
$C + CO_2 \longrightarrow 2CO$	$k_c = 3.42 T \exp(-15600/T)$ [26]	m.s <sup>-1</sup>
$C + H_2O \longrightarrow CO + H_2$	$k_c = 3.42 T \exp(-15600/T)$ [26]	m.s <sup>-1</sup>
$C + 2H_2 \longrightarrow CH_4$	$k_c = 3.42 \times 10^{-3} T \exp(-15600/T)$ [26]	m.s <sup>-1</sup>



Table 3: The composition of volatiles used in the simulations with different kinetic mechanisms.

Species	Mass fraction		
	GRI2.11	DRM22	Kilpinen97
CO	0.391	0.391	0.492
CO <sub>2</sub>	0.170	0.170	0.214
CH <sub>4</sub>	0.087	0.087	0.135
H <sub>2</sub>	0.017	0.017	0.028
H <sub>2</sub> O	0.168	0.168	0.131
N <sub>2</sub>	0.001	0.001	0.001
C <sub>2</sub> H <sub>2</sub>	0.002	0.002	-
C <sub>2</sub> H <sub>4</sub>	0.002	0.002	-
C <sub>2</sub> H <sub>6</sub>	0.056	0.056	-
CH <sub>2</sub> O	0.107	0.107	-

Table 4: The empirical constraints for the mass yield of volatiles based on Figure 4 and Figure 5.

$$\begin{aligned}
 &0.1 < \frac{m_{CO}}{m_{CO_2}} < 10 \\
 &0.1 < \frac{m_{CH_4}}{m_{CO_2}} < 1 \\
 &0.05 < \frac{m_{H_2}}{m_{CO_2}} < 0.4 \\
 &0.5 < \frac{m_{H_2O}}{m_{CO_2}} < 4 \\
 &0.1 < \frac{m_{C_2H_2} + m_{C_2H_4} + m_{C_2H_6}}{m_{CO_2}} < .15
 \end{aligned}$$

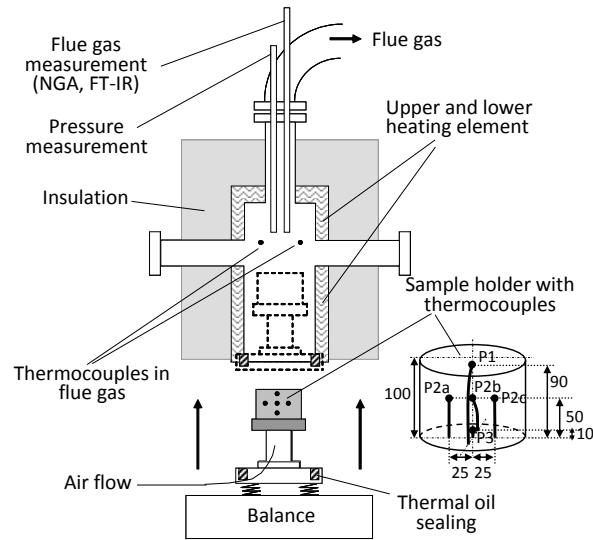


Figure 1: Scheme of the experimental setup and arrangement of the thermocouples in the fuel bed. Dimensions are in [mm].

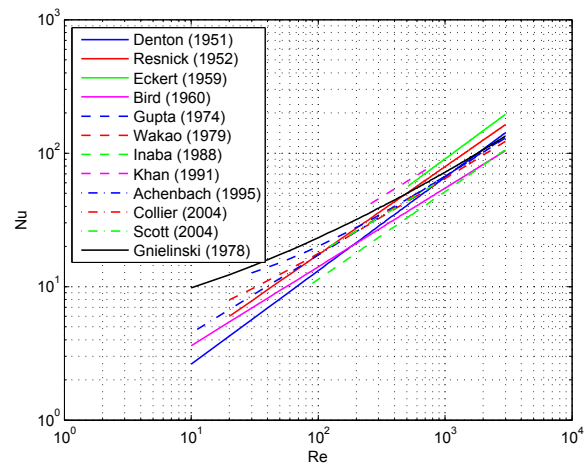


Figure 2: Nusselt number as a function of Reynolds number for packed beds, data from [31–41] and Equation 13, i.e. Gnielinski [30].

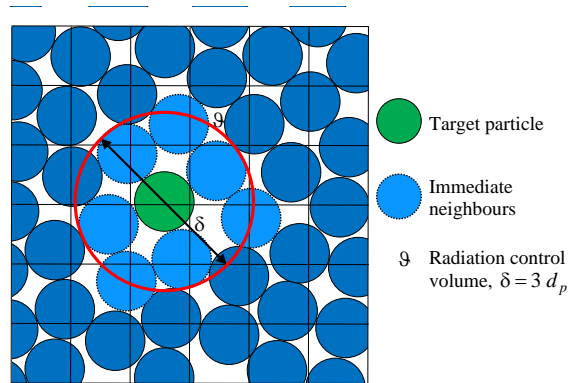


Figure 3: Radiation control volume and neighbouring particles in the packed bed radiation model

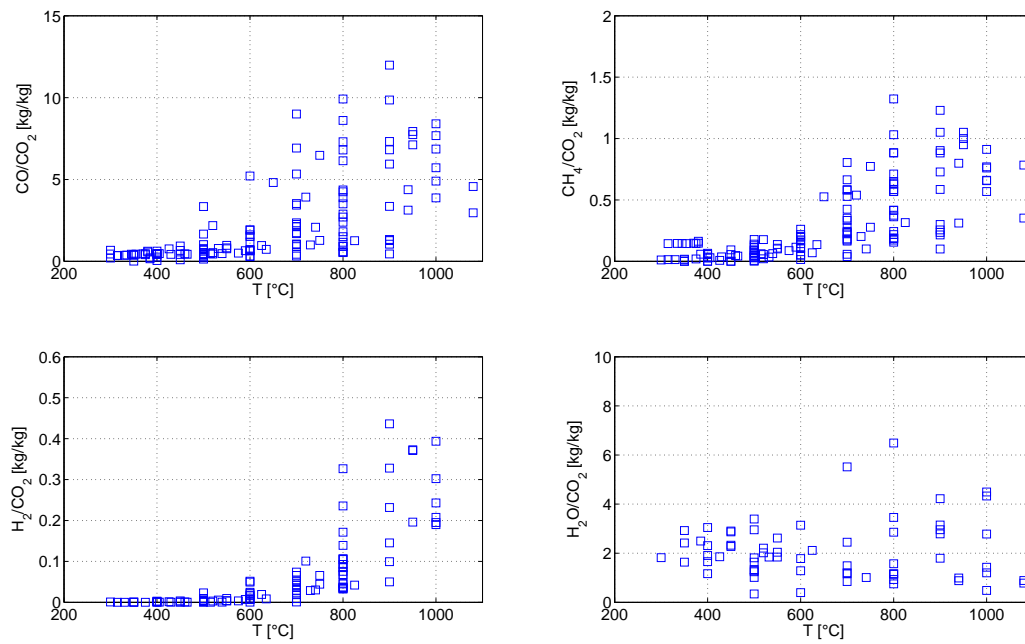


Figure 4: The mass yields of CO, CH<sub>4</sub>, H<sub>2</sub> and H<sub>2</sub>O in relation to the mass yield of CO<sub>2</sub> as a function of pyrolysis temperature, data from [48–68].

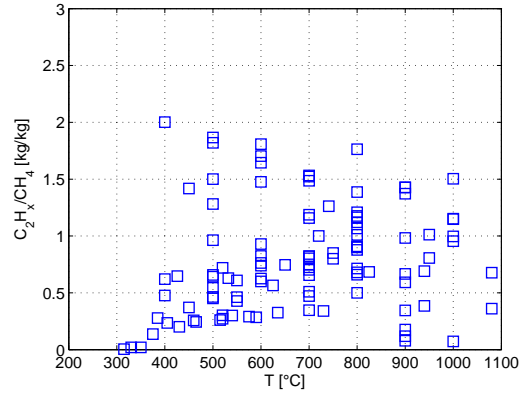


Figure 5: The mass yield of  $C_2H_x$  ( $C_2H_2+C_2H_4+C_2H_6$ ) in relation to the mass yield of  $CH_4$  as a function of pyrolysis temperature, data from [48–68].

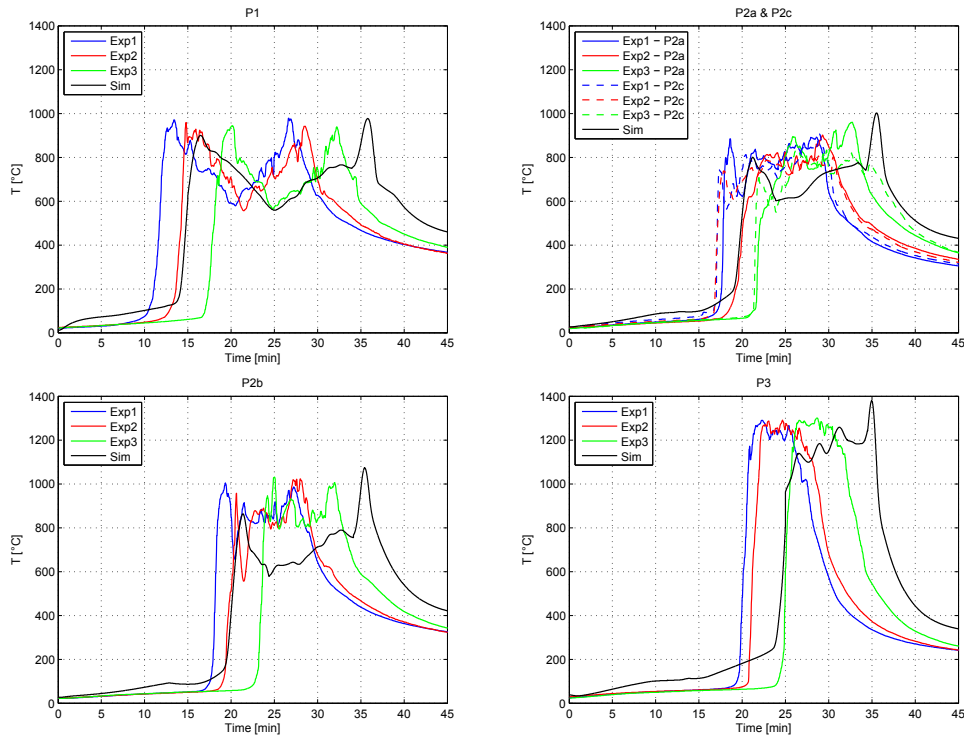


Figure 6: Comparison between simulated and measured temperatures at different positions inside the packed bed.

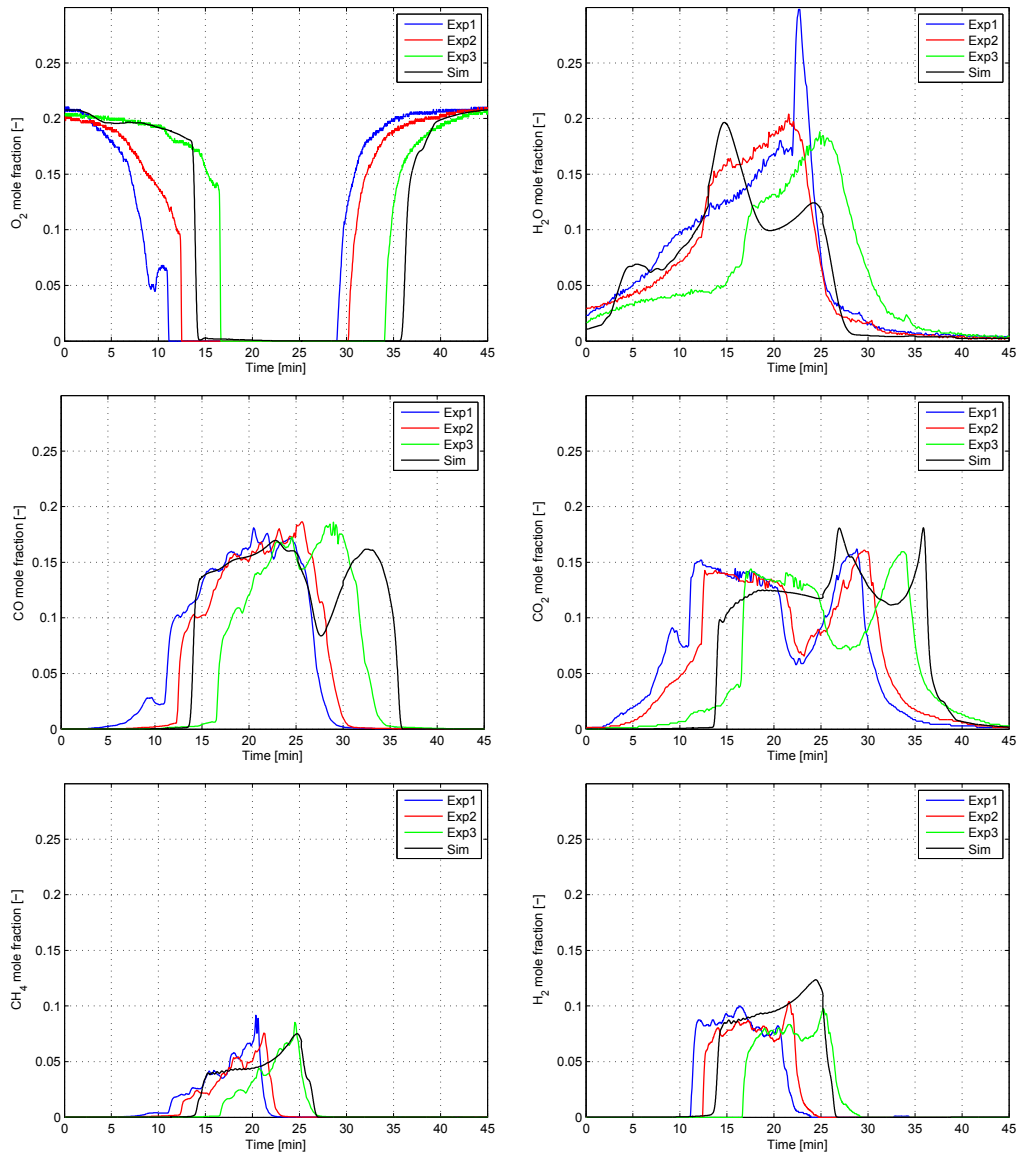


Figure 7: Comparison between simulated and measured species concentrations at a height of 11 cm above the initial surface of the packed bed.

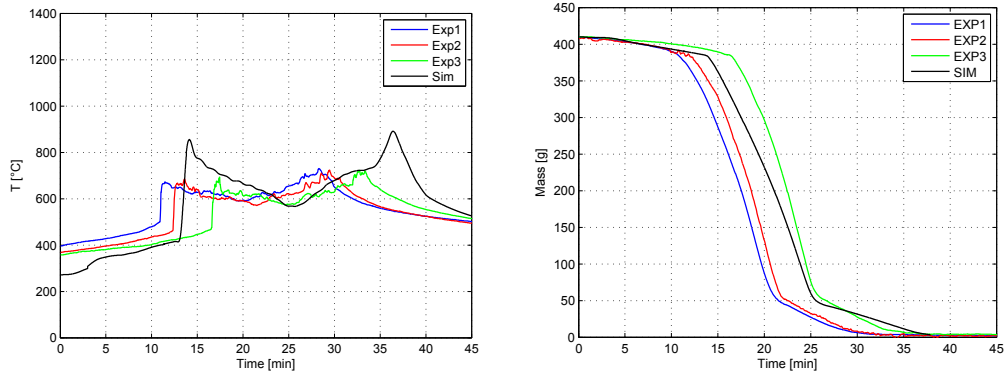


Figure 8: Left: Comparison between simulated and measured flue gas temperatures in the freeboard at a height of 7.5 cm above the initial surface of the packed bed and 4 cm away from the retort wall; Right: Comparison between simulated and measured mass loss profiles.

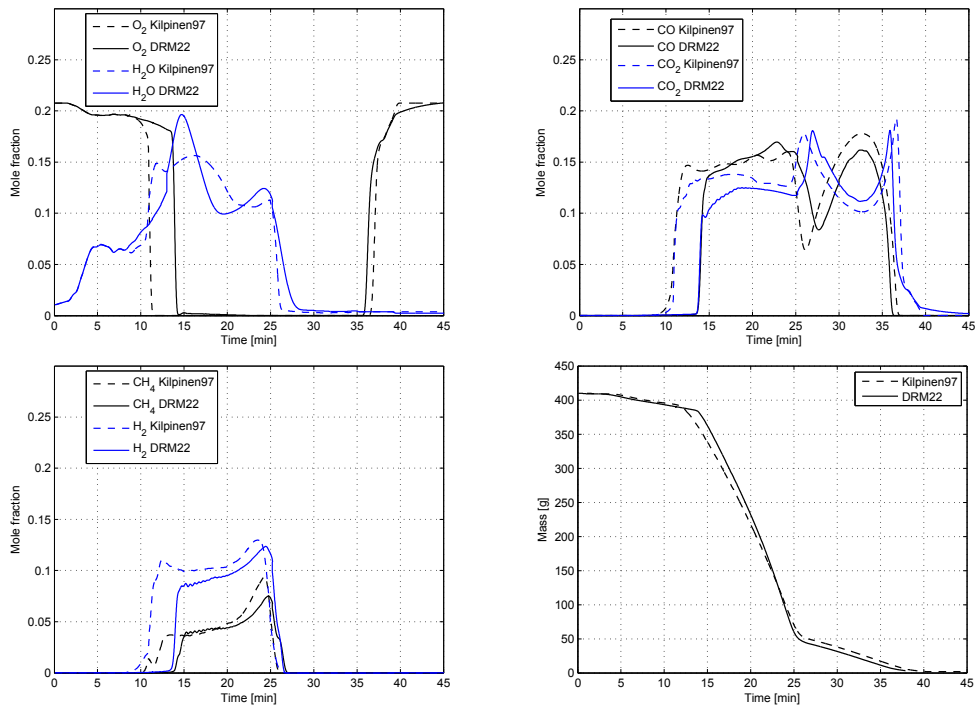


Figure 9: Comparison between the results of the DRM22 and Kilpinen97 mechanisms for species concentrations in the freeboard and mass loss profiles.

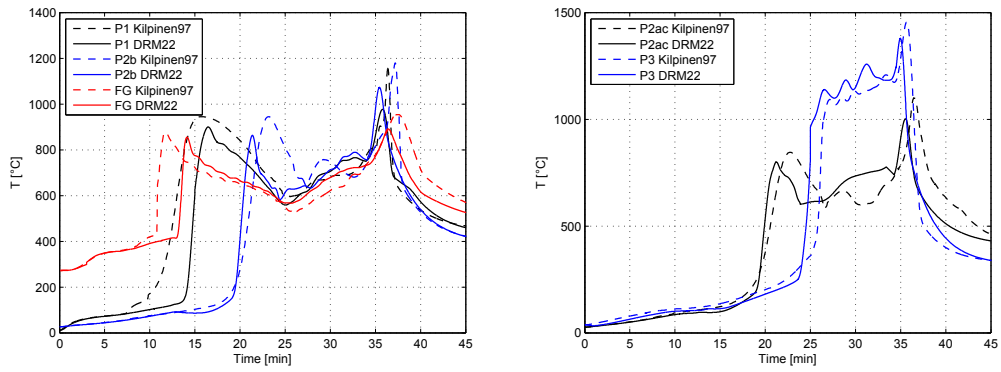


Figure 10: Comparison between the results of the DRM22 and Kilpinen97 mechanisms for temperatures inside the packed bed (P1, P2b, P2ac, P3) and freeboard (FG).

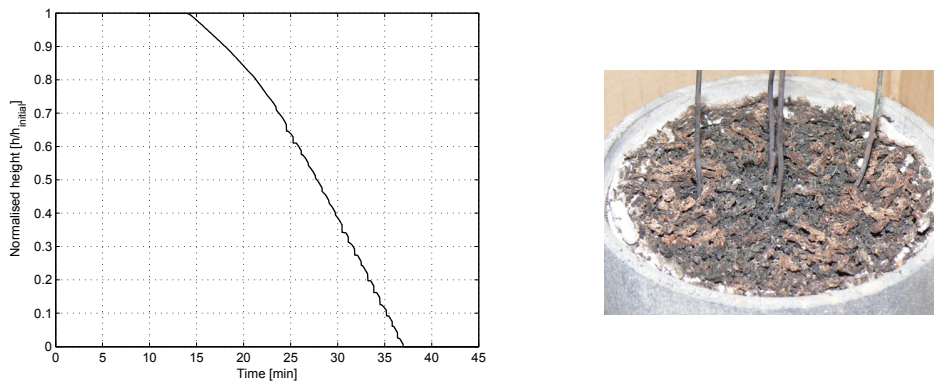


Figure 11: Left: Normalised height of the bed; Right: Picture of the remaining ash layer on the grate at the end of a test run.

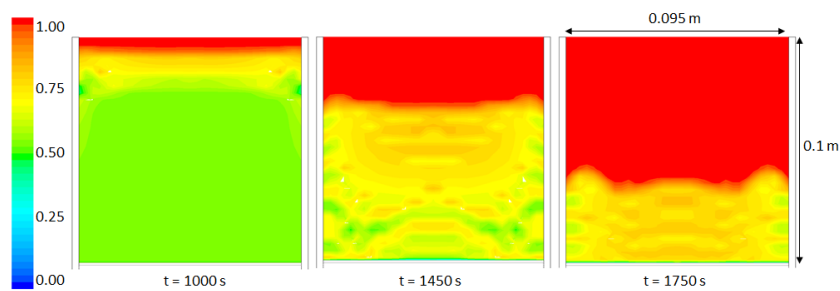


Figure 12: Porosity contours in the fuel bed at three different times.